DEPARTMENT OF PHYSICS
UNIVERSITY OF JYVÄSKYLÄ
RESEARCH REPORT No. 3/2015

DEVELOPMENTS IN MANY-BODY THEORY OF QUANTUM TRANSPORT AND SPECTROSCOPY WITH NON-EQUILIBRIUM GREEN'S FUNCTIONS AND TIME-DEPENDENT DENSITY FUNCTIONAL THEORY

BY
ANNA-MAIJA UIMONEN

ACADEMIC DISSERTATION
FOR THE DEGREE OF
DOCTOR OF PHILOSOPHY

To be presented, by permission of the
Faculty of Mathematics and Natural Sciences
of the University of Jyväskylä,
for public examination in Auditorium FYS-1 of the
University of Jyväskylä on May 27th, 2015
at 12 o'clock noon.

JYVÄSKYLÄ, FINLAND
MAY 2015

PREFACE

The research was carried out at the Department of Physics and Nanoscience Center in the University of Jyväskylä during the years 2010 and 2014.

First of all, I want to thank my supervisor, Prof. Robert van Leeuwen for his guidance and insightful discussions and help throughout my doctoral studies. I am expressing my gratitude to our collaborators Dr. Gianluca Stefanucci, Dr. Yaroslav Pavlyukh, Prof. Stefan Kurth, Dr. Adrian Stan, Dr. Elham Khosravi, Prof. Eberhard K. U. Gross, Dr. Enrico Perfetto and M.Sc. Simone Latini for insightful discussions. I also want to thank Prof. Hannu Häkkinen and Prof. Matti Manninen. In addition, I want to express my thanks to Petri Myöhänen, Niko Säkkinen, Riku Tuovinen, Daniel Karlsson, Luis Cort, Richard Lynn, Markku Hyrkäs, Esa Räsänen, Lauri Lehtovaara, Topi Korhonen, Lars Gell and Andre Clayborne for great discussions.

Jyväskylä, May 2015

Anna-Maija Uimonen

ABSTRACT

The problem of quantum dynamics in open systems has gained attention in recent decades and not the least due to the advances made in quantum transport in molecular systems. The main motivation behind quantum transport and molecular electronics is the futuristic goal to be able at some point to replace, or to complement, the silicon-based technology and to make the electronic devices faster. On a fundamental level, one has to deal with time-dependent processes where electron-electron or electron-phonon interactions are of great importance, and they can cause profound quantitative and qualitative changes on the physical and dynamical properties of electronic systems compared to the non-interacting case. Most of the studies of quantum transport have been focused on the steady-state description while neglecting the short-time dynamics. However, the dynamical effects are of great importance since fast-switching processes play a pivotal role in the operation of future devices. We studied the problem of time-dependent electron transport through the Anderson impurity model by using many-body perturbation theory (MBPT) together with Keldysh Green's functions as well as with time-dependent density functional theory (TDDFT). These methods were compared with numerically exact time-dependent density-matrix renormalization group (tDMRG) method. We found that the many-body perturbation theory results beyond Hartree-Fock approximation were in close agreement with tDMRG results. In addition we studied the possibility of multistablity in the density and current of an interacting nanoscale junction as well as how to reversibly switch between the multiple solutions in time domain.

An accurate theoretical treatment of electron correlation even in as simple model as an interacting electron gas at metallic densities still continues to be a challenge; especially description of features in the photoemission spectra due to electron correlations provides a theoretical challenge. The many-body perturbation theory yields a systematic way to study electron-electron (electron-phonon) correlations in various systems. One of the widely used approximations in MBPT is the GW approximation in which the bare interaction line is replaced with screened interaction line in the first order exchange diagram. The GW approximation gives good estimates for the band gap values close to experimental ones but especially the self-consistent GW approximation has a number of deficiencies like washing out of plasmon features and overestimation of bandwidths compared to experiment. One way to improve GW calculations is to include vertex corrections. Unfortunately, the straightforward inclusion of vertex corrections yields negative spectra in some frequency regions. We developed a diagrammatic approach to construct self-energy approximations with positive spectral properties. Our approach consists of expressing a self-energy of response diagram as a product of half-diagrams after which a minimal set of additional diagrams is identified to construct a perfect square. We applied this method to study vertex corrections in a homogeneous electron gas.

In addition we analyzed the diagrammatic content of photocurrent with density functional theory. The expression for the photocurrent was obtained as an integral over the Kohn-Sham spectral function renormalized by effective potentials that depend on the exchange correlation kernel of current density

functional theory. The expression for the photocurrent gives us the angular dependence of the photocurrent but it does not provide a direct access to the kinetic energy distribution of the photoelectrons.

AUTHOR'S ADDRESS ANNA-MAIJA UIMONEN
DEPARTMENT OF PHYSICS
UNIVERSITY OF JYVÄSKYLÄ
FINLAND

SUPERVISOR PROFESSOR ROBERT VAN LEEUWEN
DEPARTMENT OF PHYSICS
UNIVERSITY OF JYVÄSKYLÄ
FINLAND

REVIEWERS PROFESSOR FERDI ARYASETIAWAN
DEPARTMENT OF PHYSICS
UNIVERSITY OF LUND
SWEDEN

ASSOCIATE PROFESSOR ARI HARJU
DEPARTMENT OF APPLIED PHYSICS
AALTO UNIVERSITY SCHOOL OF SCIENCE
FINLAND

OPPONENT PROFESSOR REX GODBY
DEPARTMENT OF PHYSICS
UNIVERSITY OF YORK
UNITED KINGDOM

List of Publications

I A.-M. Uimonen, E. Khosravi, A. Stan, G. Stefanucci, S. Kurth, R. van Leeuwen and E. K. U. Gross, *Comparative study of many-body perturbation theory and time-dependent density functional theory in the out-of-equilibrium Anderson model*, Physical Review B **84**, 115103 (2011) [1]

II A.-M. Uimonen, E. Khosravi, G. Stefanucci, S. Kurth, R. van Leeuwen and E. K. U. Gross, *Real-time switching between multiple steady-states in quantum transport*, Journal of Physics, Conference Series **220**, 012018 (2010) [2]

III E. Khosravi, A.-M. Uimonen, A. Stan, G. Stefanucci, S. Kurth, R. van Leeuwen and E. K. U. Gross, *Correlation effects in bistability at the nanoscale: steady state and beyond*, Physical Review B **84**, 075103 (2012) [3]

IV G. Stefanucci, Y. Pavlyukh, A.-M. Uimonen and R. van Leeuwen, *Diagrammatic expansion for positive spectral functions beyond GW: Application to vertex corrections in the electron gas*, Physical Review B **90**, 115134 (2014) [4]

V A.-M. Uimonen, G. Stefanucci, Y. Pavlyukh and R. van Leeuwen, *Diagrammatic expansion for positive density-response spectra: Application to the electron gas,* Physical Review B **91**, 115104 (2015) [5]

VI S. Latini, E. Perfetto, A.-M. Uimonen, R. van Leeuwen and G. Stefanucci, *Charge dynamics in molecular junctions: Nonequilibrium Green's Function approach made fast*, Physical Review B **84**, 075103 (2014) [6]

VII A.-M. Uimonen, G. Stefanucci and R. van Leeuwen, *Ultra-nonlocality in density functional theory for photo-emission spectroscopy*, Journal of Physical Chemistry **84**, 075103 (2014) [7]

Author has done the non-equilibrium Green's function part of numerical calculations and some of the implementations on publications **I**, **II** and **III** and the Kadanoff-Baym part of the calculations on publication **VI**. Author has taken part on the theoretical development on publications **IV**, **V** and **VII.**

Contents

List of Acronyms

ALDA	Adiabatic local-density approximation
ARPES	Angle resolved photoemission spectroscopy
BALDA	Bethe-ansatz adiabatic-local density approximation
BO	Born-Oppenheimer
BSE	Bethe-Salpeter equation
CDFT	Current-density-functional theory
DFT	Density functional theory
EELS	Electron energy loss spectroscopy
GKBA	Generalized Kadanoff-Baym ansatz
GW	GW approximation for the self-energy $\Sigma(12) = iG(12)W(1^+2)$
G_0W_0	Simplified GW approximation, G and W are not solved to self-consistency.
GW_0	Simplified GW approximation, G is calculated up to self-consistency while W is not.
HF	Hartree-Fock (approximation)
HOMO	Highest occupied molecular orbital
KBE	(Keldysh-) Kadanoff-Baym Equations
KMS	Kubo-Martin-Schwinger (conditions)
KS	Kohn-Sham
LDA	Local-density approximation
LUMO	Lowest unoccupied molecular orbital
MBPT	Many-Body perturbation theory
NDR	Negative differential resistance
NEGF	Non-equilibrium Green's function
RPA	Random-phase approximation
TDCDFT	Time-dependent current-density functional theory
TDDFT	Time-dependent density functional theory
TDHF	Time-dependent Hartree-Fock
TDLDA	Time-dependent local-density approximation
TDSE	Time-dependent Schrödinger equation
VK	Vignale-Kohn
xc	Exchange-correlation
2B	Second Born (approximation) for the self-energy.

LIST OF SYMBOLS

Ψ	Interacting many-particle ground state wave function
Φ	Non-interacting many-particle ground state wave function
$\hat{H}$	Hamiltonian operator
$\hat{h}(1)$	One-body part of the Hamiltonian
$\sigma = \uparrow, \downarrow$	Spin quantum number
$\mathbf{x} \equiv (\boldsymbol{r}, \sigma)$	Position-spin coordinate
z	General time-index on Keldysh contour
t	Time-index on the real time track of the Keldysh contour
τ	Time-index on the imaginary time track of the Keldysh contour
$1 \equiv (\mathbf{x}_1, z_1)$	Position-spin-time coordinate
Z_i	Effective charge of nucleus i
$\mathcal{Z}$	Grand canonical partition function
$Z_{\mathbf{k}}$	Quasi-particle renormalization factor
w	Coulomb interaction
$\mathcal{W}$	Screened interaction
v	External potential
v_{H}	Hartree potential
v_{xc}	Exchange-correllation potential
$\boldsymbol{A}$	Vector potential
$\boldsymbol{j}$	Current density
$\hat{\psi}^\dagger_\sigma(\boldsymbol{r})$, $\hat{\psi}_\sigma(\boldsymbol{r})$	Fermionic-creation / annihilation operator in position-spin representation
$\hat{c}^\dagger_\alpha$, $\hat{c}_\alpha$	Fermionic-creation / annihilation operator in occupation number representation
$\mathcal{C}$	Keldysh contour
$\mathcal{C}_M$	Imaginary track of the Keldysh contour
$\mathcal{C}_-$	Time-ordered part of the Keldysh contour
$\mathcal{C}_+$	Anti-time ordered part of the Keldysh contour
$\mathcal{T}$	Time ordering operator
$\mathcal{T}_\mathcal{C}$	Time ordering operator on the Keldysh contour
$U(t, t')$	Time-evolution operator
$G_0(\mathbf{x}_1 t_1, \mathbf{x}_2 t_2)$	Non-interacting one-particle Green's function
$G(\mathbf{x}_1 t_1, \mathbf{x}_2 t_2)$	Interacting one-particle Green's function

$G_2(\mathbf{x}_1 t_1, \mathbf{x}_2 t_2; \mathbf{x}_1' t_1', \mathbf{x}_2' t_2')$	Two-particle Green's function
$\Sigma_{\text{MB}}(\mathbf{x}_1 t_1, \mathbf{x}_2 t_2)$	Electronic self-energy
$\Sigma_{\text{EM}}(\mathbf{x}_1 t_1, \mathbf{x}_2 t_2)$	Embedding self-energy
$\mathcal{P}(\mathbf{x}_1 t_1, \mathbf{x}_2 t_2)$	Polarizability
$\mathcal{A}(\mathbf{x}_1 t_1, \mathbf{x}_2 t_2)$	One-particle spectral function
$\tilde{\Gamma}(\mathbf{x}_1 t_1, \mathbf{x}_2 t_2 \mathbf{x}_3 t_3) = -\frac{\delta G^{-1}(\mathbf{x}_1 t_1, \mathbf{x}_2 t_2)}{\delta v(\mathbf{x}_3 t_3)}$	Vertex function
$\Gamma(\mathbf{x}_1 t_1, \mathbf{x}_2 t_2 \mathbf{x}_3 t_3) = -\frac{\delta G^{-1}(\mathbf{x}_1 t_1, \mathbf{x}_2 t_2)}{\delta v_{eff}(\mathbf{x}_3 t_3)}$	Vertex function
$\mathbf{\Gamma}$	Level-broadening
Γ_{EM}	Imaginary part of the embedding self-energy
Λ_{EM}	Real part of the embedding self-energy

1

INTRODUCTION

The role of electron-electron interaction is crucial in all of the physical systems ranging from solids and electron gas, to atoms and molecules, and they play a pivotal role in all phenomena from ground-state properties, like band gaps of semiconductors [8, 9], to the transport problem [10, 11, 12, 13, 14, 15, 16, 17], and photoexcitation and photoionization processes [18, 19] as well as to magnetism and superconductivity. The availability of ultra-short coherent light sources together with intense free-electron lasers providing up to sub-femtosecond pulses has increased the interest towards fundamental questions about the behavior of atoms, molecules and solids at the ultra-short time scales. The understanding of the many-body effects in the excitation spectrum are of crucial in phenomena like single and double ionization and excitation processes, in description of many-electron effects during photoionization and photoemission, formation of correlations and the decay of initial correlations, quantum coherence effects, and the dynamics of these systems, as interactions lead to qualitatively new excited states of the system like plasmons or the auto-ionizing states in molecules. The major complication in all of these systems, but also the most interesting to model, is the Coulomb interaction, which triggers on top of the single particle excitations, the emergence of collective behavior such as plasmon excitations. The electron-electron interaction term also crucially determines the so-called quasi-particle lifetime of electronic excitations. The one-particle and collective excitations are experimentally accessible via absorption and photoemission spectra. However, solving the Schrödinger equation directly for atoms with more than a few electrons is already beyond the present day computational capabilities.

One of the methods of tackling the many-particle problem is many-body perturbation theory (MBPT) [20, 21, 22, 23, 24, 25, 26, 27, 28, 29, 30, 31, 32] based on non-equilibrium Keldysh Green's functions [33], in which the properties of the many-particle system are obtained by expansion in powers of the interactions via self-energy insertions. The self-energy describes the effect of an electron interacting with other electrons in its neighborhood and this modified neighborhood acting back to the electron. Therefore, the electron feels a different interaction from the surrounding particles compared to the situation when its presence would have been neglected. The Green's function plays an important role in the theory of photoemission and in the theory of quantum transport since the photoemission spectrum and the spectral

density together with the time-dependent one-particle observables can be directly obtained form it. Another commonly used method is density functional theory (DFT) [34, 35, 36, 37, 38] with its time-dependent variants: time-dependent density functional theory (TDDFT) [39, 40, 41, 42, 43, 44], and time-dependent current density functional theory (TDCDFT) [39, 45, 46]. In density functional theory the main idea is to describe the system in terms of the electronic density, which can be determined by solving an effective one-particle problem.

We have used the MBPT method within non-equilibrium Keldysh Green's function theory to study the effect of *electron correlations* in non-equilibrium and equilibrium systems [1, 2, 3, 4, 5, 6]. The Keldysh Green's function method has the power to treat the Matsubara and zero-temperature formalisms as limiting cases, and although it is usually applied for systems out of equilibrium, it provides a powerful framework for calculating steady-state properties. Therefore, although the Keldysh Green's function theory being a *non-equilibrium* theory, it also provides a natural and powerful framework for theoretical development for systems in *equilibrium*.

In *non-equilibrium* we have studied the problem of quantum transport [1, 2, 3, 6], where on a fundamental level one has to deal with time-dependent processes in an open system where different scattering mechanisms such as electron-electron or electron-phonon interactions are of great importance. These factors make the transport problem not only difficult, but also very rich in physical phenomena. We have used the Kadanoff-Baym equations of motion together with the Keldysh Green's function technique to study a correlated device coupled to leads and exposed to time-dependent external fields. Since the Green's function propagator describes the propagation of added or removed particles from the system the Keldysh Green's function theory provides a natural theoretical framework to study such a problem. Another very important feature of this formalism is the fact that, if the used self-energy approximation is Φ-derivable [47, 48], then the calculated observables automatically satisfy the macroscopic conservation laws of particle number, momentum or energy. This makes the Keldysh Green's function formalism an ideal tool for studying quantum transport. Another advantage is the possibility to systematically improve, through a diagrammatic approach, the different approximations for the electron correlation term used in describing these systems. Since in the MBPT formalism the perturbation theory is done in the electron-electron interaction and not in the external field, we are able to describe the systems at fast time scales and under strong fields.

In the first part of the transport project [1] we benchmarked the MBPT method with various self-energy approximations and TDDFT with the adiabatic Bethe ansatz LDA (ABALDA) against the numerically exact solution obtained with the time-dependent density matrix renormalization group method (tDMRG) for a single interacting quantum dot connected to semi-infinite leads. We found that the MBPT method with the second order born (2B) approximation produces the time-dependent current and densities most accurately while the TDDFT approach with the ABALDA produces the time-dependent density accurately but fails considerably to produce the correct current, usually overestimating the steady-state value of the current. This problem was found to be linked with the overestimation of the density within the leads. This suggests that one needs to take into account XC-potentials which are non-local and non-zero within

the leads. In other words the improved functionals should be non-local in space and as pointed out by Vignale [49].

In the second part of the transport project [2, 3] we studied the time-dependent fast-switching phenomena in correlated quantum transport systems at the nanoscale. The possibility for a system to possess two (or more) different final steady-state solutions for the current and density is called bistability (multi-stability). This phenomenon manifests itself in the current/voltage (I/V) characteristics of the system, where two different currents can be observed for a given voltage. Depending on how the voltage is switched on the I/V characteristics show a hysteresis type behavior. At a mesoscopic level, the experimental observation [50, 51] of a hysteresis loop in the I/V characteristic of double-barrier resonant tunneling structures, prompted intense theoretical and experimental activity to gain a microscopic understanding of bistability. We studied the problem within mean-field level of the MBPT framework in which case we could solve the steady-state MBPT equation without going through the whole time propagation. We found that the steady-state self-consistency equation for the density can possess more than one fixed-point solution. Some of these fixed points can be shown to be stable and reachable by time-propagation. We found that by increasing the electron-electron interaction strength U, the system posses a bifurcation where one stable solution after a critical value U_c, bifurcates into two new symmetric stable solutions and the original stable solution becomes unstable. We found also, that by superimposing an exponentially decaying gate voltage over the bias voltage, we were able to switch between multiple steady states. For the same parameters and the same kind of driving fields we included memory effects through MBPT self-energies and calculated densities and currents from the solution of the Kadanoff-Baym equations. This was done in the 2B and GW approximations for which a remarkable agreement with numerically exact tDMRG results was found in related models [1]. In all cases bistability is destroyed and the results are qualitatively different as compared to those at the Hartree-Fock and the ABALDA level. Since the ABALDA contains correlations we conclude that the suppression of the bistability phenomenon should not be attributed to the lack of static correlations but rather to the lack of memory effects. Our results suggest that bistable regimes induced by the electron-electron interaction only, are unlikely to be found in Hubbard or extended Hubbard model nano-junctions, and other degrees of freedom, like the molecular vibrations or nuclear coordinates, must be taken into account.

At the *equilibrium* level we studied the role of vertex corrections beyond GW applied to the homogeneous 3D electron gas. In many-electron systems, like solids, the bare Coulomb interaction gets screened, when an electron polarizes its surroundings with a cloud of virtual electron-hole pairs. The self-energy approximation which describes the screening effects is called GW-approximation, in which G stands for the so-called electron propagator, *i.e.*, Green's function and $\mathcal{W}$ for the effective interaction between the electrons. In this method the self-energy Σ depends on the polarizability $\mathcal{P}$, the screened interaction $\mathcal{W}$, and on *vertex function* Γ, and the equations describing these objects should be solved self-consistently. The most common way to apply the GW approximation is to calculate the self-energy (without the vertex correction Γ) by taking the first iteration Green's function to be G_0. This leads to the so called $G_0\mathcal{W}_0$-approximation. The next step is to neglect again the vertex-function Γ and to calculate the Green's

function, G, self-consistently. This method has been successfully applied for the calculation of properties of molecules and solids [8, 9, 52, 53, 54].

It is well known that for solids the GW approximation (usually not implemented self-consistently) tends to give band gap values close to the experimental values [8, 9], thus improving over the density functional calculations (which instead underestimate the values for the band gaps [55].) In spite of some improvements over complementary theories, the self-consistent GW approximation is known to have a number of deficiencies like the washing out of plasmon features, broadened bandwidths in the electron-gas-like metals [56], and the washing out of Coulomb blockade side peaks in the Anderson Model [57]. For many decades the common argument has then been that the inclusion of vertex corrections would act as a balancing force for the self-consistency, [58, 59, 60, 61] therefore, *e.g.,* hampering the washing out of plasmon satellites. Several people have worked on this issue on various levels, [62, 63, 64, 65, 66, 67, 68] but the most interesting result from our point of view is that the straightforward inclusion of vertex corrections beyond the GW level yields *negative spectra* in some frequency regions, as first noticed by Minnhagen for the homogeneous electron gas [62]. This deficiency not only prohibits the usual probability interpretation of the spectral function but also generates Green's functions with *wrong analytic properties*. In particular the latter feature *prevents an iterative self-consistent solution* of the Dyson equation since the analytic properties deteriorate with every self-consistency cycle. This unpleasant situation is not limited to the electron gas as it has also been observed in a study of vertex corrections in finite systems [69, 70]. To tackle this problem we developed a diagrammatic method to construct positive spectral functions [4, 5].

To solve the longstanding problem of negative spectral functions within MBPT we developed a diagrammatic method to generate self-energy approximations beyond GW yielding positive spectral functions [4, 5]. The method is based on the Keldysh formalism. We extract the lesser/greater components (these components are needed to construct the spectral function) from a given self-energy, exact or approximate. Any lesser/greater self-energy or polarization diagram can be partitioned into two halves with external time vertices on opposite branches of the Keldysh contour. We then factorize each partition into half-diagrams by using the Lehmann representation of the Green's function, [71, 72] where one half of the partition consists of time-ordered quantities and the other half consists of anti-time-ordered quantities. The partitioning can be seen as cutting the diagram in half along the lesser/greater Green's function lines. After partitioning a self-energy or polarization diagram we need to find the minimal set of half-diagrams in order to write the approximation at hand as a perfect square of half-diagrams. The positivity of the spectral function is guaranteed by the fact that the sum of the products of the half-diagrams is the sum of perfect squares.

In its simplicity these cutting rules can be seen as drawing rules for diagrams, and as an extension of the Feynman rules. First we need to draw the diagrams, assign a label to the internal vertices while the external ones are kept fixed, we are able to extend any MBPT approximation to an approximation generating positive semidefinite (PSD) spectral functions. Some important MBPT approximations, such as the GW or T-matrix approximations, do not require any corrections. The straightforward inclusion of vertex corrections beyond GW inevitably ruins the PSD property and, hence, additional diagrams must

be included. Often, these additional diagrams are of higher order. For instance, the inclusion of the *full first-order vertex* leads to diagrams of fourth order in the screened interaction. Our theory applies equally well to diagrammatic expansions with non-interacting and with self-consistent Green's functions.

By *photoelectron spectroscopy* we refer to all those techniques based on the application of the photoelectric effect. With different variants of this technique it is possible to study the electronic structure of atoms and molecules in a gas, and the electronic states of solids and surfaces. The photoemission may take place as a single photon absorption process (standard photoemission) or as a result of absorption of two photons, commonly referred as two-photon-photoemission (2PPE) [73]. The standard processes in the two-photon-photoemission consist of shining electromagnetic radiation on a surface (pump) which excites the photo-electron to a certain intermediate state on which an another (probe) photon excites the final photoelectron [74].

Although photoemission spectroscopy is used with great success in a wide range of applications, the underlying theory is not sufficient and satisfactory. In the one-particle picture everything is well established in terms of the sudden approximation [74], three-step model [75] and Fermi's golden rule. In the sudden approximation the photoelectron spectrum is interpreted in terms of the one-electron spectral function, which corresponds to a sudden removal of an electron. In the one electron semi-empirical three-step model, introduced by Berglund and Spicer [75], the photoemission process is modeled to consist of three steps: (1) optical absorption, (2) transport to the surface, and (3) the transmission to the surface. Both of these models are well developed, but in order to describe realistic processes and the effect of electron-electron interactions on the photocurrent we need to go to beyond the one particle model. A way to go beyond the one particle picture is to relate the photocurrent to non-equilibrium Green's functions [76, 77, 78].

In the case of single-photon-photoemission we analyzed the diagrammatic content of the photocurrent by making a connection between the density functional expression within time-dependent current density functional theory (TDCDFT) and the diagrammatic expansion of the photocurrent in order to get more insight into the contributing electronic processes [7]. The expression for the photocurrent was obtained as an integral over the Kohn-Sham spectral function renormalized by effective potentials that depend on the exchange correlation kernel of current density functional theory. The expression for the photocurrent gives us the angular dependence of the photocurrent but it does not provide a direct access to the kinetic energy distribution of the photoelectrons. In order to obtain this information within TDCDFT we would need to split the photocurrent into various kinetic energy distributions using an external exchange-correlation field outside the sample which depends in a very non-local manner on the many-body states of the sample. This procedure would lead to very nonlocal correlations between the exchange-correlation fields in the sample and the detector. Therefore, although the density functional theory provides a relatively simple way to calculate the observables of interest, it may lead to unwanted nonlocal effects, which are hard to incorporate in practical calculations.

This thesis is organized as follows: in Chap. 2 we introduce the quantum many-particle problem together with relevant models used later in the text. In Chap. 3 we discuss the general aspects of MBPT with special attention to vertex corrections beyond GW and the construction of positive semi-definite self-energy

approximations. In Chap. 4 we discuss the basis of the TDDFT and TDCDFT in order to obtain the necessary background for the papers [1, 2, 3, 7]. In Chap. 5 we discuss how to model an open quantum system together with MBPT and TDDFT and discuss about various types of embedding for finite and infinite environments.

2

QUANTUM MANY-PARTICLE PROBLEM

The physical world consists of interacting many-particle systems and therefore they appear in many different fields from quantum chemistry and atomic physics to nuclear, solid state and low temperature physics. In the context of quantum field theory, where the point of view is in the field instead of the particle, the many-particle problem is one for which the eigenvalue of the number operator is large [79, 80]. This happens, obviously when considering a sample of solid material consisting of a number of particles of the order of Avogadro constant ($\mathcal{O}(10^{23})cm^{-3}$). But also for atoms beyond Helium the complexity of the problem increases exponentially with the number of particles. The difficulty of the many-particle problem arises from the inter-particle potentials included in the many-particle Hamiltonian $\hat{H}$, which we need to treat in order to describe the ground state properties and time-dependent dynamics of interacting quantum many-particle system accurately. The central equation in non-relativistic many-particle physics is the time-dependent Schrödinger equation,

$$\hat{H}(\{\mathbf{x}\},\{\mathbf{X}\},t)\Theta(\{\mathbf{x}\},\{\mathbf{X}\},t) = i\partial_t\Theta(\{\mathbf{x}\},\{\mathbf{X}\},t) \tag{2.1}$$

which determines the dynamics of our many-particle system together with its stationary part $\hat{H}(\{\mathbf{x}\},\{\mathbf{X}\})$ $\times\ \Theta(\{\mathbf{x}\},\{\mathbf{X}\}) = E\Theta(\{\mathbf{x}\},\{\mathbf{X}\})$. In the equation (2.1) $\Theta(\{\mathbf{x}\},\{\mathbf{X}\},t)$ is the quantum mechanical many-particle wave function giving us a complete non-relativistic description of the properties of the quantum many-particle system. The number of particles in the system is denoted by N and $\{\mathbf{x}_i\} = \{(\mathbf{r}_i,\sigma_i)\}$ denotes the set of general space-spin coordinates for the i-th electron while $\{\mathbf{X}_\alpha\} = \{(\mathbf{R}_\alpha, s_\alpha)\}$ denotes the set of general space-spin coordinates for the α-th nucleus. Equation (2.1) is the fundamental formula for describing single, and many-particle dynamics if the relativistic effects can be neglected. Therefore, the fundamental problem of many-particle physics is the determination of the eigenstates and their time-evolution under the Hamiltonian

$$\hat{H}(t) = \hat{T}_n(\mathbf{X}) + \hat{T}_e(\mathbf{x}) + \hat{W}_{nn}(\mathbf{X}) + \hat{W}_{ee}(\mathbf{x}) + \hat{W}_{en}(\mathbf{X},\mathbf{x}) + \hat{V}_{ext}(t) \tag{2.2}$$

consisting of the nuclear kinetic energy $\hat{T}_n(\mathbf{X})$, the kinetic energy of the electrons $\hat{T}_e(\mathbf{x})$ as well as the interactions between positive nuclei $\hat{W}_{nn}(\mathbf{X})$, negative electrons $\hat{W}_{ee}(\mathbf{x})$ and the interaction between

electrons and nuclei $\hat{W}_{en}(\mathbf{X}, \mathbf{x})$. The last term in the Eq. (2.2) denotes the possible external perturbation which drives our system out of equilibrium. The kinetic energy terms explicitly read as (where we drop the spin index for notational simplicity)

$$\hat{T}_n(\boldsymbol{R}) \equiv -\sum_{\alpha=1}^{N_n} \frac{\hbar^2}{2M_\alpha} \nabla^2_{\boldsymbol{R}_\alpha}, \qquad \hat{T}_e(\boldsymbol{r}) \equiv -\sum_{i=1}^{N_e} \frac{\hbar^2}{2m_i} \nabla^2_i, \tag{2.3}$$

where M_α is the mass of the α-th nucleus and the gradient is taken with respect to the coordinates $\mathbf{R}_\alpha$ of the α-th nucleus. The mass of the i-th electron is denoted by m_i, while N_e is the number of electrons and N_n is the number of nuclei. The nuclear-nuclear interaction $\hat{W}_{nn}$ and the electron-electron $\hat{W}_{ee}$ interaction respectively read

$$\hat{W}_{nn} \equiv \frac{1}{2} \sum_{\alpha \neq \beta}^{N_n} \frac{Z_\alpha Z_\beta}{|\boldsymbol{R}_\alpha - \boldsymbol{R}_\beta|}, \qquad \hat{W}_{ee} \equiv \frac{1}{2} \sum_{i \neq j}^{N_e} \frac{e^2}{|\boldsymbol{r}_i - \boldsymbol{r}_j|}, \tag{2.4}$$

where Z_α is the charge of the nucleus α and e is the charge of the electron. The last term in Eq. (2.2) $\hat{W}_{en}$ denotes the potential energy term arising from the interaction between the nuclei and electrons

$$\hat{W}_{en} \equiv -\sum_{i=1}^{N_e} \sum_{\alpha=1}^{N_n} \frac{eZ_\alpha}{|\boldsymbol{r}_i - \boldsymbol{R}_\alpha|}. \tag{2.5}$$

The solution of the many-particle problem is then obtained by solving the equation (2.1) with some initial condition $\Theta_0(\{\mathbf{x}\}, \{\mathbf{X}\}) = \Theta(\{\mathbf{x}\}, \{\mathbf{X}\}, t = 0)$, giving us the eigenstates and the time-evolution of the many-particle states. Unfortunately this equation cannot be solved exactly even for Hydrogen atom in an arbitrary field, which forces us to think various approximations. The first approximation usually done is the *Born-Oppenheimer approximation* (BO) also know as the *adiabatic approximation* where the nuclear and electronic degrees of freedom are separated. The BO approximation relies on the fact that the masses of the bare nuclei are much larger than the masses of the electrons yielding the motion of the nuclei in low temperatures to be much slower than the motion of the electrons. When the configuration of the nuclei changes, the electrons can respond instantaneously and thus remain essentially in the electronic ground state, *i.e.*, there are no transitions between the electronic states from the changes of the nuclear coordinates that is why the BO approximation is also know as the adiabatic approximation. Therefore, mainly the electron dynamics is responsible for many properties and collective phenomena in crystalline solids, such as magnetic properties, or whether the material is conducting or insulating. In conclusion, we can assume that the positions of the nuclei can be treated as fixed in the electronic point of view, and when the ground state of the electronic subsystem is solved the nuclear part of the Hamiltonian is contributing via static electric potential.

In the BO approximation the full many-particle wave function Θ is assumed to factorable into a direct product of an electronic state Ψ which depends parametrically on the nuclear coordinates $\{\mathbf{R}\}$ and a nuclear state Υ as $\Theta = \Psi \otimes \Upsilon$. This allows us to separate the Schrödinger equation (2.1) into two parts

consisting of the electronic motion and of the kinetic energy of the nuclei

$$\hat{H}\Theta \quad = \quad \hat{H}_{\text{BO}}\Psi \otimes \Upsilon + \Psi \otimes \hat{T}_n\Upsilon \tag{2.6}$$

where we defined the BO Hamiltonian is $\hat{H}_{\text{BO}}$ as (in future we will drop the subscript BO)

$$\hat{H}_{\text{BO}} = \hat{H} = \hat{H}_e + \hat{W}_{en} + \hat{W}_{nn} + \hat{V}_{ext} \tag{2.7}$$

where the electronic hamiltonian $\hat{H}_e = \hat{T}_e + \hat{W}_{ee}$, *i.e.*, it contains the electronic kinetic and interaction terms. The eigenvalue $E_i(\{\mathbf{R}\})$ of the equation (2.7) is as a result a sum of the electronic kinetic energy term and of the all potential energy terms. When neglecting the nuclear kinetic energy our many-particle problem has reduced to solving the following equation

$$\hat{H}(\{\mathbf{x}\},\{\mathbf{X}\},t)\Psi(\{\mathbf{x}\},\{\mathbf{X}\},t) = i\partial_t\Psi(\{\mathbf{x}\},\{\mathbf{X}\},t) \tag{2.8}$$

with some initial condition $\Psi_0(\{\mathbf{x}\},\{\mathbf{X}\}) = \Psi(\{\mathbf{x}\},\{\mathbf{X}\},t=0)$. For non-interacting electrons we can easily solve this equation by considering the Hamiltonian to be a sum of single-particle Hamiltonians $\hat{H} = \sum_i \hat{h}_i$. However, when several particles interact with each other, as well as with an external environment, a separation of the Hamiltonian into a sum of single-particle Hamiltonians $\hat{h}_i$ is prohibited. Thus, the motion of the particle is dependent on the position of all the other particles causing the complexity of the problem to increase very quickly. Hence, we need to find other ways to treat the many-particle system, than directly solving for the Schrödinger equation. Most of the alternative formulations of the many-particle problem are based on the second quantization, quantum field theory, and Green's function techniques or to the density functional techniques, which has been particularly successful in describing ground state properties of atoms, molecules and solids, or to resort to some other approximations. But before discussing them let us analyze the Hamiltonian of Eq. (2.8) in more detail. The electronic kinetic energy term $\hat{T}_e$ acts as a delocalizing force, while the electron-electron interaction term $\hat{W}_{ee}$ acts as localizing force, trying to keep the electrons apart from each other at fixed positions. An example of this behavior is Wigner Crystallization in weakly interacting electron liquids [81]. The relative strength of the kinetic energy term $\hat{T}_e$ and the electron-electron interaction term $\hat{W}_{ee}$ determines the true strength of the electron-electron interaction, *i.e.*, how correlated the system is. Usually the interaction term $\hat{W}_{ee}$ is assumed to be weak so that it can be treated perturbatively, like in many-body perturbation theory. At the opposite side is the strongly correlated regime where the kinetic energy terms are weak compared to the electron-electron interaction, and we need to resort other kind of approaches like the method of strictly correlated electrons [82, 83].

In this thesis we focus on the regime of weakly or moderately correlated electronic systems and try to approximate the Coulomb interaction terms in various different ways. The oldest approximation to treat the electron-electron interaction term has been to exclude all the complicated inter-particle effects and consider the particles moving independently in a potential created by the charge distributions of all the other $N-1$ electrons, *i.e.*, in an interaction mimicking mean field described by the Hartree potential

$v_{\mathrm{H}}(\mathbf{r}) = e^2 \int \frac{n(\mathbf{r}')}{|\mathbf{r}-\mathbf{r}'|} d\mathbf{r}'$. The Hartree approximation is largely based on the property that Coulomb interaction has a long range and therefore the position of a single electron does not greatly alter the potential at a given point. In this thesis we discuss only about those systems for which the antisymmetry of the wave function with respect to interchange of particles has dominating influence on the properties of the system, *i.e.*, systems consisting of fermions. In the case of the Hartree approximation the Schrödinger equation splits into a product of N electron wave functions

$$\Psi(\mathbf{x}_1, \mathbf{x}_2, ..., \mathbf{x}_N) = \psi_1(\mathbf{x}_1)\psi_2(\mathbf{x}_2)...\psi_N(\mathbf{x}_N) \tag{2.9}$$

and therefore the Hartree approximation does not incorporate the antisymmetric nature of the true solution. The only requirement of the Hartree approximation is that no more than two particles can be in each electronic state. To include the Pauli exclusion principle in the approximation we need to take into account the antisymmetric nature of the total wave function which now becomes a Slater determinant

$$\Psi(\mathbf{x}_1, \mathbf{x}_2, ..., \mathbf{x}_N) = \frac{1}{\sqrt{N!}}(-1)^P P[\psi_{P(1)}(\mathbf{x}_1)\psi_{P(2)}(\mathbf{x}_2)...\psi_{P(N)}(\mathbf{x}_N)] \tag{2.10}$$

where P is the permutation operator which permutes the particle labels. The Hartree-Fock equations and consequently the ground state energy of the Hartree-Fock approximation can be obtained by applying the variational principle to the wave function Ψ giving a set of equations for each single-particle wave function $\psi_i(\mathbf{x}_i)$. The Hartree-Fock equations read as (neglecting the nuclear terms)

$$\left(\hat{h}(\mathbf{r}) + v_{\mathrm{H}}(\mathbf{r})\right)\psi_i(\mathbf{r}) + \int d\mathbf{r}' v_{ex}(\mathbf{r}, \mathbf{r}')\psi_i(\mathbf{r}') = \varepsilon_i \psi_i(\mathbf{r}) \tag{2.11}$$

where $\hat{h}$ is the one-body part of the Hamiltonian and ε_i is the single-particle Hartree-Fock energy corresponding to the orbital i. In addition to the Hartree potential we have a nonlocal exchange potential due to the antisymmetric nature of the wave function $v_{ex}(\mathbf{r}, \mathbf{r}') = \frac{e^2}{|\mathbf{r}-\mathbf{r}'|}\sum_j \psi_j(\mathbf{r})\psi_j^*(\mathbf{r}')$.

The Pauli exclusion principle between electrons is usually more important than the correlations due to mutual repulsion between electrons. But, this is only a first order approximation, and the correlations between the electrons must be taken into account to explain some of the more detailed properties of the many-particle system. This approximation, in which the wave function of the system is approximated by an antisymmetrized product of one-particle wave functions is know as the *independent particle model*. The Pauli principle reduces the probability to find an electron in the vicinity of another electron with same spin. This effect is called the *exchange repulsion* and is totally independent of the effect of electron-electron interactions and is completely due to effect of fermionic spin statistics. A correlated electronic system is defined to be a system with non-vanishing pair correlation function between the $\uparrow$ and $\downarrow$ electrons, but the electron-electron interaction effects will also change the pair correlation function between the electrons of same spin species. For the situations when the pair correlation function for the electrons of the same spin as well as for the electrons of opposite spin is comparable in size, the system is termed *strongly correlated*. Another way to define electron correlations is via the average of a product of quantities $\langle AB \rangle$ which

usually differers from the product of averages of individual quantities $\langle A\rangle\langle B\rangle$, *i.e.,* $\langle AB\rangle \neq \langle A\rangle\langle B\rangle$. The correlations are effects that go beyond factorable approximations.

2.1 SECOND QUANTIZATION

In order to go beyond the Hartree-Fock approximation and to incorporate correlation effects into our description of the many-particle system, the methods of quantum field theory become particularly handy, allowing us to focus on the matrix elements of the quantities of interests, thus avoiding the need to deal directly with the many-particle wave function. The concept of second quantization greatly simplifies the discussion of many identical particles by reformulating the original Schrödinger equation. One of the advantages of second quantization is that it incorporates the (Bose) Fermi statistics automatically, in contrast with the more cumbersome approach of using symmetrized and anti-symmetrized products of single-particle wave functions. In addition, together with statistical mechanics and grand canonical ensemble, the second quantization provides a powerful tool to treat systems with variable number of particles, a situation, very frequent, in non-equilibrium phenomena. Let us consider N non-relativistic particles given by the square integrable wave function $\Psi(\mathbf{x}_1, ..., \mathbf{x}_N)$. A collection of all the many-particle states forms a Hilbert space

$$\mathcal{H}^N = \mathcal{L}^2(\mathbb{R}^{3N} \times \mathbb{Z}_2^N) = \left\{ \Psi(\mathbf{x}_1, .., \mathbf{x}_N); \int d\mathbf{x}_1 ....d\mathbf{x}_N \, |\Psi(\mathbf{x}_1, .., \mathbf{x}_N)|^2 < \infty \right\} \tag{2.12}$$

where $\mathcal{L}^2(\mathbb{R}^{3N} \times \mathbb{Z}_2^N)$ denotes the space of square integrable functions over the the space-spin variable $\mathbf{x} = (\boldsymbol{r}, \sigma)$, $(\int d\mathbf{x} = \sum_\sigma \int d\boldsymbol{r})$, in Euclidean three dimensional space. In second quantization the wave functions are replaced with the creation and annihilation field operators, which are mappings between the many-particle Hilbert spaces of different particle numbers. The creation operator $\hat{\psi}^\dagger(x)$ creates a particle in our case a fermion at position-spin point $x = (\mathbf{r}, \sigma)$ and is a mapping between N and $N + 1$ particle states $\hat{\psi}^\dagger(x) : \mathcal{H}^N \to \mathcal{H}^{N+1}$. The annihilation operator $\hat{\psi}$ destroys a particle at space-spin position x and is a mapping between N and $N - 1$ particle states $\hat{\psi}(x) : \mathcal{H}^N \to \mathcal{H}^{N-1}$. The creation and annihilation operators are defined as Hermitian conjugates of each other, and explicitly for fermions, these actions are

$$\hat{\psi}^\dagger(\mathbf{x})|\mathbf{x}_1, ..., \mathbf{x}_N\rangle = |\mathbf{x}_1, \mathbf{x}_2, ..., \mathbf{x}_N, \mathbf{x}\rangle, \tag{2.13}$$

$$\hat{\psi}(\mathbf{x})|\mathbf{x}_1, ..., \mathbf{x}_N\rangle = \sum_{k=1}^{N} (-1)^{N-k} \delta(\mathbf{x} - \mathbf{x}_k)|\mathbf{x}_1, ..., \mathbf{x}_{k-1}, \mathbf{x}_{k+1}, ..., \mathbf{x}_N\rangle. \tag{2.14}$$

A collection of different particle number Hilbert spaces generated by all the linear combinations of the vectors $|\phi_1\rangle \otimes |\phi_2\rangle \otimes ... \otimes |\phi_N\rangle \equiv |\phi_1 \otimes ... \otimes \phi_N\rangle$ and completed with scalar product

$$\langle \psi_1 \otimes ... \otimes \psi_N | \phi_1 \otimes ... \otimes \phi_n\rangle = \langle \psi_1|\phi_1\rangle ... \langle \psi_N|\phi_n\rangle. \tag{2.15}$$

forms a Hilbert space denoted by $\mathcal{H}\otimes ...\otimes\mathcal{H}=\mathcal{H}^{\otimes N}$. The space of arbitrary number of identical particles is called Fock space $\mathcal{F}(\mathcal{H})=\{\mathcal{H}^0,\mathcal{H}^1,...,\mathcal{H}^N,...\}$ where we have also the zero-particle space, *i.e.*, the one-dimensional space defined as $\mathcal{H}^0=\{\Psi(0)\rangle\}$ consisting only of the zero particle state $\Psi(0)=|0\rangle$. A state with variable number of particles is then a state $|\Psi\rangle$ in Fock space given as ensemble of its components in the product $\mathcal{H}^{\otimes N}$ spaces

$$|\Psi\rangle=\{|\Psi(0)\rangle,|\Psi(1)\rangle,...,|\Psi(N)\rangle,...\}=\{|\Psi(N)\rangle\}_N. \tag{2.16}$$

A general N-particle state can now be obtained by repeated action of the creation field operator on the zero particle ket $|\mathbf{x}_1...\mathbf{x}_N\rangle=\hat{\psi}^\dagger(\mathbf{x}_N)....\hat{\psi}^\dagger(\mathbf{x}_1)|0\rangle$ which demonstrates the power of second quantization nicely. The creation and annihilation operators obey the equal-time anti-commutator relations for fermions and commutator relations for bosons. For example, for fermion-field operators the antisymmetry of wave function is mapped into following anti-commutator relations

$$\{\hat{\psi}^\dagger(x),\hat{\psi}(x')\} = \delta(x-x'), \tag{2.17}$$
$$\{\hat{\psi}^{(\dagger)}(x),\hat{\psi}^{(\dagger)}(x')\} = 0. \tag{2.18}$$

We can express also operators in the second quantized form. A single particle operator $\hat{o}_i$ in Hilbert space $\mathcal{H}$ acts on the i-th factor of the tensor product $\mathcal{H}^{\otimes N}$ as

$$(\hat{I}\otimes ...\otimes\hat{o}_i\otimes ...\otimes\hat{I})|\phi_1\otimes ...\otimes\phi_i,\otimes ...\otimes\phi_n\rangle=|\phi_1\otimes ...\otimes\hat{o}_i\phi_i,\otimes ...\otimes\phi_n\rangle \tag{2.19}$$

where $\hat{I}$ is identity operator leaving the state invariant and is a basic building block in constructing an extensive operator $\hat{O}_1=\sum_{i=1}^N\hat{o}(\mathbf{x}_i)$ as a function of the coordinates $\mathbf{x}$. The second quantized form of the operator $\hat{O}_1$ is

$$\hat{O}_1=\sum_{i=1}^N\hat{o}(\mathbf{x}_i)=\int d\mathbf{x}\,\hat{\psi}^\dagger(\mathbf{x})\hat{o}(\mathbf{x})\hat{\psi}(\mathbf{x}), \tag{2.20}$$

which can be seen by acting with $\hat{O}_1$on the N-particle state and using the definitions for the fermionic creation and annihilation operators Eqs. (2.13) and (2.14). In a similar way we can define expressions for the kinetic and particle density operator, which are

$$\hat{T}=-\sum_{i=1}^N\frac{1}{2}\nabla_i^2=-\frac{1}{2}\int d\mathbf{x}\,\hat{\psi}^\dagger(\mathbf{x})\nabla^2\hat{\psi}(\mathbf{x}), \tag{2.21}$$
$$\hat{n}(\mathbf{x})=\sum_{i=1}^N\delta(\mathbf{x}-\mathbf{x}_i)=\hat{\psi}(\mathbf{x})\hat{\psi}^\dagger(\mathbf{x}). \tag{2.22}$$

In the Hamiltonian (2.7) we also have two particle operators living in the two-particle space $\mathcal{H}\otimes\mathcal{H}$. The basic example of a two-body operator is two-body interaction $\hat{W}$. The general two-particle operator $\hat{O}_2$ is

defined as

$$\hat{O}_2 = \sum_{i<j=1}^{N} \hat{o}(\mathbf{x}_i, \mathbf{x}_j) \tag{2.23}$$

with $\hat{o}(\mathbf{x}_i, \mathbf{x}_j) = \hat{o}(\mathbf{x}_j, \mathbf{x}_i)$ and where the sum is made over the $N(N-1)/2$ pairs of particles. In situations when $\hat{O}_2$ is acting on two identical particles the operator is required to be invariant under the change of two particles which implies that

$$\hat{O}_2 = \frac{1}{2} \sum_{i \neq j}^{N} \hat{o}(\mathbf{x}_i, \mathbf{x}_j) \tag{2.24}$$

which is, for example, the situation with two-body Coulomb interaction term. Hence, we can express the two-particle operator in second quantized form as

$$\hat{O}_2 = \int d\mathbf{x} d\mathbf{y}\, \hat{\psi}^\dagger(\mathbf{x}) \hat{\psi}^\dagger(\mathbf{y}) \hat{o}(\mathbf{x}, \mathbf{y}) \hat{\psi}(\mathbf{y}) \hat{\psi}(\mathbf{x}). \tag{2.25}$$

We can now define the pair correlation function in terms of the field operators

$$g_{\sigma,\sigma'}(\boldsymbol{r}, \boldsymbol{r}') \equiv \frac{\langle \hat{\psi}^\dagger_\sigma(\mathbf{r}) \hat{\psi}^\dagger_{\sigma'}(\mathbf{r}') \hat{\psi}_{\sigma'}(\mathbf{r}') \hat{\psi}_\sigma(\mathbf{r}) \rangle}{n(\mathbf{r}) n(\mathbf{r}')} \tag{2.26}$$

which being proportional to the product of two creation operators and two annihilation operators is directly related to the expectation value the electron-electron interaction. The correlation function $g_{\sigma,\sigma'}(\boldsymbol{r}, \boldsymbol{r}')$ between electrons of different spins accounts for the contributions beyond exchange effect, *i.e.*, it contains true many-body effects. As we pointed out above, the Fermi statistics of the electrons gives rise to exchange-effect between electrons of the same spin, which is signaled by a non-vanishing pair correlation function for equal spins.

The Hamiltonian (Eq. (2.7)) in the second quantized form is as follows

$$\hat{H}(t) = \int d\mathbf{x}\, \hat{\psi}^\dagger(\mathbf{x}) \hat{h}(\mathbf{x}, t) \hat{\psi}(\mathbf{x}) + \frac{1}{2} \int d\mathbf{x} d\mathbf{y}\, \hat{\psi}^\dagger(\mathbf{x}) \hat{\psi}^\dagger(\mathbf{y}) w(\mathbf{x}, \mathbf{y}) \hat{\psi}(\mathbf{y}) \hat{\psi}(\mathbf{x}) \tag{2.27}$$

where the one-body part is a sum of an external field and the positive background potential due to the nuclei

$$\hat{h}(\mathbf{r}, t) = -\frac{1}{2}\nabla^2 - \sum_{i=1}^{N} Z_i\, w(\mathbf{r}, \mathbf{R}_i) + v(\mathbf{r}, t). \tag{2.28}$$

Here w is the Coulomb interaction and Z_i is the effective positive charge of the nucleus i. The last term $v(\mathbf{r}, t)$ denotes an external field. Equation (2.27) is a reformulation of the original Hamiltonian in terms of the field operators in coordinate representation. In practical calculations we need to restrict ourselves to a suitable basis representation $\{\varphi_i(\mathbf{r}, \sigma)\}$. Then we can define the creation and annihilation operators

$\hat{c}^\dagger_{i\sigma}$,$\hat{c}_{i\sigma}$ for the state $i\sigma$ as a linear combination of field operators at different position-spin coordinates $\mathbf{x} = (\boldsymbol{r}, \sigma)$ as

$$\hat{c}^\dagger_{i\sigma} \equiv \int d\mathbf{x}\, \varphi_{i\sigma}(\mathbf{x})\hat{\psi}^\dagger(\mathbf{x}), \tag{2.29}$$

$$\hat{c}_{i\sigma} \equiv \int d\mathbf{x}\, \varphi^*_{i\sigma}(\mathbf{x})\hat{\psi}(\mathbf{x}), \tag{2.30}$$

where $\int d\mathbf{x} = \sum_\sigma \int d\mathbf{r}$. The operators $\hat{c}^\dagger$ and $\hat{c}$ obey similar anti-commutation rules as the field operators $\hat{\psi}^\dagger$ and $\hat{\psi}$. Using the definitions for the operators $\hat{c}^\dagger_i$,$\hat{c}_i$ together with their anti-commutation relations we can readily see that the second quantized Hamiltonian (2.27) has a following basis representation

$$\hat{H}(t) = \sum_{ij}\sum_{\sigma} t_{ij}(t)(\hat{c}^\dagger_{i\sigma}\hat{c}_{j\sigma} + h.c) + \frac{1}{2}\sum_{ijkl}\sum_{\sigma\sigma'} w_{ijkl}\hat{c}^\dagger_{i\sigma}\hat{c}^\dagger_{j\sigma'}\hat{c}_{k\sigma'}\hat{c}_{l\sigma}, \tag{2.31}$$

where we defined the spin-independent one-electron integral t_{ij} consisting of the kinetic terms and of the positive nuclear background term, as well as the two-electron integral w_{ijkl} as

$$t_{ij} = -\frac{1}{2}\int d\mathbf{x}\varphi^*_i(\mathbf{x})\hat{h}(\mathbf{x}, t)\varphi_j(\mathbf{x}) \tag{2.32}$$

$$w_{ijkl} = \int d\mathbf{x}d\mathbf{y}\varphi^*_i(\mathbf{x})\varphi^*_j(\mathbf{y})\hat{w}(\mathbf{x}, \mathbf{y})\varphi_k(\mathbf{y})\varphi_l(\mathbf{x}). \tag{2.33}$$

The first term on the right hand side of the Hamiltonian (Eq. 2.31) describes the transfer of an electron from spin-orbital $\varphi_i(\mathbf{r}, \sigma)$ to spin orbital $\varphi_j(\mathbf{r}, \sigma)$ and vice versa with energy scale t_{ij}. The terms $i = j$ represent the single particle on-site energy while the other terms represent the hybridization of the electrons between different orbitals. The second term represents electron-electron interactions, the most important being the direct coulomb when $i = j$ and $k = l$.

2.2 Model Hamiltonians

2.2.1 Pariser-Parr-Pople Model

In this work we focus on the transport and charge transfer properties of atomic chains and molecular systems. We describe these systems by using semi-empirical model Hamiltonians. One of them is the Pariser-Parr-Pople (PPP) model [84, 85, 86, 87, 88] which is an effective Hamiltonian for π-electrons of conjugated hydrocarbons, designed to capture the low-energy properties of these systems. In the π-electron models σ and core electrons contribute only to the static screening of the Coulomb interaction and the π-electrons are treated as independent particles moving in the average field of other electrons. The PPP-model can be derived as done by Lindberg and Öhrn in 1968 [88]. The assumptions of the frozen core orbitals motivates us to consider each atomic site i having localized spin orbital $\varphi_{i\sigma'}(\mathbf{r}\sigma) = \delta_{\sigma\sigma'}\phi_i(\mathbf{r})$ with a small but finite overlap with nearest neighbor orbitals [88]. Assuming that these Löwdin orbitals

are orthonormalized and by using the definitions for the creation and annihilation operators as Eqs. (2.29) and (2.30) together with a restriction into a spin compensated system with $\varphi_{i\sigma'}(\mathbf{r}\sigma) = \delta_{\sigma\sigma'}\phi(\mathbf{r})$, we can write the second quantized Hamiltonian in a Löwdin basis as in Eq. (2.31). Due to the assumption that basis functions are localized around each atomic site, we can focus only on the main local and non-local contributions from t_{ij} and w_{ijkl}, which are given up to the nearest neighbor terms. For the interaction term this means that we reduce the four index quantity into a two index one as $w_{ijkl} = \delta_{il}\delta_{kl}w_{ij}$, where $w_{ij} = 1/|i-j|$ is the long-range behavior of the interaction matrix elements for $i \neq j$. We can now write the PPP Hamiltonian as

$$\begin{aligned}\hat{H} &= \sum_{ij}\sum_{\sigma} t_{ij}(t)\hat{c}^{\dagger}_{i\sigma}\hat{c}_{j\sigma} + \frac{1}{2}\sum_{ij}\sum_{\sigma\sigma'} w_{ijkl}\hat{c}^{\dagger}_{i\sigma}\hat{c}^{\dagger}_{j\sigma'}\hat{c}_{k\sigma'}\hat{c}_{l\sigma} + \frac{1}{2}\sum_{ij} w_{ij}Z_iZ_j \\ &= \sum_{i\sigma}\varepsilon_i\hat{c}^{\dagger}_{i\sigma}\hat{c}_{i\sigma} + \sum_{\langle i,j\rangle}\sum_{\sigma} h_{ij}\hat{c}^{\dagger}_{i\sigma}\hat{c}_{j\sigma} + \sum_i w_{ii}\hat{n}_{i\uparrow}\hat{n}_{i\downarrow} \\ &\quad + \frac{1}{2}\sum_{i\neq j} w_{ij}(n_i - Z_i)(n_j - Z_j),\end{aligned} \tag{2.34}$$

where $\hat{c}$ and $\hat{c}^{\dagger}$ are the annihilation and creation operators for the electron in the p_z orbital on the atom i. The operator $\hat{n}_{i\uparrow}$ is the density for the up-electrons in the atom i, while $\hat{n}_{i\downarrow}$ is the density for the down-electrons in the atom i. The total density in atom i is then $\hat{n}_i = \hat{n}_{i\uparrow} + \hat{n}_{i\downarrow}$. The number of π-electrons in atom i is denoted by n_i, and therefore the $(n_i - Z_i)$-term takes into account the electron-nuclear and nuclear-nuclear interactions of the π-electron nuclei. The matrix elements of the one-body Hamiltonian are denoted as

$$t_{ij}(t) = \begin{cases} \varepsilon_i - \sum_{i\neq j} Z_i w_j + v_i(t) & i = j \\ h_{ij} \equiv V & \langle i,j\rangle \end{cases} \tag{2.35}$$

where $\sum_{i\neq j} Z_i w_j$ denotes the effective background due to surrounding ionic lattice, $v_i(t)$ is an external time-dependent potential, $v_i(t) = \int d\mathbf{r}\mu\phi^*_i(\mathbf{r})v(\mathbf{r},t)\phi_i(\mathbf{r})$ and $\langle i,j\rangle$ denotes the nearest neighbor indices. The diagonal on-site energy ε_i is defined as the expectation value of kinetic energy operator plus the local positive background by

$$\varepsilon_i = \int d\mathbf{r}\phi^*_i(\mathbf{r})\left\{-\frac{\nabla}{2} - Z_i w(\mathbf{r},\mathbf{R}_i)\right\}\phi_i(\mathbf{r}). \tag{2.36}$$

Finally, the last term in the Hamiltonian (2.34) is just an added constant due to the effective interaction between the nuclei. The off-diagonal terms denoted by the time-independent matrix elements t_{ij} are called the hopping elements which allow the lattice sites to share kinetic energy by tunneling of particles between neighboring sites. The nearest neighbor approximation is also known as the tight-binding (TB) approximation. Within the PPP model the electron-electron interaction terms for carbon backbone structures can be approximated with the semi-empirical Ohno[89, 90] or Mataga-Nishimoto potentials [91,

90], which mimic the $1/r$ behavior of the Coulomb potential at large distances for the w_{ij} matrix elements, while at small distances they recover the on-site $w_{ii} = U$ interaction between electrons at the same atom.

2.2.2 QUANTUM TRANSPORT HAMILTONIAN

The quantum transport Hamiltonian is a Hamiltonian where we connect a central system, described by some tight-binding approximation like PPP, to infinite leads. The leads mimic metallic electron reservoirs while the central system models a microscopic scattering region which is attached between these electron reservoirs (see Fig. 2.1). Thus, the model Hamiltonian describing this kind of two-terminal transport setup consists of three terms

$$\hat{H}(t) = \hat{H}_C(t) + \hat{H}_{leads}(t) + \hat{H}_T \tag{2.37}$$

where $\hat{H}_C(t)$ is the Hamiltonian for the central region which in the second quantized form reads

$$\hat{H}_C(t) = \sum_{i,j\in C} \sum_{\sigma} t_{ij}(t) \hat{d}^\dagger_{i\sigma} \hat{d}_{j\sigma} + \frac{1}{2} \sum_{ij} \sum_{\sigma\sigma'} w_{ij} \hat{d}^\dagger_{i\sigma} \hat{d}^\dagger_{j\sigma'} \hat{d}_{j\sigma'} \hat{d}_{i\sigma} \tag{2.38}$$

where the indices i, j run over the central region atomic sites and σ is a spin index, while the operators $\hat{d}^\dagger$, $\hat{d}$ are a creation and annihilation operators for the device. The matrix element $t_{ij}(t)$ denotes the one-body part of the Hamiltonian with the nearest neighbor parametrization. The two-body matrix elements w_{ij} describe the electron-electron interactions in the central system which we take to be of the form

$$w_{ij} = \begin{cases} w_{ii} & i = j \\ \frac{w_{ii}}{2|i-j|} & i \neq j \end{cases} \tag{2.39}$$

which models the Coulomb interaction. The infinite leads are described by the therm $\hat{H}_{leads}(t) = \sum_\alpha \hat{H}_\alpha(t)$ in the Hamiltonian (2.37) whose second quantized from reads

$$\hat{H}_{leads}(t) = \sum_{\alpha=L,R} \sum_{i,j\in\alpha}^{\infty} \sum_{\sigma} \left[t^\alpha_{ij} + W_\alpha(t)\delta_{ij} \right] \hat{c}^\dagger_{i\alpha\sigma} \hat{c}_{i\alpha\sigma} \tag{2.40}$$

where α denotes the left (L) / right (R) lead and t^α_{ij} is the nearest neighbor Hamiltonian of the lead α. The time-dependent bias in lead α is denoted with $W_\alpha(t)$, which we assume to be generated by applying an electric field over the system and in the simplest case is just a constant potential shift in the leads. The external electric field is assumed to be screened instantly due to the generated Hartree field. The operators $\hat{c}^\dagger$, $\hat{c}$ are the creation and annihilation operators for the leads.

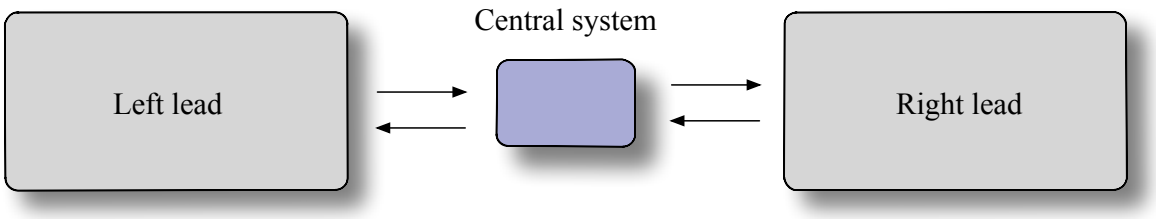

Figure 2.1: Schematics of the transport setup.

The third term $\hat{H}_T$ in the Hamiltonian (2.37) describes the contact of the central system to the lead electrodes, *i.e.,* the hybridization of the device region molecular levels with the lead region molecular levels. This coupling or tunneling Hamiltonian in nearest neighbor picture is

$$\hat{H}_T = \sum_{\alpha=L,R} \sum_{\substack{i\in C \\ j\in\alpha}} \sum_{\sigma} V_{ij,\alpha}[\hat{d}^{\dagger}_{i\sigma}\hat{c}_{j\alpha\sigma} + \hat{c}^{\dagger}_{j\alpha\sigma}\hat{d}_{i\sigma}] \tag{2.41}$$

where $V_{i,j\alpha}$ are the matrix elements of the coupling Hamiltonian.

ANDERSON IMPURITY MODEL

The Anderson impurity model was introduced by P. W. Anderson [92] to describe the effect of a single impurity to conduction electrons. In this work we use the Anderson impurity model to study electronic transport through a quantum dot, where the middle region, consisting of a single interacting site or level acting as a impurity, is connected to semi-infinite leads (large electron reservoirs) which are assumed to be metallic. The Anderson impurity model in a quantum transport setup is described by the Hamiltonian

$$\hat{H}(t) = \hat{H}_{\rm C} + \hat{H}_{leads}(t) + \hat{H}_{\rm T}, \tag{2.42}$$

where $\hat{H}_{\rm C}$, $\hat{H}_{\alpha}$, and $\hat{H}_{\rm T}$ respectively describe the impurity region, the leads α (= L,R), and the tunneling between the impurity region and the leads. The Hamiltonian for the impurity site reads

$$\hat{H}_{\rm C} = \sum_{\sigma} \varepsilon_0 \hat{d}^{\dagger}_{\sigma}\hat{d}_{\sigma} + \frac{1}{2}\sum_{\sigma,\sigma'} U \hat{d}^{\dagger}_{\sigma}\hat{d}^{\dagger}_{\sigma'}\hat{d}_{\sigma'}\hat{d}_{\sigma}, \tag{2.43}$$

where $\hat{d}^{\dagger}_{\sigma}, \hat{d}_{\sigma}$ are fermionic creation and annihilation operators and σ, σ' are the spin indices, ε_0 is the on-site energy of the interacting site and U is the interaction term or the charging energy of the impurity level. The Hamiltonian $\hat{H}_{leads}(t)$, describing the leads is $\hat{H}_{leads}(t) = \sum_{\alpha} \hat{H}_{\alpha}(t)$

$$\hat{H}_{\alpha}(t) \;=\; \sum_{\sigma}\sum_{i=1}^{\infty}\Big(\varepsilon_{\alpha} + W_{\alpha}(t)\Big)\hat{c}^{\dagger}_{i\sigma\alpha}\hat{c}_{i\sigma\alpha} - \sum_{\sigma}\sum_{i=1}^{\infty}\Big(V_{\alpha}\hat{c}^{\dagger}_{i\sigma\alpha}\hat{c}_{i+1\sigma\alpha} + H.c.\Big), \tag{2.44}$$

where ε_α is the on-site energy in the leads, W_α is the bias on the lead α and V_α is the hopping between neighboring lead sites. The tunneling Hamiltonian describes the coupling between the impurity site and the leads, and has the form

$$\hat{H}_{\text{T}} = -\sum_{\sigma} \left(V_{\text{link}}\, \hat{d}^{\dagger}_{\sigma} \hat{c}_{1\sigma L} + V_{\text{link}}\, \hat{d}^{\dagger}_{\sigma} \hat{c}_{1\sigma R} + h.c. \right), \tag{2.45}$$

where V_{link} is the hopping from the leads to the impurity site and vice versa.

3

NON-EQUILIBRIUM GREEN'S FUNCTION THEORY

Many-body perturbation theory (MBPT) provides a systematic way to study electron-electron (electron-phonon) interactions yielding understanding of the excitation properties of many-electron systems ranging form molecules to solids [23, 24, 22]. In MBPT the central object is the single-particle Green's function G which is defined as an ensemble average of time-ordered product of creation and annihilation operators. Hence, in space-time representation it gives an unnormalized probability amplitude for a propagation of an electron or a hole between two space-time points. In energy representation and in some basis describing our system at hand, the Green's function can be understood as an unnormalized probability amplitude for a transition from some initial state to an excited state in the equilibrium description [93]. The determination of the interacting single-particle Green's function requires knowledge of the self-energy Σ. The systematic diagrammatic expansion for the self-energy is an advantage of MBPT over other methods, giving the possibility to describe relevant physical processes via a selection of Feynman diagrams. The self-energy Σ is a non-local, non-hermitian operator which describes the exchange and correlation effects beyond the mean-field Hartree approximation. In practice we need to approximate the self-energy Σ. The standard approximations for the self-energy are the Hartree-Fock (HF) approximation, the second order Born (2B) approximation, which includes the second order corrections to the exchange term and to the polarizability [22]. The third standard approximation for the self-energy is called the GW approximation in which the self-energy is term expressed in terms of the screened interaction W and the single-particle propagator G [94, 30, 95, 96, 97]. A fourth standard self-energy approximation is the T-matrix approximation which is an infinite expansion of scattering events for the two-particle Green's function G_2. Therefore, T-matrix is especially useful in describing systems where a short range interactions play a major role [23, 22].

Standard zero-temperature perturbation theory fails when we are considering time-dependent expectation values and we need move to a non-equilibrium version of the perturbation theory also know as the Keldysh Green's function theory [33, 23, 22]. Non-equilibrium Green's function theory together with many-body perturbation theory provides a natural and powerful framework for theoretical study of systems with variable particle number both in *equilibrium* and *non-equilibrium*, since it incorporates naturally the

zero temperature (time-ordered) and Matsubara formalism as limiting cases. Consequently, it provides a powerful framework for calculating steady-state properties. In addition, since perturbation theory is done in the interaction rather than in the external field, we are able to study interacting fermion (and boson) many-particle systems at finite temperatures under arbitrary strong external fields.

In this chapter we introduce the basic quantities of non-equilibrium many-body perturbation theory. Every now and then we will take the equilibrium or steady-state limit together with assumption of a homogeneous electron gas. This allows us to substantiate the physical meaning of otherwise abstract objects. A homogeneous electron gas or a jellium model describes interacting electrons within a uniform background of positive charge. It provides a first approximation to alkali metals as well as to any system whose Fermi surface of conducting electrons is nearly spherical.

3.1 TIME-EVOLUTION AND STATISTICAL AVERAGES

For the description of the non-equilibrium properties of a many-particle quantum system we need to know the time-dependent expectation values of the quantum mechanical operators. For the many-particle systems at equilibrium consisting of a mixture of states described by the statistical operator or density matrix $\hat{\rho}$ in $\mathcal{F}(\mathcal{H})$, the expectation value of an operator $\hat{O}$ in grand canonical ensemble is defined by

$$\langle \hat{O} \rangle \equiv \mathrm{Tr}\{\hat{\rho}\,\hat{O}\}. \tag{3.1}$$

The statistical operator $\hat{\rho}$ in Eq (3.1) is defined as

$$\hat{\rho} = \frac{1}{\mathcal{Z}} e^{-\beta(\hat{H}-\mu\hat{N})} = \frac{e^{-\beta(\hat{H}-\mu\hat{N})}}{\mathrm{Tr}\left\{e^{-\beta(\hat{H}-\mu\hat{N})}\right\}} = \sum_{N=0}^{\infty}\sum_{i=1}^{\infty} p_{N_i} |\varphi_{N_i}\rangle\langle\varphi_{N_i}| \tag{3.2}$$

where the normalization constant $\mathcal{Z} = \mathrm{Tr}\{e^{-\beta(\hat{H}-\mu\hat{N})}\}$ is the partition function, $\beta = 1/k_B T$ is the inverse temperature with k_B being the Boltzmann constant and T the temperature. The chemical potential is denoted by μ while N is the total number of particles, and $p_{N_i} = \frac{1}{\mathcal{Z}} e^{-(E_{N_i}-\mu N_i)/k_B T}$ denotes the probability that the systems described by Hamiltonian $\hat{H}$ is in an eigenstate $|\varphi_i\rangle$ with energy $E_{N_i} = \varepsilon_{N_i} - \mu N_i$. Since the total number operator $\hat{N}$ and the Hamiltonian commute, the term $\mu\hat{N}$ is merged to the definition of the Hamiltonian $\hat{H}$. Thus, we can write $\hat{\rho} = \frac{e^{-\beta\hat{H}}}{\mathrm{Tr}\{e^{-\beta\hat{H}}\}}$. The statistical operator $\hat{\rho}$ is Hermitian $\hat{\rho}^\dagger = \hat{\rho}$ and positive with trace equal to unity, $\mathrm{Tr}\{\hat{\rho}\} = 1$. In principle, knowledge of the density operator in Fock space gives all of the microscopic information available regarding the system, allowing one to calculate the mean values of all observables. We can now define the grand canonical expectation value of a time-dependent operator $\hat{O}(t)$ as

$$\langle \hat{O}(t) \rangle \;=\; \sum_i p_i \langle \varphi_i(t)|\hat{O}|\varphi_i(t)\rangle = \frac{1}{\mathcal{Z}} \sum_i e^{-\beta E_i} \langle \varphi_i|\hat{U}(t_0,t)\hat{O}\hat{U}(t,t_0)|\varphi_i\rangle$$

$$= \frac{1}{\mathcal{Z}}\sum_i e^{-\beta E_i}\langle\varphi_i|\hat{O}_H(t)|\varphi_i\rangle = \mathrm{Tr}\{\hat{\rho}\hat{O}_{\mathrm{H}}(t)\} \tag{3.3}$$

where we used the Heisenberg representation for the operator $\hat{O}_{\mathrm{H}}(t) = \hat{U}(t_0,t)\hat{O}\hat{U}(t,t_0)$ which relates the time-dependent Heisenberg operator to the time independent Schödinger operator via the unitary time-evolution operator $\hat{U}$. In mathematicians language the evolution operator is a mapping between the wave functions at times t and t' i.e.

$$|\Psi(t)\rangle = \hat{U}(t,t')|\Psi(t')\rangle \tag{3.4}$$

with following properties

$$\begin{aligned} i\partial_t\hat{U}(t,t') &= \hat{H}(t)\hat{U}(t,t'), && (3.5)\\ -i\partial_t\hat{U}(t',t) &= \hat{U}(t',t)\hat{H}(t), && (3.6)\\ \hat{U}(t,t) &= 1. && (3.7) \end{aligned}$$

The first property can be obtained by taking the time-derivative of Eq. (3.4) with respect to t together with the time-dependent Schrödinger equation yielding the result

$$i\partial_t\hat{U}(t,t')|\Psi(t')\rangle = \hat{H}(t)\hat{U}(t,t')|\Psi(t')\rangle. \tag{3.8}$$

From which the property (3.5) follows, since the state $|\Psi(t')\rangle$ is arbitrary. An expression for the time-evolution operator $\hat{U}$ can be solved from Eqs (3.5) and (3.6) which we can formally write as a time-ordered product of the exponential of the Hamiltonian $\hat{H}$ [25, 27, 22]

$$\begin{aligned} \hat{U}(t,t') &= \mathcal{T}\left[\exp\left(-i\int_{t'}^{t} d\tau\,\hat{H}(\tau)\right)\right], \quad \text{if } t'<t,\\ \hat{U}(t,t') &= \tilde{\mathcal{T}}\left[\exp\left(i\int_{t}^{t'} d\tau\,\hat{H}(\tau)\right)\right], \quad \text{if } t'>t. \end{aligned} \tag{3.9}$$

where $\mathcal{T}$ is the so-called time-ordering operator, arranging the latest time to the left and $\tilde{\mathcal{T}}$ is the anti-time ordering operator, arranging the latest time operator to the right. The time-ordering operator constructs all the possible chronological products of the operators $\hat{A}_1, \hat{A}_2, ..., \hat{A}_n$ as

$$\mathcal{T}\left[\hat{A}_1(t_1)...\hat{A}_n(t_n)\right] = \sum_P (-1)^{F_p}\theta(t_{P_{(1)}} - t_{P_{(2)}})...\theta(t_{P_{(n-1)}} - t_{P_{(n)}})\hat{A}_{P_{(1)}}(t_{P_{(1)}})...\hat{A}_{P_{(n)}}(t_{P_{(n)}})$$

where P runs over permutations and F_p denotes the number of fermionic permutations, *i.e.*, for fermionic operators the interchange of two operators will change the sign of the product. In the equal time limit, the time-ordering operator leaves the operator product untouched. Similarly, the anti-time order operator constructs all the possible anti-chronological products of operators $\hat{A}_1, \hat{A}_2, ..., \hat{A}_n$. The equations (3.9) are central for the perturbation theory calculations of many-particle systems. Furthermore, by noting that

a connection between the statistical operator $\hat{\rho}$ and the imaginary time-propagator

$$e^{-\beta\hat{H}} \equiv \hat{U}(t_0 - i\beta, t_0), \tag{3.10}$$

which also means that the partition function and the trace of the evolution operator are related by $\mathcal{Z} = \mathrm{Tr}\{e^{-\beta\hat{H}}\} = \mathrm{Tr}\{\hat{U}(t_0 - i\beta, t_0)\}$. We can rewrite the expectation value of the time-dependent operator $\langle\hat{O}(t)\rangle = \mathrm{Tr}\{\hat{\rho}\, O_{\mathrm{H}}(t)\} = \langle\hat{U}(t_0, t)O(t)\hat{U}(t, t_0)\rangle$ in a following form

$$\langle\hat{O}(t)\rangle = \frac{\mathrm{Tr}\{\hat{U}(t_0 - i\beta, t_0)\hat{O}_{\mathrm{H}}(t)\}}{\mathrm{Tr}\{\hat{U}(t_0 - i\beta, t_0)\}} = \frac{\mathrm{Tr}\{\hat{U}(t_0 - i\beta, t_0)\hat{U}(t_0, t)\hat{O}\hat{U}(t, t_0)\}}{\mathrm{Tr}\{\hat{U}(t_0 - i\beta, t_0)\}}. \tag{3.11}$$

From this expression it is seen that the system evolves first from an initial time $(t_0, 0)$ to a time $(t, 0)$, the operator $\hat{O}$ acts and the system evolves back to time $(t_0, 0)$ from where the system is evolving along the imaginary track to the time $(t_0, -i\beta)$. This time-contour in the complex time-plane (see Fig. 3.1a) was originally introduced by Keldysh [33]. Because of the semi-group property of the time-evolution operator, the time contour can be expanded up to the infinity. Times are ordered on the contour in such a way that t_+ is later than t_- [22]. It is also to be noted that by the relation between the partition function and the imaginary time propagation $\mathcal{Z} = \mathrm{Tr}\{e^{-\beta\hat{H}}\} = \mathrm{Tr}\{\hat{U}(t_0 - i\beta, t_0)\}$, the formalisms of equilibrium statistical mechanics, and quantum mechanics can seen to be equivalent, whose physical significance is the formal equivalence of quantum and thermal fluctuations.

The piece-wise time-propagation procedure in the calculation of the expectation value (3.11) takes place on the Keldysh contour $\mathcal{C} = \mathcal{C}_M \cup \mathcal{C}_- \cup \mathcal{C}_+$ (see Fig. 3.1a), which is piece-wise defined and consists of the Matsubara part $\mathcal{C}_M$, time-ordered part $\mathcal{C}_-$ and of the backward branch, *i.e.,* the anti-time ordered part $\mathcal{C}_+$, with each branch having its own time-evolution operator. Thus, the expectation value of an operator $\hat{O}$ can be generalized to apply on the whole contour. Let z be a variable on the contour $\mathcal{C}$. After using exponent expression for the time-evolution operator we can formally write the expectation value of the one-particle operator $\hat{O}$ as

$$\begin{aligned}
\langle\hat{O}(z)\rangle &= \frac{\mathrm{Tr}\left\{e^{-\beta\hat{H}^M}\mathcal{T}_{\mathcal{C}}\left[\left(e^{-i\int_{\mathcal{C}_-} d\tilde{z}\,\hat{H}(\tilde{z}) - i\int_{\mathcal{C}_+} d\tilde{z}\,\hat{H}(\tilde{z})}\right)\hat{O}(z)\right]\right\}}{\mathrm{Tr}\left\{e^{-\beta\hat{H}^M}\mathcal{T}_{\mathcal{C}}\left[e^{-i\int_{\mathcal{C}_-} d\tilde{z}\,\hat{H}(\tilde{z}) - i\int_{\mathcal{C}_+} d\tilde{z}\,\hat{H}(\tilde{z})}\right]\right\}} \\
&= \frac{\mathrm{Tr}\left\{\mathcal{T}_{\mathcal{C}}\left[e^{-i\int_{\mathcal{C}} d\tilde{z}\,\hat{H}(\tilde{z})}\hat{O}(z)\right]\right\}}{\mathrm{Tr}\left\{\mathcal{T}_{\mathcal{C}}\left[e^{-i\int_{\mathcal{C}} d\tilde{z}\,\hat{H}(\tilde{z})}\right]\right\}}.
\end{aligned} \tag{3.12}$$

The operator $\mathcal{T}_{\mathcal{C}}$ is the time-ordering operator on the Keldysh contour, which rearranges the operators in chronological order; $\tilde{\mathcal{T}}_{\mathcal{C}}$ is the anti-chronological time-ordering operator. In the equation (3.12) we denoted the ground-state Matsubara-Hamiltonian as $\hat{H}^M$, we also assumed that the time-ordered and anti-time ordered contours are governed by the same Hamiltonian $\hat{H}$, this does not necessarily need to be the case and indeed in some applications it might even be advantageous to differentiate the Hamiltonian between forward and backward branch. If the Hamiltonian is time-independent, the expression (3.12)

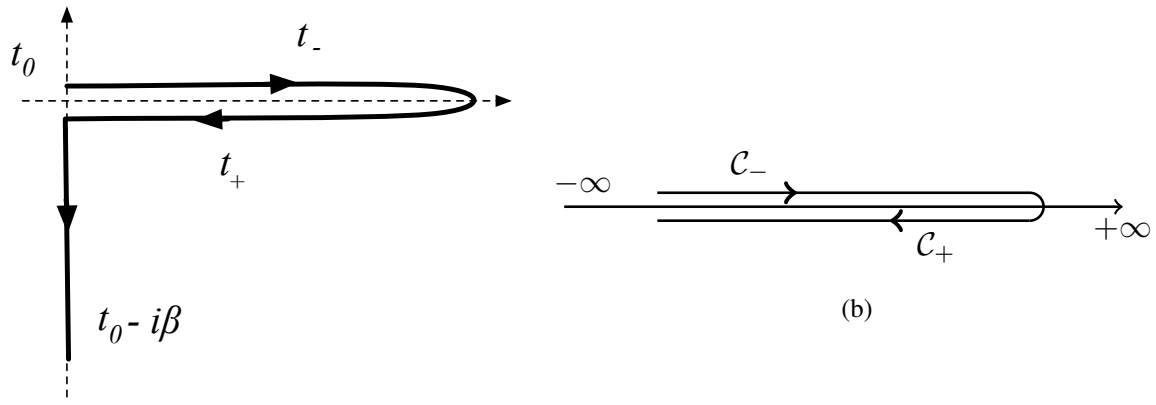

Figure 3.1: Keldysh contours. (a) Keldysh contour with initial correlations in a from of grand canonical ensemble. (b) The closed time-loop contour $\mathcal{C}$. The forward time-ordered branch is denoted with a "$-$" label while the backward anti-time ordered branch is denoted by a "$+$" label.

simplifies to the equilibrium expectation value. For the system in equilibrium at a finite temperature we obtain the Matsubara formalism on the contour $\mathcal{C}_M$, while for the equilibrium at zero temperature we obtain the standard time-ordered formalism on the contour $\mathcal{C}_-$. The power of the Eq. (3.12) is that it correctly includes the initial correlations in ensemble formalism and after external perturbation gives the expectation value of the operator $\hat{O}$. It should be noted that the initial state is a grand canonical ensemble average and therefore any specific information about the states of the many-particle system is lost. If we want to prepare our system for a specific initial state, for example an excited state of a molecule, we need to resort to the formalism of general initial states [98, 22].

LANGRETH RULES

For an object $a(z, z')$ on the Keldysh contour $\mathcal{C}$ we can definite different components, depending on which branch the time-arguments locate. Here z is the general contour time argument defined as z consisting of the time argument on the real axis, denoted by t, and of the imaginary time component of denoted by τ. If both of the time-arguments lie on the upper branch we obtain the time-ordered $a^{--}(t, t')$ component of the object $a(z, z')$, while for the situation that both of the time-arguments are on the lower-branch we have the anti-time ordered $a^{++}(t, t')$ component. Similarly, if z-time argument is on the upper branch and the z'-time argument is on the lower branch we obtain $a^{-+}(t, t')$ component or more familiarly the lesser component $a^<$, and for $z \in \mathcal{C}_+$ and $z' \in \mathcal{C}_-$ we have a^{+-} *i.e.,* the greater component $a^>$. In addition to the lesser and greater components, we also have components where one of the time-arguments lies on the imaginary track and other one one the real axis. We call these ones as the mixed components are they are defined as $a^\lceil(-i\tau, t') = a^<(-i\tau, t')$ and $a^\rceil(t, -i\tau) = a^>(t, -i\tau)$ where $i\tau \in \mathcal{C}_M$ and $t, t' \in \mathcal{C}_\pm$. If both of the time arguments are on the imaginary track we obtain the Matsubara component $a^M(-i\tau, -i\tau')$.

From the greater and lesser pieces we can obtain retarded and advanced components as

$$a^R(t,t') \equiv a^\delta(t)\delta(t-t') + \theta(t-t')[a^>(t,t') - a^<(t,t')], \tag{3.13}$$
$$a^A(t,t') \equiv a^\delta(t)\delta(t-t') - \theta(t'-t)[a^>(t,t') - a^<(t,t')], \tag{3.14}$$

where $a^\delta(t)$ is a time-local part of $a(t,t')$ satisfying $a^\delta(t_-) = a^\delta(t_+) \equiv a^\delta(t)$, the delta function is denoted by $\delta(t-t')$ and $\theta(t-t')$ denotes the Heaviside function on the real axis. Furthermore, we note that the general form of the object $a(z,z')$ on the Keldysh contour $\mathcal{C}$ is of the form

$$a(z,z') = a^\delta(t)\delta(t-t') + \theta(t,t')a^>(t,t') + \theta(t',t)a^<(t,t') \tag{3.15}$$

where $\theta(t,t')$ is the Heaviside step function on the contour Keldysh $\mathcal{C}$.

If the object $a(z,z')$ on the Keldysh contour is a product of two other objects $b(z,z')$ and $c(z,z')$ given by $a(z,z') = b(z,z')c(z,z')$, we can obtain the greater and lesser component of $a(z,z')$ as $a^{\xi\xi'}(t,t') = b^{\xi\xi'}(t,t')c^{\xi\xi'}(t,t')$, where $\xi,\xi' = \pm$. The mixed terms will be $a^\rceil(t,-i\tau) = b^\rceil(t,-i\tau)c^\rceil(t,-i\tau)$ and $a^\lceil(-i\tau,t) = b^\lceil(-i\tau,t)c^\lceil(-i\tau,t)$ On the other had if $a(z,z')$ is a convolution between the operators $b(z,z')$ and $c(z,z')$ given by

$$a(z,z') = \int_{\mathcal{C}_-\cup\mathcal{C}_+} d\bar{z}\, b(z,\bar{z})c(\bar{z},z') \tag{3.16}$$

we can obtain the greater and lesser components as

$$a^{\xi\xi'}(t,t') = \sum_{\bar{\xi}} \int_{\mathcal{C}} d\bar{t}\, b^{\xi\bar{\xi}}(t,\bar{t})c^{\bar{\xi}\xi'}(\bar{t},t') = \sum_{\bar{\xi}=+,-} \bar{\xi} \int d\bar{t}\, b^{\xi\bar{\xi}}(t,\bar{t})c^{\bar{\xi}\xi'}(\bar{t},t') \tag{3.17}$$

where on the second equality we used the fact that the contour integration on the real time splits in forward and backward integration $\int_{\mathcal{C}} dt = \int_{\mathcal{C}^-} dt + \int_{\mathcal{C}^+} dt = \int dt^- - \int dt^+$. Utilizing the $\pm$ notation it is now very easy to obtain the Langreth components of general operator product. For example, a very common object encountered in MBPT is of the form

$$a(z_1,z_2) = \int_{\mathcal{C}} dz_3 dz_4\, b(z_1,z_3)c(z_2,z_3)b(z_3,z_4)b(z_4,z_2)c(z_4,z_1) \tag{3.18}$$

whose lesser and greater component can be obtained as

$$\begin{aligned} a^{\xi_1\xi_2}(t_1,t_2) &= \sum_{\xi_3\xi_4=+,-} \xi_3\xi_4 \int dt_3 dt_4\, b^{\xi_1\xi_3}(t_1,t_3)c^{\xi_2\xi_3}(t_2,t_3)b^{\xi_3\xi_4}(t_3,t_4) \\ &\quad \times b^{\xi_4\xi_2}(t_4,t_2)c^{\xi_4\xi_1}(t_4,t_1). \end{aligned} \tag{3.19}$$

The mixed terms can be obtained from the greater and lesser ones by setting one of the external time vertices on the imaginary axis according to $a^\lceil(-i\tau,t') = a^<(-i\tau,t')$ and $a^\rceil(t,-i\tau) = a^>(t,-i\tau)$. The $\pm$- formalism for the Langreth rules is especially handy when drawing Feynman diagrams since it allows

us to obtain the greater or lesser component just by drawing the diagram, fixing the external vertex points, and distributing $+$ and $-$ labels all the possible ways for the internal vertices (see Fig. 3.2).

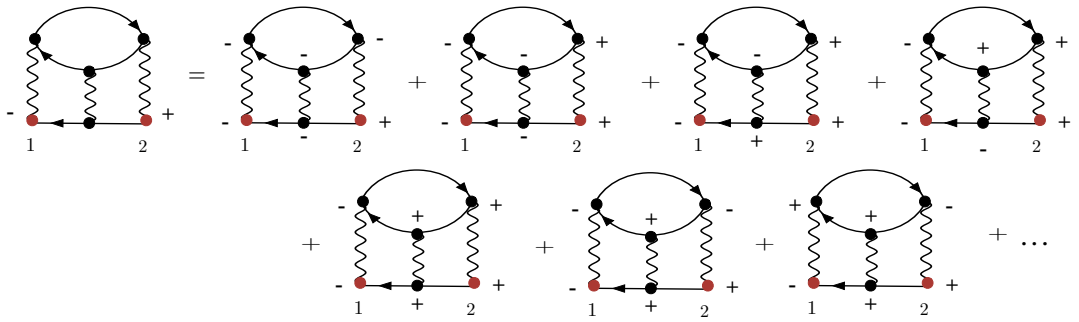

Figure 3.2: Example of distribution of plus and minus signs for a lesser self-energy diagram with non-instantaneous interaction.

3.2 ONE-PARTICLE GREEN'S FUNCTION

For the description of the dynamics of the many-particle system we are looking at various correlation functions, the central one being the one-particle Green's function. Due to the form of the time-evolution operator Eq. (3.9) the quantum dynamics is governed by time-ordered products of non-commuting objects. The standard correlation function is the one-particle Green's function $G(\mathbf{x}_1 t_1, \mathbf{x}_2 t_2)$ defined as the expectation value of a time-ordered product of creation and annihilation operators, which gives us the expectation values of the one-particle operators, such as the average probability density of the particles and ground state energy. We develop now the many-body perturbation theory for the interacting fermions under the Hamiltonian (atomic units are used)

$$\begin{aligned} \hat{H}(t) &= \sum_{\sigma} \frac{1}{2} \int d^3\mathbf{r}\, \hat{\psi}^\dagger_\sigma(\mathbf{r}) \Big[-i\nabla^2 + qv(\mathbf{r},t) \Big] \hat{\psi}_\sigma(\mathbf{r}) \\ &+ \sum_{\sigma\sigma'} \frac{1}{2} \int d^3\mathbf{r} d^3\mathbf{r}'\, w(\mathbf{r},\mathbf{r}') \hat{\psi}^\dagger_\sigma(\mathbf{r}) \hat{\psi}^\dagger_{\sigma'}(\mathbf{r}') \hat{\psi}_{\sigma'}(\mathbf{r}') \hat{\psi}_\sigma(\mathbf{r}) \end{aligned} \tag{3.20}$$

where $\hat{\psi}^\dagger, \hat{\psi}$ are the creation and annihilation operators for electrons at space-spin position $\mathbf{x} = (\mathbf{r}, \sigma)$. The external potential is denoted by $v(\mathbf{r}, t)$ and the two-body Coulomb interaction is denoted by $w(\mathbf{r}, \mathbf{r}')$. Within the Keldysh formalism the operators are defined on the time-loop contour like the one shown in Fig. 3.1b. Operators on the *minus*-branch are ordered chronologically while operators on the *plus*-branch are anti-chronologically ordered. The Green's function is defined as an expectation value of time-ordered

product of creation and annihilation operators as

$$G(\mathbf{x}_1 z_1, \mathbf{x}_2 z_2) \equiv -i\left\langle \mathcal{T}_{\mathcal{C}}[\hat{\psi}_{\rm H}(\mathbf{x}_1 z_1)\hat{\psi}^{\dagger}_{\rm H}(\mathbf{x}_2 z_2)]\right\rangle = -i\frac{\mathrm{Tr}\left\{\hat{U}(t_0 - i\beta, t_0)\mathcal{T}_{\mathcal{C}}[\hat{\psi}_{\rm H}(\mathbf{x}_1 z_1)\hat{\psi}^{\dagger}_{\rm H}(\mathbf{x}_2 z_2)]\right\}}{\mathrm{Tr}\left\{\hat{U}(t_0 - i\beta, t_0)\right\}}, \tag{3.21}$$

where $\mathcal{T}_{\mathcal{C}}$ denotes the time ordering operator along the contour $\mathcal{C}$, and the average is taken over the grand canonical ensemble. If we consider only the time-ordered part of the Keldysh contour $\mathcal{C}$ we obtain the standard zero temperature formalism [27, 29]. The Green's function $G^{\xi_1\xi_2}(\mathbf{x}_1 z_1, \mathbf{x}_2 z_2)$ $(\xi_1, \xi_2 = +/-)$ defined on the contour $\mathcal{C}$, where z is contour parameter, can be divided into different components depending on the branch $\mathcal{C}_-, \mathcal{C}_+$ to which z_1 and z_2 belong. For both time-arguments belonging to the minus branch $(\xi_1 = \xi_2 = -)$ we have the *time-ordered* Green's function. If both of the time-arguments lie on the plus branch of the contour $(\xi_1 = \xi_2 = +)$, *i.e.,* the time-arrow is reversed we have the *anti-time-ordered* Green's function G^{++}. These time-ordered and anti-time-ordered Green's functions are defined as

$$\begin{aligned} G^{--}(\mathbf{x}_1 t_1, \mathbf{x}_2 t_2) &= -i\left\langle \mathcal{T}_{\mathcal{C}}\left[\hat{\psi}_{\rm H}(\mathbf{x}_1 t_1)\hat{\psi}^{\dagger}_{\rm H}(\mathbf{x}_2 t_2)\right]\right\rangle, \\ G^{++}(\mathbf{x}_1 t_1, \mathbf{x}_2 t_2) &= -i\left\langle \tilde{\mathcal{T}}_{\mathcal{C}}\left[\hat{\psi}_{\rm H}(\mathbf{x}_1 t_1)\hat{\psi}^{\dagger}_{\rm H}(\mathbf{x}_2 t_2)\right]\right\rangle, \end{aligned} \tag{3.22}$$

where the operators are in the Heisenberg picture and the statistical average $\langle ... \rangle$ is taken with respect to some density matrix $\hat{\rho}$. The time-ordering operator $\mathcal{T}_{\mathcal{C}}$ orders the operator with earliest time on the right and the latest to the left. The operator $\tilde{\mathcal{T}}$ denotes the anti-time-ordering operator, *i.e.*, it orders the earliest time to the left and latest time to the right. The time-ordered and anti-time-ordered Green's function are sums of two other Green's function. If $t_1 \in \mathcal{C}_-$ and $t_2 \in \mathcal{C}_+$ we have the *lesser* component of the Green's function, commonly denoted as $G^{<}$ which describes the propagation of a hole. If $t_1 \in \mathcal{C}_+$ and $t_2 \in \mathcal{C}_-$ we have the *greater* component usually denoted as $G^{>}$ which describes the propagation of a particle. These lesser and greater Green's functions are defined as

$$G^{-+}(\mathbf{x}_1 t_1, \mathbf{x}_2 t_2) = i\left\langle \hat{\psi}^{\dagger}_{\rm H}(\mathbf{x}_2 t_2)\hat{\psi}_{\rm H}(\mathbf{x}_1 t_1)\right\rangle, \tag{3.23}$$

$$G^{+-}(\mathbf{x}_1 t_1, \mathbf{x}_2 t_2) = -i\left\langle \hat{\psi}_{\rm H}(\mathbf{x}_1 t_1)\hat{\psi}^{\dagger}_{\rm H}(\mathbf{x}_2 t_2)\right\rangle. \tag{3.24}$$

These components are equivalently written as $G^{-+} = G^{<}$ (*lesser* Green's function) and $G^{+-} = G^{>}$ (*greater* Green's function), and describe the propagation of an added hole ($G^{<}$) or particle ($G^{>}$) in the medium. These four Green's functions $G^{\xi_1\xi_2}$ are not independent of each other. The G^{--} and G^{++} are given in terms of $G^{\lessgtr}$ according to the equations below (omitting the position-spin variables)

$$\begin{aligned} G^{--}(t_1, t_2) &= \theta(t_1 - t_2)G^{>}(t_1, t_2) + \theta(t_2 - t_1)G^{<}(t_1, t_2), \\ G^{++}(t_1, t_2) &= \theta(t_1 - t_2)G^{<}(t_1, t_2) + \theta(t_2 - t_1)G^{>}(t_1, t_2). \end{aligned}$$

In addition of the above four Green's function we can define the retarded and advanced Green's functions as an expectation value of the anti-commutator of the two field operators $\hat{\psi}$ and $\hat{\psi}^\dagger$

$$\begin{aligned} G^R(\mathbf{x}_1 t_1, \mathbf{x}_2 t_2) &= -i\theta(t_1 - t_2) \left\langle \left\{ \hat{\psi}_{\text{H}}(\mathbf{x}_1 t_1), \hat{\psi}^\dagger_{\text{H}}(\mathbf{x}_2 t_2) \right\} \right\rangle \\ &= \theta(t_1 - t_2) \left[G^{+-}(\mathbf{x}_1 t_1, \mathbf{x}_2 t_2) - G^{-+}(\mathbf{x}_1 t_1, \mathbf{x}_2 t_2) \right], \qquad (3.26) \\ G^A(\mathbf{x}_1 t_1, \mathbf{x}_2 t_2) &= i\theta(t_2 - t_1) \left\langle \left\{ \hat{\psi}_{\text{H}}(\mathbf{x}_1 t_1), \hat{\psi}^\dagger_{\text{H}}(\mathbf{x}_2 t_2) \right\} \right\rangle \\ &= \theta(t_2 - t_1) \left[G^{-+}(\mathbf{x}_1 t_1, \mathbf{x}_2 t_2) - G^{+-}(\mathbf{x}_1 t_1, \mathbf{x}_2 t_2) \right], \qquad (3.27) \end{aligned}$$

where $\theta(t_2 - t_1)$ is the Heaviside step-function on the real axis. Although, the Green's function does not contain the full information carried by the wave function, it contains, nevertheless, the useful one-particle statistical and dynamical information such as ground state properties (one-body observables and the ground state energy) and ionization energies. The expectation value of a one-body operator $\hat{O}(\mathbf{x}_1 t_1)$ is generally given by

$$\begin{aligned} \langle \hat{O}(\mathbf{x}_1 t_1) \rangle &= \int d\mathbf{x}_1 \left[\hat{O}(\mathbf{x}_2 t_1) \langle \hat{\psi}_H(\mathbf{x}_1 t_1) \hat{\psi}^\dagger_H(\mathbf{x}_2 t_1) \rangle \right]_{\mathbf{x}_1 = \mathbf{x}_2} \\ &= -i \int d\mathbf{x}_1 \left[\hat{O}(\mathbf{x}_2 t_1) G^<(\mathbf{x}_1 t_1, \mathbf{x}_2 t_1) \right]_{\mathbf{x}_1 = \mathbf{x}_2}, \end{aligned} \qquad (3.28)$$

i.e., the lesser Green's function gives us a way to calculate any one-particle observable. For example, the particle and current are given by

$$\begin{aligned} \langle \hat{n}(\mathbf{x}_1 t_1) \rangle &= -iG^<(\mathbf{x}_1 t_1, \mathbf{x}_1 t_1^+), \\ \langle \mathbf{j}(\mathbf{x}_1 t_1) \rangle &= -i \left\{ \left[\frac{\nabla_1 - \nabla_2}{2i} \right] G(\mathbf{x}_1 t_1, \mathbf{x}_2 t_2) \right\}_{1=2^+}, \end{aligned} \qquad (3.29)$$

where the notation $^+$ means that in the time-contour, time variable t^+ approaches t from an infinitesimally later time, $t^+ = t + \delta$ and the operator must act before the limit $\mathbf{x}_1 \to \mathbf{x}_2$ is taken. In a similar fashion, we can find the expectation value of any one-particle operator in terms of the one-particle Green's function [22].

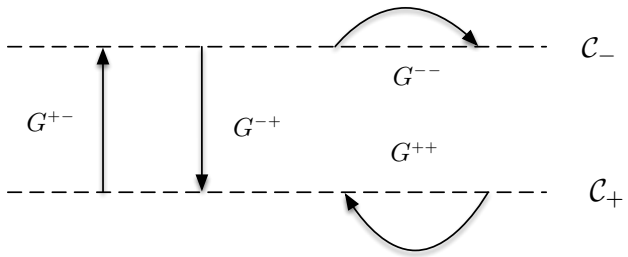

Figure 3.3: Schematic picture demonstrating the time-arguments of different real-time components of the Keldysh Green's function

LEHMANN REPRESENTATION

In equilibrium the Green's function will become time-translationally invariant and the Green's function does not depend anymore on two time arguments t_1 and t_2 separately but rather on their difference $t_1 - t_2$. Consequently, the Green's function can be Fourier transformed (in non-equilibrium steady-state we need to let the initial time $t_0 \to -\infty$) to obtain the removal and addition energies of the system [20, 21, 22]. This information is given by spectral function which gives us the correlated quasiparticle spectrum. We start by inserting a complete set of eigenstates of the Hamiltonian between the creation and annihilation operators in the definition of greater and lesser Green's function giving us

$$G^<(\mathbf{x}_1 t_1, \mathbf{x}_2 t_2) = \frac{i}{\mathcal{Z}} \sum_{ij} e^{-\beta E_i} e^{i(E_i - E_j)(t_2 - t_1)} g^*_{ij}(\mathbf{x}_2) g_{ji}(\mathbf{x}_1), \tag{3.30a}$$

$$G^>(\mathbf{x}_1 t_1, \mathbf{x}_2 t_2) = -\frac{i}{\mathcal{Z}} \sum_{ij} e^{-\beta E_i} e^{i(E_j - E_i)(t_2 - t_1)} f_{ij}(\mathbf{x}_1) f^*_{ji}(\mathbf{x}_2), \tag{3.30b}$$

where $\mathcal{Z} = \mathrm{Tr}[e^{-\beta H}] = \mathrm{Tr}[\hat{U}(t_0 - i\beta, t_0)]$ is the grand partition function, E_i is the eigenenergy corresponding to the state Ψ_i of the Hamiltonian $\hat{H}$. We also introduced the Feynman-Dyson amplitudes using the notation

$$f_{ij}(\mathbf{x}_1) = \langle \Psi_{N,i} | \hat{\psi}(\mathbf{x}_1) | \Psi_{N+1,j} \rangle, \tag{3.31}$$

$$g_{ji}(\mathbf{x}_1) = \langle \Psi_{N-1,j} | \hat{\psi}(\mathbf{x}_1) | \Psi_{N,i} \rangle, \tag{3.32}$$

which can be seen as *quasi-particle amplitudes* f_{ij} and *quasi-hole amplitudes* g_{ij}. These amplitudes are non-zero only if the states Ψ_i and Ψ_j contain different number of particles, which is indeed the case, since the states $\Psi_{j,N\pm1}$ contain $N \pm 1$ particles if the state $\Psi_{i,N}$ contains N particles.

Fourier transforming the expressions for the lesser and greater Green's functions as given in Eq. (3.30) gives us

$$G^<(\mathbf{x}_1, \mathbf{x}_2, \omega) = \frac{i}{\mathcal{Z}} \sum_{ij} \delta(\omega + E_j - E_i) e^{-\beta E_i} g^*_{ij}(\mathbf{x}_2) g_{ji}(\mathbf{x}_1), \tag{3.33a}$$

$$G^>(\mathbf{x}_1, \mathbf{x}_2, \omega) = -\frac{i}{\mathcal{Z}} \sum_{ij} \delta(\omega + E_i - E_j) e^{-\beta E_i} f_{ij}(\mathbf{x}_1) f^*_{ji}(\mathbf{x}_2), \tag{3.33b}$$

from which we see that the Fourier transform of $G^<$ is peaked at the removal energies of the system while the Fourier transform of $G^>$ is peaked at the addition energies of the system. The spectrum possesses peaks at possible removal and addition energies but since the particle has the possibility to scatter with all the other particles, it does not have well defined energy. As a consequence the quasiparticle in the interacting systems has a finite lifetime (see Fig. 3.4). Substituting the expressions (3.33a) and (3.33b)

into the equation for the Green's function we obtain the Lehmann representation as

$$\begin{aligned} G(\mathbf{x}_1,\mathbf{x}_2;\omega) &= \frac{i}{Z}\sum_{ij}\left[\frac{e^{-\beta E_i} f_{ij}(\mathbf{x}_1) f^*_{ji}(\mathbf{x}_2)}{\omega - E_j - \varepsilon_i + i\eta} + \frac{e^{-\beta E_i} g^*_{ij}(\mathbf{x}_2) g_{ij}(\mathbf{x}_1)}{\omega + E_i - E_j - i\eta}\right] \\ &= \frac{i}{Z}\int d\tilde{\omega}\left[\frac{\mathcal{A}^{>}(\mathbf{x}_1,\mathbf{x}_2,\tilde{\omega})}{\omega + \tilde{\omega} + i\eta} + \frac{\mathcal{A}^{<}(\mathbf{x}_1,\mathbf{x}_2,\tilde{\omega})}{\omega - \tilde{\omega} - i\eta}\right]. \end{aligned} \tag{3.34}$$

where we defined the spectral weight functions by

$$\mathcal{A}^{<}(\mathbf{x}_1,\mathbf{x}_2,\omega) = \frac{i}{\mathcal{Z}}\sum_{ij}\delta(\omega + E_j - E_i) e^{-\beta\varepsilon_i} g^*_{ij}(\mathbf{x}_2) g_{ji}(\mathbf{x}_1), \tag{3.35}$$

$$\mathcal{A}^{>}(\mathbf{x}_1,\mathbf{x}_2,\omega) = -\frac{i}{\mathcal{Z}}\sum_{ij}\delta(\omega + E_i - E_j) e^{-\beta\varepsilon_i} f_{ij}(\mathbf{x}_1) f^*_{ji}(\mathbf{x}_2), \tag{3.36}$$

which give a measure how well the system can be treated as consisting of noninteracting quasiparticles. If the system is non-interacting, the spectral function is just a sum of delta functions in an infinite system. The interactions change profile of the spectral function from the ideal delta functions to more broad Lorentzian or Gaussian peaks (see Fig. 3.6). We will also notice that the retarded and advanced Green's functions are related to the lesser and greater components via relation $G^{+-}(\omega) - G^{-+}(\omega) = G^R(\omega) - G^A(\omega)$. From the Fourier transform of the retarded and advanced Green's functions we see that the retarded is analytic in the upper and the advanced in lower complex ω half-plane respectively. Solving the equation (3.34) for the spectral function gives us

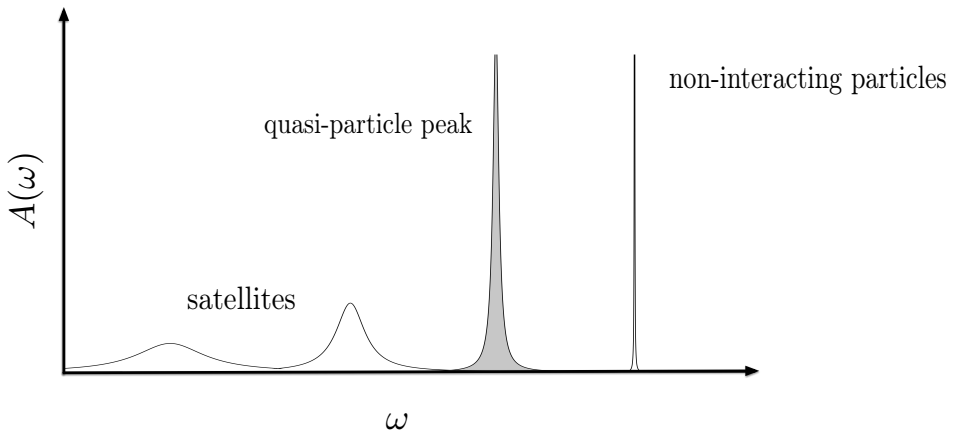

Figure 3.4: Schematics demonstrating the difference between non-interacting particles having a delta-function spectra compared to the spectra of quasi-particles.

the standard definition via greater and lesser Green's functions

$$\mathcal{A}(\omega) = i[G^{+-}(\omega) - G^{-+}(\omega)] = i[G^R(\omega) - G^A(\omega)] \tag{3.37}$$

The spectral function has the property that for a homogeneous system, when integrated over frequency up to chemical potential μ gives the momentum distribution $n_{\mathbf{k}}$, *i.e.*, $\int_{-\infty}^{\mu} \frac{d\omega}{2\pi} A(\mathbf{k},\omega) = n_{\mathbf{k}}$, *i.e.*, the spectral function integrates to the number of particles with momentum $\mathbf{k}$. If we, on the other hand, integrate over the momentum variable we obtain the density of states $\rho(\omega) = \frac{1}{2\pi}\int \frac{d\mathbf{k}}{(2\pi)^3} A(\mathbf{k},\omega)$. In frequency space and at zero temperature $-iG^<(\omega)$ relates to the spectral function below the Fermi energy and zero otherwise whereas $iG^>(\omega)$ relates to the spectral function above the Fermi energy and zero otherwise. Thus, we can relate the lesser and greater Green's function with the lesser and greater spectral function as

$$\begin{aligned} G^{-+}(\omega) &= if(\omega-\mu)\mathcal{A}(\omega) \\ G^{+-}(\omega) &= -i\left[1-f(\omega-\mu)\right]\mathcal{A}(\omega). \end{aligned} \tag{3.38}$$

where $f(\omega-\mu)$ is the Fermi distribution. On the imaginary time axis, *i.e.*, in equilibrium at finite temperature and when the system is described by canonical ensemble, the fluctuation-dissipation relations [99] or the so called Kubo-Martin-Schwinger (KMS) boundary conditions stress the fact that the Green's function is *anti-periodic* for fermions or *periodic* for bosons under a translation of its time arguments where the interval for periodicity is determined by the inverse temperature β. These periodic Kubo-Martin-Schwinger (KMS) boundary conditions for the fermionic case are

$$\begin{aligned} G\left(\mathbf{x}_1(t_0-i\beta),\mathbf{x}_2t_2\right) &= -G\left(\mathbf{x}_1t_0,\mathbf{x}_2t_2\right), \\ G\left(\mathbf{x}_1t_1,\mathbf{x}_2(t_0-i\beta)\right) &= -G\left(\mathbf{x}_1t_1,\mathbf{x}_2t_0\right). \end{aligned} \tag{3.39}$$

The fluctuation-dissipation theorem tells us that the greater and lesser correlation functions also carry information about the fluctuations of the system which are proportional to the dissipative part given by the spectral function $\mathcal{A}(\mathbf{k},\omega)$, which being given by the imaginary part of the Green's function is related to the decay in time domain, giving us the dissipation of the system. The proportionality factor in the fluctuation-dissipation theorem is given by the Fermi distribution.

To this end, we note that for a expectation values of the greater and lesser functions $G^{\gtrless}$ we have a well defined sign for all frequencies ω

$$\langle\phi|iG^>(\omega)|\phi\rangle \geq 0 \quad \langle\phi|-iG^<(\omega)|\phi\rangle \geq 0. \tag{3.40}$$

and therefore $iG^>$ and $-iG^<$ are positive-semidefinite (PSD) matrices in $(\mathbf{x},\omega)$-space.

NON-EQUILIBRIUM SPECTRAL FUNCTION

In description of the time-dependent processes it is sometimes useful to define the non-equilibrium spectral function as a Fourier transform of $G^{>} - G^{<}$ with respect to the relative time coordinate $t = t_1 - t_2$ as

$$\mathcal{A}(\mathbf{x}_1, \mathbf{x}_2, T, \omega) = -\mathrm{Im} \int \frac{dt}{2\pi} e^{i\omega t} \left[G^{>} - G^{<}\right] \left(\mathbf{x}_1, T + \frac{t}{2}; \mathbf{x}_2, T - \frac{t}{2}\right) \tag{3.41}$$

for a given center of time-coordinate $T = (t_1 + t_2)/2$. when the system reaches time-translational invariance, *i.e.,* the expression (3.41) becomes independent of T, and we recover the standard definition of the equilibrium spectral function [10].

As a short summary, we have defined the Green's function as an expectation value of a time-ordered product of two field operators on the time contour. We were able to express the expectation value of an operator using the time-evolution operator, which lead us to the definition of the Keldysh-contour. The Fourier-transform of the Green's function allows us to determine the spectral function. The poles of the spectral function determine the allowed energies of the quasi-particles.

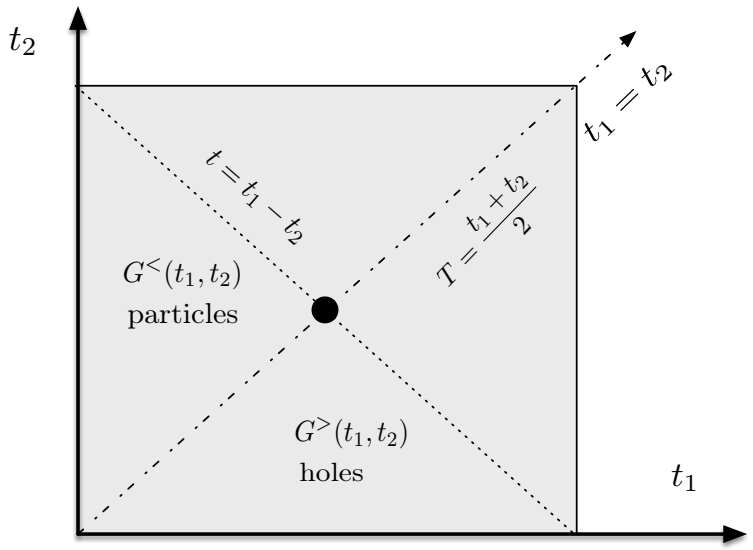

Figure 3.5: The double time-plane for the greater and lesser Green's functions $G^{\gtrless}(t_1, t_2)$.

3.3 EQUATION OF MOTION OF THE GREEN'S FUNCTION

For description of non-equilibrium dynamics of a many-particle system we need to know how the system evolves in time starting from an initial state Ψ_0, which in the Keldysh Green's function theory corresponds to finding the time-evolution of the one-particle Green's function $G(\mathbf{x}_1 z_1, \mathbf{x}_2 z_2)$. Thus, we need to find the equation of motion for one-particle Green's function. This is easily done by using the Heisenberg equation of motion for the time-dependent operators defined as

$$i\partial_z \hat{O}_{\text{H}}(z) = \left[\hat{O}_{\text{H}}(z), \hat{H}(z)\right] \tag{3.42}$$

with the Hamiltonian defined in Eq. (3.20). For the fermionic creation and annihilation field operators $\hat{\psi}^\dagger_{\text{H}}(\mathbf{x}_1 z_2)$, $\hat{\psi}_{\text{H}}(\mathbf{x}_1 z_2)$ we obtain the following equations of motion

$$[i\partial_{z_1} - \hat{h}(\mathbf{x}_1 z_1)]\hat{\psi}_{\text{H}}(\mathbf{x}_1 z_1) = \hat{\gamma}_{\text{H}}(\mathbf{x}_1 z_1) \tag{3.43}$$

$$\hat{\psi}^\dagger_{\text{H}}(\mathbf{x}_2 z_2)[-i\overleftarrow{\partial}_{z_2} - \hat{h}(\mathbf{x}_2 z_2)] = \hat{\gamma}^\dagger_{\text{H}}(\mathbf{x}_2 z_2) \tag{3.44}$$

where we introduced the $\hat{\gamma}_{\text{H}}$ operator defined as

$$\hat{\gamma}_{\text{H}}(\mathbf{x}_1 z_1) \equiv \int d\mathbf{x}_3 \int_{\mathcal{C}} dz_3\, w(\mathbf{x}_1 z_1, \mathbf{x}_3 z_3)\hat{n}_H(\mathbf{x}_3 z_3)\hat{\psi}_{\text{H}}(\mathbf{x}_1 z_1), \tag{3.45a}$$

$$\hat{\gamma}^\dagger_{\text{H}}(\mathbf{x}_1 z_1) \equiv \int d\mathbf{x}_3 \int_{\mathcal{C}} dz_3\, w(\mathbf{x}_1 z_1, \mathbf{x}_3 z_3)\hat{\psi}^\dagger_{\text{H}}(\mathbf{x}_1 z_1)\hat{n}_{\text{H}}(\mathbf{x}_3 z_3), \tag{3.45b}$$

consisting of the Coulomb interaction w, the density operator $\hat{n}_{\text{H}}(\mathbf{x}_1 z_1) = \hat{\psi}^\dagger_{\text{H}}(\mathbf{x}_1 z_1)\hat{\psi}_{\text{H}}(\mathbf{x}_1 z_1)$ and of an annihilation operator for $\hat{\gamma}_{\text{H}}$, and a creation operator for $\hat{\gamma}^\dagger_{\text{H}}$. Consequently, the operator $\hat{\gamma}_{\text{H}}$ can be viewed as describing a process where a created electron-hole pair interacts with a created hole. Similarly the operator $\hat{\gamma}^\dagger_{\text{H}}$ describes a process where an electron-hole pair interacts with a created electron. Using the equations of motion for the field operators (Eqs. (3.43) and (3.44)) we can derive the equation of motion for the single-particle Green's function together with its adjoint

$$\left[i\partial_{z_1} - \hat{h}(1)\right] G(1,2) = \delta(1,2) - i\left\langle \mathcal{T}_C[\hat{\gamma}_{\text{H}}(1)\hat{\psi}^\dagger_{\text{H}}(2)]\right\rangle, \tag{3.46a}$$

$$G(1,2)\left[-i\overleftarrow{\partial}_{z_2} - \hat{h}(2)\right] = \delta(1,2) - i\left\langle \mathcal{T}_C[\hat{\psi}_{\text{H}}(1)\hat{\gamma}^\dagger_{\text{H}}(2)]\right\rangle, \tag{3.46b}$$

where we introduced a compact short hand notation $1 = (\mathbf{x}_1, t_1)$. The term $\left\langle \mathcal{T}_C[\hat{\gamma}_{\text{H}}(1)\hat{\psi}^\dagger_{\text{H}}(2)]\right\rangle$ is related to the two-particle Greens's function $G_2(1,2;1',2')$ defined as a time-ordered product of two creation and two annihilation operators by

$$G_2(12;1'2') = (-i)^2\left\langle \mathcal{T}_C[\psi_{\text{H}}(1)\psi_{\text{H}}(2)\psi^\dagger_{\text{H}}(2')\psi^\dagger_{\text{H}}(1')]\right\rangle \tag{3.47}$$

which describes a motion of two particles, two holes, or a particle and a hole, depending on the orderings of the field operators. Using the definition of $\hat{\gamma}_{\text{H}}(1)$ we can write the time-ordered product of the $\hat{\gamma}_{\text{H}}$

operator and $\hat{\psi}^\dagger$ operator in Eq. (3.46a) as

$$\int d3\, w(1^+,3) \left\langle \mathcal{T}_\mathcal{C}[\hat{\psi}_H(1)\hat{\psi}^\dagger_{\text{H}}(2)\hat{\psi}^\dagger_{\text{H}}(3)\hat{\psi}_{\text{H}}(3)] \right\rangle \tag{3.48}$$

with notation $\int d3 = \int d\mathbf{x}_3 \int_\mathcal{C} dz_3$ and $1^+ = \mathbf{x}_1, t_1 + \delta$ denoting a time infinitesimally larger than t_1 on the Keldysh contour $\mathcal{C}$. The equation of motion for the one-particle Green's function, together with it's adjoint now read

$$\left[i\partial_{z_1} - \hat{h}(1)\right] G(1,2) = \delta(1,2) - i\int d3\; w(1^+,3) G_2(1,3;3^+,2), \tag{3.49a}$$

$$G(1,2)\left[-i\overleftarrow{\partial}_{z_2} - \hat{h}(2)\right] = \delta(1,2) - i\int d3\; w(2^+,3) G_2(1,3;3^+,2). \tag{3.49b}$$

We see that the equation of motion for the one-particle Green's function is related to the two-particle Green's function. To solve for this we need the equation of motion of the two-particle Green's function. This will be related to the three-particle Green's function, and so forth. This is very natural, since the addition or removal of a particle with its propagation in the medium creates more and more complicated interactions to the system. These higher order interactions are incorporated via higher order Green's functions and consequently the equation of a motion of n-particle Green's function

$$G_n(1,..,n;1',..,n') = (-i)^n \left\langle \mathcal{T}_\mathcal{C}[\hat{\psi}_{\text{H}}(1)...\hat{\psi}_{\text{H}}(n)\hat{\psi}^\dagger_{\text{H}}(n')...\hat{\psi}^\dagger_{\text{H}}(1')] \right\rangle \tag{3.50}$$

will depend of the $n+1$-particle Green's function. This hierarchy of equations of motion is called the Martin-Schwinger hierarchy [79, 22].

A standard way to continue from here is to truncate the hierarchy by introducing an integral kernel, which in our case will be the electron self-energy Σ_{MB} such that $-iG_2 w = \Sigma_{\text{MB}}[G]G$, which is a functional of the one-particle Green's function. The many-particle self-energy Σ_{MB} describes the effects of the interaction of an electron with its surroundings (ions, other electrons, etc.) causing polarization which will act back on the original particle. In other words the self-energy includes all of the interaction effects of the particle with itself. With this integral kernel the equation of motion for the one-particle Green's function attains a closed form

$$\left[i\partial_{z_1} - \hat{h}(1)\right] G(1,2) = \delta(1,2) + \int d3\, \Sigma_{\text{MB}}(1,3) G(3,2), \tag{3.51a}$$

$$G(1,2)\left[-i\overleftarrow{\partial}_{z_2} - \hat{h}(2)\right] = \delta(1,2) + \int d3\, G(1,3)\bar{\Sigma}_{\text{MB}}(3,2). \tag{3.51b}$$

where $\bar{\Sigma}_{\text{MB}}$ is the adjoint of the Σ_{MB} operator. These two self-energy operators are the same for systems initially in equilibrium, but for general initial states this does not need to be the case [22, 21]. To see this and to derive a general expression for the self-energy Σ_{MB} we will study the definitions for the self-energy kernel in terms of the expectation value of time-ordered product of the $\hat{\gamma}_{\text{H}}$ and $\hat{\psi}^\dagger_{\text{H}}$ operators

$$\int d3\,\Sigma_{\text{MB}}[G](1,3)G(3,2) \equiv -i\left\langle \mathcal{T}_C[\hat{\gamma}_{\text{H}}(1)\hat{\psi}^\dagger_{\text{H}}(2)]\right\rangle, \tag{3.52}$$

$$\int d3\,G(1,3)\bar{\Sigma}_{\text{MB}}[G](3,2) \equiv -i\left\langle \mathcal{T}_C[\hat{\psi}_{\text{H}}(1)\hat{\gamma}^\dagger_{\text{H}}(2)]\right\rangle. \tag{3.53}$$

Multiplying Eq. (3.52) with $\left[-i\overleftarrow{\partial}_{z_2} - \hat{h}(2)\right]$ from the right and Eq. (3.53) with $[i\partial_{z_1} - h(1)]$ from the left, we obtain

$$\begin{aligned}
\Sigma_{\text{MB}}(1,2) &+ \int d3 \int d4\,\Sigma_{\text{MB}}(1,3)G(3,4)\bar{\Sigma}_{\text{MB}}(4,2) \\
&= \delta(t_1,t_2)\left\langle\left\{\hat{\gamma}_{\text{H}}(1),\hat{\psi}^\dagger_{\text{H}}(2)\right\}\right\rangle - i\left\langle \mathcal{T}_C[\hat{\gamma}_{\text{H}}(1)\hat{\gamma}^\dagger_{\text{H}}(2)]\right\rangle \qquad (3.54)\\
\bar{\Sigma}_{\text{MB}}(1,2) &+ \int d3 \int d4\,\Sigma_{\text{MB}}(1,3)G(3,4)\bar{\Sigma}_{\text{MB}}(4,2) \\
&= \delta(t_1,t_2)\left\langle\left\{\hat{\psi}(1),\hat{\gamma}^\dagger_{\text{H}}(2)\right\}\right\rangle - i\left\langle \mathcal{T}_C[\hat{\gamma}_{\text{H}}(1)\hat{\gamma}^\dagger_{\text{H}}(2)]\right\rangle, \qquad (3.55)
\end{aligned}$$

where due to the delta function $\delta(t_1,t_2)$ the equal-time anti-commutators

$$\left\langle\left\{\hat{\gamma}_{\text{H}}(1),\hat{\psi}^\dagger_{\text{H}}(2)\right\}\right\rangle = \left\langle\left\{\hat{\psi}(1),\hat{\gamma}^\dagger_{\text{H}}(2)\right\}\right\rangle \tag{3.56}$$

are equal and we have $\Sigma_{\text{MB}}(1,2) = \bar{\Sigma}_{\text{MB}}(1,2)$ with the following general expression for the electronic many-particle self-energy

$$\Sigma_{\text{MB}}(\mathbf{x}_1t_2,\mathbf{x}_2t_2) = \Sigma^\delta(\mathbf{x}_1t_1,\mathbf{x}_2t_2) + \theta(t_1,t_2)\Sigma_c^>(\mathbf{x}_1t_1,\mathbf{x}_2t_2) + \theta(t_2,t_1)\Sigma_c^<(\mathbf{x}_1t_1,\mathbf{x}_2t_2) \tag{3.57}$$

where the time-local part

$$\begin{aligned}
\Sigma^\delta(1,2) &= \delta(t_1,t_2)\left\langle\left\{\hat{\gamma}_{\text{H}}(1),\hat{\psi}^\dagger_{\text{H}}(2)\right\}\right\rangle \\
&= -i\delta(1,2)\int d\mathbf{x}_3 w(\mathbf{x}_1,\mathbf{x}_3)G^<(\mathbf{x}_3t_1,\mathbf{x}_3t_1) + i\delta(t_1,t_2)w(\mathbf{x}_1,\mathbf{x}_2)G^<(\mathbf{x}_1t_1,\mathbf{x}_2t_1) \qquad (3.58)
\end{aligned}$$

is nothing but the Hartree-Fock part $\Sigma_{\text{HF}}(1,2)$ of the self-energy, while the correlation part of the self-energy taking into account all the effects beyond mean-field theory, is the greater and lesser part

$$\begin{aligned}
\Sigma_c(1,2) &= \theta(t_1,t_2)\Sigma_c^>(\mathbf{x}_1t_1,\mathbf{x}_2t_2) + \theta(t_2,t_1)\Sigma_c^<(\mathbf{x}_1t_1,\mathbf{x}_2t_2) \\
&= -i\left\langle \mathcal{T}_C[\hat{\gamma}_H(1)\hat{\gamma}^\dagger_H(2)]\right\rangle_{irr} \qquad (3.59)
\end{aligned}$$

defined as an expectation value of the time-ordered product of $\hat{\gamma}_{\text{H}}$ operators (compare with the definition of the one-particle Green's function). The subscript "irr" refers to the irreducible representation of the self-energy, *i.e.*, to the presentation of the self-energy in terms of the Feynman diagrams which are not dividable into two other self-energy expressions by cutting a Green's function line [22]. By using the definitions for the $\hat{\gamma}_{\text{H}}$ operators we actually see that the correlation part of the self-energy is

proportional to the three-particle Green's function where some space-time arguments are set equal. It is also to be noted that the exact self-energy will satisfy the KMS-boundary conditions.

To conclude this section, let us get back to the equation of motion for the one-particle Green's function (3.51) and (3.51b) and rewrite it with the help of the non-interacting Green's function $G_0(1,2)$ defined via the relation $\left(i\partial_{z_1} - \hat{h}(1)\right) G_0(1,2) = \delta(1,2)$ in the from of a standard Dyson-equation

$$\begin{aligned} G(1,2) &= G_0(1,2) + \int d3 \int d4\, G_0(1,3)\Sigma_{\text{MB}}(3,4)G(4,2) \\ &= G_0(1,2) + \int d3 \int d4\, G(1,3)\Sigma_{\text{MB}}(3,4)G_0(4,2) \end{aligned} \tag{3.60}$$

in which uniqueness of the solution is guaranteed by the KMS-boundary conditions. This equation shows us that by starting from the non-interacting solution we can obtain the full interacting Green's function G at the level of the chosen self-energy approximation Σ_{MB} via an iterative procedure. This iterative procedure of generating the full interacting Green's function from the non-interacting one is called dressing of the Green's function.

Let us now consider a time-translationally invariant system which allows us to perform a Fourier transform to frequency space together with translationally invariant system in space allowing us to go from the position representation to the momentum representation. By taking the retarded component of the Dyson equation (Eq. (3.60)) and Fourier-transforming into $(\omega, \mathbf{k})$-domain we can write the spectral function by using the definition (3.37) as

$$\mathcal{A}(\mathbf{k},\omega) = \frac{1}{\pi} \frac{\operatorname{Im}\Sigma^R_{\text{MB}}(\mathbf{k},\omega)}{\left(\omega - \varepsilon_{\mathbf{k}} - \operatorname{Re}\Sigma^R_{\text{MB}}(\mathbf{k},\omega)\right)^2 + \left(\operatorname{Im}\Sigma^R_{\text{MB}}(\mathbf{k},\omega)\right)^2}. \tag{3.61}$$

When the many-particle self-energy is non-zero this is of a Lorenzian shape where the broadening of the peak is controlled by the imaginary part of the self-energy. For the non-interacting many-particle system Eq. (3.61) reduces to a (sum of) delta-function(s). The imaginary part of the retarded self-energy relates to the life-time of the quasi-particle as $\tau_{\mathbf{k}} \propto 1/\operatorname{Im}\Sigma^R$, while the real-part of the self-energy will shift the poles of the non-interacting system by the real part of the self-energy resulting the quasi-particle energy to be $E_{\mathbf{k}} = \varepsilon_k - \operatorname{Re}\Sigma^R_{\text{MB}}(\mathbf{k},\omega)$ (see 3.6 and 3.7c). In conclusion, the singularities of the interacting Green's function give the dispersion relations of the system. In addition to the single-particle excitations, characterized by the quasi-particle peaks, our system might also sustain collective excitations, like plasmon excitations in metallic structures. The collective excitations manifest itself in the spectra as satellite side structure, whose spectral weight is smaller and it is more broad compared to the quasi-particle peak. The broad peak structure of the collective excitations characterize the shorter life time of these excitations (see Fig. 3.6).

The weight of the quasi-particle peak is characterized by the $Z_{\mathbf{k}}$-factor, which tells us how single-particle like our excitation is. For a non-interacting electrons at zero temperature the $Z_{\mathbf{k}}$-factor is unity and for interacting electrons $Z_{\mathbf{k}} < 1$, *i.e*, the more correlated our system the smaller the $Z_{\mathbf{k}}$-factor and therefore the

excitations are less single-particle-like (see Fig. 3.7b)). By expanding the self-energy around the pole of the one-particle Green's function $E_{\mathbf{k}}$ we can write one-particle Green's function as $G(\mathbf{k},\omega) \approx Z_{\mathbf{k}}/(\omega - E_{\mathbf{k}})$ where we defined the $Z_{\mathbf{k}}$ as

$$Z_{\mathbf{k}} = \frac{1}{1 - \frac{\partial \mathrm{Re}\,\Sigma^R_{\mathrm{MB}}(\mathbf{k},\omega)}{\partial\omega}\Big|_{\omega=E_{\mathbf{k}}}} \tag{3.62}$$

we will also see that the life-time of the quasi-particle is proportional to the product of the quasi-particle weight times the imaginary part of the self-energy $\tau^{-1}_{\mathbf{k}} = Z_{\mathbf{k}}\,\mathrm{Im}\,\Sigma^R_{\mathrm{MB}}(\mathbf{k},\omega)$. As a consequence we can approximate the spectral function in terms of the quasi-particle weight and quasi-particle life-time

$$\mathcal{A}(\mathbf{k},\omega) \sim Z_{\mathbf{k}} \frac{1/\tau_{\mathbf{k}}}{(\omega - E_{\mathbf{k}})^2 + (1/\tau_{\mathbf{k}})^2}. \tag{3.63}$$

The spectral function $\mathcal{A}(\mathbf{k},\omega)$ can be mapped out for solids via an angle-resolved photoemission technique (ARPES) [100, 101, 102] which is the best technique to observe the band structure of solids on the resolution of individual bands (see Fig. 3.7c)). Thus we can relate our approximations directly to experimental data.

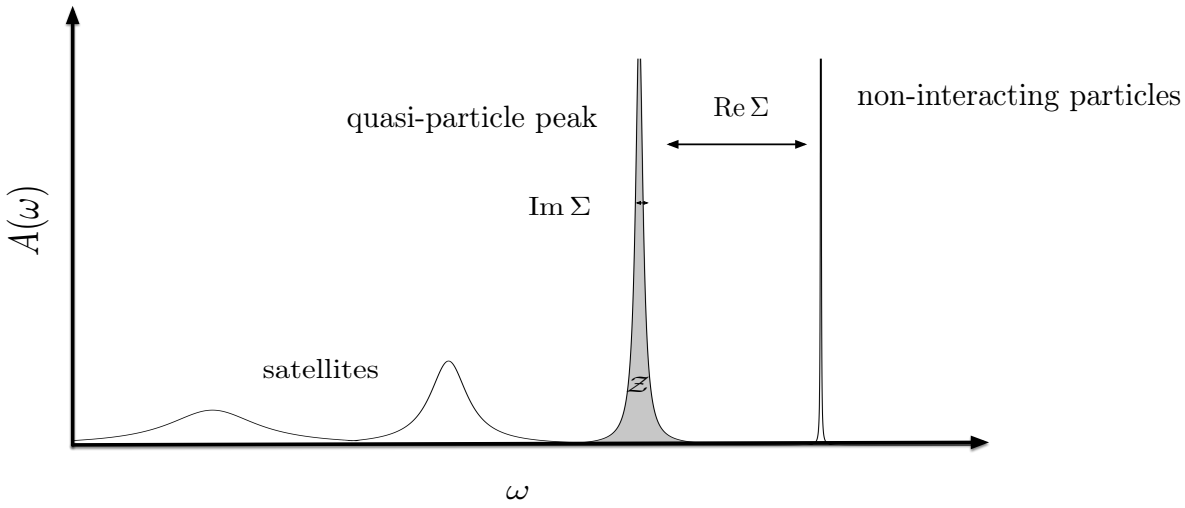

Figure 3.6: Schematics demonstrating the difference between non-interacting particles having a delta-function spectra compared to the spectra of quasi-particles. The real part of the self-energy will induce a shift to the main quasi-particle peak, while the imaginary part will induce a finite life time for the quasi-particle. In addition we might also have satellite structure due to collective excitations such as plasmon excitations.

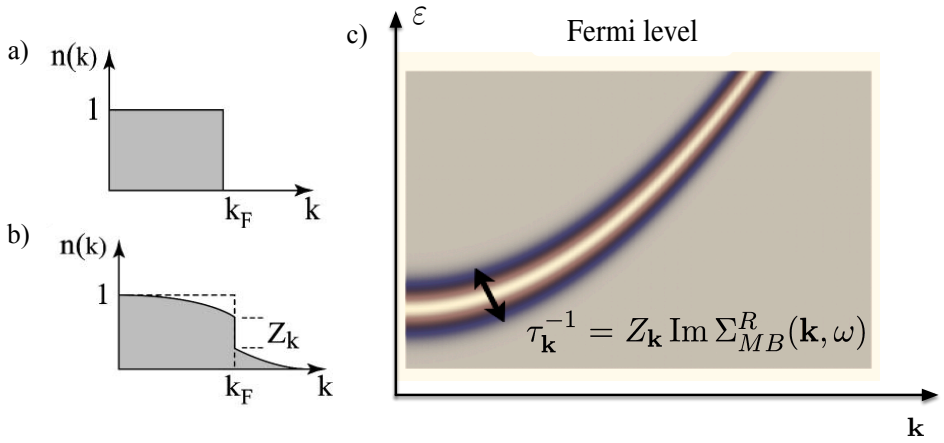

Figure 3.7: Fermi distributions a) for non-interacting electrons at zero temperature. b) interacting electrons at zero temperature. The vertical part of the distribution at k_φ is characterized by the quasi-particle factor or $Z_{\mathbf{k}}$-factor. (Fig. from Damascelli *Rev. Mod. Phys.* **75** 473 (2003) [100]). c) Demonstration of a possible measured band structure giving the quasiparticle dispersion and the quasiparticle life time (Fig. from GW and ARPES, F. Giustino (talk) [103]).

3.4 Many-Particle Self-Energy Approximations

In this section we introduce the standard self-energy approximations beyond Hartree-Fock (HF) approximation: the 2nd order Born (2B) approximation, the GW approximation and the T-matrix approximation. We will also show that these approximations are Φ-derivable, *i.e.*, they fulfill the standard conservation laws, like the continuity equation, which is very important especially for the non-equilibrium description of many-particle systems.

The many-particle self-energy approximations can be derived by using a brute force expansion of the full interacting Green's function in powers of the interaction w together with utilization of Wick's theorem [22]. A much more elegant way of deriving many-particle self-energy approximations is via variational techniques where the core idea is to study variations of the external potential v to the one-particle Green's function, *i.e.*, to study the quantity $\delta G(1,2)/\delta v(3)$.

3.4.1 2nd Order Born Approximation

Our starting point is the definition of the time-evolution operator on the Keldysh contour $\mathcal{C}$ (see Eq. (3.9)). Small variations to the Hamiltonian cause a change in the evolution operator $\hat{U}$. These changes can be investigated by using an exponential expression for the time-evolution operator (Eq. (3.9)) as a generating functional. A small perturbation $\delta v(t)$ to the Hamiltonian causes a change $\delta\hat{U}(t,t')$ to the time-evolution

operator given as

$$\delta\hat{U}(t,t') = -i\int_{t'}^{t} d\tau\ \hat{U}(t,\tau)\delta v(\tau)\hat{U}(\tau,t'). \tag{3.64}$$

where the response arises from the small changes in the external perturbation of the form $\delta v = \int \delta\mathbf{x}\,\delta v(\mathbf{x}t)$ $\times\ \hat{n}_{\text{H}}(\mathbf{x})$, where $\hat{n}_{\text{H}}(\mathbf{x}) = \hat{\psi}^{\dagger}_{\text{H}}(\mathbf{x})\hat{\psi}_{\text{H}}(\mathbf{x})$ is the density operator. Now the change in $\hat{U}$ due to an external perturbation $v(\mathbf{x}t)$ is

$$\frac{\delta\hat{U}(t,t')}{\delta v(\mathbf{x}t)} = i\hat{U}(t_0 - i\beta, t_0)\hat{n}_{\text{H}}(\mathbf{x}t). \tag{3.65}$$

Using this equation we can calculate the change in expectation values due to external perturbation v, and especially the change in the expectation value of the time-ordered product of two field operators (compare with the one-particle Green's function). The functional derivative of the Green's function with respect to the external perturbation can readily seen to be

$$\begin{aligned}\frac{\delta G(1,2)}{\delta v(3)} &= -i\frac{\delta}{\delta v(3)}\langle\mathcal{T}_{\mathcal{C}}[\hat{\psi}_{\text{H}}(1)\hat{\psi}^{\dagger}_{\text{H}}(2)]\rangle \\ &= -\langle\mathcal{T}_{\mathcal{C}}[\hat{\psi}(1)\hat{\psi}^{\dagger}_{\text{H}}(2)\hat{n}_{\text{H}}(3)]\rangle + \langle\hat{n}_{\text{H}}(3)\rangle\langle\mathcal{T}_{\mathcal{C}}[\hat{\psi}_{\text{H}}(1)\hat{\psi}^{\dagger}_{\text{H}}(2)]\rangle,\end{aligned} \tag{3.66}$$

from which it follows that the two-particle Green's function G_2 can be seen as a variation of one-particle Green's function plus the product of the expectation value of the density at the space-time point 3 multiplied by the propagator $G(1,2)$ (see Fig. 3.8). Thus, we have found a new useful link between the one-particle and two-particle Green's functions

$$G_2(1,3;3^+,2) = -\frac{\delta G(1,2)}{\delta v(3)} + \langle n_{\text{H}}(3)\rangle G(1,2). \tag{3.67}$$

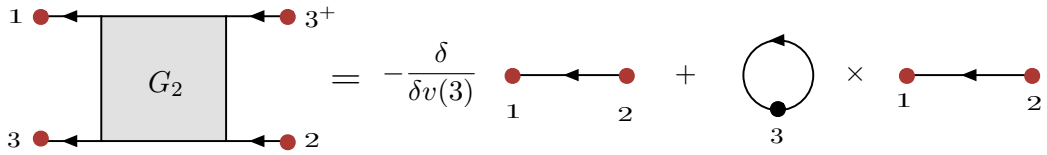

Figure 3.8: Diagrammatic expression of Eq. (3.67).

Substituting this expression for the two-particle Green's function into the equation of motion (3.51) gives

$$\left[i\partial_{z_1} - \hat{h}(1)\right] G(1,2) = \delta(1,2) + G(1,2)\int d3\, w(1^+,3)\langle\hat{n}_H(3)\rangle \tag{3.68}$$

$$+i\int d3\, w(1,3)\frac{\delta G(1,2)}{\delta v(3)} \tag{3.69}$$

where the functional derivative of the one-particle Green's function with respect to the external potential can be written in terms of self-energy by introducing a vertex function $\Gamma(12;3)$, an identity for the inverse

of the Green's function $\int d3\, G^{-1}(1,3)G(3,2) = \delta(1,2)$ this gives

$$\frac{\delta G(1,2)}{\delta v(3)} = \int d4d5\, G(1,4)\tilde{\Gamma}(45;3)G(5,2), \tag{3.70}$$

where we have defined the vertex function as $\tilde{\Gamma}(12;3) = -\frac{\delta G^{-1}(1,2)}{\delta v(3)}$. From the Dyson equation we find the following relation for the inverse Green's function $G^{-1}(1,2) = [\partial_{z_1} - \hat{h}(1)]\delta(1,4) - \Sigma_{\text{MB}}(1,4)$. Inserting this in the definition of the $\tilde{\Gamma}$ gives the more familiar looking definition for the vertex function in terms of the many-particle self-energy

$$\tilde{\Gamma}(14;3) = \delta(1,3)\delta(1,4) + \frac{\delta\Sigma_{\text{MB}}(1,4)}{\delta v(3)}. \tag{3.71}$$

In calculating $\delta G/\delta w$ we ignored a possible arbitrary constant term C with property $G^{-1}C = 0$, yielding the actual derivative to be $\delta G/\delta v = -G(\delta G^{-1}/\delta v)G + C$. The constant term C is closely related to initial correlations, and in the situation where the system is initially a statistical average of states at equilibrium and at finite temperature, *i.e.,* the initial Green's function obeys KMS boundary conditions, the term C can be readily seen to be zero [22]. Inserting the equation (3.70) back into the equation (3.68) we obtain the equation of motion for the single-particle Green's function (3.51) with the following definition for the electronic many-particle self-energy

$$\begin{aligned}
\Sigma_{\text{MB}}[G,w](1,2) &= i\int d3d4\, G(1,3)w(1^+,4)\Gamma(32;4) - i\delta(1,2)\int d3\, w(1,3)G(3,3^+) && (3.72)\\
&= iG(1,2)w(1^+,2) - i\delta(1,2)\int d3\, w(1,3)G(3,3^+) \\
&\quad + i\int d3d4\, G(1,3)w(1^+,4)\frac{\delta\Sigma(3,2)}{\delta v(4)} && (3.73)
\end{aligned}$$

where the first line gives us the first-order approximation for the self-energy namely the Hartree-Fock approximation

$$\Sigma_{\text{HF}}[G,w](1,2) = iG(1,2)w(1^+,2) + i\delta(1,2)\int d3\, w(1,3)G(3,3^+) \tag{3.74}$$

and by making the next iteration for the equation (3.72) we obtain the second-order Born (2B) approximation for the electron self-energy

$$\begin{aligned}
\Sigma^{2B}[G,w](1,2) = \Sigma^{\text{HF}}[G,w](1,2) &+ i^2\int d3d4\, G(1,3)w(1^+,4)G(3,4)G(4,2)w(3^+,2) \\
&- i^2\int d4d5\; G(1,2)w(1^+,4)w(2,5)G(5,4)G(4,5^+),
\end{aligned} \tag{3.75}$$

where in addition to the time-local part of the self-energy (Σ^{HF}) we have terms second order in the Coulomb interaction w. The first term after the HF-part of the self-energy is generally denoted as first order bubble diagram (see Fig. (3.9)) which describes a propagation of a particle (or hole) while interacting

with particle hole-pair, *i.e.,* it includes to first order the polarization of the media due to inserted particle (or hole). The last term is nothing but the second order correction to the exchange term.

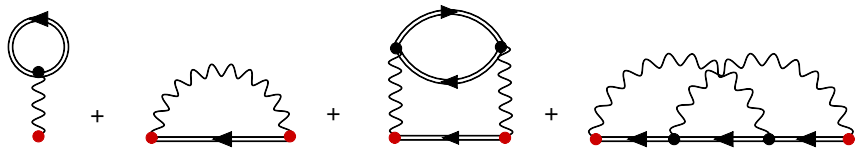

Figure 3.9: Feynman diagrams constituting 2B approximation. The first two diagrams being Hartree and Fock diagrams respectively. The third diagram is generally referred as first order bubble-diagram or polarization diagram while the last diagram is the second-order correction to the exchange.

3.4.2 HEDIN'S EQUATIONS, GW APPROXIMATION AND VERTEX CORRECTIONS

In metallic systems, as well as for a finite systems close to metallic surface where image charge effects are important, the long-range screening effects play a major role. The standard way to proceed is to replace the bare Coulomb interaction w with a dynamically screened interaction $\mathcal{W}$ to include the long-range screening effects. This approximation is called GW approximation where the electronic self-energy takes a form $\Sigma = iG\mathcal{W}$ [94, 104, 97, 95, 105, 96]. In this way, the GW approximation can be seen as a dynamically screened exchange approximation. The GW approximation has successfully been used to calculate quasi-particle energies and band-gaps of various materials [8, 9] as well as properties of molecules [52, 54]. In this section we discuss how to obtain GW approximation rigorously from the Hedin equations [94], vertex corrections, the relation between vertex corrections and dressing, and the physical meaning of these objects.

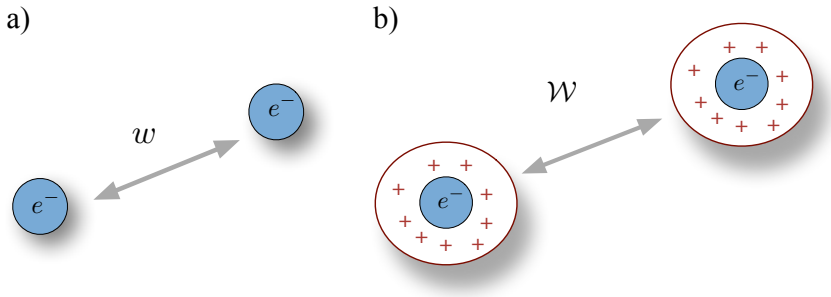

Figure 3.10: (a) The bare Coulomb interaction w between electrons. (b) The screened interaction $\mathcal{W}$ between polarized electrons.

The derivation of the GW approximation is very similar to the derivation of 2B approximation. But now, instead of studying variations of the Green's function with respect to the external perturbation $v(1)$, we will study variations with respect to external perturbation which gets screened by the Hartree potential produced by the surrounding medium. Thus, our perturbation is of the form

$$v_{\text{eff}}(1) = v(1) + \int d3\; w(1,3)\langle \hat{n}_{\text{H}}(3)\rangle. \tag{3.76}$$

We now can calculate the change of the single-particle Green's function $G(1,2)$ due to the effective perturbation $v_{\text{eff}}(3)$. This results in a similar expression for the two-particle Green's function G_2 as in Eq. (3.67). Now for the term $\delta G(1,2)/\delta v(3)$ we need to utilize the chain rule $\frac{\delta}{\delta v(3)} = \int d4\, \frac{\delta v_{\text{eff}}(4)}{\delta v(3)} \frac{\delta}{\delta v_{\text{eff}}}$ (this assumes a one-to-one correspondence between v_{eff} and v) giving us the following equation of motion for the one-particle Green's function

$$\left(i\partial_{z_1} - \hat{h}(1)\right) G(1,2) = \delta(1,2) + G(1,2)\int d3\, w(1^+,3)\langle \hat{n}_{\text{H}}(3)\rangle \tag{3.77}$$

$$+i\int d3d4\, w(1,3)\frac{\delta G(1,2)}{\delta v_{\text{eff}}(4)}\frac{\delta v_{\text{eff}}(4)}{\delta v(3)} \tag{3.78}$$

where we can calculate the change of the Green's function due to the effective potential by utilizing chain rule and equation (3.70) yielding

$$\frac{\delta G(1,2)}{\delta v_{\text{eff}}(3)} = \int d4d5\, G(1,4)\Gamma(45;3)G(5,2). \tag{3.79}$$

Here we have defined the vertex function as $\Gamma(12;3) = -\frac{\delta G^{-1}(1,2)}{\delta v_{\text{eff}}(3)}$. Inserting this back to the Eq. (3.77) we obtain the equation of motion for the one-particle Green's function (3.51) with the following definition for the electronic many-particle self-energy

$$\Sigma_{\text{MB}}(1,2) = \Sigma_{\text{H}}(1,2) + \Sigma_{\text{xc}}(1,2), \tag{3.80}$$

where the self-energy Σ_{MB} consists of the Hartree and exchange-correlation part. The Hartree part reads

$$\Sigma_{\text{H}}(1,2) = \delta(1,2)\int d3\, w(1,3)\langle \hat{n}_{\text{H}}(3)\rangle \tag{3.81}$$

while the exchange-correlation part is

$$\Sigma_{xc}(1,2) = i\int d3d4\, \mathcal{W}(1,3)G(1,4)\Gamma(42;3), \tag{3.82}$$

where we introduced the screened interaction $\mathcal{W}$ as

$$\mathcal{W}(1,2) = \int d3 \frac{\delta v_{\text{eff}}(2)}{\delta v(3)} w(1,3) = \mathcal{W}(2,1), \tag{3.83}$$

which is proportional to the inverse dielectric function $\mathcal{E}^{-1}$. In classical electrodynamics the dielectric function is defined by the relation between displacement field $\boldsymbol{D}$ and the electric-field $\boldsymbol{E}$ as $\boldsymbol{D}(\mathbf{x},t) = \int d\mathbf{x}'\mathcal{E}(\mathbf{x},\mathbf{x}',t-t')\boldsymbol{E}(\mathbf{x}',t')$. Analogously, we can now obtain the dielectric response by considering the change in the effective potential due to a small change in external potential as $v_{\text{eff}}(\mathbf{r}) = \int d\mathbf{r}'dt'\,\mathcal{E}^{-1}(\mathbf{r}t,\mathbf{r}'t')v(\mathbf{r}',t)$. Hence the dielectric response describing the screening of the system is given by

$$\mathcal{E}^{-1}(1,2) = \frac{\delta v_{\text{eff}}(1)}{\delta v(2)} = \delta(1,2) + \int d3\, w(1,3)\frac{\delta\langle\hat{n}_{\text{H}}(3)\rangle}{\delta v(2)}. \tag{3.84}$$

We notice that the inverse dielectric function is related to the density fluctuations (see also section 3.6 in chapter 3). The inverse dielectric function in frequency space is closely related to the elementary excitations of the many-particle system. We can rewrite equation (3.83) as,

$$W(1,2) = \int d3\,\mathcal{E}^{-1}(2,3)w(1,3), \tag{3.85}$$

i.e., the screened interaction is proportional to the inverse dielectric function. This equation describes the effect on a test charge at point 2, including the polarization effects to the potential at point 1. If we again assume a homogeneous system with time-translational invariance and perform o Fourier transform into $(\mathbf{k},\omega)$-space, we see that the screened interaction can be written as $W(\mathbf{k},\omega) = v(\mathbf{k})/\mathcal{E}(\mathbf{k},\omega)$. Hence, the zeros of the $\mathcal{E}(\mathbf{k},\omega)$ appear as poles in the interaction, and thus they will contribute to the Green's function via the self-energy. On the other hand, if we write the effective potential in terms of the dielectric function we have $\delta v_{\text{eff}}(\mathbf{k},\omega) = \delta v(\mathbf{k},\omega)/\mathcal{E}(\mathbf{k},\omega)$.This tells us that when the dielectric function $\mathcal{E}$ is close to zero, it is possible to have a large effective (internal) field with very small external field. At the poles of the dielectric function we have self-sustaining oscillatory behavior in the sample, like plasma oscillations. If the dielectric function has a complex component, we have damped collective oscillations.

Let us now go back to our derivation. We can now evaluate the screened the expression for the screened interaction further by utilizing the variation of the effective potential with respect to the external potential as

$$\frac{\delta v_{\text{eff}}(1)}{\delta v(2)} = \delta(1,2) + \int d4\frac{\delta\langle\hat{n}_{\text{H}}(4)\rangle}{\delta v(2)}w(1,2) \tag{3.86}$$

giving us the standard Dyson-like expression as

$$\mathcal{W}(1,2) = w(1,2) + \int d3d4\;\mathcal{W}(1,3)\mathcal{P}(3,4)w(4,2), \tag{3.87}$$

where we have defined the polarization propagator as the irreducible density-response at space-time point 1 due to the effective field v_{eff} at space-time point 2

$$\mathcal{P}(1,2) = -i\frac{\delta\langle\hat{n}_{\text{H}}(1)\rangle}{\delta v_{\text{eff}}(2)} = -i\frac{\delta G(1,1^+)}{\delta v_{\text{eff}}(1)} = i\int d3d4\;G(1,3)\Gamma(34,2)G(4,1^+). \tag{3.88}$$

From the above equation we see that it is also possible to relate the polarization $\mathcal{P}$ to the inverse dielectric function as

$$\mathcal{E}(1,2) = \delta(1,2) - \int d3\, w(1,3)\mathcal{P}(3,2). \tag{3.89}$$

This is a very useful expression since the imaginary part inverse dielectric function can be measured via electron energy loss spectroscopy (EELS) [19, 106] where an electrons are bombarded through the sample and the corresponding electron distribution is measured at the exit $L[\varepsilon^{-1}] = -\mathrm{Im}\left[\mathcal{E}^{-1}\right]$, where L denotes the energy-loss function. It tells us which frequencies and momenta dissipate energy [22]. Hence, the name electron energy loss spectroscopy. The EELS spectroscopy is especially useful in measuring the plasmon excitations [19]. To this end, we also note that the inverse dielectric function can also be related to the dynamical structure factor $S(\mathbf{k},\omega) \propto -\mathrm{Im}\left[\mathcal{E}^{-1}\right]$. In conclusion, we can relate the polarization P into a measurable quantity, which allows us to determine the quality of our approximations. The screening effects play usually a major role in producing non-trivial spectral features like satellite structures.

Furthermore, we can rewrite the vertex function $\Gamma(12;3) = -\frac{\delta G^{-1}(1,2)}{\delta v_{\text{eff}}(3)}$ with the help of the definition for the inverse Green's function via the Dyson equation $G^{-1}(1,2) = [\partial_{t_1} - \hat{h}(1) - v_{\text{eff}}(2)]\delta(1,4) - \Sigma_{\text{MB}}(1,4)$ as

$$\begin{aligned}
\Gamma(12;3) &= \delta(1,2)\delta(2,3) + \frac{\delta\Sigma_{xc}(1,2)}{\delta v_{\text{eff}}(3)} \\
&= \delta(1,2)\delta(2,3) + \int d4d5\, \frac{\delta\Sigma_{\text{xc}}(1,2)}{\delta G(4,5)}\frac{\delta G(4,5)}{\delta v_{\text{eff}}(3)} \\
&= \delta(1,2)\delta(2,3) + \int d4d5d6d7\, \frac{\delta\Sigma_{\text{xc}}(1,2)}{\delta G(4,5)} G(4,6)\Gamma(67,3)G(7,5).
\end{aligned} \tag{3.90a}$$

This gives us a way to construct approximations for the vertex function in terms of the many-particle self-energy.

We have now derived Hedin's equations which is a key set of equations in many-body perturbation theory

$$\mathcal{W}(1,2) = w(1,2) + \int d3d4\, \mathcal{W}(1,3)\mathcal{P}(3,4)w(4,2), \tag{3.90b}$$

$$\mathcal{P}(1,2) = i\int d3d4\, G(1,3)\Gamma(34,2)G(4,1^+), \tag{3.90c}$$

$$\Sigma(1,2) = \Sigma_H(1,2) + i\int d3d4\, \mathcal{W}(1,3)G(1,4)\Gamma(42;3), \tag{3.90d}$$

$$\Gamma(12;4) = \delta(1,2)\delta(2,3) + \int d4d5d6d7\, \frac{\delta\Sigma_{xc}(1,2)}{\delta G(4,5)} G(4,6)\Gamma(67,3)G(7,5). \tag{3.90e}$$

This set of equations can be closed via the Dyson equation $G(1,2) = G_0(1,2) + \int d3d4\, G_0(1,3)\Sigma_{\text{MB}}(3,4) \times G(4,2)$. Furthermore, since all the quantities $\mathcal{W}$, Σ and $\mathcal{P}$ are functionals of the Green function, these equations have to be solved self-consistently.

In Fig. 3.11 we see the diagrammatic structure for the Hedin's equations. The screened interaction $\mathcal{W}$ is denoted by the double wiggly line whereas the bare Coulomb interaction w is denoted by the single

wiggly line. The polarization propagator is denoted by grey bubble. Therefore, we see that the Dyson-like expression for the screened interaction $\mathcal{W}$ causes the bare interaction to be renormalized due to the polarization effects caused by the added particle or hole. The vertex function in Fig. 3.11 is denoted by the grey triangle shown in the diagrams for the polarization and the self-energy. The last diagram denotes the structure for the Dyson-equation. The single lines denote bare propagators whereas the double lines denote the dressed propagators.

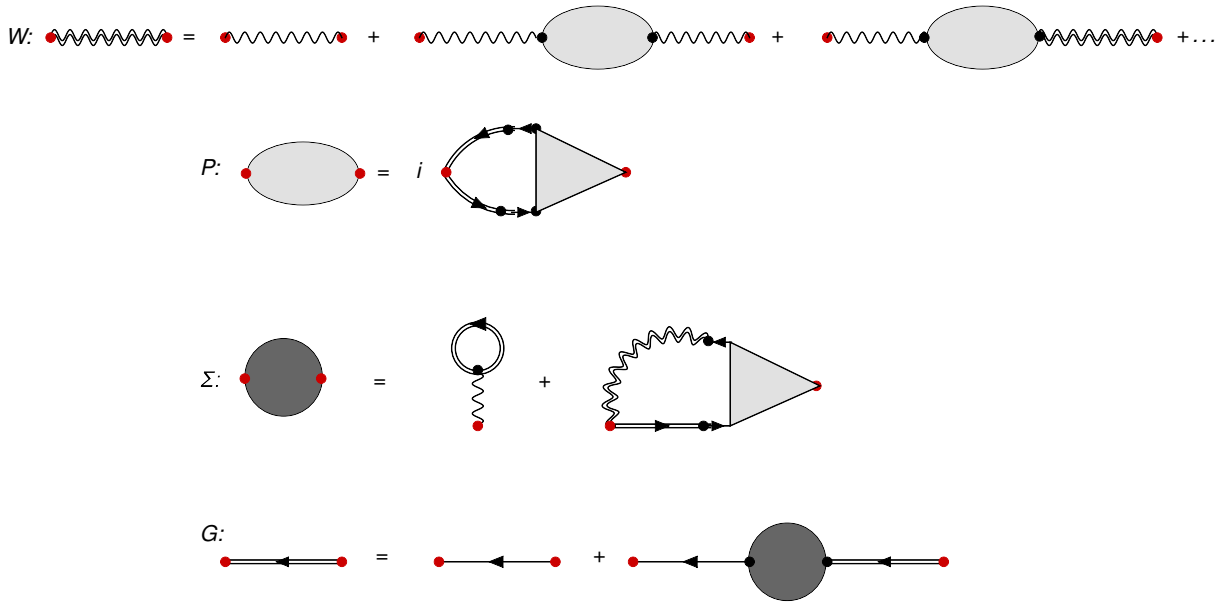

Figure 3.11: Feynman diagrams constituting Hedin's equations.

By taking the vertex function in Hedin's equations (3.90) to be proportional to delta function we recover the first order in $\mathcal{W}$ for self-energy, *i.e.*, the standard $G\mathcal{W}$ approximation

$$\Gamma^{(0)}(1,2;3) = \delta(1,2)\delta(1,3) \tag{3.91}$$

$$\mathcal{P}^{0}(1,2) = -iG(2,1)G(1,2^{+}) \tag{3.92}$$

$$\Sigma^{(1)}_{xc}(1,2) = i\mathcal{W}(1^{+},2)G(1,2). \tag{3.93}$$

These equations form a coupled set of equations together with the Dyson equations for the screened interaction $\mathcal{W}$ as well for the single-particle Green's function (Eq. (3.60)) and they should be solved up to self-consistency. The diagrammatic structure of the $G\mathcal{W}$ self-energy is presented in the Fig. 3.12. In literature there are many variants of the $G\mathcal{W}$ approximation which often use the HF or some DFT based Green's function to do a single shot $G\mathcal{W}$ calculation. Such an approximation is called $G_0\mathcal{W}_0$ approximation.

With the first order approximation for the polarization $\mathcal{P}_0(1,2) = iG(1,2)G(2,1)$, constituting of a particle-hole pair, we can solve the screened interaction by repeated substitution writing formally as

$$\mathcal{W} = w + w\mathcal{P}_0\mathcal{W} = w + w\mathcal{P}_0 w + w\mathcal{P}_0 w\mathcal{P}_0 w + \dots \,. \tag{3.94}$$

If we substitute this into the equation of the self-energy $\Sigma^{(1)}$, together with the definition of the polarization propagator $\mathcal{P}_0$, we obtain

$$\begin{aligned} \Sigma^{(1)}_{xc}(1,2) &= iw(1,2)G(1,2) && (3.95)\\ &\quad + i\int d3d4\; w(1,3)G(3,4)G(4,1)w(4,2)G(1,2) + .., \ , && (3.96) \end{aligned}$$

which is an infinite expansion of the self-energy in terms of the bare interaction. The use of screened interaction, therefore can be seen as a selected set of self-energy terms summed up to finite order. The particles in the interacting system respond to the potential, which includes the induced potential due to the response of the system to the external potential (see Fig. 3.12).

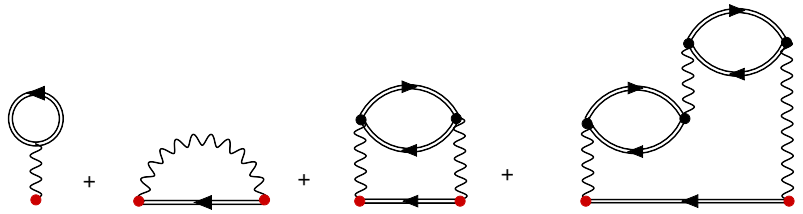

Figure 3.12: Feynman diagrams constituting the GW approximation. We have again the Hartree-Fock approximation as a subset, but now in addition we have also an infinite sum of polarization diagrams.

By evaluating the next iteration for the vertex function in Eq. (3.90), we obtain the first order terms of Γ and $\mathcal{P}$ in terms of the screened interaction $\mathcal{W}$

$$\begin{aligned} \Gamma^{(1)}(1,2;3) &= i\mathcal{W}(1^+,2)G(1,2)G(3,2), && (3.97)\\ \mathcal{P}^1(1,2) &= -i^2\int d3d4\; G(2,3)G(4,2^+)\mathcal{W}(3^+,4)G(3,1)G(1,4), && (3.98) \end{aligned}$$

as well as the second order term in $\mathcal{W}$ of the self-energy

$$\Sigma^{(2)}_{xc}(1,2) = i^2\int d3d4\; \mathcal{W}(1^+,2)G(1,4)\mathcal{W}(4^+,2)G(4,3)G(3,2). \tag{3.99}$$

This set of equations is commonly referred as the *first-order vertex correction*, or simply *vertex correction of the GW self-energy*. The diagrammatic structure of the vertex correction is presented in the Fig. 3.13. By continuing this iterative procedure of Hedin's equations, we can generate infinite partial summations for the self-energy and polarizability in terms of the screened interaction $\mathcal{W}$.

In order to rigorously include the vertex corrections, one should include them at the same level for the self-energy and polarizability [48, 47, 107]. Since the contributions from these two factors mainly cancel each other[108, 109]. Another important point is the relation between self-consistency and vertex corrections, as noted by Dubois [110, 111], is that the self-consistency procedure makes the correlation function smaller while the vertex effects make them larger. Thus, one needs to find the right mix between vertex correction for the self-energy and the polarizability together with self-consistency to capture the effects of interest. In addition, vertex corrections in diagrammatic approximations to the polarizability are known to be crucial for capturing double and higher particle-hole excitations, excitons, multiple plasmon excitations, *etc.*, as well as for estimating excitation life-times.

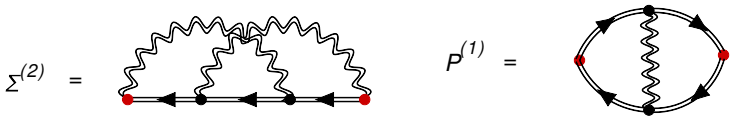

Figure 3.13: Feynman diagrams for the 1st-order vertex for the self-energy and polarization.

$G_0\mathcal{W}_0$ FOR HOMOGENEOUS 3D ELECTRON GAS

To substantiate the discussion of the $G\mathcal{W}$ approximation we consider as an example the $G_0\mathcal{W}_0$ approximation for the homogeneous electron gas. This section is also motivated by the fact that the second part of this thesis was to study the role of the vertex corrections and dressing of the Green's function, a question which still remains unanswered.

From the early days of the $G\mathcal{W}$ approximation, after its introduction by Lars Hedin [94] in 1965, the question of vertex corrections versus self-consistency has been triggering new research. The self-consistency procedure in $G\mathcal{W}$ approximation is know to lead to deterioration of the description of the bandwidth of metals and semiconductors, leading to overestimation of experimental results. In addition, the self-consistency procedure causes damping of the plasmon satellite structure [56, 112] compared to the $G_0\mathcal{W}_0$ approximation. This damping procedure is a very similar to the one observed for the Coulomb side peak structure in the Anderson impurity model [57]. For the Anderson impurity model the Coulomb side peak structure as well as an approximation for the Kondo peak can be obtained by doing a single shot 2B calculation [11], *i.e.,* a calculation without self-consistency. Since the 2B approximation contains the second order exchange term, this could imply that the second order exchange coming from the vertex corrections to the $G\mathcal{W}$ self-energy could restore the plasmon features. To this end, we note that the reason for doing self-consistent $G\mathcal{W}$ calculations is that it is conserving (see section 3.5 in chapter 3).

The homogeneous electron gas or the jellium model is described by the density parameter r_s which is related to the electron density by $1/n = 4\pi r_s^3 a_0^3/3$. In other words r_s gives the radius of a sphere in units of the Bohr radii a_0 which encloses one unit of charge in an electron case with density $n = N/V$ where

N is the number of electrons. The density parameter r_s can be related to the Fermi wave vector via the relation

$$k_F a_0 = \left(\frac{9}{3}\right)^{1/3} \frac{1}{r_s}. \tag{3.100}$$

For metallic systems r_s is usually on range from 2 to 5. The parameter r_s is a measure of relative importance of the Coulomb interaction in a metal. A typical value for the Coulomb interaction in a metal is approximately $w \sim e^2/r_s$ and the characteristic kinetic energy is of the order of the Femi energy ε_F yielding for the ratio to be proportional to the density parameter r_s, $w/\varepsilon_F \sim r_s$.

Since the homogeneous 3D electron gas is a translational invariant system in space and time we can perform Fourier transforms of G_0 and $\mathcal{W}_0$ into the $(\omega, \mathbf{k})$ space

$$G_0(1,2) = \int \frac{d\mathbf{k}}{(2\pi)^3} \int \frac{d\omega}{2\pi} e^{i\mathbf{k}\cdot(\mathbf{r}_1-\mathbf{r}_2)} e^{-i\omega(t_1-t_2)} G_0(\mathbf{k},\omega), \tag{3.101}$$

$$\mathcal{W}_0(1,2) = \int \frac{d\mathbf{k}}{(2\pi)^3} \int \frac{d\omega}{2\pi} e^{i\mathbf{k}\cdot(\mathbf{r}_1-\mathbf{r}_2)} e^{-i\omega(t_1-t_2)} \mathcal{W}_0(\mathbf{k},\omega), \tag{3.102}$$

$$\mathcal{P}(\mathbf{k},\omega) = -i \int \frac{d\mathbf{k}}{(2\pi)^3} \int \frac{d\nu}{2\pi} G_0(\mathbf{k},\nu) G_0(\mathbf{k}+\mathbf{p},\omega+\nu) \tag{3.103}$$

Within $G_0\mathcal{W}_0$ approximation the self-energy $\Sigma(1,2) = iG_0(1,2)\mathcal{W}_0(1^+,2) = i\mathcal{W}_0(2,1^+)G_0(1,2)$ we will approximate the one-particle Green's function with the non-interacting Green's function

$$G_0(\mathbf{k},\omega) = \frac{n_\mathbf{k}}{\omega - \varepsilon_\mathbf{k} - i\eta} + \frac{1-n_\mathbf{k}}{\omega - \varepsilon_\mathbf{k} + i\eta}, \tag{3.104}$$

where $n_\mathbf{k}$ denotes the occupation of the state with the momentum $\mathbf{k}$. To obtain a more accurate description of the spectral properties we will add a small kinetic self-energy renormalization Δ to the denominator of the G_0 to mimic self-consistency effects. We can choose this quantity by doing two separate calculations for the self-energy Σ^R and by requiring $\mu - \varepsilon_{k_F} - \Sigma^R(k_F,\mu) = 0$. From this we can determine the shift in the pole of the Green's function for the next iteration to be $\Delta = \mu - \varepsilon_{k_F}$ [113].

In Fig. 3.14 we show the self-energy and spectral function for an homogeneous electron gas at $G_0\mathcal{W}_0$ level. In the upper panel of Fig. 3.14 we show the real and imaginary part of the self-energy for $r_s = 4.0$ with wave vectors below and above the Fermi wave number. According to Luttinger the imaginary part of the self-energy close to the Fermi surface goes as $\mathrm{Im}\,[\Sigma^R(\mathbf{k},\omega)] = \mathrm{sgn}(\mu-\omega)c(\mathbf{k})(\omega-\mu)^2$, *i.e.* close to Fermi surface the imaginary part of the retarded self-energy approaches zero as ω^2 [22]. This we can see for the imaginary parts of the self-energy plotted in the upper plane of Fig. (3.14). Remembering that $\mathrm{Im}\,\Sigma$ represents a life-time or inverse of the decay rate of a quasiparticle $\tau_\mathbf{k}^{-1} = Z_\mathbf{k}\,\mathrm{Im}\,\Sigma^R_{MB}(\mathbf{k},\omega)$. Implies this that quasiparticles are well defined on the Fermi surface. In the lower panel of the Fig. 3.14 we show the spectral functions with $r_s = 2.0, 4.0, 6.0$ for wave numbers $k = 0.5k_F, k_F, 1.5k_F$. A figure of the spectral function as a function of k and ω can be seen in Fig 3.16a. We see that quasiparticle peak has a non-zero width for $k = 0.5k_F$ and $k = 1.5k_F$, *i.e,* for the states which are not on the Fermi surface. The non-zero width of the quasi-particle peak can be understood the density fluctuation spectrum which at

the RPA level includes both continuum of electron-hole pair and plasmon excitations. For the states not on the Fermi surface, the quasiparticle is damped due to excitation of particle hole pairs, and at higher momenta also due to excitation of plasmons. We also notice, that the $G_0\,W_o$ spectral function contains the first plasmon peak next to the quasiparticle peak.

The lowest order approximation for the polarization $\mathcal{P}_0$ will lead to the Random Phase Approximation (RPA) (see also section 3.6 in chapter 3) for the dielectric function and for the effective interaction, which we can see to be the Lindhard dielectric function [113]. In Fig. 3.15 we show the RPA response at the $G_0\mathcal{W}_0$ level, *i.e.* the RPA response for $r_s = 3.0$. At low frequencies the real part of dielectric function has a large positive contribution which means the low frequency charge distribution is strongly screened. The cut-off for the imaginary part gives us the maximum energy for single particle excitations. If $\mathrm{Re}\,[\varepsilon]$ contains a pole in the region where $\mathrm{Im}\,[\varepsilon] = 0$ our system can possess a plasmon. For the situation $\mathrm{Im}\,[\varepsilon] = \mathrm{Re}\,[\varepsilon] = 0$ the system possess an undamped plasma oscillation. In the left panel of Fig. 3.15 we show the Lindhard function below the critical wave number, *i.e.* before the plasmon excitation reaches the electron-hole continuum (left panel) and at the critical wave number (middle panel), and in the (right panel) we show the standard dispersion relation curves for the electron gas. In Fig 3.16b we illustrate the inverse of the dielectric function. The high resonance is the plasmon peak while the lower order excitations describe electron-hole pairs.

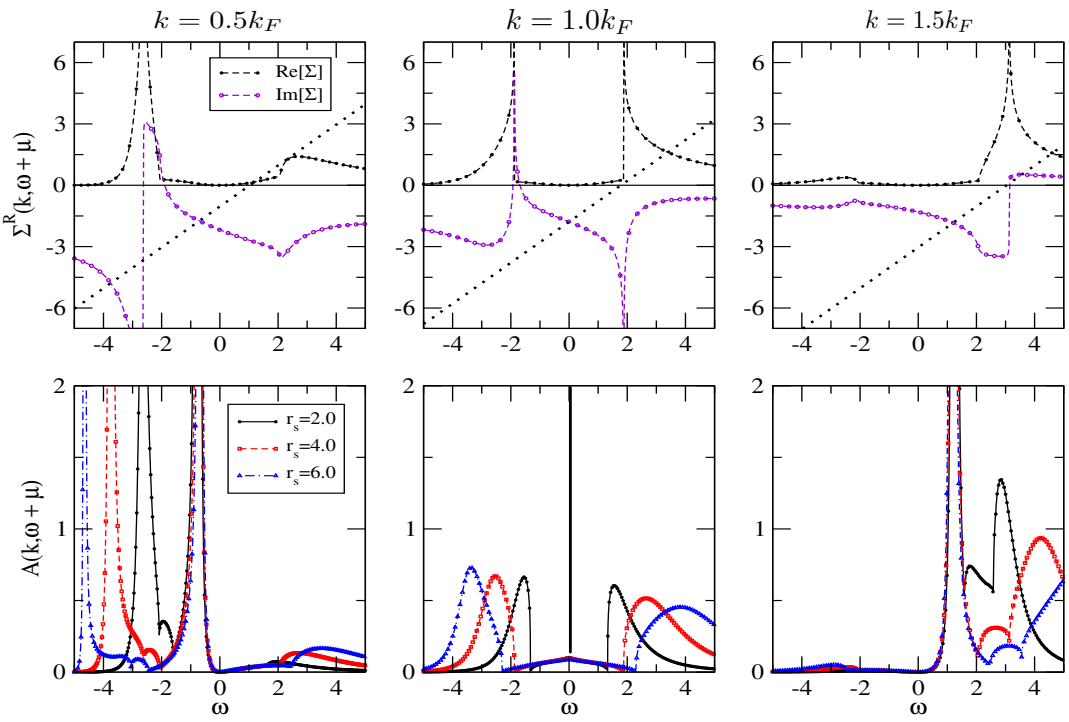

Figure 3.14: $G_0\mathcal{W}_0$ self-energy for the homogeneous electron gas. On the upper row we show the real and imaginary part of the Σ^R for $r_s = 4.0$. The dotted line represents the line $\varepsilon + \mu - \varepsilon_k$. In the lower panels we show the spectral function for different values of r_s.

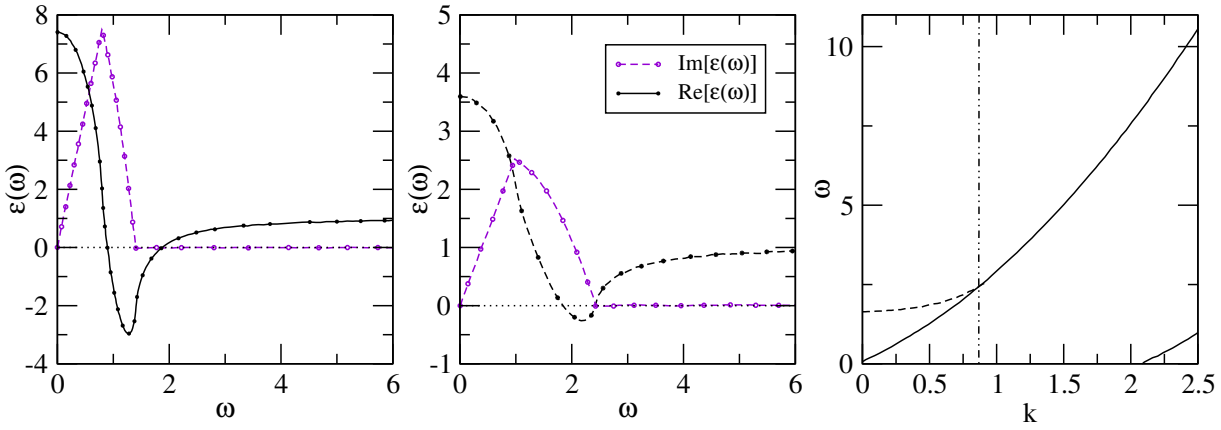

Figure 3.15: Real and imaginary part of the dielectric response with $G_0\mathcal{W}_0$ approximation for $r_s = 3$. Left panel $k < k_F$, middle panel $k = k_F$. In right panel we show the dispersion relation for 3D homogeneous electron gas consisting of plasmon branch and particle-hole continuum.

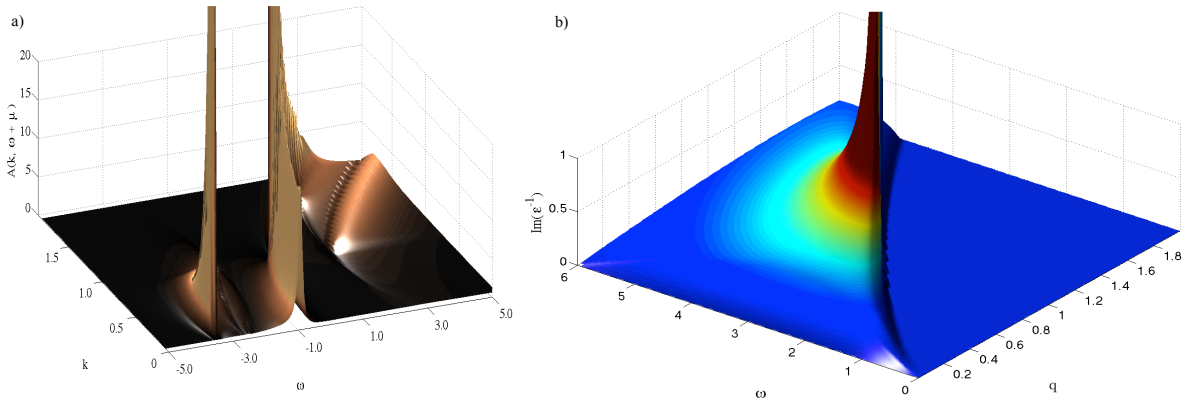

Figure 3.16: $G_0\mathcal{W}_0$ self-energy (a) and the inverse dielectric function (b) for the homogeneous electron gas with $r_s = 3.0$.

3.4.3 T-MATRIX APPROXIMATION

The third correlated many-particle approximation we used in this thesis work is the T-matrix approximation which is particularly useful in studying strongly correlated systems where the short range interaction plays a dominant role. The T-matrix approximation can be derived by approximating the two-particle Green's function G_2 as an infinite sum of two-particle collision terms

$$\begin{aligned} G_2(12;1'2') &= G(1,1')G(2,2) - G(1,2')G(2,1') \\ &\quad + i\int d3d4\, G(1,3)G(2,4)w(3,4)G_2(34;1'2') \end{aligned} \tag{3.105}$$

where the first two terms describing free propagation of two particles is just Hartree-Fock approximation while the integral kernel takes into account all the other collision processes where the particles interact one or several times before or after the collision. We can now define the T-operator (or transfer-operator) as

$$\begin{aligned} T(12;1'2') &= w(1,2)\delta(1,1')\delta(2,2') + \\ &\quad i\int d3d4\, T(12;34)K(34;1'2')w(1',2'), \end{aligned} \tag{3.106}$$

where $K(12;1'12') = G(1,1')G(2,2')$ is a propagator for two-particles (or two holes). which allows us to write the wG_2 term in the equation of motion of the one-particle Green's function (3.51) as

$$w(1,2)G_2(12;1'2') = \int d3d4\, T(12;34)\left[G(2,1')G(4,2') - G(3,2')G(2,1')\right] \tag{3.107}$$

yielding us the following T-matrix expression of the many-particle self-energy

$$\Sigma^{\text{TMAT}}_{\text{MB}}(1,2) = -i\int d3d4\, \left[T(12;34) - T(12;34)\right] G(3,4^+) \tag{3.108}$$

which we need naturally solve up to self-consistency in a similar fashion as the GW approximation. In Fig. 3.17 we show the diagrammatic expansion of the T-matrix self-energy

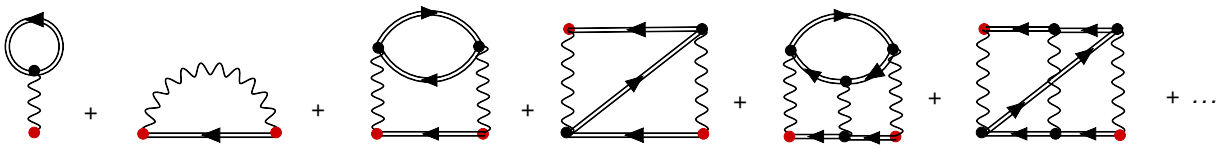

Figure 3.17: Feynman diagrams for T-matrix approximation.

We have now introduced the standard many-particle self-energy approximations. These are the approximations that are also used in the quantum transport section of this thesis.

3.5 CONSERVING APPROXIMATIONS

When developing theory for the non-equilibrium problem it is important to have self-energy approximations which satisfy the basic conservation laws for particle number, momentum and energy. Otherwise, the chosen scheme for transport problem will be unable to answer the basic questions, like what is the current through the system, and in worst scenarios leads to unphysical results and to inability of numerical time-propagation. All the approximations discussed so far are conserving in the sense of Kadanoff and Baym [48, 47], *i.e.*, the observables calculated form the Green's function with these self-energy approximations will obey the fundamental conservation laws like particle conservation which can be expressed via continuity equation

$$\partial_t n(\mathbf{r}, t) = -\nabla \cdot \mathbf{j}(\mathbf{r}, t). \tag{3.109}$$

The momentum conservation, for example, is expressed as the sum of translational part, being proportional to the electric field $\boldsymbol{E}(1) = -\nabla_1 v(1) - \partial_t \boldsymbol{A}(1)$, and the rotational part, being proportional to the magnetic field $\boldsymbol{B} = \nabla \times \boldsymbol{A}$, as

$$\frac{d}{dt}\langle \hat{\boldsymbol{P}} \rangle = -\int d\mathbf{x}_1 \left[\langle \hat{n}(1) \rangle \boldsymbol{E}(1) + \langle \hat{\mathbf{j}}(1) \rangle \times \boldsymbol{B}(1) \right]. \tag{3.110}$$

According to Baym and Kadanoff [48, 47] a sufficient condition that the self-energy approximation is conserving, is that it is obtainable from gauge-invariant Φ-functional according to

$$\Sigma(1,2) = \frac{\delta \Phi[G]}{\delta G(2, 1^+)}. \tag{3.111}$$

Due to this, the conserving approximations are often called Φ-derivable approximations. If the functional is symmetric under infinitesimal variations of the Green's function we have

$$\delta\Phi = \int d1 \int d2\, \Sigma(1,2) \delta G(2, 1^+) = 0. \tag{3.112}$$

The requirement for the symmetry under variations guarantees the satisfaction of the conservation laws. Luttinger and Ward [114] showed that a closed gauge invariant Φ-functional could be constructed by summing over the irreducible self-energy diagrams closed with additional Green's function line

$$\Phi[G] = \sum_{nk} \frac{1}{2n} \int d1 \int d2\, \Sigma_k^{(n)}(1,2) G(2, 1^+) = \sum_{nk} \frac{1}{2n} \mathrm{tr}_{\mathcal{C}} \left[\Sigma_k^{(n)} G \right]. \tag{3.113}$$

where k labels the Σ-diagrams, n labels the number of interaction lines, and $\mathrm{tr}_{\mathcal{C}}$ indicates integration over all internal vertex points on the Keldysh contour $\mathcal{C}$. In other words, the exact self-energy is a sum of all dressed skeleton diagrams, *i.e.,* Green's functions without self-energy insertions, closed with extra self-energy line (see Fig. 3.18).

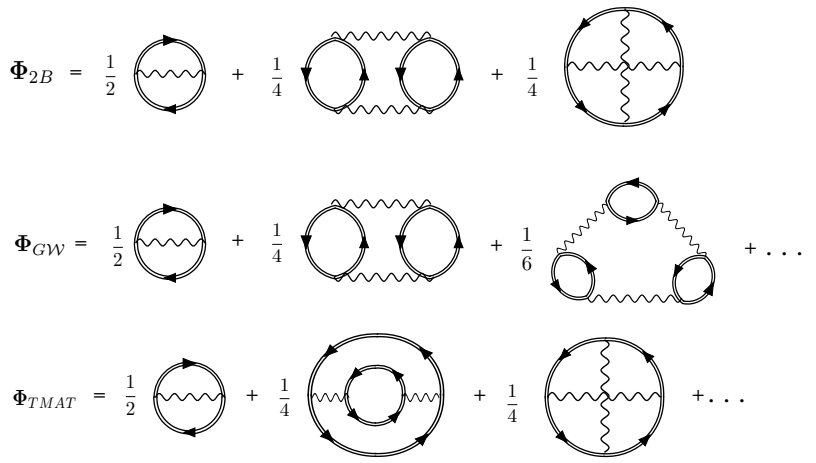

Figure 3.18: Φ functionals for the standard conserving self-energy approximations.

CHARGE CONSERVATION

Now we demonstrate how the Φ-derivability of the self-energy implies the fulfillment of the continuity equation

$$\partial_1 \langle \hat{n}(1) \rangle = -\nabla_1 \langle \mathbf{j}(1) \rangle, \tag{3.114}$$

where the expectation values for density and current operators are expressed with the help of one-particle Green's function

$$\langle \hat{n}(1) \rangle = iG(1,1^+), \tag{3.115}$$

$$\langle \hat{\mathbf{j}}(1) \rangle = -i \left\{ \left[\frac{\nabla_1}{2i} - \frac{\nabla_{1^+}}{2i} \right] G(1,1^+) \right\}_{1'=1^+}. \tag{3.116}$$

The continuity equation or number conservation follows from the symmetry of $\Phi[G]$ under variations. Therefore, if we consider the perturbing potential to transform under gauge as $\mathbf{v} \to \mathbf{v}' + \partial_{t_1}\lambda(1)$ (and in the case of vector potential $\mathbf{A} \to \mathbf{A}' + \nabla\lambda(1)$) the one-particle part of the Hamiltonian transforms as

$$\hat{h}' = \frac{1}{2}[\nabla + \nabla\lambda]^2 + v' + \partial_t\lambda - \mu, \tag{3.117}$$

where λ is an arbitrary function which satisfies the KMS boundary condition $\lambda(t_0) = \lambda(t_0 - i\beta)$. The only constraint for the transformation of the Green's function under the chosen gauge is that it satisfies the equation of motion with the transformed Hamiltonian

$$(i\partial_{t_1} - \hat{h}')G(1,2;\lambda) = \delta(1,2) + \int d3\, \Sigma(1,3;\lambda)G(3,2;\lambda). \tag{3.118}$$

Starting from the noninteracting Green function, which satisfies the following equation of motion $(i\partial_{t_1} - \hat{h}')G_0(1,2;\lambda) = \delta(1,2)$ we find out that G_0 transforms according to

$$G_0(1,2;\lambda) \to e^{-i\lambda(1)}G_0(1,2)e^{i\lambda(2)}, \tag{3.119}$$

which can be seen by considering the change of wave functions under the chosen gauge transformation, which define the transformed non-interacting Green's function in terms of the transformed field operators. Another way to see this just by direct differentiation. Together with Dyson equation and the transformation of G_0 it is straightforward to see that the interacting Green's function and a diagrammatically given self-energy will also transform as

$$G(1,2;\lambda) \to e^{-i\lambda(1)}G(1,2)e^{i\lambda(2)} \tag{3.120}$$

$$\Sigma(1,2;\lambda) \to e^{-i\lambda(1)}\Sigma(1,2)e^{i\lambda(2)}. \tag{3.121}$$

These transformations also follow from the particle conservation in the internal vertex points [48, 47]. Now the invariance of Φ under a gauge change gives [22]

$$0 = \delta\Phi[G] = \mathrm{tr}\{\Sigma\delta G\} = \int d1 \int d2\, \Sigma(1,2)\delta G(2,1), \tag{3.122}$$

where the first order change in G with respect to λ is $\delta G(1,2) = -i(\lambda(1) - \lambda(2))G(1,2)$ yielding

$$\begin{aligned}\delta\Phi[G] &= -i\int d1 \int d2\, \Sigma(1,2)(\lambda(2) - \lambda(1))G(2,1) \\ &= i\int d1 \int d2\, \left[\Sigma(1,2)G(2,1) - G(1,2)\Sigma(2,1)\right]\lambda(1).\end{aligned} \tag{3.123}$$

This has to hold for all λ and consequently

$$\int d2\, \left[\Sigma(1,2)G(2,1) - G(1,2)\Sigma(2,1)\right] = 0. \tag{3.124}$$

This relation will imply the validity of continuity equation as we will see below. From the equation of motion of the Green's function (3.51), by subtracting the adjoint equation and letting $2 \to 1^+$, we obtain

$$\left[i\partial_1 + i\partial_{1^+} - \hat{h}(1) + \hat{h}(1^+)\right] G(1,1^+) = \int d\bar{1}\, \left[\Sigma(1,\bar{1})G(\bar{1},1^+) - G(1,\bar{1})\Sigma(\bar{1},1^+)\right]. \tag{3.125}$$

Now since the integral in the right hand side is proven to be zero, we have

$$\left[i\partial_1 + i\partial_{1^+}\right] G(1,1^+) = [\hat{h}(1) - \hat{h}(1^+)]G(1,1^+) \tag{3.126}$$

which reduces to $\left[i\partial_1 + i\partial_{1^+}\right] G(1,1^+) = [(\nabla_1 + \nabla_{1^+})(\nabla_1 - \nabla_{1^+})]G(1,1^+)$, yielding the continuity equation.

$$\partial_1\langle\hat{n}(1)\rangle = -\nabla_1\langle\mathbf{j}(1)\rangle. \tag{3.127}$$

The momentum conservation follows from the invariance of $\Phi[G]$ under translations whereas the angular momentum conservation is consequence of the invariance of $\Phi[G]$ under rotations. The energy conservation follows from the invariance of $\Phi[G]$ when observer uses a flexible clock [48, 47, 23, 22].

3.6 Density Response Function

The response theory is an essential tool in determining various physical properties of a many-electron system. Response function of a system to an external electric or magnetic field reveals neutral excitation spectrum of the system, while the imaginary part of the density response function relates to collective excitations. Like we saw in previous section also the optical absorption spectra and EELS spectra can be related to the response function of the studied many-particle system. In linear response regime we can define the density response function to a weak external perturbation as

$$\delta\langle\hat{n}(\mathbf{x}_1 t_1)\rangle = \int d\mathbf{x}_2 \int dt_2\, \chi^R(\mathbf{x}_1 t_1, \mathbf{x}_2 t_2)\delta v(\mathbf{x}_2 t_2) \tag{3.128}$$

where we have defined the retarded density-response function giving us the neutral excitation spectrum as

$$\chi^R(\mathbf{x}_1 t_1, \mathbf{x}_2 t_2) = -i\theta(t_1 - t_2)\langle[\hat{n}_{\text{H}}(\mathbf{x}_1 t_1), \hat{n}_{\text{H}}(\mathbf{x}_2 t_2)]\rangle. \tag{3.129}$$

The retarded component guarantees correct causal properties, *i.e.,* the disturbance at $\mathbf{r}_2$ can lead changes in density at all spatial points, but the disturbance at time t_1 can lead to changes at the observed quantity only for later times than t_1. The expression for the retarded density-response function follows from studying systems in response to an external perturbation $\delta v(t)$ where the full Hamiltonian reads (omitting the spatial index)

$$\hat{H}(t) = \hat{H}_0 + \delta v(t) \tag{3.130}$$

where $\delta v(t) = 0$ for $t < t_0$. The expectation value of an operator $\hat{O}$, $\langle\hat{O}_{\text{H}}(t)\rangle = \text{Tr}\{\hat{\rho}\hat{O}_{\text{H}}(t)\}$ will now change due to the perturbation as

$$\delta\langle\hat{O}_{\text{H}}(t)\rangle = \langle\hat{O}_{\text{H}}(t)\rangle - \langle\hat{O}_{\text{H}}(t_0)\rangle. \tag{3.131}$$

Furthermore, the time-evolution operator can now be written as

$$\hat{U}'(t, t_0) = \hat{U}(t, t_0) + \delta\hat{U}(t, t_0) \tag{3.132}$$

which will allow us to write the expectation value of operator $\hat{O}$ at time t as

$$\begin{aligned}\langle\hat{O}(t)\rangle &= \text{Tr}\left\{\hat{\rho}\hat{U}'(t_0, t)\hat{O}\hat{U}'(t, t_0)\right\} \\ &= \text{Tr}\left\{\hat{\rho}\hat{U}(t_0, t)\hat{O}\hat{U}(t, t_0)\right\} + \text{Tr}\left\{\hat{\rho}\hat{U}(t_0, t)\hat{O}\delta\hat{U}(t, t_0)\right\} + \text{Tr}\left\{\hat{\rho}\delta\hat{U}(t_0, t)\hat{O}\hat{U}(t, t_0)\right\} + \mathcal{O}((\delta v)^2)\end{aligned}$$

$$= \langle \hat{O}(t_0)\rangle + \mathrm{Tr}\left\{\hat{\rho}\delta\hat{U}(t_0,t)\hat{O}\hat{U}(t,t_0)\right\} + \mathrm{Tr}\left\{\hat{\rho}\hat{U}(t_0,t)\hat{O}\delta\hat{U}(t,t_0)\right\} + \mathcal{O}((\delta v)^2) \quad (3.133)$$

which then allows us the write the linear response equation for operator $\hat{O}$ due to the perturbation $\delta\hat{H}(t)$ as

$$\delta O(t) = -\int_{t_0}^{t} dt' \,\langle[\delta\hat{O}_{\mathrm{H}_0}(t), \delta\hat{O}_{\mathrm{H}_0}(t')]\rangle. \quad (3.134)$$

This allows us to write the density deviation $\delta\langle\hat{n}(\mathbf{x}_1 t_1)\rangle$ as [115]

$$\begin{aligned}\delta\langle\hat{n}(\mathbf{x}_1 t_1)\rangle &= \langle\hat{n}(\mathbf{x}_1,t_1)\rangle_v - \langle\hat{n}(\mathbf{x}_1,t_1)\rangle \\ &\approx \int_{-\infty}^{\infty} dt_2 \int d\mathbf{x}_2\, \theta(t_1-t_2)\langle[\hat{n}_{\mathrm{H}}(\mathbf{x}_1 t_1), \hat{n}_{\mathrm{H}}(\mathbf{x}_2 t_2)]\rangle\delta v(\mathbf{x}_2,t_2). \end{aligned} \quad (3.135)$$

We can now define the density response function χ on the contour $\mathcal{C}$ as the contour-ordered product of density deviation operators

$$\chi(\mathbf{x}_1 z_1, \mathbf{x}_2 z_2) = -i\langle\mathcal{T}_{\mathcal{C}}[\Delta\hat{n}_H(\mathbf{x}_1 z_1)\Delta\hat{n}_H(\mathbf{x}_2 z_2)]\rangle,$$

where $\Delta\hat{n}(\mathbf{x}) = \hat{n}(\mathbf{x}) - \langle\hat{n}(\mathbf{x})\rangle$ and $\mathcal{T}_{\mathcal{C}}$ is the contour-ordering operator and the average $\langle\ldots\rangle$ is performed over the many-body state of the system. The greater $\chi^{+-} \equiv \chi^{>}$ and lesser $\chi^{-+} \equiv \chi^{<}$ response functions read

$$\chi^{>}(\mathbf{x}_1 t_1, \mathbf{x}_2 t_2) = -i\langle\Delta\hat{n}_H(\mathbf{x}_1 t_1)\Delta\hat{n}_H(\mathbf{x}_2 t_2)\rangle \quad (3.136)$$

$$\chi^{<}(\mathbf{x}_1 t_1, \mathbf{x}_2 t_2) = -i\langle\Delta\hat{n}_H(\mathbf{x}_2 t_2)\Delta\hat{n}_H(\mathbf{x}_1 t_1)\rangle \quad (3.137)$$

and fulfill the symmetry relation $i\chi^{\lessgtr}(\mathbf{x}_1 t_1, \mathbf{x}_2 t_2) = [i\chi^{\lessgtr}(\mathbf{x}_2 t_2, \mathbf{x}_1 t_1)]^*$. We can now express the retarded response function in terms of the greater and lesser componentes as

$$\chi^{R}(\mathbf{x}_1 t_1, \mathbf{x}_2 t_2) = \theta(t_1-t_2)(\chi^{>} - \chi^{<})(\mathbf{x}_1 t_1, \mathbf{x}_2 t_2). \quad (3.138)$$

Like for the one-particle Green's function, we can write a Lehmann representation for the density-response function

$$\chi^{>}(\mathbf{x}_1 t_1, \mathbf{x}_2 t_2) = -i\sum_j e^{-i(E_j - E_0)(t_1-t_2)} f_j(\mathbf{x}_1) f_j^*(\mathbf{x}_2) \quad (3.139)$$

$$\chi^{<}(\mathbf{x}_1 t_1, \mathbf{x}_2 t_2) = -i\sum_j e^{-i(E_0 - E_j)(t_1-t_2)} f_j^*(\mathbf{x}_1) f_j(\mathbf{x}_2) \quad (3.140)$$

where we have used the completeness relation $\sum_j |\Psi_j\rangle\langle\Psi_j|$ of states j which can be both discrete and continuous and we have introduced the so-called excitation amplitudes $f_j(\mathbf{x}) = \langle\Psi_0|\Delta\hat{n}(\mathbf{x})|\Psi_j\rangle$ between the ground state $|\Phi_0\rangle$ and the excited state $|\Phi_j\rangle$. The excitation amplitudes vanish if the number of particles

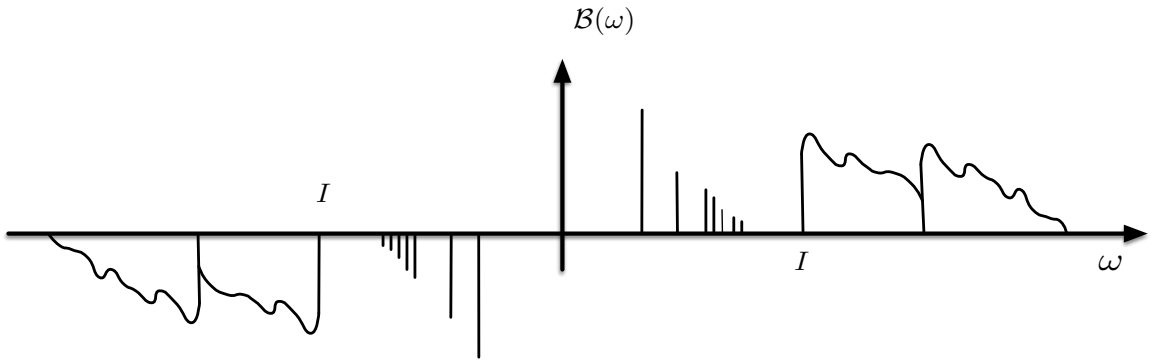

Figure 3.19: The neutral excitation spectrum of atom or molecule given by imaginary part of the density response function. I denotes the ionization edge.

for the ground state and excited state differ. In equilibrium, the Green's function and as a consequence the response function will depend on the time-difference $t_1 - t_2$ only, allowing us to perform a Fourier transform with respect to $t_1 - t_2$ giving us

$$\chi^{>}(\mathbf{x}_1, \mathbf{x}_2, \omega) = -i \sum_j \delta(\omega - (E_j - E_0)) f_j(\mathbf{x}_1) f_j^*(\mathbf{x}_2) \tag{3.141}$$

$$\chi^{<}(\mathbf{x}_1, \mathbf{x}_2, \omega) = -i \sum_j \delta(\omega + (E_j - E_0)) f_j^*(\mathbf{x}_1) f_j(\mathbf{x}_2) \tag{3.142}$$

which after substitution to the equation for the retarded response function (3.138) gives us the Lehmann representation

$$\begin{aligned} \chi^R(\mathbf{x}_1, \mathbf{x}_2, \omega) &= \sum_j \left[\frac{f_j(\mathbf{x}_1) f_j^*(\mathbf{x}_2)}{\omega - (E_j - E_0) - i\eta} - \frac{f_j^*(\mathbf{x}_1) f_j(\mathbf{x}_2)}{\omega + (E_j - E_0) + i\eta} \right] \\ &= \int \frac{d\omega'}{2\pi} \frac{\mathcal{B}(\omega')}{\omega - \omega' + i\eta} \end{aligned} \tag{3.143}$$

where η is a positive infinitesimal and we defined the spectral function $\mathcal{B}$ for the density response as $\mathcal{B}(\omega) = i[\chi^{>}(\omega) - \chi^{<}(\omega)]$ which contains information on the energy of the neutral excitations and can be measured in optical absorption experiments. From equation (3.141) we see that due to the symmetry relation $\chi^R(-\omega) = \chi^R(\omega)^*$ (where $\omega \in \mathbb{R}$) the real part of χ^R is an even function and the imaginary part is a odd function, a result we will utilize later. We will also see that the χ^R has simple poles for discrete and branch cuts for the continuous part of the spectrum j. Hence, the spectral function $\mathcal{B}$ has delta-like peaks for the discrete excitation energies and a continuum of excitations as shown in Fig. 3.19. We also notice that $\chi^{>}(\omega)$ is only nonzero for positive frequencies and gives the excitation energies while the lesser component $\chi^{<}(\omega)$ is only nonzero for negative frequencies and describes the de-excitation processes. The two functions are related by $\chi^{>}(\omega) = \chi^{<}(-\omega)$.

Since the density response function $\chi^R(\mathbf{x}_1 t_1, \mathbf{x}_2 t_2)$ depends on the density given as a product of creation and annihilation operators $\hat{n}_{\rm H}(\mathbf{x}_1, t_1) = \hat{\psi}^\dagger_{\rm H}(\mathbf{x}_1 t_1)\hat{\psi}_{\rm H}(\mathbf{x}_1, t_1)$, it can be viewed as the probability of electron-hole pair created at space-time point $(\mathbf{x}, t_2)$ and to be observed at space-time point $(\mathbf{x}_1, t_1)$. If the electron-hole pair does not interact, *i.e.*, we are describing the free-propagation of electrons, we obtain single bubble diagram denoted by χ_0, the first diagram after the equality sign in Fig. 3.20 . In reality due to Coulomb interaction electron and hole can interact all the possible ways, which we denote by the grey block in Fig. 3.20. The Fig 3.20 also shows some possible lowest order scattering process for the response function χ. We note that the expansion for χ contains diagrams which can be reduced to two or more response diagrams by cutting an interaction line. Therefore, χ is called interaction line reducible response function. In many-body perturbation theory it is often more convenient to calculate the irreducible part $\mathcal{P}$ of the response function χ defined by the Dyson equation

$$\begin{aligned}\chi(\mathbf{x}_1 z_1, \mathbf{x}_2 z_2) &= \mathcal{P}(\mathbf{x}_1 z_1, \mathbf{x}_2 z_2) \\ &+ \int d\mathbf{x}_3 d\mathbf{x}_4 \int_{\mathcal{C}} dz_3 dz_4\, \mathcal{P}(z_1, \mathbf{x}_3 z_3) w(\mathbf{x}_3 z_3, \mathbf{x}_4 z_4) \chi(\mathbf{x}_4 z_4, \mathbf{x}_2 z_2), \quad (3.144)\end{aligned}$$

which elaborates the fact the the reducible diagrams can be constructed by connecting irreducible diagrams by interaction lines in a sequence.

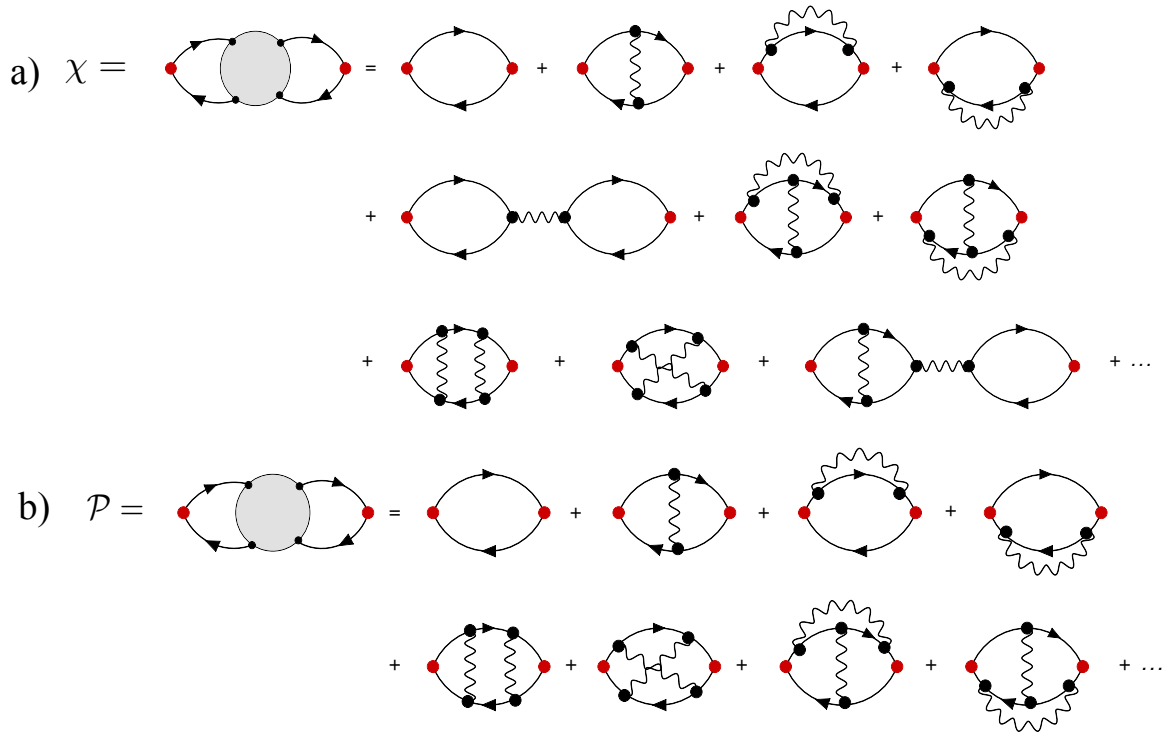

Figure 3.20: Feynman diagrams for the reducible density response function (a) and irreducible response function (b). The grey bubble represents all the possible scattering events for the electron-hole pair.

Approximating the irreducible response by the zeroth order term in interaction denoted by $\mathcal{P}$ we obtain the Random Phase Approximation (RPA) form of the dielectric function and effective interaction (see Fig. 3.21)

$$\begin{aligned}\chi(\mathbf{x}_1 z_1, \mathbf{x}_2 z_2) &= \mathcal{P}_o(\mathbf{x}_1 z_1, \mathbf{x}_2 z_2) \\ &\quad + \int d\mathbf{x}_3 d\mathbf{x}_4 \int_{\mathcal{C}} dz_3 dz_4 \, \mathcal{P}_0(z_1, \mathbf{x}_3 z_3) w(\mathbf{x}_3 z_3, \mathbf{x}_4 z_4) \chi(\mathbf{x}_4 z_4, \mathbf{x}_2 z_2), \quad (3.145)\end{aligned}$$

which corresponds to an infinite summation particle-hole diagrams. The RPA approximation performs well for high-density homogeneous electron system ($r_s \leqq 1$) since Coulomb interaction is large for small momenta ($V(\mathbf{q}) \to \infty$ for $\mathbf{q} \to 0$), so that in perturbation theory the higher order terms containing extra e^2 will be compensated with $1/\mathbf{q}^2$ term yielding us RPA response in the from of geometric series

$$\chi(\mathbf{q}, \psi) = \frac{\mathcal{P}_0(\mathbf{q}, \omega)}{1 - \frac{4\pi e^2}{\mathbf{q}^2} \mathcal{P}_0(\mathbf{q}, \omega)} \quad (3.146)$$

where the $\mathcal{P}_0$ corresponds to the free propagation of an electron–hole pair, without scattering processes. The higher order terms correspond to a special subset of all possible scattering processes. The electron–hole pair is annihilated in an interaction process creating another electron–hole pair.

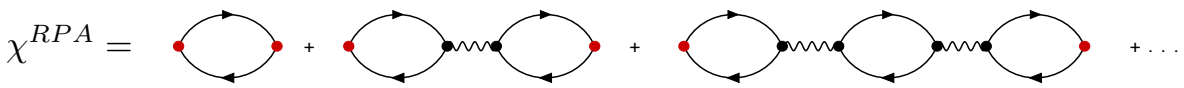

Figure 3.21: Feynman diagrams for RPA response illustrating the propagation of electron-hole pair.

3.6.1 BETHE-SALPETER EQUATION

We can obtain the optical absorption spectrum from the time-dependent equations of motion for the Green's function by applying an external perturbation such as a sudden delta function kick, after which we calculate the time-dependent density from the lesser Green's function [116, 117]. By Fourier transforming the density response $\chi^R(t) = \int d\bar{t} \; \delta G^<(t, \bar{t}) \delta v(\bar{t})$, where $\delta G^<(t,t) = -i[G^<(t,t) - G^<(t_0, t_0)]$, we then obtain the optical absorption spectrum. This spectrum corresponds to an infinite series of response diagrams generated by the Bethe-Salpeter equation (BSE) [118, 20] and it provides standard and systematic way to go beyond RPA response. The BSE is a Dyson-like equation for the four-point reducible polarizability $\mathcal{L}(12; 34)$ which, since the variation of the Green's function is related to the two-particle Green's function, is related to the two-particle excitation spectrum. The function $\mathcal{L}(12; 34)$ is obtained as the response to a non-local scalar potential $u(4, 3)$ [20]

$$\mathcal{L}(12;34) \;=\; -\frac{\delta G(1,2)}{\delta u(4,3)} = \mathcal{L}_0(12;34) + \int d(5678)\, G(1,5)G(7,3)\mathcal{K}(56;78)\mathcal{L}(82;64) \quad (3.147)$$

where $\mathcal{L}_0(12;34) = G(1,4)G(2,3)$ and the four-point reducible kernel $\mathcal{K}$ is given by $\mathcal{K}(12;34) = -i\delta\Sigma(1,3)/\delta G(4,2)$. By taking the limit $3 \to 1^+$ and $4 \to 2^+$ we obtain an equation for the response function since $\chi(1,2) = i\mathcal{L}(12;1^+2^+)$.

The standard self-energy approximations, *e.g.*, the Hartree-Fock (HF), the second order Born (2B) or the GW approximation can be utilized to derive diagrammatic approximations for the $\mathcal{K}$ which are shown in Fig. 3.22. By defining a two-particle irreducible and one interaction line irreducible kernel $\tilde{\mathcal{K}}$ as (see Fig. 3.22d)

$$\tilde{\mathcal{K}}(12;34) = \mathcal{K}(12;34) - i\delta(1,3)\delta(2,4)w(1,2), \quad (3.148)$$

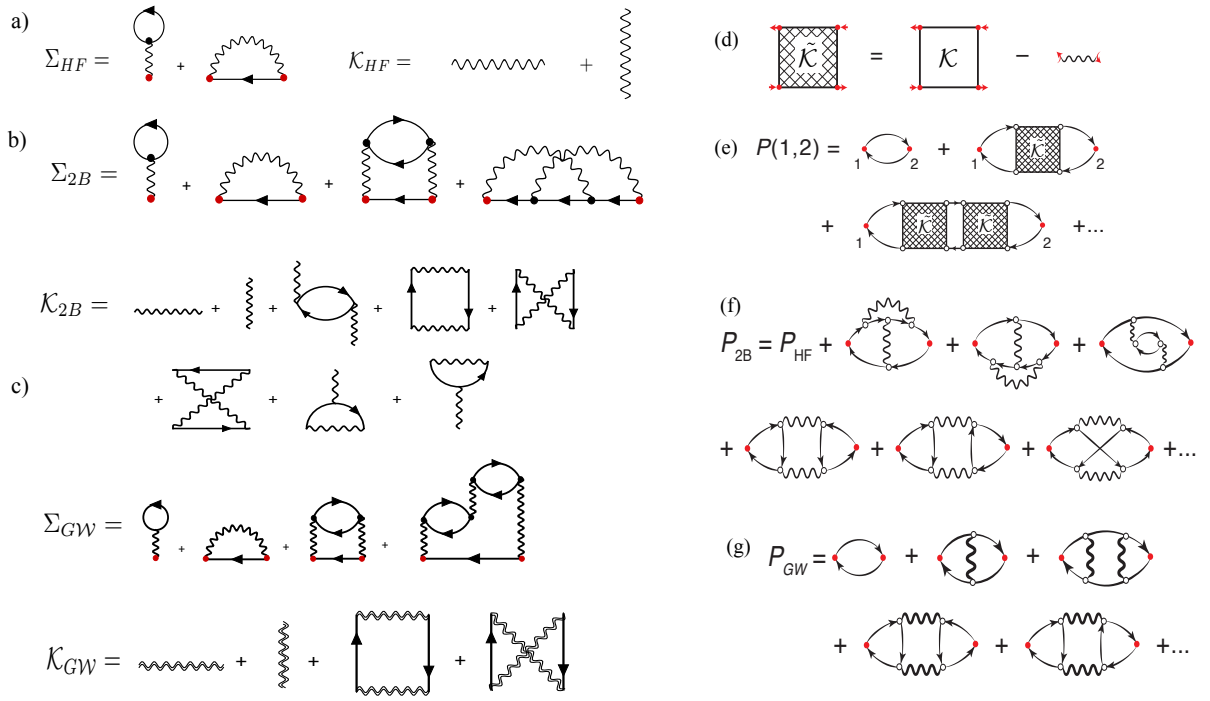

Figure 3.22: a) Hartree-Fock approximation for self-energy Σ and the corresponding BSE kernel $\mathcal{K}$. b) Second order born approximation for the self-energy and The BSE kernel corresponding to the 2B approximation. c) GW self-energy and the corresponding irreducible kernel $\mathcal{K}$. (d) Two-particle irreducible and one interaction line irreducible kernel $\tilde{\mathcal{K}}$. (e) The diagrammatic expression for the polarizability in terms of BSE kernel $\tilde{\mathcal{K}}$ as well as with (f) 2B approximation and (g) GW approximation. (Fig. from Uimonen *et al.* Phys. Rev. B **91** 115104 (2015)

we can write the polarizability as an infinite series of response diagrams

$$\mathcal{P}(1,2) = \mathcal{P}_0(1,2) + i\int d(3456)\, G(5,1)G(1,3)\tilde{\mathcal{K}}(34;56)G(4,2)G(2,6) + \dots. \tag{3.149}$$

where $\mathcal{P}_0(1,2) = -iG(1,2)G(2,1)$. The diagrammatic expression for this equation is shown in Fig. 3.22e. By using the kernels in Fig. 3.22a, 3.22b, and 3.22c,, removing the Hartree part, we obtain the approximations shown in Fig. 3.22f and Fig 3.22g. A very commonly used approximation to study the exitonic properties of solids is the *static GW* approximation [20, 119, 120] where in the *GW* kernel $\tilde{\mathcal{K}}_{GW}$

$$\tilde{\mathcal{K}}_{GW}(12;34) \quad = \quad i\delta(1,2)\delta(3,4)\mathcal{W}(1,3) + iG(1,3)\frac{\delta\mathcal{W}(1,3)}{\delta G(2,4)} \tag{3.150}$$

the functional derivative of $\mathcal{W}$ is neglected giving us a *static GW* kernel

$$\tilde{\mathcal{K}}^{(0)}_{\text{GW}}(12;34) = i\delta(1,2)\delta(3,4)\mathcal{W}(1,3) \tag{3.151}$$

which leads to the polarizability of similar to the HF, but in which the bare interaction lines are replaced by statically screened ones.

3.7 Positive Semi-Definite Approximations

So far we have discussed conserving Φ-derivable approximations for the self-energy as well as for the response function. Another class of self-energy approximations are positive semi-definite (PSD) approximations. These are self-energy approximations which will yield a PSD spectrum for the self-energy or for the response function. In this section we will discuss the systematic way to construct PSD approximations introduced in articles [4, 5]. We start from an expression of the self-energy derived by Danielewicz [21] and use the Keldysh formalism [33] to extract the lesser/greater components (these components are needed to construct the spectral function). The lesser and greater components are factorable by using the Lehmann representation of the Green's function [71, 72]. This partitioning can be seen as a cutting of the Feynman diagram. A similar cutting procedure is used in high-energy physics to calculate the imaginary part of diagrams contributing to the scattering amplitudes [121, 122, 123, 124, 125, 126]. In high-energy physics the discussion of the positivity is not addressed. A scheme to construct positive-definite photoemission current [127] as proposed by Almbladh for a diagrammatic perturbation theory of the photoemission current initiated the work towards PSD approximations.

The need for PSD approximations arises from the observation that the vertex corrections will yield negative domains for the spectral function as observed by Peter Minnhagen in 1974 [62]. Negative domains in the BSE response spectra were also observed by Sangalli *et al.* [119]. They proposed an another cutting rule based on the time-ordered half-diagrams to guarantee that the BSE density response function does not have any spurious poles.

We start by showing that the exact self-energy will be PSD. Since the time-local Hartree-Fock part of the self-energy will yield positive spectra we will focus our attention to the correlation part. We can write the self-energy as

$$\Sigma_{\text{MB}}(1,2) = \Sigma^{\delta}(1,2) + \theta(t_1,t_2)\Sigma_c^{>}(1,2) + \theta(t_2,t_1)\Sigma_c^{<}(1,2) \tag{3.152}$$

where the greater and lesser components of the self-energy are given in terms of $\hat{\gamma}$ operators by Eq. (3.45)

$$\Sigma_c^{<}(\mathbf{x}_1t_1,\mathbf{x}_2t_2) = i\langle\hat{\gamma}_{\text{H}}^{\dagger}(\mathbf{x}_2t_2)\hat{\gamma}_{\text{H}}(\mathbf{x}_1t_1)\rangle_{\text{irr}}\,, \tag{3.153a}$$

$$\Sigma_c^{>}(\mathbf{x}_1t_1,\mathbf{x}_2t_2) = -i\langle\hat{\gamma}_{\text{H}}(\mathbf{x}_1t_1)\hat{\gamma}_{\text{H}}^{\dagger}(\mathbf{x}_2t_2)\rangle_{\text{irr}}\,, \tag{3.153b}$$

where the subscript "irr" denotes the irreducible part of the self-energy. From the Dyson equation on the Keldysh contour $\mathcal{C}$ we can derive a relation between the self-energy and the Green's function as [22]

$$G^{\lessgtr}(\mathbf{x}_1,\mathbf{x}_2,\omega) = \int d\mathbf{x}_3 \int d\mathbf{x}_4\, G^{\text{R}}(\mathbf{x}_1,\mathbf{x}_3,\omega)\Sigma_c^{\lessgtr}(\mathbf{x}_3,\mathbf{x}_4,\omega)G^{\text{A}}(\mathbf{x}_4,\mathbf{x}_2,\omega), \tag{3.154}$$

where we have performed Fourier transform with respect to the time-difference $t_1 - t_2$. As we discussed already in Sec. 3.2 the retarded and advanced Green's functions are given as

$$G^{\text{R/A}}(\mathbf{x}_1,\mathbf{x}_2,\omega) = i\int \frac{d\omega'}{2\pi}\frac{G^{>}(\mathbf{x}_1,\mathbf{x}_2,\omega') - G^{<}(\mathbf{x}_1,\mathbf{x}_2\omega')}{\omega - \omega' \pm i\eta} \tag{3.155}$$

and they are adjoints of each other $G^{\text{A}}(\omega) = [G^{\text{R}}(\omega)]^{\dagger}$. In Sec. 3.2 we saw that the greater and lesser functions $G^{\gtrless}$ have a well defined sign for all frequencies ω, $\langle\phi|iG^{>}(\omega)|\phi\rangle \geq 0$ and $\langle\phi| - iG^{<}(\omega)|\phi\rangle \geq 0$. This followed from the the Lehmann representation. Therefore, $iG^{>}$ and $-iG^{<}$ are PSD matrices in $(\mathbf{x},\omega)$-space. Thus, the PSD of $\mp iG^{\lessgtr}$ implies that $\mp i\Sigma_c^{\lessgtr}$ is PSD and vice versa.

As an example we will study the lesser self-energy, *e.g.*, $\Sigma_c^{<}$ (the same reasoning applies to $\Sigma_c^{>}$ as well as for the response functions χ and $\mathcal{P}$). We will consider systems at zero temperature possessing a non-degenerate ground state Ψ_0. Using the definition of operators in the Heisenberg picture we can write Eq. (3.153b) as

$$\Sigma_c^{<}(\mathbf{x}_1t_1,\mathbf{x}_2t_2) = i\langle\Psi_0|\hat{U}(t_0,t_2)\hat{\gamma}^{\dagger}(\mathbf{x}_2)\hat{U}(t_2,t_0)\hat{U}(t_0,t_1)\hat{\gamma}(\mathbf{x}_1)\hat{U}(t_1,t_0)|\Psi_0\rangle_{\text{irr}}\,, \tag{3.156}$$

where we have taken the expectation value with respect to the non-degenerate ground state. We will assume that we can obtain the interacting ground state Ψ_0 by utilizing the adiabatic theorem. *i.e.*, the interaction is switched on adiabatically $\hat{\mathcal{H}} = \hat{H}_0 + e^{-\eta|t-t_0|}w$, where $\eta > 0$ is a small infinitesimal (in units of energy) and at time $t = t_0$ we have the full Hamiltonian of the interacting system. Hence, the interacting ground state can be obtained by evolving backward the noninteracting ground state Φ_0 from a distant future time τ to the arbitrary initial time t_0 as $|\Psi_0\rangle = \hat{\mathcal{U}}(t_0,\tau)|\Phi_0\rangle$ where the time-evolution operator is given as

$$\hat{U}(t_0,\tau) = \sum_{n=1}^{\infty} \frac{(-i)^n}{n!} \int_{t_0}^{\tau} dt_1 ... \int_{t_0}^{\tau} dt_n e^{-\eta(|t_1|+...+|t_n|)} \mathcal{T}[\hat{\mathcal{H}}_1(t_1)...\hat{\mathcal{H}}_n(t_n)], \tag{3.157}$$

and eventually taking the limit $\tau \to \infty$. In this way we obtain the ground state of the interacting system from the ground state of the non-interacting system which is a standard assumption of the zero-temperature formalism [27]. The reason why we want to expand the self-energy with respect to non-interacting ground state is that it allows us to expand an arbitrary N particle state Φ_i in terms of annihilation and creation operators.

Now we can write the Eq. (3.156) as

$$\Sigma_c^<(\mathbf{x}_1 t_1, \mathbf{x}_2 t_2) = i\langle\Phi_0|\hat{U}(\tau,t_2)\hat{\gamma}^\dagger(\mathbf{x}_2)\hat{U}(t_2,\tau)\hat{U}(\tau,t_1)\hat{\gamma}(\mathbf{x}_1)\hat{U}(t_1,\tau)|\Phi_0\rangle_{\text{irr}}, \tag{3.158}$$

where we have used the semi-group property of time-evolution operator $\hat{\mathcal{U}}(t_1,t_0)\hat{\mathcal{U}}(t_0,\tau) = \hat{\mathcal{U}}(t_1,\tau)$ and $\hat{\mathcal{U}}^\dagger(t_0,\tau)\hat{\mathcal{U}}(t_0,t_2) = \hat{\mathcal{U}}(\tau,t_2)$. Also the limit $\tau \to \infty$ is implied. We can now insert a complete set of states in Fock space $\mathcal{F}(\mathcal{H})$ as $\sum_i |\Phi_i\rangle\langle\Phi_i| = 1$ (i runs over all states in $\mathcal{F}(\mathcal{H})$) allowing us to write the self-energy in product form

$$\Sigma_c^<(\mathbf{x}_1 t_1, \mathbf{x}_2 t_2) = i\left[\sum_i \langle\Phi_0|\hat{U}(\tau,t_2)\hat{\gamma}^\dagger(\mathbf{x}_2)\hat{U}(t_2,\tau)|\Phi_i\rangle\langle\Phi_i|\hat{U}(\tau,t_1)\hat{\gamma}(\mathbf{x}_1)\hat{U}(t_1,\tau)|\Phi_0\rangle\right]_{\text{irr}}. \tag{3.159}$$

We can now generate any N-particle state in Fock-space $\mathcal{F}(\mathcal{H})$ by applying the (fermionic) creation $\hat{a}_k^\dagger$ and annihilation $\hat{a}_k$ operators of k-th eigenstate of the noninteracting problem. Due to the form of the $\hat{\gamma}$ and $\hat{\gamma}^\dagger$ operators which annihilate or create a fermion respectively (see Fig. 3.23) only states $|\Phi_i\rangle$ of the form $\hat{a}_{q_N}^\dagger \dots \hat{a}_{q_1}^\dagger \hat{a}_{p_{N+1}} \dots \hat{a}_{p_1}|\Phi_0\rangle \equiv |\Phi_{\underline{pq}}^{(N)}\rangle$ contribute. We used a compact notation for the indices $\underline{p} = (p_1,\dots,p_{N+1})$ and $\underline{q} = (q_1,\dots,q_N)$ in $\Phi_{\underline{pq}}^{(N)}$ which specify the quantum numbers of the $\hat{a}$ and $\hat{a}^\dagger$ operators respectively.

Figure 3.23: Diagrammatic expression of $\hat{\gamma}$-operator.

The expansion of the non-interacting ground state in terms of the creation and annihilation operators will yield us the same N particle state for different permutations of $\underline{p}$ and $\underline{q}$ labels, *i.e.,* $|\Phi^{(N)}_{\underline{pq}}\rangle = |\Phi^{(N)}_{P(\underline{p})Q(\underline{q})}\rangle$. By denoting the permutation group of N elements by π_N we can write the inner product of intermediate N particle states as

$$\langle\Phi^{(N)}_{\underline{pq}}|\Phi^{(N')}_{\underline{p}'\underline{q}'}\rangle = \delta_{N,N'}\sum_{P\in\pi_{N+1}}\sum_{Q\in\pi_N}(-)^{P+Q}\delta_{P(\underline{p}),\underline{p}'}\delta_{Q(\underline{q}),\underline{q}'},$$

where P and Q run over all possible permutations of $N+1$ and N indices with parities $(-)^P$ and $(-)^Q$, respectively. Therefore, the resolution of identity takes the form

$$\sum_i |\Phi_i\rangle\langle\Phi_i| \to \sum_{N=0}^{\infty}\frac{1}{(N+1)!N!}\sum_{\underline{pq}}|\Phi^{(N)}_{\underline{pq}}\rangle\langle\Phi^{(N)}_{\underline{pq}}|, \tag{3.160}$$

where the prefactor cancels the contribution from the permutations yielding an identical state. The outer summation runs over the different N particle states, and the inner summation denotes integrations or summations over sets of $\underline{p}$ and $\underline{q}$ quantum numbers. Since $\underline{p}$ denotes quantum numbers for annihilation operators and $\underline{q}$ denotes the quantum numbers for creation operators, the $\underline{p}$ integration runs over the occupied and $\underline{q}$ integration runs over the unoccupied states, respectively.

We can now rewrite the lesser self-energy in Eq. (3.159) compactly as

$$\Sigma^<_c(\mathbf{x}_1t_1,\mathbf{x}_2t_2) = i\left[\sum_{N=0}^{\infty}\frac{1}{(N+1)!N!}\sum_{\underline{pq}}S_{N,\underline{pq}}(\mathbf{x}_2t_2)S^*_{N,\underline{pq}}(\mathbf{x}_1t_1)\right]_{\text{irr}}, \tag{3.161}$$

where we defined the following scattering amplitudes

$$\begin{aligned} S^*_{N,\underline{pq}}(\mathbf{x}_1t_1) &\equiv \langle\Phi^{(N)}_{\underline{pq}}|\hat{U}(\tau,t_1)\hat{\gamma}(\mathbf{x}_1)\hat{U}(t_1,\tau)|\Phi_0\rangle, \\ S_{N,\underline{pq}}(\mathbf{x}_2t_2) &\equiv \langle\Phi_0|\hat{U}(\tau,t_2)\hat{\gamma}^\dagger(\mathbf{x}_2)\hat{U}(t_2,\tau)|\Phi^{(N)}_{\underline{pq}}\rangle. \end{aligned}$$

We have now managed to write the self-energy as a product form of a quantity S and its complex conjugate S^*. To analyze the content of the scattering amplitudes further we use the result from the adiabatic assumption stating that the evolution of the noninteracting ground state Φ_0 from $-\tau$ to τ yields Φ_0 up to a phase factor, i.e., $\hat{\mathcal{U}}(\tau,-\tau)|\Phi_0\rangle = e^{i\alpha}|\Phi_0\rangle$ with $e^{i\alpha} = \langle\Phi_0|\hat{\mathcal{U}}(\tau,-\tau)|\Phi_0\rangle$. In conclusion, we can expand S and S^* as

$$\begin{aligned} S^*_{N,\underline{pq}}(\mathbf{x}_1t_1) &= \langle\Phi_0|\hat{c}^\dagger_{p_1}\dots\hat{c}^\dagger_{p_{N+1}}\hat{c}_{q_1}\dots\hat{c}_{q_N}\hat{\mathcal{U}}(\tau,t_1)\hat{\gamma}(\mathbf{x}_1)\hat{\mathcal{U}}(t_1,-\tau)|\Phi_0\rangle\times e^{-i\alpha} \\ &= \frac{\langle\Phi_0|\mathcal{T}\{e^{-i\int_{-\tau}^{\tau}dt\hat{H}(t)}\hat{c}^\dagger_{p_1}(\tau^+)\dots\hat{c}^\dagger_{p_{N+1}}(\tau^+)\hat{c}_{q_1}(\tau)\dots\hat{c}_{q_N}(\tau)\hat{\gamma}(\mathbf{x}_1t_1)\}|\Phi_0\rangle}{\langle\Phi_0|\mathcal{T}\{e^{-i\int_{-\tau}^{\tau}dt\hat{H}(t)}\}|\Phi_0\rangle}, \end{aligned} \tag{3.162}$$

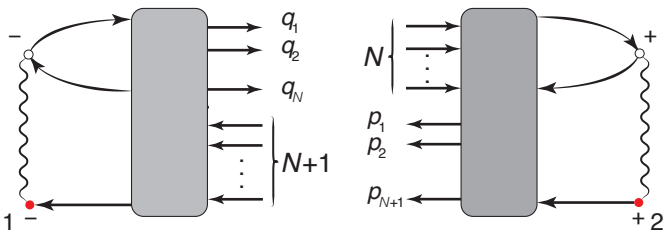

Figure 3.24: Diagrammatic structure of the functions $S(1)$ and $S^*(2)$ for the lesser self-energy. The external vertex points 1 and 2 have times on the $-$ and $+$ branch respectively (Fig. from Stefanucci et al. Phys. Rev. B **90** 115134 (2014) [4]).

and

$$\begin{aligned} S_{N,\underline{pq}}(\mathbf{x}_2 t_2) &= \langle\Phi_0|\hat{\mathcal{U}}(-\tau,t_2)\hat{\gamma}(\mathbf{x}_2)\hat{\mathcal{U}}(t_2,\tau)\hat{c}^\dagger_{q_1}\dots\hat{c}^\dagger_{q_N}\hat{c}_{p_1}\dots\hat{c}_{p_{N+1}}|\Phi_0\rangle \times e^{i\alpha} \\ &= \frac{\langle\Phi_0|\bar{\mathcal{T}}\{e^{i\int_{-\tau}^{\tau}d\tau\hat{H}(t)}\hat{\gamma}^\dagger(\mathbf{x}_2 t_2)\hat{c}^\dagger_{q_N}(\tau)\dots\hat{c}^\dagger_{q_1}(\tau)\hat{c}_{p_{N+1}}(\tau^+)\dots\hat{c}_{p_1}(\tau^+)\}|\Phi_0\rangle}{\langle\Phi_0|\bar{\mathcal{T}}\{e^{i\int_{-\tau}^{\tau}dt\hat{H}(t)}\}|\Phi_0\rangle}, \end{aligned} \tag{3.163}$$

where $\mathcal{T}$, $\bar{\mathcal{T}}$ denote the time and anti-time ordering operators, the time-argument in the operators specifies their position along the interval $(-\tau,\tau)$, and the superscript $+$ denotes times infinitesimally later on the Keldysh contour $\mathcal{C}=\mathcal{C}_-\cup\mathcal{C}_+$ assuring the correct ordering of the operators. Since $\hat{\gamma}(\mathbf{x}_1 t_1)$ is composed of an annihilation operator in $\mathbf{x}_1$, a density operator in some internal point $\mathbf{x}_3$, and an interaction line connecting $\mathbf{x}_1$ to $\mathbf{x}_3$, see Eq. (3.45) and Fig. 3.23, the amplitude S^*_N is an interacting *time-ordered* $(N+2)$-Green's function multiplied by $w(\mathbf{x}_1,\mathbf{x}_3)$ and integrated over $\mathbf{x}_3$. Thus, we can expand S^*_N in powers of the inter-particle interaction w by means of Wick's theorem, yielding an diagrammatic expansion in terms of half-diagrams. The generic term of the expansion for $S^*(\mathbf{x}_1 t_1)$ is a connected diagram for the noninteracting *time ordered* Green's functions G_0^{--} with external vertices $1=\mathbf{x}_1 t_1$ and $\underline{p}$, $\underline{q}$ at time τ, while for the $S(\mathbf{x}_2 t_2)$ the generic term of the expansion is a connected diagram of the noninteracting *anti-time ordered* Green's functions G_0^{++} with external vertices $2=\mathbf{x}_2 t_2$ and $\underline{p}$, $\underline{q}$ at time τ. The general structure for the amplitudes S and S^* is shown in Fig. 3.24. The grey region characterizes all the possible scattering processes taking place between $N+2$ particles.

We have now partitioned a generic self-energy diagram. Let us now study the properties of the half-propagator lines and the multiplication of S diagram by a S^* diagram involving a sum $\underline{p}$ and $\underline{q}$ labels. Let us focus first on the $S^*_{N,\underline{pq}}(\mathbf{x}_1 t_1)$ diagram described by time-ordered quantities where the half-propagators have the latest possible time τ yielding

$$\begin{aligned} G^{--}_{0,q\mathbf{x}}(\tau,t_x) &= G^{>}_{0,q\mathbf{x}}(\tau,t_x), \\ G^{--}_{0,\mathbf{x}p}(t_x,\tau) &= G^{<}_{0,\mathbf{x}p}(t_x,\tau), \end{aligned}$$

where we introduced a short hand notation $G_0^{\alpha\beta}(\mathbf{x}_1 t_1,\mathbf{x}_2 t_2)=G^{\alpha\beta}_{0,\mathbf{x}_1\mathbf{x}_2}(t_1,t_2)$ and $(\mathbf{x},t_x)$ denotes an internal space-spin-time vertex. In the same way, since for the diagram $S_{N,\underline{pq}}(\mathbf{x}_2 t_2)$ the half-propagators

are also calculated at the latest possible time τ giving us

$$\begin{aligned} G^{++}_{0,\mathbf{y}q}(t_y,\tau) &= G^{>}_{0,\mathbf{y}q}(t_y,\tau), \\ G^{++}_{0,p\mathbf{y}}(\tau,t_y) &= G^{<}_{0,p\mathbf{y}}(\tau,t_y). \end{aligned}$$

These relations tell us that the partitioning of a generic self-energy diagram is made along $-/+$ - line, *i.e.,* along the greater and lesser propagators. The multiplication of S and S^* diagrams therefore involves a sum over q of $G^{>}_{0,q\mathbf{x}}G^{>}_{0,\mathbf{y}q}$ and the sum over p of $G^{<}_{0,\mathbf{x}p}G^{<}_{0,p\mathbf{y}}$. Using the expansion of the lesser and greater Green's function in the basis of the noninteracting one-particle eigenstates we find [22]

$$G^{<}_{0,\mathbf{x}\mathbf{x}'}(t,t') = i\sum_p f(\epsilon_p)e^{-i\epsilon_p(t-t')}u_p(\mathbf{x})u^*_p(\mathbf{x}'), \tag{3.164}$$

$$G^{>}_{0,\mathbf{x}\mathbf{x}'}(t,t') = -i\sum_q \bar{f}(\epsilon_q)e^{-i\epsilon_q(t-t')}u_q(\mathbf{x})u^*_q(\mathbf{x}'), \tag{3.165}$$

where ϵ_p is the energy of the one-particle eigenstate $|p\rangle$, f is the zero-temperature Fermi function and $\bar{f} = 1 - f$. Taking into account that $f^2(\epsilon_p) = f(\epsilon_p)$ and $\bar{f}^2(\epsilon_q) = \bar{f}(\epsilon_q)$ we find that the sum over q states for the greater Green's function and the sum over p states for the lesser Green's function are

$$\sum_q G^{>}_{0,\mathbf{y}q}(t_y,\tau)G^{>}_{0,q\mathbf{x}}(\tau,t_x) = -iG^{>}_{0.\mathbf{y}\mathbf{x}}(t_y,t_x), \tag{3.166}$$

$$\sum_p G^{<}_{0,\mathbf{x}p}(t_x,\tau)G^{<}_{0,p\mathbf{y}}(\tau,t_y) = iG^{<}_{0,\mathbf{x}\mathbf{y}}(t_x,t_y), \tag{3.167}$$

i.e., when multiplying two half-propagators we obtain back the full one-particle propagator which guarantees the possibility of *cutting* a diagram. This property is not restricted to the noninteracting Green's functions and can be extended to dressed Green's functions by utilizing the Lehmann-representation of the Green's function. In frequency space the greater and lesser Green's function read

$$G^{\gtrless}(\mathbf{x}_1t_1,\mathbf{x}_2t_2) = \mp i\int\frac{d\omega}{2\pi}\mathcal{A}^{\gtrless}(\mathbf{x}_1,\mathbf{x}_2;\omega)e^{-i\omega(t_1-t_2)}, \tag{3.168}$$

where $\mathcal{A}^{<}(\omega) \equiv f(\omega)\mathcal{A}(\omega)$ is the removal part of the spectral function $\mathcal{A}(\omega)$ whereas $\mathcal{A}^{>}(\omega) \equiv (1 - f(\omega))\mathcal{A}(\omega)$ is the addition part of $\mathcal{A}(\omega)$, and $f(\omega)$ is the zero temperature Fermi function. If the self-energy is PSD then both $\mathcal{A}^{>}$ and $\mathcal{A}^{<}$ are PSD. We expand the matrix $\mathcal{A}^{\gtrless}(\omega)$ in terms of its eigenvalues $a^{\gtrless}_n(\omega) \geq 0$ and eigenvectors $u_n(\omega,\mathbf{x})$

$$\mathcal{A}^{\gtrless}(\mathbf{x}_1,\mathbf{x}_2;\omega) = \sum_n a^{\gtrless}_n(\omega)u_n(\omega,\mathbf{x}_1)u^*_n(\omega,\mathbf{x}_2) \tag{3.169}$$

and define the square root matrix as

$$\sqrt{\mathcal{A}^{\gtrless}}(\mathbf{x}_1,\mathbf{x}_2;\omega) = \sum_n \sqrt{a^{\gtrless}_n(\omega)}u_n(\omega,\mathbf{x}_1)u^*_n(\omega,\mathbf{x}_2). \tag{3.170}$$

We then make the rule that when cutting a partition the internal lines are G^{--} for the left half, G^{++} for the right half, and

$$\sqrt{G^{\gtrless}}(\mathbf{x}_1 t_1, \mathbf{x}_2 t_2) = \int \frac{d\omega}{2\pi} \sqrt{\mathcal{A}^{\gtrless}}(\mathbf{x}_1, \mathbf{x}_2; \omega) e^{-i\omega(t_1 - t_2)} \tag{3.171}$$

for the dangling lines of the two halves. For the reverse operation of gluing the two halves we make the rule that the "product" of two dangling lines is defined according to

$$\int d\mathbf{y} dt \, \sqrt{G^{<}}_{\mathbf{x}_1 \mathbf{y}}(t_1, t) \sqrt{G^{<}}_{\mathbf{y}\mathbf{x}_2}(t, t_2) = iG^{<}(\mathbf{x}_1 t_1, \mathbf{x}_2 t_2), \tag{3.172a}$$

$$\int d\mathbf{y} dt \, \sqrt{G^{>}}_{\mathbf{x}_1 \mathbf{y}}(t_1, t) \sqrt{G^{>}}_{\mathbf{y}\mathbf{x}_2}(t, t_2) = -iG^{>}(\mathbf{x}_1 t_1, \mathbf{x}_2 t_2). \tag{3.172b}$$

which gives us the gluing procedure for dressed Green's functions.

In a summary, to partition a $\Sigma^<$ diagram we first assign the external vertices appropriate $-$ and $+$ sign together with internal vertices having all the possible combinations of $\pm$ labels. Secondly, we obtain the half-diagrams by cutting along the greater and lesser Green's function lines. A procedure we refer to as *cutting rule* for a diagram. Due to the structure of the S and S^* diagrams as a objects with time ordered or anti-time ordered quantities only, we see that some of the partitions are vanishing. The vanishing partitions, are the ones in which an internal vertex $+(-)$ is surrounded by $-(+)$ vertices, *i.e.,* an internal vertex is disconnected from the external vertex (see Fig. 3.25). This result is equivalent to the requirement of the energy conservation on each vertex, an argument used by Veltman [122] and Kobes and Semenoff [123] to show that any disconnected diagram, *i.e*, a diagram with no external vertex points, obtained by the cutting procedure must vanish.

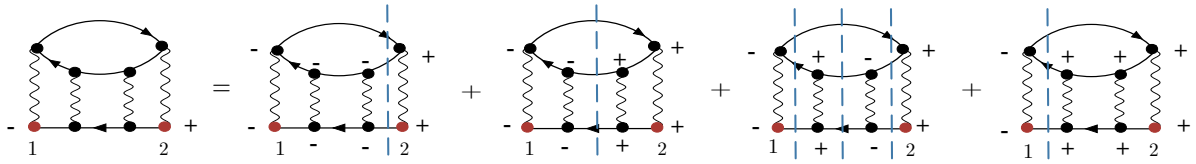

Figure 3.25: An example of the distribution of $+$ and $-$ labels over the internal vertices of a lesser fourth order self-energy diagram. Divisions with lines w^{+-} or w^{-+} vanish due to the time-locality of the interaction and therefore are not shown. The third term after the equality sign must be discarded because it contains an isolated island of plus signs upon cutting the $+/-$ G_0-lines.

We also note that the self-energy in Eq. (3.161) is not the sum of all possible SS^* diagrams due to the subscript "irr". Therefore, after the gluing procedure we have to discard all the reducible diagrams, *i.e.,* the diagrams which fall apart in two disjoint pieces by cutting a single Green's function line. If we now define $\tilde{S}$ as the sum of irreducible S-diagrams we can rewrite the lesser self-energy as

$$\Sigma_c^<(\mathbf{x}_1 t_1, \mathbf{x}_2 t_2) = i \sum_{N=1}^{\infty} \frac{1}{(N+1)!N!} \sum_{\underline{pq}} \tilde{S}_{N,\underline{pq}}(\mathbf{x}_2 t_2) \tilde{S}^*_{N,\underline{pq}}(\mathbf{x}_1 t_1), \tag{3.173}$$

which is a Lehmann-like expression for the self-energy, where the irreducible part of products in Eq. (3.161) has been transformed into products of irreducible parts in Eq. (3.173). We call this product a *partition* of the self-energy diagram. It is now easy to show that the Fourier transform of the $-i\Sigma^<$ is positive semidefinite. Fourier transforming $\tilde{S}$ and $\tilde{S}^*$ and omitting the dependence on the position-spin variables we find

$$-i\Sigma_c^<(\mathbf{x}_1,\mathbf{x}_2,t_1-t_2) = \sum_{N=1}^{\infty}\frac{1}{(N+1)!N!}\int\frac{d\omega}{2\pi}\frac{d\omega'}{2\pi}e^{-i\omega t_2+i\omega' t_1}\sum_{\underline{pq}}\tilde{S}_{N,\underline{pq}}(\omega)\tilde{S}^*_{N,\underline{pq}}(\omega'), \quad (3.174)$$

where $\Sigma^<$ depends on the time-difference t_1-t_2 and the product of $\tilde{S}$ and $\tilde{S}^*$ depend on t_1 and t_2 respectively and thus the Fourier transform is performed over respective time-argument and not over the time difference, which is ill-defined for $\tau\to\infty$. For the right hand side to depend only on t_1-t_2 the following property

$$\sum_{N=1}^{\infty}\frac{1}{(N+1)!N!}\sum_{\underline{pq}}\tilde{S}_{N,\underline{pq}}(\omega)\tilde{S}^*_{N,\underline{pq}}(\omega')=\mathcal{F}(\omega)\delta(\omega-\omega')$$

has to be fulfilled. Since for $\omega=\omega'$ the left hand side is the sum of modulus squares we have that $\mathcal{F}(\omega)\geq 0$, and inserting this result back into equation (3.174) we see that $\mathcal{F}(-\omega)$ is the Fourier transform of the function $-i\Sigma_c^<(1,2)$ with respect to the time difference t_1-t_2. Thus we have shown that the exact self-energy will have a PSD spectra.

In a similar way we can also show that the exact neutral excitation spectra calculated from the response function will be PSD. Utilizing the expression for the reducible response function as contour-ordered product of density deviation operators

$$\chi(\mathbf{x}_1z_1,\mathbf{x}_2z_2)=-i\langle\mathcal{T}_\mathcal{C}[\Delta\hat{n}_H(\mathbf{x}_1z_1)\Delta\hat{n}_H(\mathbf{x}_2z_2)]\rangle,$$

we can expand the with respect to non-interacting degenerate ground state with help of adiabatic theorem, in a similar fashion as we did for the self-energy. This will yield an expression in terms of S and S^* scattering amplitudes as

$$i\chi^<(\mathbf{x}_1t_1,\mathbf{x}_2t_2) = \sum_{N=1}^{\infty}\frac{1}{N!}\frac{1}{N!}\sum_{\underline{pq}}\mathcal{S}^{(N)}_{\underline{pq}}(\mathbf{x}_2t_2)\mathcal{S}^{(N)*}_{\underline{pq}}(\mathbf{x}_1t_1), \quad (3.175)$$

where the generic structure for half-diagrams is shown in Fig. 3.26. Restricting ourselves to the irreducible part we obtain a similar expression for the polarizability

$$i\mathcal{P}^{<}(\mathbf{x}_1 t_1, \mathbf{x}_2 t_2) \;=\; \sum_{N=1}^{\infty} \frac{1}{N!}\frac{1}{N!} \sum_{\underline{pq}} \tilde{\mathcal{S}}^{(N)}_{\underline{pq}}(\mathbf{x}_2 t_2)\tilde{\mathcal{S}}^{(N)*}_{\underline{pq}}(\mathbf{x}_1 t_1). \tag{3.176}$$

Both of these quantities can be Fourier transformed to show that they are PSD just like we just did with the self-energy.

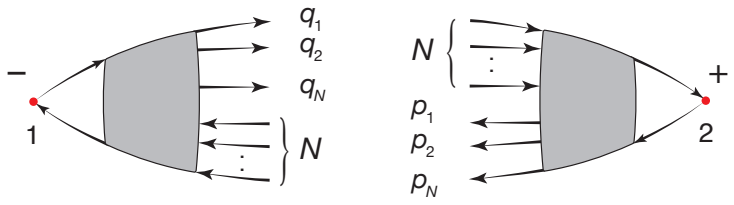

Figure 3.26: Typical diagram for $S^*(1)$ (left) and $S(2)$ (right) forming the lesser reducible response function. Labels p and q on the arrows denote quantum numbers of particles and holes respectively (Fig. from Uimonen *et al.* Phys. Rev. B **91** 115104 (2015)).

POSITIVE SEMI-DEFINITE DIAGRAMMATIC EXPANSION

For the construction of PSD approximations we need to address the possible issue of double counting when gluing half diagrams together, *i.e.* $\tilde{S}\tilde{S}^*$ partitions yielding the same self-energy diagram after gluing. We can address this question by expanding the scattering amplitudes $\tilde{S}$ and $\tilde{S}^*$ in terms of Feynman diagrams. Let us denote by $\{D^{(j)}_{\underline{pq}}\}$ with $j \in I_N$ the set of topologically inequivalent half-diagrams for S, *i.e.,* half-diagrams obtained after cutting procedure, where I_N labels the sets of half-diagrams with different number of dangling particle-hole lines. Due to the anti-commutation relations of fermionic creation and annihilation operators, a permutation of P of $\underline{p}$ labels and, a permutation Q of $\underline{q}$ labels will only change the sign of the amplitude S. In conclusion we need to write the half-scattering amplitude as a sum of half-diagrams D in a way where we take into account the change of sign of the half-diagram due to permutation of $\underline{p}$ and $\underline{q}$ labels as

$$\tilde{S}_{N,\underline{pq}} = \sum_{j\in I_N} \sum_{\substack{P\in\pi_{N+1}\\ Q\in\pi_N}} (-)^{P+Q} D^{(j)}_{P(\underline{p})Q(\underline{q})}. \tag{3.177}$$

Here we denoted the permutation group for $\underline{p}$ labels as π_{N+1} and the permutation group for $\underline{q}$ labels as π_N, where the subscript $N+1$ refers to the number of a_p operators and N to the number of $\hat{a}^\dagger_q$ operators in the complete set of states (see text below Eq. (3.159)). Inserting Eq. (3.177) back into Eq. (3.173) and

restricting the sum over N to start from 1, since the $N = 0$ term will yield a reducible diagram, we find

$$\Sigma_c^<(\mathbf{x}_1 t_1, \mathbf{x}_2 t_2) = i \sum_{N=1}^{\infty} \sum_{j_1, j_2 \in \mathcal{I}_N} \sum_{\substack{P \in \pi_{N+1}^{(j_1,j_2)} \\ Q \in \pi_N^{(j_1,j_2)}}} (-)^{P+Q} \sum_{\underline{pq}} D_{\underline{pq}}^{(j_2)}(\mathbf{x}_2 t_2) D_{P_1(\underline{p})Q_1(\underline{q})}^{(j_1)^*}(\mathbf{x}_1 t_1) \tag{3.178}$$

where $\mathcal{I}_N$ is a subset of the product set $I_N \times I_N$ and for any given couple (j_1, j_2) the sum over P runs over a subset $\pi_{N+1,p}^{(j_1 j_2)}$ of the permutation group π_{N+1} and the sum over Q runs over a subset $\pi_{N,q}^{(j_1 j_2)}$ of the permutation group π_N (see Fig. 3.27). In the equation (3.178) every term of the form $\sum_{\underline{pq}} D_{\underline{pq}}^{(j_2)}(\mathbf{x}_2 t_2) D_{P_1(\underline{p})Q_1(\underline{q})}^{(j_1)^*}(\mathbf{x}_1 t_1)$ corresponds to a unique partition of a $\Sigma_c^<$ diagram. We also note that the half-diagrams obey the standard Feynman rules and our expression Eq. (3.178) will have the correct properties as well as the correct sign of the original diagram after the gluing procedure. In deriving Eq. (3.178) we used the observation that the composite permutations $P \circ P_i$ and $Q \circ Q_i$ with $i = 1, 2$ yield the same contribution as the permutations P_i and Q_i. The minimal set of additional half-diagrams to be added is obtained as follows. Let $\{\tilde{I}_N^\alpha\}$ be a set of disjoint subsets of I_N ($\tilde{I}_N \subset I_N$) with the property that the union of the product sets (see Fig. 3.27)

$$\bigcup_\alpha \tilde{I}_N^\alpha \times \tilde{I}_N^\alpha \supset \mathcal{I}_N \tag{3.179}$$

and contains the least number of elements of $I_N \times I_N$. Since the subsets $\tilde{I}_N^\alpha$ are disjoint, the sets $\mathcal{I}_N^\alpha = \mathcal{I}_N \cap (\tilde{I}_N^\alpha \times \tilde{I}_N^\alpha)$ are disjoint also. Due to Eq. (3.179) we have that $\bigcup_\alpha \mathcal{I}_N^\alpha = \mathcal{I}_N$. For any given α we then consider the smallest subgroups of the permutation group π_N with the property that

$$\tilde{\pi}_{N+1,p}^\alpha \supset \bigcup_{(j_1 j_2) \in \mathcal{I}_N^\alpha} \pi_{N+1,p}^{(j_1,j_2)}, \tag{3.180}$$

$$\tilde{\pi}_{N,q}^\alpha \supset \bigcup_{(j_1 j_2) \in \mathcal{I}_N^\alpha} \pi_{N,q}^{(j_1,j_2)}. \tag{3.181}$$

Thus by construction the self-energy

$$i\Sigma_{\mathrm{PSD}}^<(\mathbf{x}_1 t_1, \mathbf{x}_2 t_1) \;=\; \sum_{N=1}^{\infty} \sum_\alpha \sum_{j_1, j_2 \in \tilde{I}_N^\alpha} \sum_{\substack{P \in \tilde{\pi}_{N+1,p}^\alpha \\ Q \in \tilde{\pi}_{N,q}^\alpha}} (-)^{P+Q} \sum_{\underline{pq}} D_{\underline{pq}}^{(j_2)}(2) D_{P(\underline{p})Q(\underline{q})}^{(j_1)^*}(1) \tag{3.182}$$

contains all partitions of Eq. (3.178) plus the minimal number of additional partitions to form a perfect square and consequently yielding a PSD spectrum, *i.e.,* its Fourier transform is of the from of modulus squared. In this expression the sum over N goes over the cut particle hole lines, α denotes the number of disjoint product sets, j_i labels the topologically different half-diagrams, and P and Q denote the permutations of $\underline{p}$ and $\underline{q}$ labels respectively. This is a rather abstract looking definition which becomes more clear when we look at some examples. In conclusion, the PSD diagrammatic approximation for the

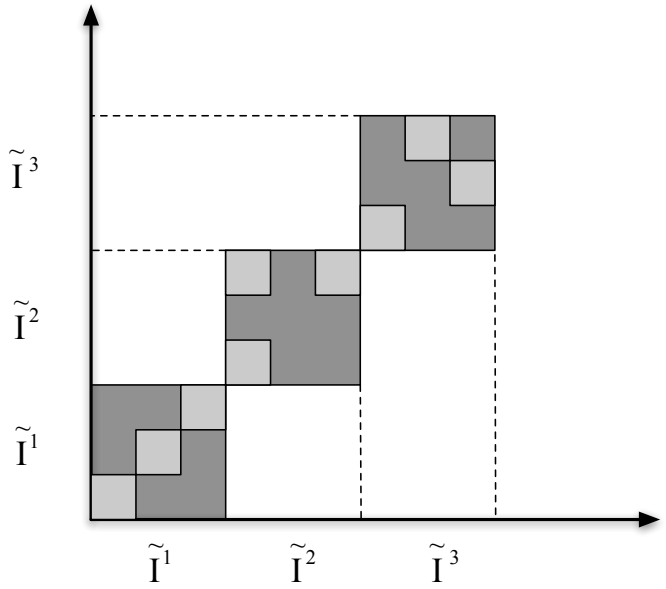

Figure 3.27: Decomposition $\bigcup_\alpha \mathcal{I}_N^\alpha = \mathcal{I}_N$ of the $\mathcal{I}_N$ subset (denoted as three disjoint gray areas) into a union of (tree in this example) product sets.

self-energy Σ is a sum of partial diagrams with internal vertices either on the minus or the plus branch of the Keldysh contour. Similarly we can also construct the PSD polarizability as

$$i\mathcal{P}^<_{\mathrm{PSD}}(1,2) = \sum_{N=1}^{\infty}\sum_{\alpha}\sum_{j_1,j_2\in\tilde{I}_N^\alpha}\sum_{\substack{P\in\tilde{\pi}^\alpha_{N,p}\\ Q\in\tilde{\pi}^\alpha_{N,q}}}(-)^{P+Q}\sum_{\underline{pq}} D^{(j_2)}_{\underline{pq}}(2)D^{(j_1)^*}_{P(\underline{p})Q(\underline{q})}(1), \tag{3.183}$$

where the half-diagrams D are now time-ordered and anti-time ordered halves of the response diagrams. From the construction of the minimal PSD approximation we notice that any reduction of half-diagrams or permutations would not fulfill the PSD property. This concluded the diagrammatic theory for MBPT self-energy and response.

CONNECTION BETWEEN PSD PROPERTY AND ANALYTIC STRUCTURE

From the Lehmann representation it follows that the Green's function has poles at excitation energies of the system which lie just below the real axis on the complex frequency plane. Therefore, the Green's function of the complex variable $G^R(z)$ is an analytic function on complex upper half plane. The correct analytic properties are very important in MBPT, since in the self-consistency cycle wrong analytic properties of $G^R(z)$ would lead to incorrect quantities at the next iteration cycle as well as to incorrect causal properties. From the Lehmann representation for the density response function it follows that χ^R has poles at the neutral excitation energies of the system, which also lie just below the real axis on the complex frequency plane. Therefore, $\chi^R(z)$ is an analytic function on complex upper half plane. The correct analytic property

of χ^R plays a role in the GW approximation, for example. Since $\mathcal{W}$ is calculated by using the response function, wrong analytic properties of χ would yield wrong analytic properties for the Green's function. It is therefore crucial that the quantities of interest have the correct analytic properties. It is also to be noted that, the correct analytic properties for the response function are highly desirable since it relates directly to the correct causality relations.

We start the analysis between PSD property and analytic structure by solving the Dyson equation for the full retarded Green's function (we omit the spatial indicies for clarity)

$$G^R(\omega) = G_0^R(\omega)\left(1 - G_0^R(\omega)\Sigma^R(\omega)\right)^{-1} = (\omega - \varepsilon_0 - \Sigma^R(\omega))^{-1}. \tag{3.184}$$

We want to know if $G^R(z)$ has a pole on the upper half of the complex plane ($z = x + iy$ with $y > 0$). Since the non-interacting Green's function does not have poles on the complex plane, this can happen only when $\omega - \varepsilon_0 - \Sigma^R(\omega)$ has a zero. Utilizing the Lehmann representation for the self-energy function

$$\Sigma^R(x + iy) = \int \frac{d\omega'}{2\pi} \frac{\Gamma(\omega')}{x - \omega' + iy} \tag{3.185}$$

we obtain the real and imaginary part of the retarded self-energy

$$\operatorname{Im}\Sigma^R(z) = -y \int \frac{d\omega'}{2\pi} \frac{\Gamma(\omega')}{(x-\omega')^2 + y^2}, \tag{3.186}$$

$$\operatorname{Re}\Sigma^R(z) = \int \frac{d\omega'}{2\pi} \frac{\Gamma(\omega')(x-\omega')}{(x-\omega')^2 + y^2}. \tag{3.187}$$

Since $y > 0$ and the spectral function $\Gamma(\omega)$ is an integrable function, both integrals are well defined and finite. Now we consider the possibility that the operator $\omega - \varepsilon_0 - \Sigma^R(\omega)$ has a zero eigenvalue. This implies that there exists an eigenvector $|\lambda\rangle$ for which $\left(\omega - \varepsilon_0 - \Sigma^R(\omega)\right)|\lambda\rangle = 0$. Implying

$$\langle\lambda| x - \varepsilon_0 - \operatorname{Re}\Sigma^R(z)|\lambda\rangle = 0, \tag{3.188}$$

$$\langle\lambda| y - \operatorname{Im}\Sigma^R(z)|\lambda\rangle = 0. \tag{3.189}$$

Using Eq. (3.186) we can write the imaginary as

$$\langle\lambda|\operatorname{Im}\Sigma^R(z)|\lambda\rangle = -y \int \frac{d\omega}{2\pi} \frac{\langle\lambda|\Gamma(\omega')|\lambda\rangle}{(x-\omega')^2 + y^2}. \tag{3.190}$$

Since we assumed that $y > 0$ and $\langle\lambda|\Gamma(\omega)|\lambda\rangle \geq 0$. Now $\langle\lambda| y - \operatorname{Im}\Sigma^R(z)|\lambda\rangle = 0$ cannot never be zero for $y > 0$ which concludes our proof and $G^R(z)$ has the correct analytic properties.

For the response function the proof is similar with a minor extra complication arising from the fact that the spectral function satisfies the relation $\tilde{B}(\omega) = -\tilde{B}(-\omega)$ (where tilde refers to the spectral function of the irreducible response, similar relation holds naturally also for the reducible response).

From the Dyson equation for the response function we can write the retarded component in terms of the polarizability as

$$\chi^R(\omega) = \mathcal{P}^R(\omega)\left(1 - w\mathcal{P}^R(\omega)\right)^{-1}, \tag{3.191}$$

which we will symmetrize to a more useful form for our proof as

$$w^{1/2}\chi^R w^{1/2} = \frac{w^{1/2}\mathcal{P}^R(\omega)w^{1/2}}{1 - w^{1/2}\mathcal{P}^R(\omega)w^{1/2}} - \tag{3.192}$$

Here we used the PSD property of w to take the square root operation, and since $w^{1/2}$ is frequency independent it does not change the analytic properties of $\chi^R(\omega)$. The symmetric form $w^{\frac{1}{2}}\mathcal{P}^R(\omega)w^{\frac{1}{2}}$ is PSD whereas $w\mathcal{P}^R(\omega)$ does not need to PSD. The response function $\chi^R(z)$ has a pole in upper half of the complex plane, *i.e.,* for $z = x + iy$ with $y > 0$. This is either the case when $\mathcal{P}^R(z)$ has a pole at z or when $1 - w^{1/2}\mathcal{P}^R(z)w^{1/2}$ has a zero. Utilizing the Lehmann representation for the response function

$$\mathcal{P}^R(x + iy) = \int \frac{d\omega'}{2\pi} \frac{\tilde{\mathcal{B}}(\omega')}{x - \omega' + iy} \tag{3.193}$$

we can write the imaginary and real part of the retarded response function as

$$\mathrm{Im}\,\mathcal{P}^R(z) = -y \int \frac{d\omega'}{2\pi} \frac{\tilde{\mathcal{B}}(\omega')}{(x-\omega')^2 + y^2}, \tag{3.194}$$

$$\mathrm{Re}\,\mathcal{P}^R(z) = \int \frac{d\omega'}{2\pi} \frac{(x-\omega')\tilde{\mathcal{B}}(\omega')}{(x-\omega')^2 + y^2}. \tag{3.195}$$

Following the reasoning of the G^R we notice that the only possibility χ^R to have a pole in the complex plane is when the operator $1 - w^{1/2}\mathcal{P}^R(z)w^{1/2}$ has a zero eigenvalue. Hence,

$$\langle\lambda|\, 1 - w^{1/2}\mathrm{Re}\,\mathcal{P}^R(z)w^{1/2}\,|\lambda\rangle = 0, \tag{3.196a}$$

$$\langle\lambda|\, w^{1/2}\mathrm{Im}\,\mathcal{P}^R(z)w^{1/2}\,|\lambda\rangle = 0. \tag{3.196b}$$

Rewriting the the imaginary part with help of spectral representation Eq. (3.196b) as

$$\langle\lambda|w^{1/2}\mathrm{Im}\,\mathcal{P}^R(x+iy)w^{1/2}|\lambda\rangle = -y\int_0^\infty \frac{d\omega'}{2\pi}\langle\lambda|w^{1/2}\tilde{\mathcal{B}}(\omega')w^{1/2}|\lambda\rangle\ell(\omega'), \tag{3.197}$$

where due to the fact that $\tilde{\mathcal{B}}(\omega) = -\tilde{\mathcal{B}}(-\omega)$ we can write the integral from 0 to ∞. We also defined the function $\ell(\omega)$ as

$$\ell(\omega) = \left[\frac{1}{(x-\omega)^2 + y^2} - \frac{1}{(x+\omega)^2 + y^2}\right]. \tag{3.198}$$

Now we come to the conclusion that the only possibility to χ^R to have a pole on the complex plane is when $x = 0$. If $x = 0$ then $\ell(\omega) = 0$ and the Eq. (3.196b) is automatically satisfied. The Eq. (3.196a) now reads

$$\langle\lambda|1 - w^{1/2}\mathrm{Re}\,\mathcal{P}^R(z)w^{1/2}|\lambda\rangle = 1 + 2\int_0^\infty \frac{d\omega'}{2\pi}\,\frac{\langle\lambda|w^{1/2}\tilde{\mathcal{B}}(\omega')w^{1/2}|\lambda\rangle\omega'}{\omega'^2 + y^2} \geq 1 \qquad (3.199)$$

since $w^{1/2}\tilde{\mathcal{B}}w^{1/2}$ is PSD for positive frequencies. In this case also the Eq. (3.196a) cannot be satisfied and therefore χ^R cannot have poles in the upper half plane when $\mathcal{P}^R$ and v are PSD.

The connection between positivity and analytic structure has important consequences for the *Kramers-Kronig relations*, relating the real (imaginary) part of a function to its imaginary (real) part, as well as for the *f-sum rule*, which relates the first momentum of the retarded density response function to the equilibrium density $n_0(\mathbf{x})$ [22]. Both of these theorems involve an integral on the complex plane in which the integrand needs to be analytic for the integral to be well defined. Thus, we see that the approximations which fulfill the PSD property the *Kramers-Kronig relations* and *f-sum rule* are well defined.

EXAMPLES

Let us now clarify the cutting procedure and especially the completion of a square with minimal substitution of half-diagrams with some illustrative examples. In Fig. 3.28A we show the first order bubble diagram appearing in both 2B and GW approximations. By taking the lesser component of this self-energy diagram

$$\Sigma_c^<(1,2) \;=\; \int d\mathbf{x}_3 \int d\mathbf{x}_4 w(\mathbf{x}_1,\mathbf{x}_3)G^<_{0,\mathbf{x}_1\mathbf{x}_2}(t_1,t_2)G^<_{0,\mathbf{x}_3\mathbf{x}_4}(t_1,t_2)G^>_{0,\mathbf{x}_4\mathbf{x}_3}(t_2,t_1)w(\mathbf{x}_2,\mathbf{x}_4), \quad (3.200)$$

we see that it can be partitioned in only one way by cutting along the $+/-$ G_0-lines. The cutting procedure will yield three dangling G_0 lines which we label by p_1, p_2 for in-going Green's function line and by q_2 for out-going Green's function line. We see that the resulting half-diagrams $D^{(a)}_{p_1p_2q_1}$ and $D^{(a*)}_{p_1p_2q_1}$ are complex conjugates of each other and form immediately a perfect square. In conclusion, the first order bubble self energy diagram can be written as

$$\Sigma_c^<(1,2) = i\sum_{\underline{pq}} D^{(a)}_{p_1p_2q_1}(2)D^{(a)^*}_{p_1p_2q_1}(1), \qquad (3.201)$$

in terms of the D half-diagrams given by

$$D^{(a)^*}_{p_1p_2q_1}(1) \;=\; \int d\mathbf{x}_3 w(\mathbf{x}_1,\mathbf{x}_3)G^<_{0,\mathbf{x}_1\,p_1}(t_1,\tau)G^<_{0,\mathbf{x}_3\,p_2}(t_1,\tau)G^>_{0,q_1\,\mathbf{x}_3}(\tau,t_1). \qquad (3.202)$$

Thus, since the first order bubble diagram can be written in the form of PSD self-energy (see Eq. (3.182)) and it will produce a PSD spectrum.

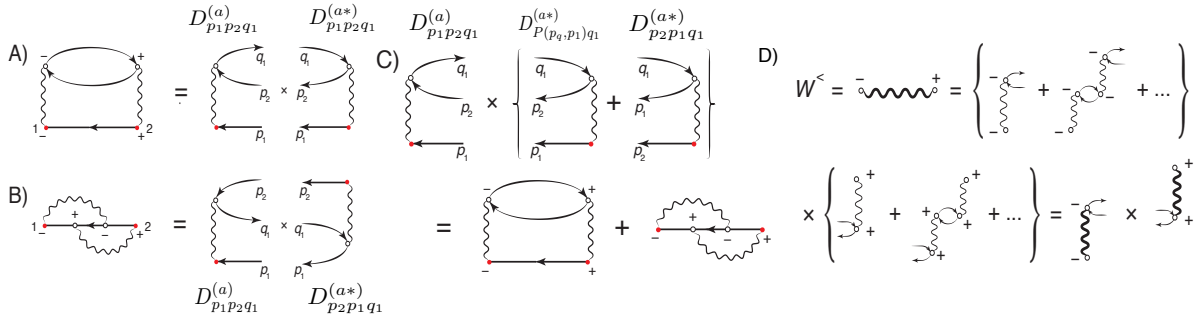

Figure 3.28: A) Partition of first order bubble diagram. B) Partition of second order exchange diagram. C) PSD construction of second order exchange diagram. D) Decomposition of screened interaction $W^<$ in half-diagrams (Fig. from Stefanucci et al. Phys. Rev. B **90** 115134 (2014) [4] and from Uimonen *et al.* Phys. Rev. B **91** 115104 (2015) [5].

Another common self-energy approximation occurring in MBPT is the second-order exchange diagram shown in Fig. 3.28B. By taking the lesser component

$$\Sigma^<_c(1,2) \;=\; -\int d\mathbf{x}_3 \int d\mathbf{x}_4 w(\mathbf{x}_1,\mathbf{x}_3) G^<_{0,bx_1\mathbf{x}_4}(t_1,t_2) G^>_{0,\mathbf{x}_4\mathbf{x}_3}(t_2,t_1) G^<_{0,\mathbf{x}_3\mathbf{x}_2}(t_1,t_2) v(\mathbf{x}_4,\mathbf{x}_2) \quad (3.203)$$

and cutting along the greater and lesser Green's function lines, we obtain the half-diagrams shown on the right hand side of the equality sign in Fig. 3.28B. We now notice that we get two partitions $D^{(a)}_{p_1p_2q_1}$ and $D^{(a*)}_{p_2p_1q_1}$ that differ by the permutation of p_1 and p_2 labels for the in-going Green's function lines. In order to make the spectra produced by the second-order exchange self-energy PSD we need to add a half diagram with permuted p_1 and p_2 labels $D^{(a*)}_{P(p_1,p_2)q_1}$, where P denotes the permutations of p labels as $P(p_1,p_2) = (p_2,p_1)$ as shown in Fig. 3.28C. We can now write the PSD form of the second order exchange self-energy as

$$\Sigma^<_c(1,2) = i\sum_{\underline{pq}} (-)^P D^{(a)}_{p_1p_2q_1}(2) D^{(a)*}_{p_2p_1q_1}(1), \quad (3.204)$$

where $D^{(a)}_{p_1p_2q_1}$ is the same half-diagram as in Eq. (3.202). Thus, the second-order exchange self-energy is not PSD. To obtain the PSD self-energy from the 2nd order exchange diagram we need to add the first order bubble diagram to our self-energy approximation. To elaborate the connection between the equation (3.204) and the general expression for the PSD self-energy Eq. (3.182) we will find the smallest subgroups $\tilde{\pi}$ and product sets $\tilde{I} \times \tilde{I}$. The smallest subgroup for P permutations of π_2 which contains P is π_2 itself. Furhermore, we have $j_1 = a$ and $j_2 = a$ which is already of the form $\tilde{I}_1 \times \tilde{I}_1$. Therefore, we can form a PSD self-energy by taking $\tilde{I}_1 = \{a\}$, $\tilde{\pi}_{2,p} = \pi_2$ and $\tilde{\pi}_{1,q} = \{1\} = \pi_1$. In this way we end up with the diagrams shown in Fig. 3.28C. An important conclusion of this example is that a conserving self-energy approximation does not need to a PSD approximation. The second order exchange self-energy being the simplest example of a conserving self-energy which is not PSD. Furthermore, we note that the

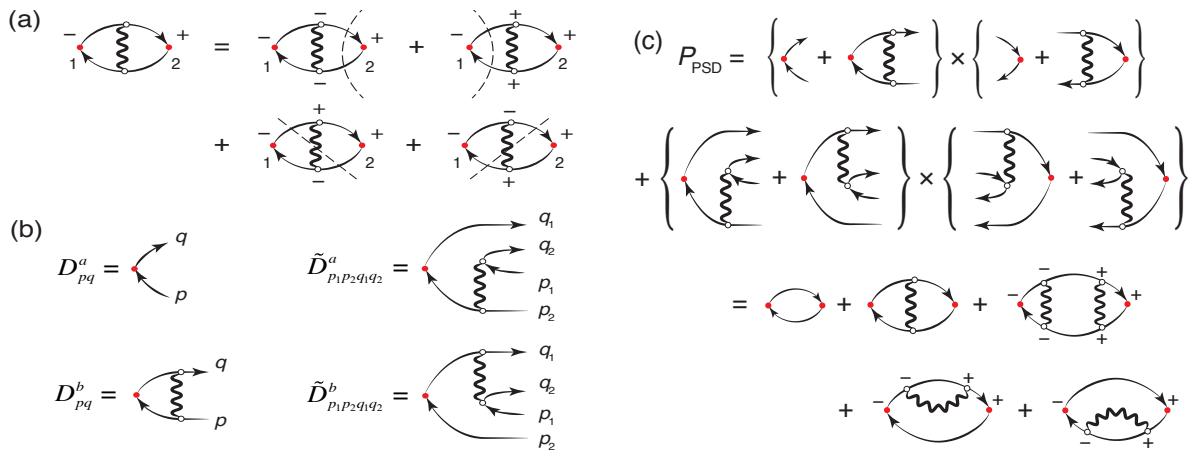

Figure 3.29: (a) Decomposition the vertex diagram for the response function with screens interaction lines into half-diagrams. (b) Constituent half-diagrams. (c) Resulting PSD polarizability (Fig. from Uimonen *et al.* Phys. Rev. B **91** 115104 (2015) [5].

GW and T-matrix approximations will be PSD approximations as shown in reference [4]. In Fig. 3.28D we also demonstrate how to write the screened interaction into half-diagrams.

The next example consists of the fist order vertex diagram for the response function with screened interaction $\mathcal{W}$ (see Fig. 3.29). We start again by taking the lesser component of the Feynman diagram. In this case, since the screened interaction $\mathcal{W}$ is non-local in time and we can have different times at the internal vertices (compare with the bare Coulomb interaction which is instantaneous in time, therefore forcing the time-arguments to be at the same time for both ends of the interaction). We can now partition the lesser vertex diagram (Fig. 3.29a) into half-diagrams along the greater and lesser Green's function lines. The greater and lesser screened interactions $\mathcal{W}^{\gtrless}$ will be partitioned as illustrated in the Fig. 3.28D. The cutting procedure results half-diagrams illustrated in Fig. 3.29b. The cutting of the screened interaction ($\mathcal{W}$ lines) results half-diagrams with four dangling lines. Thus, in this example we have two half-diagrams with one particle-hole (ph) line ($D^{(a)}_{pq}$ and $D^{(b)}_{pq}$) and two half-diagrams with two ph-lines ($\tilde{D}^{(a)}_{p_2p_1q_2q_1}$ and $\tilde{D}^{(b)}_{p_2p_1q_2q_1}$). Therefore, for the PSD construction of the PSD response function Eq. (3.183) we have $N = 2$, *i.e.,* we have two classes of half-diagrams: (a) with one ph-line and (b) two ph-lines. We need to make both of these two classes PSD. The lesser response diagram constructed from Fig. 3.29b is

$$i\mathcal{P}^{<} = \left\{ D^{(a)}_{pq} D^{(b)*}_{pq} + D^{(b)}_{pq} D^{(a)*}_{pq} \right\} + \left\{ \tilde{D}^{(a)}_{p_2p_1q_2q_1} \tilde{D}^{(b)*}_{p_2p_1q_2q_1} + \tilde{D}^{(b)}_{p_2p_1q_2q_1} \tilde{D}^{(a)*}_{p_2p_1q_2q_1} \right\}, \tag{3.205}$$

where we omitted the integrals over the vertices for notational simplicity and we used the brackets to group the one particle hole diagrams and the two particle hole diagrams into their own respective sums for extra clarification.

The structure for the response function in Eq. (3.205) is not of the form of Eq. (3.183) and hence it is not PSD. We can construct the corresponding PSD approximation by finding the minimal set of partitions to

add in order to make the first order vertex diagram for the response function PSD. The PSD approximation can be found by taking the one ph-line diagrams and squaring them with their conjugate diagrams, as well as squaring the two ph-line diagrams with their conjugate diagrams (see Fig. 3.29C). The resulting PSD response is

$$i\mathcal{P}^{<}_{\mathrm{PSD}} = \sum_{ij=a,b} D^{(i)}_{pq} D^{(j)*}_{pq} + \sum_{ij=a,b} \tilde{D}^{(i)}_{p_1p_2q_1q_2} \tilde{D}^{(j)*}_{p_1p_2q_1q_2}, \tag{3.206}$$

where in each of the sums the indices i and j independently take values a, b. The resulting diagrammatic approximation for $\mathcal{P}$ is illustrated in Fig. 3.29c. This example demonstrates the important point that the additional diagrams do not need be skeletonic in G. In conclusion, one needs to be careful when constructing PSD approximations for dressed Green's functions and to avoid double countings one should not dress the G with the same self-energy appearing in the diagrams of the PSD polarizability.

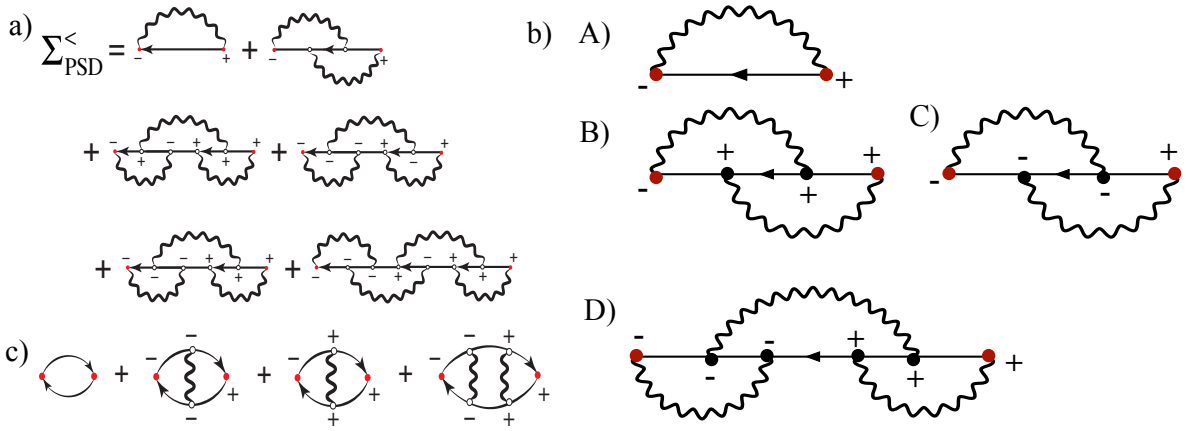

Figure 3.30: (a) PSD self-energy corresponding to the 1st order vertex correction for the self-energy. (b) A simplified PSD vertex. (c) PSD diagrams for the 1st order response function. The interaction is a bare Coulomb. (Fig (a) and (b) from Stefanucci et al. Phys. Rev. B **90** 115134 (2014) [4] Fig. (c) from Uimonen *et al.* Phys. Rev. B **91** 115104 (2015)

To this end, we demonstrate that the cutting procedure works also in practice, thanks to the impressive numerical power of Dr. Yaroslav Pavlyukh. The PSD approximation corresponding to the first order vertex function with bare coulomb interaction lines is demonstrated in Fig. 3.30a. We see that in order to make the spectra positive we need to include diagrams which are of fourth order in interaction. However, we notice that we can write a simplified vertex shown in Fig. 3.30b. The numerical results corresponding to this approximation are shown in Fig. 3.31a. The green curve corresponds to the contribution coming from the first order diagram (A) of Fig. 3.30b, while the red curve corresponds to the contribution from second order diagrams (B) and (C) of Fig. 3.30b. The contribution from these is seen to be negative. The contribution from third order diagram (D) of Fig. 3.30b is denoted by the blue curve. The sum of all these contributions to the spectra is denoted by the black curve which is PSD.

The PSD approximation corresponding to the first order vertex correction to the response function with bare Coulomb interaction lines is shown in Fig. 3.30b. We see that in order to make the spectra PSD

we need to include terms which are of second oder in the interaction. The numerical results are shown in Fig. 3.31b. In the upper left panel we show the contribution from the zeroth order term, which is the Lindhard function. The contribution from the first order term is shown in the upper right panel of Fig. 3.31b. We see that this approximation has a domain with negative spectrum. The contribution from the second order term is illustrated in the lower left panel of Fig. 3.31b while the sum of all three orders is demonstrated in the lower right panel of Fig. 3.31b which we see to be PSD.

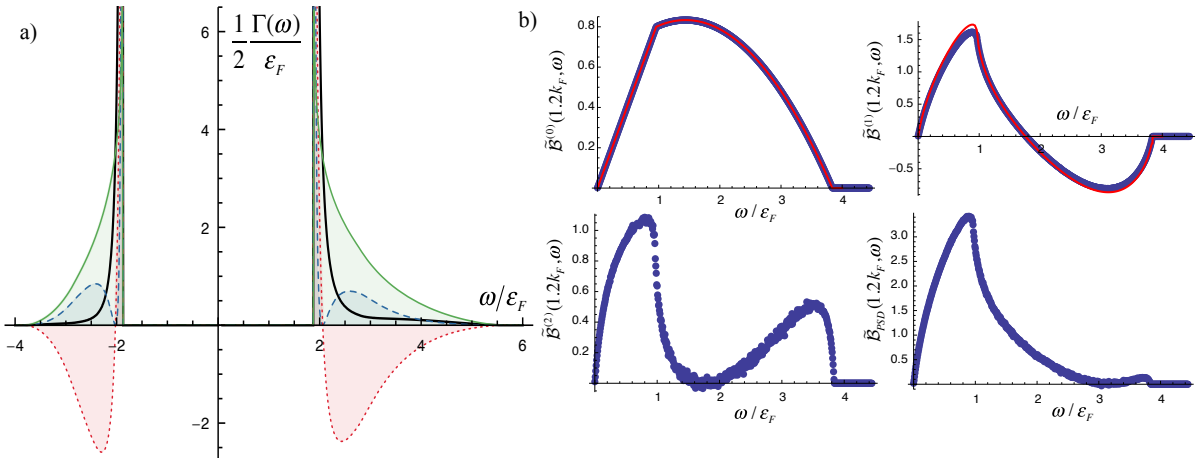

Figure 3.31: (a) The rate operator $\frac{1}{2}\Gamma(k,\omega) = -\mathrm{Im}\,\Sigma_c^{\mathrm{R}}(k,\omega)$ for a different momentum $k = 1.2k_F$ (b) The spectral function for the polarizability $\mathcal{P}$ of homogeneous electron gas at $r_s = 3$. Top left: zeroth order contribution $\tilde{\mathcal{B}}^{(0)}$. Top right: first order contribution $\tilde{\mathcal{B}}^{(1)}$. Bottom left: second order contribution $\tilde{\mathcal{B}}^{(2)}$. Bottom right: the sum of all three contributions $\tilde{\mathcal{B}}_{\mathrm{PSD}}$ which is positive. Dots (blue) denote numerical Monte Carlo results. Solid lines (red) stand for analytical results. (Fig. (a) from Stefanucci et al. Phys. Rev. B **90** 115134 (2014) [4] Fig. (b) from Uimonen *et al.* Phys. Rev. B **91** 115104 (2015) [5]).

4

DENSITY FUNCTIONAL THEORY

Ground state density functional theory (DFT) has been one of the most used theories in condensed matter physics and quantum chemistry in past decades due to its power, if applied carefully, to calculate ground state properties of various electronic systems, yielding especially good estimates for the ground state charge density and ground state energy. The original idea behind DFT, introduced by Hohenberg, Kohn and Sham in the 1960s [128, 129], is to describe the system via the density. Therefore, the complexity of the problem is reduced from the many particle Schrödinger equation for ground state Ψ_0

$$\hat{H}\Psi_0(\mathbf{x}_1, ..., \mathbf{x}_N) = \left(\hat{T} + \hat{w} + \hat{v}\right) \Psi_0(\mathbf{x}_1, ..., \mathbf{x}_N) = E\Psi_0(\mathbf{x}_1, ..., \mathbf{x}_N)$$

to an effective one-particle problem, where each quantum mechanical observable is written as a functional of the density [34, 35, 36, 38, 37, 40, 41]. In the Hamiltonian $\hat{T}$ denotes the kinetic energy operator, $\hat{w}$ is the electron-electron interaction term and $\hat{v}$ is the external potential.

The Hohenberg-Kohn theorem states that for a finite interacting many-particle system there exists a one-to-one correspondence between the external potential $v(\mathbf{r})$ and the ground-state density $n(\mathbf{r})$. This means that the external potential is a unique functional of the ground-state density $n(\mathbf{r})$ up to an arbitrary constant [128, 39]. This one-to-one correspondence implies that the external potential and the ground state density are conjugated variables, which allows us to use the total energy functional

$$E[v] = \langle \Psi([v], \mathbf{r}) | \hat{T} + \hat{w} + \hat{v} | \Psi([v], \mathbf{r}) \rangle, \tag{4.1}$$

where the expectation value is taken with respect to normalized antisymmetrized N-particle wave functions Ψ in a such a way that the total energy is minimized for a given density. The total energy functional is associated with a given external potential $v(\mathbf{r})$ to the electron density $n(\mathbf{r})$ via the Legendre Transform

$$F[n] = E[v] - \int d\mathbf{r}\, v(\mathbf{r}) n(\mathbf{r}) = \langle \Psi([v], \mathbf{r}) | \hat{T} + \hat{w} | \Psi([v], \mathbf{r}) \rangle \tag{4.2}$$

where the external potential v now depends on the density, since by utilizing the Hellmann-Feynman theorem we see that $\frac{\delta E[v]}{\delta v(\mathbf{r})} = n(\mathbf{r})$ and $\frac{\delta F[n]}{\delta n(\mathbf{r})} = -v(\mathbf{r})$. It is to be noted that $F[n]$ is defined for v-representable densities, *i.e.,* which densities that are obtainable by solution of Schrödinger equation. The derivation is also valid for $\hat{w} = 0$. In that case we consider a non-interacting system, with density n, which we will call the Kohn-Sham (KS) system. Then the functional $F[n]$ is denoted by $T_{\text{KS}}[n] = \langle \Psi_{\text{KS}}[n] | \hat{T} | \Psi_{\text{KS}}[n] \rangle$ and has the property $\frac{\delta T_{\text{KS}}[n]}{\delta n(\mathbf{r})} = v_{\text{KS}}(\mathbf{r})$, where $v_{\text{KS}}(\mathbf{r})$ is the potential that produces density $n(\mathbf{r})$ in non-interacting system and the wave function $\Psi_{\text{KS}}[n]$ corresponds the ground state. Since the interaction term $\hat{w}$ is zero the total Hamiltonian for the KS system $\hat{H}_{\text{KS}}$ will be a sum of the kinetic and the potential terms and we can write the total energy functional as

$$E_{\text{KS}}[n] = T_{\text{KS}}[n] + \int d\mathbf{r}\, v_{\text{KS}}(\mathbf{r}) n(\mathbf{r}). \tag{4.3}$$

Separating the KS kinetic energy and the Hartree potential from the universal functional $F[n]$ we can define the *exchange-correlation* functional $E_{xc}[n]$ as

$$E_{\text{xc}}[n] = F[n] - T_{\text{KS}}[n] - \frac{1}{2} \int d\mathbf{r} d\mathbf{r}' n(\mathbf{r}) n(\mathbf{r}') w(|\mathbf{r} - \mathbf{r}'|). \tag{4.4}$$

If we differentiate the *exchange-correlation* functional with respect to the density, we obtain the exchange-correlation potential. Via this relation we can define the KS potential as the sum of external potential v, Hartree potential v_{H} and the exchange-correlation potential v_{xc}

$$v_{\text{KS}}([n], \mathbf{r}) = v(\mathbf{r}) + \int d\mathbf{r}'\, n(\mathbf{r}') w(|\mathbf{r} - \mathbf{r}'|) + v_{\text{xc}}([n], \mathbf{r}). \tag{4.5}$$

Explicitly written, the *exchange-correlation potential* $v_{\text{xc}}(\mathbf{r})$ is defined as

$$v_{\text{xc}}([n], \mathbf{r}) = \frac{\delta E_{\text{xc}}[n]}{\delta n(\mathbf{r})}. \tag{4.6}$$

The exchange-correlation energy is a sum of exchange energy $E_{\text{x}}[n]$ and correlation energy $E_c[n]$, where the exchange energy functional is defined as difference between the contribution to the total energy from the electron-electron repulsion and the Hartree energy functional as

$$E_{\text{x}}[n] = \langle \Psi_{\text{KS}}([n], \mathbf{r}) | \hat{w} | \Psi_{\text{KS}}([n], \mathbf{r}) \rangle - E_{\text{H}}[n] \tag{4.7}$$

with

$$E_{\text{H}}[n] = \frac{1}{2} \int d\boldsymbol{r} \int d\boldsymbol{r}'\, n(\boldsymbol{r}) n(\boldsymbol{r}') w(|\boldsymbol{r} - \boldsymbol{r}'|). \tag{4.8}$$

For a system of non-interacting particles we can write the ground-state wave function as a Slater determinant, *i.e.* as an anti-symmetrized product of single-particle orbitals $\phi_i(\mathbf{r})$ allowing us to write the Shcrödinger equation as a set of single-particle Kohn-Sham equations

$$\left(-\frac{1}{2}\nabla^2 + v(\mathbf{r}) + \int d\mathbf{r}'\, n(\mathbf{r}')w(|\mathbf{r}-\mathbf{r}'|) + v_{\text{xc}}(\mathbf{r}')\right)\phi_i(\mathbf{r}) = \varepsilon_i\phi_i(\mathbf{r}) \tag{4.9}$$

where ε_i is the KS orbital eigenvalue and the ground state density is obtained from the N lowest occupied single-particle orbitals as $n(\mathbf{r}) = \sum_{i=1}^{N}|\phi_i(\mathbf{r})|^2$. This is the Kohn-Sham description of non-interacting particles moving in effective local single-particle Kohn-Sham potential $\hat{v}_{\text{KS}} = \hat{v} + \hat{v}_{\text{H}} + \hat{v}_{\text{xc}}$ where the complicated many-particle effects are hidden in the exchange-correlation potential v_{xc}. The exact form of the exchange-correlation potential as well as the exchange-correlation energy functional are unknown and in practice these quantities need to be approximated. When compared to the self-energy approximations in the many-body perturbation theory, the main drawback is that DFT lacks strategies allowing systematically to construct approximations for the exchange-correlation terms, except only at a formal level with the use of many-body perturbation theory [130, 131]. The lack of systematics can sometimes be also an advantage since one might find clever shortcuts in deriving better and more accurate functionals.

4.1 TIME-DEPENDENT DENSITY-FUNCTIONAL THEORY

Despite the success of DFT, it is only a ground state theory. To be able to describe time-dependent processes we need to go beyond ground state DFT to time-dependent density-functional theory (TDDFT) [132, 133, 134, 135, 136]. TDDFT is based on the Runge-Gross theorem [132, 133, 134] which states that the time-dependent potential $v(\mathbf{r},t)$ is a functional of the time-dependent density $n(\mathbf{r},t)$ up to a time-dependent constant. In other words two densities $n(\mathbf{r},t)$ and $n'(\mathbf{r}',t)$ evolving from a common initial state Φ_0 under two different external potentials $v(\mathbf{r},t)$ and $v'(\mathbf{r},t) \neq v(\mathbf{r},t) + c(t)$ will become different infinitesimally later than t_0. The time-dependent constant is related to a time-dependent phase factor since the external potential determines the time-dependent wave function which can be seen as a functional of the time-dependent density modulo a phase. Therefore, the expectation value of an operator $\hat{O}(t)$ is a unique functional of the density since the ambiguity of the phase cancels out. The one-to-one correspondence only ensures the uniqueness of $v([n],\mathbf{r},t)$ for all v-representable densities but not its existence for an arbitrary $n(\mathbf{r},t)$. The Runge-Gross theorem is not a simple extension of the Hohenberg-Kohn theorem, which is based on the Rayleigh-Ritz variational principle for the ground state energy which is not well defined on the time-dependent case, and the proof is based directly to the time-dependent Schrödinger equation [132, 133, 134].

Extensions of the Runge-Gross theorem [133, 134] guarantee that the time-dependent density $n(\mathbf{r},t)$ of an interacting system evolving under a time-dependent potential $v(\mathbf{r},t)$ from an initial state Ψ_0 can be described in terms of the time-dependent non-interacting density moving in a effective time-dependent potential $v_{\text{KS}}[n,\Psi_0,\Phi_0](\mathbf{r},t)$ [39, 137], where Φ_0 is the non-interacting initial state. The Kohn-Sham

potential in analogy with stationary KS-theory can be written as

$$v_{\text{KS}}[n](\mathbf{r},t) = v[n](\mathbf{r},t) + \int d^3\boldsymbol{r}' \frac{n(\mathbf{r}',t)}{|\mathbf{r}-\mathbf{r}'|} + v_{\text{xc}}[n](\mathbf{r},t) \tag{4.10}$$

where v is again the external potential, the second term on the right hand side is the time-dependent Hartree potential, and as in the static case the exchange-correlation effects are incorporated via the exchange-correlation potential $v_{\text{xc}}[n](\mathbf{r},t)$ which now is time-dependent and is even more involved than static case due to the involvement of non-local memory effects. Most of the applications of TDDFT are in the regime of linear response and utilize the fact that the excitation energies of a finite system are obtained as finite poles $\Omega = E_i - E_0$ of the density response function [138, 139, 135, 140].

In the time-dependent situation it is not possible to define the exchange-correlation potential as a functional derivative of the exchange-correlation energy functional, since if we assume that $v_{\text{xc}}(\mathbf{r},t)$ is obtainable from some action functional $A_{\text{xc}}[n]$ as

$$v_{\text{xc}}(\mathbf{r},t) = \frac{\delta A_{\text{xc}}[n]}{\delta n(\mathbf{r},t)} \tag{4.11}$$

would this mean that

$$\frac{\delta v_{\text{xc}}(\mathbf{r},t)}{\delta n(\mathbf{r}',t)} = \frac{\delta^2 A_{\text{xc}}[n]}{\delta n(\mathbf{r},t)\delta n(\mathbf{r}',t)} \tag{4.12}$$

where the right hand side is symmetric under interchange of the coordinates but the left hand side is not due to the causality requirement of the KS-potential [141, 142]. Due to this contradiction the exchange-correlation potential cannot be written as a functional derivative of any functional. The contradiction between symmetry and causality can only be circumvented by constructing an action functional on the

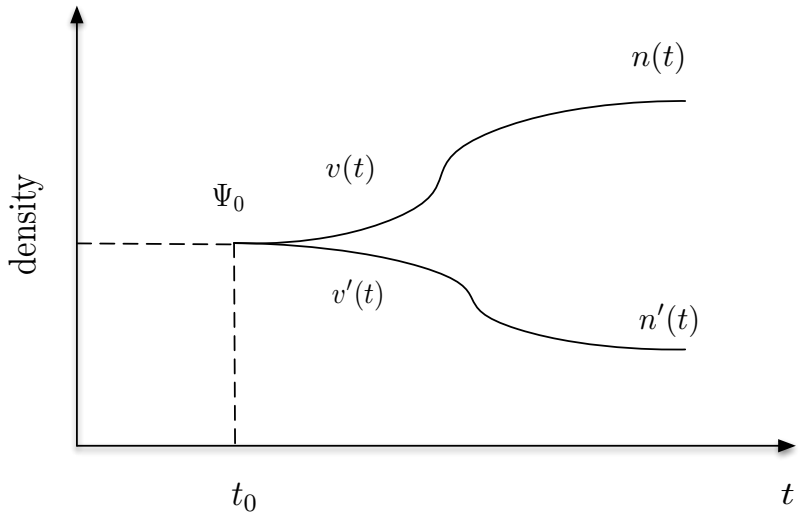

Figure 4.1: Graphical illustration of the Runge-Gross theorem.

Keldysh contour [143, 137] which allows us to define the time-dependent density functional as a Legendre transformation on the Keldysh contour $\mathcal{C}$ (see also section 4.2 in chapter 4).

In a similar fashion as in the static DFT, we can also derive the time-dependent Kohn-Sham (KS) equations. Assuming that the initial state wave function Ψ_0 can be written as a Slater determinant of the single-particle orbitals we can write the time-dependent Schrödinger equation as a set of single particle equations

$$i\partial_t \phi_j(\mathbf{r},t) = \left(-\frac{1}{2}\nabla^2 + v([n],\mathbf{r},t) + \int d^3\mathbf{r}' \frac{n(\mathbf{r}',t)}{|\mathbf{r}-\mathbf{r}'|} + v_{\text{xc}}([n],\mathbf{r},t)\right)\phi_j(\mathbf{r},t) \tag{4.13}$$

where initial orbital ϕ_j^0 is obtained form solving the stationary KS-equations. The time-dependent density is now given as the sum over time-dependent occupied orbitals $n(\mathbf{r},t) = \sum_{j=1}^{N} |\phi_j(\mathbf{r},t)|^2$. In the time-dependent KS scheme we have to assume non-interacting v-representability, *i.e*, we have to assume that a potential v_s exists that produces the time-dependent density of the interacting system of interest.

THE EXCHANGE-CORRELATION KERNEL

In the linear response regime we perturb the system by a sufficiently small external potential $\delta v(\mathbf{r}_1,t_1)$ which is zero for times t_1 before some initial time t_0 at which the perturbation is switched on. Thus, the total external potential in the linear response regime is $v(\mathbf{r}_1,t_1) = v_0(\mathbf{r}_1) + \delta v(\mathbf{r}_1,t_1)$, where $v_0(\boldsymbol{r})$ is the time-independent external potential. The one-to-one correspondence between the time-dependent potentials and the time-dependent densities provided by the Runge-Gross theorem allows us to formally write the time-dependent external potential as a functional of the density $v(\mathbf{r}_1 t_1) = v([n],\mathbf{r}_1,t_1)$, while from the time-dependent Schrödinger equation it follows that the time-dependent density can be seen as a functional of the external potential as $n(\mathbf{r}_1,t_1) = n([v],\mathbf{r}_1,t_1)$. For small perturbations δv we can expand the density $n([v],\mathbf{r}_1,t_1)$ as Taylor series around the perturbation δv. Retaining only the first order term we obtain the first order density response as

$$\delta n(\mathbf{r}_1,t_1) = \int d\mathbf{r}_2 \int dt_2\, \chi(\mathbf{r}_1,t_1;\mathbf{r}_2,t_2)\delta v(\mathbf{r}_2,t_2) \tag{4.14}$$

where χ is the density response function, defined as the functional derivative of the time-dependent density with respect to the time-dependent perturbation

$$\chi(\mathbf{r}_1,t_1;\mathbf{r}_2,t_2) = \frac{\delta n[v](\mathbf{r}_1,t_1)}{\delta v(\mathbf{r}_2,t_2)}. \tag{4.15}$$

Naturally, the Runge-Gross theorem holds also for the non-interacting particles moving in an external field proceeded by the KS potential $v_{\text{KS}}[n](\mathbf{r}_1,t_1)$, implying it to be invertible as well, *i.e.,* $v_{\text{KS}}(\mathbf{r},t) = v_{\text{KS}}[n](\mathbf{r},t)$ and $n(\mathbf{r},t) = n[v_{\text{KS}}](\mathbf{r},t)$. Furthermore, since the KS system has the same density as the true interacting system, there exist an analogous relation to Eq. (4.14) for KS particles

$$\delta n(\mathbf{r}_1,t_1) = \int d\mathbf{r}_2 \int dt_2\, \chi_{\text{KS}}(\mathbf{r}_1,t_1;\mathbf{r}_2,t_2)\delta v_{\text{KS}}(\mathbf{r}_2,t_2). \tag{4.16}$$

where the KS response function is defined as

$$\chi_{\text{KS}}(\mathbf{r}_1, t_1; \mathbf{r}_2, t_2) = \left.\frac{\delta n([v_{\text{KS}}], \mathbf{r}_1, t_1)}{\delta v_{\text{KS}}(\mathbf{r}_2, t_2)}\right|_{v_{\text{KS}}[n_0]}. \tag{4.17}$$

and evaluated with the density n_0 corresponding to the time-independent potential v_0. We can relate the response function χ of the true interacting system to the KS response function by applying a chain rule for the functional derivative of the density with respect to the external potential in Eq. (4.15) as

$$\chi(\mathbf{r}_1, t_1; \mathbf{r}_2, t_2) = \int d\mathbf{r}_3 \int dt_3 \frac{\delta n([v], \mathbf{r}_1, t_1)}{\delta v_{\text{KS}}(\mathbf{r}_3, t_3)} \frac{\delta v_{\text{KS}}(\mathbf{r}_3 t_3)}{\delta v(\mathbf{r}_2, t_2)}. \tag{4.18}$$

where the functional derivative of the KS potential with respect to the external potential reads explicitly as

$$\begin{aligned} \left.\frac{\delta v_{\text{KS}}(\mathbf{r}_1, t_1)}{\delta v(\mathbf{r}_2, t_2)}\right|_{v_{\text{KS}}[n_0]} &= \delta(\mathbf{r}_1 - \mathbf{r}_2)\delta(t_1 - t_2) \\ &+ \int d\mathbf{r}_3 \int dt_3 \left(w(\mathbf{r}_1 t_1, \mathbf{r}_3 t_3) + \frac{\delta v_{\text{xc}}(\mathbf{r}_1, t_1)}{\delta n(\mathbf{r}_3, t_3)} \right) \frac{\delta n(\mathbf{r}_3, t_3)}{\delta v(\mathbf{r}_2, t_2)}. \end{aligned} \tag{4.19}$$

where $w(\mathbf{r}_1 t_1, \mathbf{r}_2 t_2) = \delta(t_1 - t_2)/|\mathbf{r}_1 - \mathbf{r}_2|$ is the Coulomb interaction. Combining the above equations gives us a Dyson-type equation relating the true interacting response function to the non-interacting KS response function

$$\begin{aligned} \chi(\mathbf{r}_1, t_1; \mathbf{r}_2, t_2) &= \chi_{\text{KS}}(\mathbf{r}_1, t_1; \mathbf{r}_2, t_2) \\ &+ \int d\mathbf{r}_3 \int dt_3 \left[w(\mathbf{r}_1 t_1, \mathbf{r}_3 t_3) + f_{\text{xc}}([n_0], \mathbf{r}_1, t_1; \mathbf{r}_3, t_3) \right] \chi(\mathbf{r}_3, t_3; \mathbf{r}_2, t_2) \end{aligned} \tag{4.20}$$

where we defined the exchange correlation kernel f_{xc} as a functional of the ground state density as

$$f_{\text{xc}}[n_0](\boldsymbol{r}_1, t_1; \boldsymbol{r}_2, t_2) = \left.\frac{\delta v_{\text{xc}}(\boldsymbol{r}_1, t_1)}{\delta n(\mathbf{r}_2, t_2)}\right|_{n_0(\mathbf{r})}. \tag{4.21}$$

Due to the one-to-one correspondence between the density and the KS potential we can see that the exchange-correlation kernel relates the change in xc potential due to the change in density n as

$$\delta v_{\text{xc}}(\boldsymbol{r}_1, t_1) = \int d\mathbf{r}_2 \int dt_2 \left.\frac{\delta v_{\text{xc}}([n], \mathbf{r}, t)}{\delta n(\mathbf{r}_2, t_2)}\right|_{n_0(\mathbf{r})} \delta n(\mathbf{r}_2, t_2). \tag{4.22}$$

It can be shown that the interacting and non-interacting response functions depend only on the difference between the time-arguments which will imply similar dependence for the xc-kernel and can be therefore Fourier transformed [39] giving us the definition of the frequency-dependent xc-kernel

$$f_{\text{xc}}(\mathbf{r}_1, \mathbf{r}_2, \omega) = \int d(t_1 - t_2) e^{i\omega(t_1 - t_2)} \left.\frac{\delta v_{\text{xc}}([n], \mathbf{r}_1, t_1)}{\delta n(\mathbf{r}_2, t_2)}\right|_{n_0(\mathbf{r})}. \tag{4.23}$$

SHAM-SCHLÜTER EQUATION

Another concept within TDDFT what we will to utilize later in the discussion of quantum transport results is the Sham-Schlüter equation relating the exchange-correlation potential to the many-body self-energy. The Sham-Schlüter equation can be derived by taking the equation of motion for the full interaction Green's function (Eq. (3.51)) and solving the Dyson equation with the KS reference Green's function. The KS Green's function satisfies the following equation of motion

$$\left(i\partial_{z_1} - \hat{h}_{\text{KS}}(\boldsymbol{r}_1, z_1)\right) G^{\text{KS}}(\boldsymbol{r}_1, z_1; \boldsymbol{r}_2, z_2) = \delta(\boldsymbol{r}_1 - \boldsymbol{r}_2)\delta(z_1, z_2) \tag{4.24}$$

where the KS-hamiltonian is a sum of kinetic energy term and the KS potential, *i.e.*, $\hat{h}_{KS} = \hat{t} + v_{\text{KS}}$. This yield the following equation for the fully self-consistent Green's function

$$\begin{aligned} G(\mathbf{r}_1, z_1; \mathbf{r}_2, z_2) &= G^{\text{KS}}(\mathbf{r}_1, z_1; \mathbf{r}_2, z_2) + \int \mathrm{d}\mathbf{r}_3 d\mathbf{r}_4 \int_{\mathcal{C}} dz_3 dz_4 G^{\text{KS}}(\mathbf{r}_1 z_1, \mathbf{r}_3 z_3)[\Sigma_{\text{xc}}(\mathbf{r}_3 z_3, \mathbf{r}_4 z_4) \\ &- \delta(z_3, z_4)\delta(\mathbf{r}_3 - \mathbf{r}_4) v_{\text{xc}}(\mathbf{r}_4, z_4)] G(\mathbf{r}_4, z_4; \mathbf{r}_2, z_2). \end{aligned} \tag{4.25}$$

Since the exact density is given by both the KS and the exact Green's function, *i.e.*,

$$n(\mathbf{r}, z) = -iG(\mathbf{r}, z; \mathbf{r}, z^+) = -iG^{\text{KS}}(\mathbf{r}, z; \mathbf{r}, z^+), \tag{4.26}$$

it follows that

$$\begin{aligned} &\int d\mathbf{r}_3 \int_{\mathcal{C}} \mathrm{d}z_3\, G^{\text{KS}}(\mathbf{r}_1, z_1; \mathbf{r}_3, z_3) v_{\text{xc}}(\mathbf{r}_3, z_3) G(\mathbf{r}_3, z_3; \mathbf{r}_1, z_1) \\ &= \int d\mathbf{r}_3 d\mathbf{r}_4 \int_{\mathcal{C}} \mathrm{d}z_3 \mathrm{d}z_4\, G^{\text{KS}}(\mathbf{r}_1, z_1; \mathbf{r}_3, z_3) \Sigma_{\text{xc}}(\mathbf{r}_3, z_3; \mathbf{r}_4, z_4) G(\mathbf{r}_3, z_3; \mathbf{r}_1, z_1), \end{aligned} \tag{4.27}$$

where Σ_{xc} is the many-body self-energy with the Hartree potential subtracted. If the self-energy is exact then the corresponding xc-potential that solves this Sham-Schlüter equation [131] yields the exact density of the system.

THE ADIABATIC LOCAL DENSITY APPROXIMATION

To perform practical calculations within TDDFT we need to approximate the exchange-correlation potential v_{xc} somehow. The simplest approximation for the v_{xc} potential is the adiabatic local density approximation (ALDA) given as

$$v_{\text{xc}}^{ALDA}(\mathbf{r}, t) = \left.\frac{d\varepsilon_{xc}^{h}[n]}{dn}\right|_{n=n(\mathbf{r},t)} \tag{4.28}$$

where $\varepsilon_{\text{xc}}^{h}(n)$ is the exchange-correlation energy per unit volume of homogeneous system of density n whose derivative, with respect to the density, is evaluated at the instantaneous time-dependent density

$n(\mathbf{r},t)$ which means that ALDA is local in time and in space, *i,.e.,*

$$\frac{\delta v_{\rm xc}([n],t)}{\delta n(t')} = \delta(t-t')\frac{dv_{\rm xc}(n)}{dn}. \tag{4.29}$$

Therefore, ALDA neglects the memory effects. Despite its simplicity ALDA performs quite well even for systems which are not slowly varying in space and time [144, 1].

In the lattice systems we can construct a BALDA approximation for the xc-potential, which is based on the local density approximation (LDA) for the static, non-uniform one-dimensional Hubbard model derived from the Bethe ansatz, (Bethe ansatz LDA, BALDA). From the Bethe-ansatz solution for the 1D Hubbard model below the half-filling of the energy band we have the following total energy expressions for the limiting cases $U \to \infty$ and $U = 0$

$$\varepsilon^{<}(n, U\to\infty) = -\frac{2V}{\pi}\sin(\pi n) \tag{4.30}$$

$$\varepsilon^{<}(n, U=0) = -\frac{4V}{\pi}\sin\left(\frac{\pi}{2}n\right) \tag{4.31}$$

where the superscript " $<$ " denotes below the half-filling, V is the hopping between sites and U is the on-site interaction strength. The analytical formula for the total energy at half-filling is

$$\varepsilon^{n=1}(U) = -4\int_0^\infty \frac{J_0(x)J_1(x)}{x(1+\exp(Ux/2))}dx \tag{4.32}$$

as given by Lieb and Wu [145]. Here $J_{i=0,1}(x)$ are Bessel functions. Capelle *et al.* [146] showed that for the infinite Hubbard chain the total energy density can be interpolated from the limiting cases

$$\varepsilon^{<}(n,U) = -\frac{2\xi(U)}{\pi}\sin\left(\frac{\pi n}{\xi(U)}\right) \tag{4.33}$$

where the parameters ξ is determined from the solution at half-filling

$$-\frac{2\xi}{\pi}\sin\left(\frac{\pi}{\xi}\right) = -4\int_0^\infty \frac{J_0(x)J_1(x)}{x[1+\exp(Ux/2)]}dx \tag{4.34}$$

to guarantee the correct result at the particle-hole symmetric point. In the transport situation the parameter U/V_{link}, where V_{link} is the coupling between central region and leads, determines the strength of the correlations and therefore in the modified version of ABALDA for the transport setup [147] we need to take into account the different hopping between the impurity site and the leads. For the transport problem the half-filling condition therefore takes the form

$$\frac{2\xi}{\pi}\sin(\pi/\xi) = 4\int_0^\infty {\rm d}x\,\frac{J_0(x)J_1(x)}{x[1+\exp(Ux/(2\,V_{\rm link}))]}. \tag{4.35}$$

We can obtain the exchange correlation energy from the total energy by utilizing the symmetry relation for the 1D Hubbard chain around the half-filling point *i.e.,* $\varepsilon^{>}_{\rm xc}(n) = \varepsilon^{<}_{xc}(2-n)$. Since, the total energy

is a sum of the kinetic, Hartree and exchange energy, we can obtain the exchange correlation energy by subtracting the non-interacting kinetic energy and the Hartree energy from the total energy

$$\varepsilon_{\rm xc}(n,U) = \varepsilon(n,U) - \varepsilon(n,U=0) - \varepsilon_{\rm H}(n,U) \tag{4.36}$$

where the kinetic energy is obtained from the total energy for non-interacting particles. By differentiating with respect to the density we obtain the exchange-correlation potential for BALDA as

$$v_{\rm xc}^{\rm BALDA}[n] = \theta(1-n)v_{\rm xc}^{<}(n) - \theta(n-1)v_{\rm xc}^{<}(2-n), \tag{4.37}$$

where

$$v_{\rm xc}^{<}(n) = -\frac{1}{2}Un - 2\,V_{\rm link}\left[\cos\left(\frac{\pi n}{2}\right) - \cos\left(\frac{\pi n}{\xi}\right)\right]. \tag{4.38}$$

A particularly interesting property of the interpolated BALDA is its discontinuity at half-filling [148]: $v_{\rm xc}(1^+) - v_{\rm xc}(1^-) = U - 4V_{\rm link}\cos(\frac{\pi}{\xi})$ which can be either positive or negative depending on the parameter used as seen in Fig. 4.2 but the results are not to affected by the change in sign due to the symmetry of the dynamics of 1D Hubbard model around the particle-hole symmetric point [147].

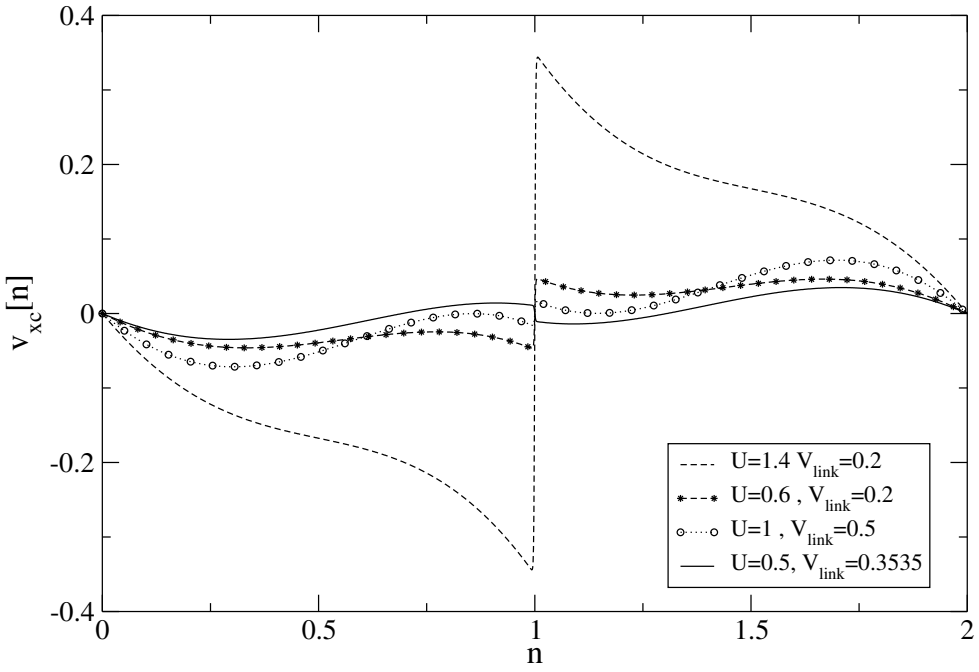

Figure 4.2: The BALDA XC-potential as a function of the density.

4.2 TIME-DEPENDENT CURRENT DENSITY FUNCTIONAL THEORY

In this section we give a brief discussion of time-dependent current density-functional theory (TDCDFT) for the purposes of providing background for the article VII [7], where we study the diagrammatic content of the photocurrent with TDDFT. One motivation to switch from TDDFT to TDCDFT is that TDCDFT provides a natural framework to construct non-adiabatic approximations [39] for $v_{\rm xc}$ which in TDDFT lead to violation of basic theorems [39]. The problem with TDDFT is that it can break down when considering uniform local changes in density as illustrated in Fig. 4.3. Let us look at the time-dependent density at point x_0 where the system is moving in time to the right. The movement causes the density distribution to change which by continuity equation induces a flow of current. If we just observe the density at the point x_0 it is impossible to notice any change as long as the edges of the slab are far away. Thus, one needs to look at the current density to observe the movement of the slab, and a theory based on the ALDA will fail to describe this situation correctly within standard TDDFT (see Ref. [39]).

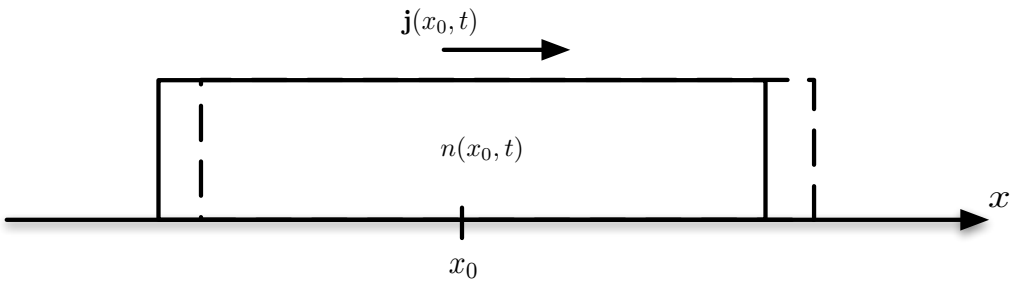

Figure 4.3: Schematics demonstrating how the local density $n(x_0,t)$ remains constant when the slabs is moving to the right while generating current $\mathbf{j}(x_0,t)$.

In TDCDFT we are considering systems which are moving in general time-dependent electromagnetic fields depending on both of the external scalar potential $v(\mathbf{r},t)$ and of the external vector potential $\boldsymbol{A}$(r,t) described by the Hamiltonian

$$\hat{H}(t)=\sum_{j=1}^{N}\left(\frac{1}{2}\left[-i\nabla_j+\boldsymbol{A}(\mathbf{r}_j,t)\right]^2+v(\mathbf{r}_j,t)\right)+\frac{1}{2}\sum_{i,j\neq i}^{N}w(\mathbf{r}_i-\mathbf{r}_j) \tag{4.39}$$

The electric $\boldsymbol{E}(\boldsymbol{r},t)$ and magnetic $\boldsymbol{B}(\boldsymbol{r},t)$ fields are naturally given in terms of the vector potential $\boldsymbol{A}(\mathbf{r},t)$ as $\boldsymbol{E}=-\nabla v(\mathbf{r},t)-\frac{\partial \boldsymbol{A}(\mathbf{r},t)}{\partial t}$ and $\boldsymbol{B}=\nabla\times\boldsymbol{A}(\mathbf{r},t)$. The electric and magnetic fields will transform under the Coulomb gauge $\nabla\cdot A=0$ as

$$v(\mathbf{r},t) \;\rightarrow\; v(\mathbf{r},t)+\frac{\partial\lambda(\mathbf{r},t)}{\partial t} \tag{4.40}$$

$$\boldsymbol{A}(\mathbf{r},t) \;\rightarrow\; \boldsymbol{A}(\mathbf{r},t)+\nabla\lambda(\mathbf{r},t) \tag{4.41}$$

which leaves the Hamiltonian invariant.

In TDCDFT one can prove that the current density $\boldsymbol{j}$ and the vector potential $\boldsymbol{A}$ will be conjugate variables *i.e.* the vector potential determines the current density uniquely up to a gauge. The proof goes in the same spirit as the Runge-Gross proof for the TDDFT. Assuming that all the potentials are Taylor expandable around the initial time t_0 one can prove that two current densities $\boldsymbol{j}_1(\mathbf{r},t)$ and $\boldsymbol{j}_2(\mathbf{r},t)$ evolving from common initial state and generated by external potentials $\{\mathbf{v}_1(\mathbf{r},t),\boldsymbol{A}_1(\mathbf{r},t)\}$ and $\{\mathbf{v}_2(\mathbf{r},t),\boldsymbol{A}_2(\mathbf{r},t)\}$ cannot be the same provided that the set of potentials differ by more than a gauge transformation of the form of the Coulomb gauge. Like for the TDDFT also for TDCDFT one can write down the Kohn-Sham equations

$$\left[\frac{1}{2}\big(-i\nabla+\boldsymbol{A}_{\text{KS}}(\mathbf{r},t)\big)^2+v_{\text{ext}}(\mathbf{r})\right]\phi_j(\mathbf{r},t)=i\partial_t\phi_j(\mathbf{r},t),$$

where we included the KS vector potential defined as

$$\boldsymbol{A}_{\text{KS}}(\mathbf{r},t)=\boldsymbol{A}(\mathbf{r},t)+\boldsymbol{A}_{\text{H}}(\mathbf{r},t)+\boldsymbol{A}_{xc}(\mathbf{r},t). \tag{4.42}$$

In TDCDFT the xc-vector potential can be obtained as functional derivative from a functional $\mathcal{F}[\boldsymbol{j}]$ defined as a Legendre transformation of the action functional $\tilde{\mathcal{F}}[\boldsymbol{A}]$ defined on the Keldysh contour $\mathcal{C}$ as

$$\tilde{\mathcal{F}}[\boldsymbol{A}]=i\ln\langle\Psi_0|\hat{U}(t_0,t_0)|\Psi_0\rangle$$

where the time-evolution operator $\hat{U}$ is defined on the Keldysh contour $\mathcal{C}$ as (here we chose a gauge such that all time-dependence is in the vector potential, this same convention is used in the article VII [7])

$$U(t,t')=T_{\mathcal{C}}\,e^{-i\int_{\mathcal{C}}dz\hat{H}(z)}, \tag{4.43}$$

where $T_{\mathcal{C}}$ denotes contour ordering on the contour $\mathcal{C}$ running from t_0 back to t_0. It is now easy to see that the functional derivative of the time-evolution operator with respect to the vector potential is

$$\frac{\delta\hat{U}(t,t')}{\delta\boldsymbol{A}(\mathbf{r},t')}=-i\hat{U}(t,t')[\hat{\boldsymbol{j}}_p(\mathbf{r})+\hat{n}\boldsymbol{A}(\mathbf{r},t')]\hat{U}(t,t'), \tag{4.44}$$

yielding the following functional derivative for the action functional

$$\frac{\delta\tilde{\mathcal{F}}}{\delta\boldsymbol{A}(\mathbf{r},z)}=\langle\hat{\boldsymbol{j}}_{\text{p}}(\mathbf{r},z)\rangle+\langle\hat{n}(\mathbf{r},z)\rangle\boldsymbol{A}(\mathbf{r},z)=\boldsymbol{j}(\mathbf{r},z), \tag{4.45}$$

where $\boldsymbol{j}_{\text{p}}$ is the paramagnetic current and $\boldsymbol{j}$ is the physical gauge-invariant current. In general the physical gauge-invariant current $\boldsymbol{j}$, which is a central object in TDCDFT, is given as

$$\boldsymbol{j}(\mathbf{r},t) = \langle\Phi(t)|\hat{\boldsymbol{j}}(\mathbf{r})|\Phi(t)\rangle = \boldsymbol{j}_p(\mathbf{r},t) + n(\mathbf{r},t)\boldsymbol{A}(\mathbf{r},t), \tag{4.46}$$

where $\Phi(t)$ is time-dependent many-particle wave function and $\boldsymbol{j}_p$ is the paramagnetic current density and the second term in the right hand side is the diamagnetic current density. Since the vector potential and the current density are conjugate variables we obtain current functional $\mathcal{F}[\boldsymbol{j}]$ by a Legendre transform

$$\mathcal{F}[\boldsymbol{j}] = -\tilde{\mathcal{F}}[\boldsymbol{A}] + \int d\mathbf{r} \int_{\mathcal{C}} dz\, \boldsymbol{j}(\mathbf{r},z)\cdot\boldsymbol{A}(\mathbf{r},z) \tag{4.47}$$

such that

$$\frac{\delta\mathcal{F}[\boldsymbol{j}]}{\delta\boldsymbol{j}(\mathbf{r},z)} = \boldsymbol{A}(\mathbf{r},z). \tag{4.48}$$

Similarly, as in the static DFT for the universal functional, we can start from the non-interacting system with $|\Psi_{0,s}\rangle$ and obtain a KS-current functional $\mathcal{F}_{\text{KS}}[\boldsymbol{j}]$ and define the exchange correlation part of the action function $\mathcal{F}_{\text{xc}}$ as the difference between true interacting and non-interacting functionals

$$\mathcal{F}[\boldsymbol{j}] = \mathcal{F}_{\text{KS}}[\boldsymbol{j}] - \mathcal{A}_{\text{xc}}[\boldsymbol{j}] - \frac{1}{2}\int d\mathbf{r}_1 d\mathbf{r}_2 \int_{\mathcal{C}} dt_1\, n(\mathbf{r}_1,t_1)n(\mathbf{r}_1t_1)w(|\mathbf{r}_1-\mathbf{r}_2|) \tag{4.49}$$

where w is the Coulomb interaction and the density $n(\boldsymbol{r},z)$ is regarded a functional of the current through the continuity equation. Differentiating this equation with respect to $\boldsymbol{j}$ gives us the xc-vector potential

$$\boldsymbol{A}_{\text{xc}}(\mathbf{r},t) = \boldsymbol{A}_{\text{KS}}(\mathbf{r},t) - \boldsymbol{A}(\mathbf{r},t) - \boldsymbol{A}_{\text{H}}(\mathbf{r},t) \tag{4.50}$$

where we defined

$$\boldsymbol{A}_{\text{xc}}(\mathbf{r}_1,t_1) = \frac{\delta\mathcal{F}_{\text{xc}}(\mathbf{r}_1,t_1)}{\delta\boldsymbol{j}(\mathbf{r}_2,t_2)} \tag{4.51}$$

$$\boldsymbol{A}_{\text{H}}(\mathbf{r}_1,t_1) = \frac{\delta\mathcal{F}_{\text{H}}(\mathbf{r}_1,t_1)}{\delta\boldsymbol{j}(\mathbf{r}_2,t_2)}. \tag{4.52}$$

Like in TDDFT the KS scalar potential is such a non-interacting potential which produced the density of the true system. In a same way the KS vector potential $\boldsymbol{A}_{\text{KS}}$ is the vector potential that for a non-interacting system gives the current density $\boldsymbol{j}$. We can also study the linear response with TDCDFT due to sufficiently small external perturbing vector potential and obtain the current-current response function as

$$\begin{aligned}\chi_{\mu\nu}(\boldsymbol{r}_1t_1,\boldsymbol{r}_2t_2) &= \frac{\delta\boldsymbol{j}_\mu(\boldsymbol{r}_1,t_1)}{\delta\boldsymbol{A}_\nu(\mathbf{r}_2t_2)} \\ &= \delta_{\mu\nu}n(\mathbf{r},t)\delta(t_1,t_2)\delta(\mathbf{r}_1-\mathbf{r}_2) - i\langle\mathcal{T}_{\mathcal{C}}[\Delta\hat{\boldsymbol{j}}_p(\mathbf{r}_1,t_1)\Delta\hat{\boldsymbol{j}}_p(\mathbf{r}_2,t_2)]\rangle\end{aligned} \tag{4.53}$$

where the fluctuation operator is defined as $\Delta\hat{\boldsymbol{j}}_p(\mathbf{r},t) = \hat{\boldsymbol{j}}_p(\mathbf{r},t) - \langle\hat{\boldsymbol{j}}_p(\mathbf{r},t)\rangle$. Like we did in the TDDFT section, we can now proceed via application of the chain rule and the definition for the KS vector potential and find the relation between the true response function and the KS-response function as a Dyson equation

$$\begin{aligned}\chi(\mathbf{r}_1,t_1;\mathbf{r}_2,t_2) &= \chi_{\text{KS}}(\mathbf{r}_1,t_1;\mathbf{r}_2,t_2)+\int d\mathbf{r}_3dt_3\int d\mathbf{r}_4t_4\,\chi_{\text{KS}}(\mathbf{r}_1,t_1;\mathbf{r}_2,t_2)\big[f_{\text{H}}(\mathbf{r}_3,t_3;\mathbf{r}_4,t_4)\\ &\quad +f_{\text{xc}}(\mathbf{r}_3,t_3;\mathbf{r}_4,t_4)\big]\chi(\mathbf{r}_4,t_3;\mathbf{r}_2,t_2) \qquad (4.54)\end{aligned}$$

where we defined the Hartree and exchange-correlation kernels as

$$\begin{aligned}f_{\text{H}}(\mathbf{r}_1,t_1;\mathbf{r}_2,t_2) &= \frac{\delta \boldsymbol{A}_{\text{H}}(\mathbf{r}_1,t_1)}{\delta \boldsymbol{j}(\mathbf{r}_2,t_2)}\\ f_{\text{xc}}(\mathbf{r}_1,t_1;\mathbf{r}_2,t_2) &= \frac{\delta \boldsymbol{A}_{\text{H}}(\mathbf{r}_1,t_1)}{\delta \boldsymbol{j}(\mathbf{r}_2,t_2)}. \qquad (4.55)\end{aligned}$$

This concludes our introduction regarding density functional theories used in this thesis.

4.3 GLANCE INTO PHOTOEMISSION SPECTROSCOPY

One of the fundamental questions in solid state physics is the spectrum of the one-particle and collective excitations of a system of correlated electrons. Information on the excitation spectrum of a many-particle system can be gained via photoemission spectroscopy techniques and the theoretical understanding of this spectrum constitutes a long-standing and not yet generally solved problem of many-particle physics. The complication of the theoretical description of the photo-emission process is due to several reasons. First of all the accurate description constitutes a description of the equilibrium and excited electronic structure of a many-particle system as well as the interaction of the many-particle system with the perturbing electromagnetic fields. In addition, we need to solve this problem in the vicinity of the surface, through which all system properties change dramatically.

The basic approximation done in the many-particle theoretical description of photoemission process is called the sudden approximation. In sudden approximation the photo-electron is directly excited into vacuum, *i.e.*, the electron is removed suddenly from the material without leaving any time for the system to relax. Hence, for example the many-particle effects, like the energy losses experienced by the photo-electron during its travel inside the material are neglected. Since we are removing an electron suddenly we can calculate the photoemission spectra from the single-particle spectral function $\mathcal{A}(\omega)$. The photocurrent within the sudden approximation can be obtained via Fermi's golden rule as

$$\begin{aligned}I(\mathbf{k},\omega) &\propto |\langle\Psi_{N-1}|\hat{c}_{\mathbf{k}}|\Psi_{N,0}\rangle|^2\delta(E_{N-1}+\omega-E_{N,0}-\hbar\nu)\\ &= \mathcal{A}(k,\omega-\hbar\nu)f(\omega-\hbar\nu), \qquad (4.56)\end{aligned}$$

where Ψ_{N-1} is the excited state of the system after removal of an electron while $\Psi_{N,0}$ is the N-particle ground state. The annihilation operator $\hat{c}_{\mathbf{k}}$ removes an electron with momentum $\mathbf{k}$, E_{N-1} is the energy of the excited state and $E_{N,0}$ is the energy of the ground state. The photon has an energy $\hbar\nu$ and f denotes a Fermi function. In Fig. 4.4 we show the standard photo-current Feynman diagram contributing

to photocurrent within sudden approximation. At the point $\mathbf{r}_1 t$ the photoelectron is excited by the photons, after which the photoelectron travels freely to the detector at $\mathbf{R}$. The excitation of the electron leaves an photo-hole behind in the material. The propagation of the hole is described by the bulk Green's function. A neutralizing electrical contact between the detector and the sample is described by the electric field coupling at point $\mathbf{r}_2$.

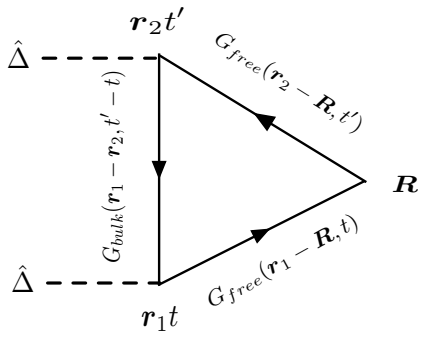

Figure 4.4: The no-loss diagram of the photocurrent in the sudden approximation,

In reality the photoelectron is not excited directly into the vacuum and it might travel a certain distance in the system and may undergo energy losses on its way out. The energy losses can be divided into extrinsic losses and intrinsic losses. The extrinsic losses are related to the interaction of the photoelectron with the system (material), like impurity scattering, scattering of the photoelectron against other electrons or electron-phonon scatterings. Intrinsic losses, on the other hand, are related to the damping of the effects, causing the excitations to have a finite life-time. In order to take theses processes into account we need to expand the expression for the photocurrent diagrammatically [149, 127].

To see which kind of processes constitute the photocurrent with density functional theory we examined its diagrammatic content. We will consider a many-particle system described by a Hamiltonian of the form $\hat{H}(t) = \hat{H}_0 + \hat{\Delta}(t)$ where $\hat{\Delta}$ describes the electromagnetic field applied for times $t > t_0$ and $\hat{H}_0$ is the many-body Hamiltonian of the sample before the field is applied. In the photo-emission problem the quantity of interest is the current density outside the sample which is a one-particle observable and can be calculated from the lesser Green's function as

$$\hat{\mathbf{j}}(\boldsymbol{r}, t) = -\frac{1}{2} \sum_{\sigma} (\nabla - \nabla') G^{<}(\mathbf{x}t, \mathbf{x}'t')|_{\mathbf{x}=\mathbf{x}'}. \tag{4.57}$$

Let us now expand the expectation value for the current $\boldsymbol{j}(\boldsymbol{r}, t) = \langle \Phi(t) | \hat{\boldsymbol{j}}(\boldsymbol{r}) | \Phi(t) \rangle$ in terms of the electromagnetic coupling $\hat{\Delta}$. To do this we first expand the time-dependent many-body state in powers of $\hat{\Delta}$, after which we are able to find the lowest non-zero contribution to the photo-current in terms of the

one-particle Green's function. The expansion of the many-particle wave function in powers of $\hat{\Delta}$ is

$$|\Psi(t)\rangle = |\Psi^{(0)}(t)\rangle + |\Psi^{(1)}(t)\rangle + |\Psi^{(2)}(t)\rangle + ... \tag{4.58}$$

with $|\Psi^{(0)}(t)\rangle = e^{-i\varepsilon_0(t-t')}|\Phi_0\rangle$. Therefore, the expectation value for the current is

$$\begin{aligned}\langle\hat{j}(\boldsymbol{r}t)\rangle &= \langle\Psi^{(0)}(t)|\hat{j}(\boldsymbol{r})|\Psi^{(0)}(t)\rangle + \langle\Psi^{(0)}(t)|\hat{j}(\boldsymbol{r})|\Psi^{(1)}(t)\rangle \\ &+\langle\Psi^{(1)}(t)|\hat{j}(\boldsymbol{r})|\Psi^{(0)}(t)\rangle + \langle\Psi^{(1)}(t)|\hat{j}(\boldsymbol{r})|\Psi^{(1)}(t)\rangle + \langle\Psi^{(0)}(t)|\hat{j}(\boldsymbol{r})|\Psi^{(2)}(t)\rangle \\ &+\langle\Psi^{(2)}(t)|\hat{j}(\boldsymbol{r})|\Psi^{(0)}(t)\rangle + O(\hat{\Delta}^3).\end{aligned} \tag{4.59}$$

Since we are interested in the photo-emission current outside the sample the zeroth order term does not contribute since $|\Psi^{(0)}(t)\rangle$ is localized to the sample in position space and all matrix elements with $|\Psi^{(0)}(t)\rangle$ vanish outside the sample. Therefore the lowest order contribution to the photocurrent is

$$\langle\hat{j}^{(2)}(\mathbf{r}t)\rangle = \langle\Psi^{(1)}(t)|\hat{\boldsymbol{j}}_p(\mathbf{r})|\Psi^{(1)}(t)\rangle \tag{4.60}$$

which is second order in the applied field and we restricted ourselves to the paramagnetic current since the diamagnetic current $\hat{n}(\boldsymbol{r}t)\boldsymbol{A}(\mathbf{r}t)$ is even smaller due to the terms higher order in the applied field. Since the lowest order non-zero contribution for the photocurrent involves the expectation value with respect to the many-particle wave function in first order of the applied field, we need to find the first order change in the many-particle state. If $\hat{U}(t,t') = e^{-iH_0(t-t')}$ is the time-evolution operator of the unperturbed system and the operator in the Heisenberg representation is $\hat{A}_H(t) = \hat{U}_0(t_0,t)\hat{A}\hat{U}_0(t,t_0)$, we find the first order change to the unperturbed ground state $|\Phi_0\rangle$ to be

$$|\Psi^{(1)}(t)\rangle = \int_{t_0}^{t} dt'\hat{U}_0(t,t')\hat{\Delta}(t')\hat{U}(t',t)|\Phi_0\rangle. \tag{4.61}$$

It can be readily seen that $(i\partial_t - \hat{H}_0)|\Psi^{(1)}(t)\rangle = \hat{\Delta}(t)|\Psi^{(1)}(t)\rangle$ with the initial condition $|\Psi^{(1)}(t_0)\rangle = 0$. We can now write the photocurrent as

$$\langle\hat{j}(\boldsymbol{r}t)\rangle^{(2)} = \int_{t_0}^{t} dt_1 \int_{t_0}^{t} dt_2 \langle\Phi_0|\hat{U}(t_0,t_2)\hat{\Delta}(t_2)\hat{U}(t_2,t)\hat{j}(\mathbf{r})\hat{U}_0(t,t_1)\hat{\Delta}(t_1)\hat{U}(t_1,t_0)|\Phi_0\rangle \tag{4.62}$$

$$= \int_{t_0}^{t} dt_1 \int_{t_0}^{t} dt_2 \langle\Phi_0|\hat{\Delta}_{H_0}(t_2)\hat{j}_H(\mathbf{r}t)\hat{\Delta}_{H_0}(t_1)|\Phi_0\rangle \tag{4.63}$$

where the operators are now in the Heisenberg representation with respect to $\hat{H}_0$. This is equivalent to the calculation of the equal-time lesser Green's function to second order in the external perturbation as

$$G^{(2)<}(\mathbf{x}t,\mathbf{x}'t) = i\int_{t_0}^{t} dt_1 dt_2 \,\langle\Phi_0|\hat{\Delta}_{H_0}(t_2)\hat{\psi}^{\dagger}_{H_0}(\mathbf{x}'t)\hat{\psi}_{H_0}(\mathbf{x}t)\hat{\Delta}_{H_0}(t_1)|\Phi_0\rangle \tag{4.64}$$

which we can expand in terms of the Feynman diagrams. Since $t_1, t_2 \leq t$ and the $\hat{\Delta}(t_1)$ appears to the right of $\hat{\psi}^\dagger_{H_0}(\mathbf{x}, t)\hat{\psi}_{H_0}(\mathbf{x}, t)$ while $\hat{\Delta}^\dagger(t_2)$ appears to the left, we can write the Eq. (4.64) on the Keldysh contour $\mathcal{C}$ where $\hat{\Delta}(t_1)$ is on the upper branch and $\hat{\Delta}^\dagger(t_2)$ lives on the lower branch. Thus, it is advantageous to rewrite the Eq. (4.64) as

$$G^{(2)<}(\mathbf{x}t, \mathbf{x}'t) = i \int_{t_0}^{t} dt_1 dt_2 \, \langle \Phi_0 | \hat{\Delta}_+(t_2) \hat{\psi}^\dagger(\mathbf{x}') \hat{\psi}(\mathbf{x}) \hat{\Delta}_-(t_1) | \Phi_0 \rangle \tag{4.65}$$

where we defined

$$\hat{\Delta}_-(t_1) = \hat{U}_0(t, t_1)\hat{\Delta}(t_1)\hat{U}_0(t_1, t_0),$$
$$\hat{\Delta}_+(t_2) = \hat{U}_0(t_0, t_2)\hat{\Delta}(t_2)\hat{U}_0(t_2, t).$$

We notice that $\hat{\Delta}_-(t_1)$ is surrounded by vertices labeled with $-$ sign while $\hat{\Delta}_+(t_2)$ is surrounded by vertices labeled with $+$ sign. Hence, operator $\hat{\Delta}_-(t_1)$ can now be expanded in time-ordered powers of the many-body interaction, whereas $\hat{\Delta}_+(t_2)$ can be expanded in anti-time-ordered powers of the interaction. An example, of the resulting expansion can be seen in Fig. 4.5.

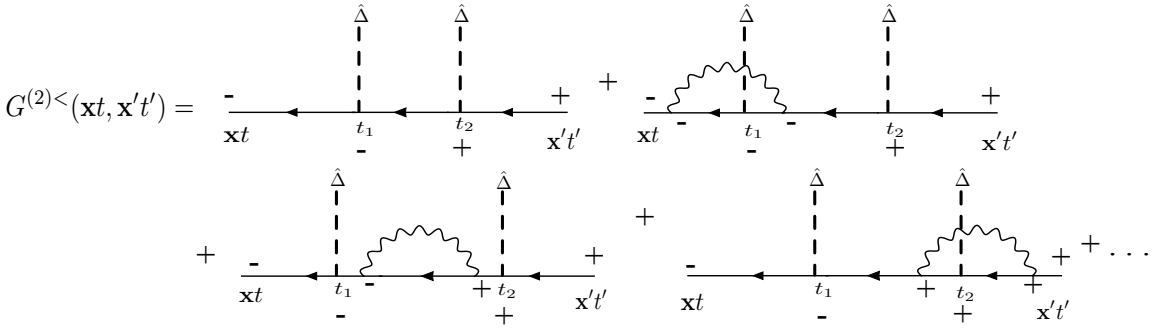

Figure 4.5: Expansion of $G^{(2)<}(\mathbf{x}t, \mathbf{x}'t)$ in Eq. (4.5) in G and $\mathcal{W}$.

Since the incoming and outgoing vertices are evaluated at the same time, it is customary to draw these diagrams in closed from as a triangles as in Fig. 4.6. In Fig 4.6. we show the skeleton diagram expansion of $G^{(2)<}$ to lowest order in the screened interaction $\mathcal{W}$ and the dressed Green's function G. These diagrams are the lowest order contributions to the photocurrent beyond sudden approximation. In Fig. 4.6 diagrams (a)-(c) contribute to the no-loss current while diagrams (d)-(f), including an interaction line between upper and lower branch of the Keldysh contour, describe extrinsic losses. Diagrams (g)-(h) describe renormalisation of the photo field inside (close) the sample within RPA.

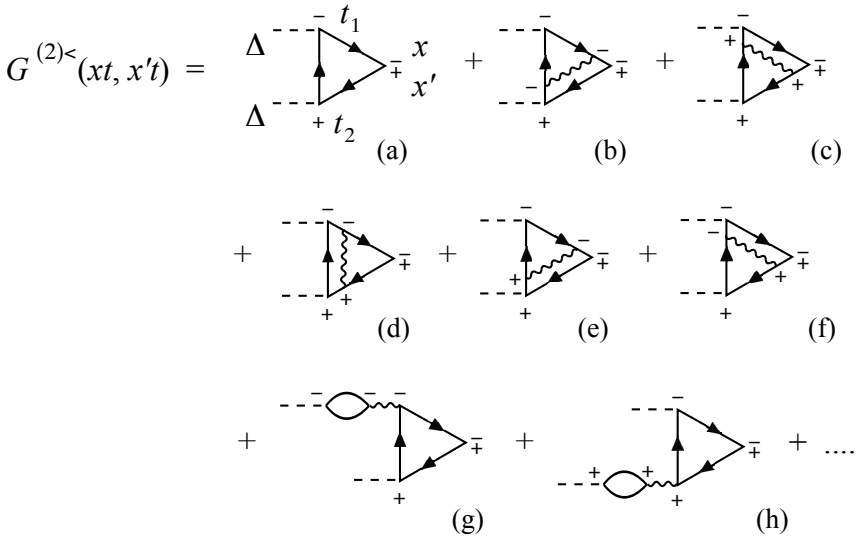

Figure 4.6: Skeleton expansion of $G^{(2)<}$ in G and $\mathcal{W}$ to the first order.

5

Non-equilibrium Dynamics of Open Quantum Systems

The problem of quantum dynamics in open systems has gained attention in recent decades and not the least due to the advances made in quantum transport in molecular systems [11, 15, 12, 17, 14, 13, 16, 150, 151]. The main motivation behind the quantum transport and molecular electronics is the futuristic goal to be able at some point to replace or to complement the silicon-based technology with molecular electronics to make the electronic devices faster [152]. Although, the replacement of silicon-based electronics with a molecular one will not very likely ever happen molecular electronics has established itself in recent decades as a field of study of its own. One of the boosts for molecular electronics was due to the work by Mark Reed *et al.* who was the first to be able to measure current through molecules between small nanoscale-structures between metals or semi-conductors [153]. The miniaturization of the silicon-based electronics and the research done on the molecular devices has given need for a truly quantum mechanical description of the transport problem where the electron-electron and electron-phonon interactions are taken into account. Examples of non-classical behavior in transport problem are, for instance, negative differential resistance (NDR), bistability and hysteresis or polaronic conduction due to electron-phonon interactions. The understanding of the different phenomena in quantum transport does not rely solely on understanding the underlying physical phenomena, but in addition understanding of the structure-function relationships in transport devices plays a crucial role.

Density functional (DFT) and non-equilibrium Green's function (NEGF) based methods are widely used nowadays in electron transport calculations [154, 10, 155, 156, 157, 57, 158, 159, 160, 161] which solve a system of nonlinear equations for the non-equilibrium density and current via self-consistent iterations. The power of DFT and NEGF based methods is that they can treat the underlying electronic structure of the transport device from the first principles together with electron-electron and electron-phonon interactions, hence answering the very question of phenomena-structure-function of molecular electronics.

In this thesis we focus on the description of time-dependent phenomena by using non-equilibrium Green's functions together with the Kadanoff-Baym equations and try to answer the fundamental question of how

the electrons move through nanoscale junctions. The time-dependent description of quantum transport is motivated by the constant need to speed up electronic devices, which means that they are most of the time operating in non-equilibrium and there is hardly any time for the steady-state to equilibrate. Therefore, it is important to understand the underlying mechanism of non-equilibrium dynamics and the mechanisms for reaching a steady-state, and whether the steady-state is unique, and if not, how we can determine which steady-states are obtainable via time-propagation.

This chapter is organized as follows. At first we introduce the time-propagation scheme with the Kadanoff-Baym (KB) equations followed by introduction to generalized Kadanoff-Baym ansatz (GKBA) and an introduction to two different types of embedding schemes after which we will show how the standard Meir-Wingreen formula [162] relates to the current calculated via KB-equations. Finally, we will study some basic quantum transport situations.

5.1 KELDYSH-KADANOFF-BAYM EQUATIONS

In the transport calculations, we take the system to be initially in thermal equilibrium described by a statistical grand canonical ensemble. At time t_0 the system is perturbed by an external perturbation after which its time-evolution is followed. This process is described by the Keldysh contour of Fig. 3.1b, where we have the vertical imaginary track describing the ground state and the time-loop contour on the real axis describing the non-equilibrium dynamics. By utilizing the Langreth rules we are able to distinguish, from the equation of motion for the one-particle Green's function (3.51), different components on the contour $\mathcal{C}$. These different componets are commonly called the Kadanoff-Baym equations and they read as

$$\left[i\partial_{t_1} - \hat{h}(t_1)\right] G^{\gtrless}(t_1,t_2) = \left[\Sigma^R \cdot G^{\gtrless} + \Sigma^{\gtrless} \cdot G^A + \Sigma^{\rceil} \star G^{\lceil}\right](t_1,t_2) = I_1^{\gtrless}(t_1,t_2), \tag{5.1a}$$

$$G^{\gtrless}(t_1,t_2)\left[-i\overleftarrow{\partial}_{t_2} - \hat{h}(t_2)\right] = \left[G^R \cdot \Sigma^{\gtrless} + G^{\gtrless} \cdot \Sigma^A + G^{\rceil} \star \Sigma^{\lceil}\right](t_1,t_2) = I_2^{\gtrless}(t_1,t_2), \tag{5.1b}$$

$$\left[i\partial_{t_1} - \hat{h}(t_1)\right] G^{\rceil}(t_1,\tau_2) = \left[\Sigma^R \cdot G^{\rceil} + \Sigma^{\rceil} \star G^M\right](t_1,\tau_2) = I^{\rceil}(t_1,\tau_2), \tag{5.1c}$$

$$G^{\lceil}(\tau_1,t_2)\left[-i\overleftarrow{\partial}_{t_2} - \hat{h}(t_2)\right] = \left[G^{\lceil} \cdot \Sigma^A + G^M \star \Sigma^{\lceil}\right](\tau_1,t_2) = I^{\lceil}(\tau_1,t_2), \tag{5.1d}$$

$$\left[-\partial_{\tau_1} - \hat{h}^M\right] G^M(\tau_1,\tau_2) = i\delta(\tau_1-\tau_2) + \left[\Sigma^M \star G^M\right](\tau_1,\tau_2) = I^M(\tau_1,\tau_2), \tag{5.1e}$$

$$G^M(\tau_1,\tau_2)\left[\partial_{\tau_2} - \hat{h}^M\right] = i\delta(\tau_1-\tau_2) + \left[G^M \star \Sigma^M\right](\tau_1,\tau_2) = I^M(\tau_1,\tau_2). \tag{5.1f}$$

Here we omitted the spatial indices, introduced a short-hand notation $I^{\gtrless,\rceil,\lceil}$ called collision integrals for the inhomogeneous part of the equations as well as defined the convolution integrals on the real and imaginary axis as $[a\cdot b](t_1,t_2) = \int_{t_0}^{\infty} a(t_1,t)b(t,t_2)dt$ and $[a\star b](t_1,t_2) = -\int_0^{\beta} a(t_1,\tau)b(\tau,t_2)d\tau$. The greater and lesser collision integrals $I^{\gtrless}$, due to the integration over all the earlier times, take into account the history dependence for self-energy approximations which are time non-local, *i.e.,* have non-zero greater and lesser component. The mixed terms in the collision integrals, $I^{\rceil,\lceil}$, take into account the initial correlations of the system, being components having one time-argument on the imaginary track and other

on the real axis. The boundary conditions for solving the initial Green's function on the imaginary axis are given by the Kubo-Martin-Schwinger (KMS) boundary conditions as $G(\mathbf{x}_1 t_0, 2) = -G(\mathbf{x}_1 t_0 - i\beta, 2)$ and $G(1, \mathbf{x}_2 t_0) = -G(1, \mathbf{x}_2 t_0 - i\beta)$. The self-energy will also fulfill KMS boundary conditions due to the structure of the Dyson equation. For the mixed $\rceil, \lceil$ components of the Green's function and the self-energy we have the following conditions

$$\left[G^{\lceil}(-i\tau, t)\right]^{\dagger} = G^{\rceil}(t, -i(\beta - \tau)), \tag{5.2}$$

$$\left[\Sigma^{\lceil}(-i\tau, t)\right]^{\dagger} = \Sigma^{\rceil}(t, -i(\beta - \tau)), \tag{5.3}$$

which imply for the mixed collision integrals a similar condition $\left[I^{\lceil}(-i\tau, t)\right]^{\dagger} = I^{\rceil}(t, -i(\beta - \tau))$. The equal time relation for the lesser and greater Green's function

$$G^{>}(\mathbf{x}_1 t, \mathbf{x}_2 t) = -i\delta(\mathbf{x}_1, \mathbf{x}_2) + G^{<}(\mathbf{x}_1 t, \mathbf{x}_2 t) \tag{5.4}$$

together with the symmetry relations for the Green's function and self-energy

$$\left[G^{\gtrless}(t_1, t_2)\right]^{\dagger} = -G^{\lessgtr}(t_2, t_1), \tag{5.5}$$

$$\left[\Sigma^{\gtrless}(t_1, t_2)\right]^{\dagger} = -\Sigma^{\lessgtr}(t_2, t_1), \tag{5.6}$$

imply similar symmetry relation also for the greater and lesser collision integral $\left[I^{\gtrless}_{1,2}(t_1, t_2)\right]^{\dagger} = -I^{\gtrless}_{2,1}(t_2, t_1)$. We see that in practice we need to propagate only a part of the Kadanoff-Baym equations, namely (see Fig. 5.1)

$$G^{<}(t_1, t_2) \quad \& \quad \Sigma^{<}(t_1, t_2), \quad \text{for } t_1 \leq t_2, \tag{5.7}$$

$$G^{>}(t_1, t_2) \quad \& \quad \Sigma^{>}(t_1, t_2), \quad \text{for } t_1 > t_2, \tag{5.8}$$

involving only $I_1^{>}$, $I_2^{<}$ and $I^{\rceil}$. The rest of the components are obtainable via the symmetry relations. Now the initial conditions for the time-propagation can be seen to be

$$G^{>}(t_0, t_0) = -iG^{M}(\tau_0^{+}), \tag{5.9a}$$

$$G^{<}(t_0, t_0) = iG^{M}(\tau_0^{-}), \tag{5.9b}$$

$$G^{\rceil}(t_0, t_0 - i\tau) = iG^{M}(-\tau), \tag{5.9c}$$

$$G^{\lceil}(t_0 - i\tau, t_0) = -iG^{M}(\tau). \tag{5.9d}$$

The numerical procedure for solving the Kadanoff-Baym equations starts by determining the Matsubara component of the Green's function after which the Green's function on the real axis is initialized with the initial conditions (5.9). All these conditions together with Kadanoff-Baym equations determine the one-particle Green's function at all times when an approximation for the self-energy has been made [163, 164].

DYSON EQUATION

The first step is to solve the equilibrium ground state system. This amounts to solving the system on the imaginary time axis, *i.e.,* solving the Matsubara component of the Green's function. In our discussion we will consider only spin-compensated systems and therefore the Green's function has the form

$$G(\mathbf{x}_1 z_1, \mathbf{x}_2 z_2) = \delta_{\sigma_1\sigma_2} G(\boldsymbol{r}_1 z_1, \boldsymbol{r}_2 z_2). \tag{5.10}$$

Furthermore, since the system is initially in equilibrium both the Green's function and the self-energy will depend only on the time difference of their time-arguments and therefore it is convenient to introduce the following notation

$$G^M(\tau_1 - \tau_2) = -iG^M(-i\tau_1, -i\tau_2), \tag{5.11}$$
$$\Sigma^M(\tau_1 - \tau_2) = -i\Sigma^M(-i\tau_1, -i\tau_2), \tag{5.12}$$

where we omitted the spatial arguments, and due to the factor i, the Matsubara Green's function G^M and the self-energy Σ^M are real quantities if the Hamiltonian on the imaginary axis $\hat{h}^M$ and the interaction term w are real quantities. Therefore, the equation of motion for the Matsubara component of the Green's can be written as

$$\sum_k (-\delta_{ik}\partial_{\tau_1} - h^0_{ik}) G^M_{kj}(\tau_1) = \delta_{ij}\delta(\tau_1) + \int_0^\beta d\tau_3 \sum_k \Sigma^M_{ik}(\tau_1 - \tau_3) G^M_{kj}(\tau_3), \tag{5.13}$$

where the integration over the spatial coordinates is replaced by a matrix multiplication. We have also set $\tau_2 = 0$. Since the Green's function G^M and the self-energy Σ^M are symmetric on the interval $[-\beta, \beta]$ we need to calculate it only on the half of the interval. We have reduced the full domain to $[-\beta, 0]$, since $G(0^-)$ is related to the density matrix. We can now cast the equation (5.13) into a form of a Dyson equation with help of a reference Green's function $G_0(\tau)$ satisfying the homogeneous equation

$$\sum_k (-\delta_{ik}\partial_\tau - h^0_{ik} - \Sigma^0_{ik}) G_{0,kj}(\tau) = \delta_{ij}\delta(\tau). \tag{5.14}$$

where Σ^0 is the static part of the self-energy, yielding

$$G^M_{ij}(\tau_1) = G_{0,ij}(\tau_1) + \int_{-\beta}^0 d\tau_4 \int_0^\beta d\tau_3 \sum_{kl} G_{0,ik}(\tau_1 - (\tau_3 - \beta)) \Sigma^{M,c}_{kl}(\tau_3 - (\tau_4 + \beta)) G^M_{lj}(\tau_4), \tag{5.15}$$

where we used the Kubo-Martin-Schwinger boundary conditions for the G_0 and G^M and defined the time nonlocal part of the self-energy to be $\Sigma^{M,c}_{ij}(\tau) = \Sigma^M_{ij}(\tau) - \delta(\tau)\Sigma^0_{ij}$. This equation is solved to self-consistency for the Matsubara Green's function G^M. In other words, for the first iteration the reference Green's function $G_0(\tau)$ is calculated either from the Hartree-Fock or DFT calculation from which the first approximation for the self-energy is obtained. The equation (5.15) will yield a new approximation for the

G^M Green's function from which we get a new estimate for the self-energy. This procedure is applied until the desired convergence is reached. The converged Green's function is then used as a starting point for the time-propagation along the real time-axis on the contour $\mathcal{C}$.

The Dyson equation (5.15) can be cast into a system of linear equations of the form $\mathbf{Ax} = \mathbf{b}$ which we can solve very efficiently by utilizing biconjugate gradient methods [165, 166]. First of all, we notice that the the Dyson equation (5.15) can be written as a Fredholm integral equation

$$G^M_{ij}(\tau) - \int_{-\beta}^{0} d\tau' \sum_k F_{ik}(\tau,\tau') G^M_{kj}(\tau') = G_{0,ij}(\tau), \tag{5.16}$$

where the integral kernel is given as

$$F_{ij}(\tau,\tau') = \int_0^{\beta} d\tau_1 \sum_k G_{0,ik}(\tau - (\tau_1 - \beta)) \Sigma^{M,c}_{kj}(\tau_1 - (\tau' + \beta)). \tag{5.17}$$

By discretizing the Dyson equation in the Fredholm form (5.16) we are able to write our problem as a set of linear equations of the form $\mathbf{Ax} = \mathbf{b}$

$$\sum_{k=1}^{n}\sum_{q=0}^{m} A_{(ip),(kq)} G^M_{kj}(\tau_q) = \delta_{ij} G_{0,i}(\tau) \tag{5.18}$$

where our matrix $\mathbf{A}$ consists of the Fredholm integral kernel

$$A_{(ip),(kq)} = \delta_{ik}\delta_{pq} \quad - \quad F_{ik}(\tau_p,\tau_q) \tag{5.19}$$

The unknown $\mathbf{x}$ is naturally the Matsubara component of the Green's function which we want to solve $G^M_{kj}(\tau_q)$ and the inhomogenous part $\mathbf{b}$ is given by our reference Green's function $\delta_{ij}G_{0,i}(\tau)$. In appendix A we present the BiCGSTAB and BiCGSTAB(l) algorithms applied to the solution of the Dyson equation.

TWO-TIME PROPAGATION

From the obtained solution of the Dyson equation Eq. (5.15) we can start our two-time propagation with the initial conditions Eq. (5.9). Due to the symmetries discussed earlier we have only a subset of equations of motion which we need to propagate which are

$$i\partial_{t_1} G^{>}(t_1,t_2) = \hat{h}(t_1)G^{>}(t_1,t_2) + I^{>}_1(t_1,t_2) \tag{5.20a}$$
$$-i\partial_{t_1} G^{<}(t_2,t_1) = G^{<}(t_2,t_1)\hat{h}(t_1) + I^{<}_2(t_2,t_1) \tag{5.20b}$$
$$i\partial_{t_1} G^{\rceil}(t_1,-i\tau) = \hat{h}(t_1)G^{\rceil}(t_1,-i\tau) + I^{\rceil}(t_1,-i\tau) \tag{5.20c}$$
$$-i\partial_{t_1} G^{\lceil}(-i\tau,t_1) = G^{\lceil}(-i\tau,t_1)\hat{h}(t_1) + I^{\lceil}(-i\tau,t_1), \tag{5.20d}$$

where we again suppressed spatial indices for the notational simplicity. We will now propagate these equations with a small time step Δ from $t \to t + \Delta$. From the symmetry relations of equations (5.20) it follows that we need to take time-step in the first time-argument for the greater Green's function $G^{>}(t + \Delta, t_2)$ and for the second time-argument for the lesser Green's function $G^{<}(t_1, t + \Delta)$ (see Fig. 5.1). For the time-diagonal part $t_1 = t_2$ we need to take a time-step in both time-arguments as $G^{<}(t, t) \to G^{<}(t + \Delta, t + \Delta)$. For the mixed components $G^{\lceil}$ and $G^{\rceil}$ the time-stepping is done in the real-time argument while the imaginary time τ is kept fixed. We define new Green's functions with the help of the time-evolution operator $\hat{U}$ as

$$
\begin{aligned}
G^{\gtrless}(t_1, t_2) &= \hat{U}(t_1) g^{\gtrless}(t_1, t_2) \hat{U}^{\dagger}(t_2), && (5.21)\\
G^{\rceil}(t_1, -i\tau) &= \hat{U}(t_1) g^{\rceil}(t_1, -i\tau), && (5.22)\\
G^{\lceil}(-i\tau, t_2) &= g^{\lceil}(-i\tau, t_2) \hat{U}^{\dagger}(t_2). && (5.23)
\end{aligned}
$$

The time-propagation is done by using HF Hamiltonian, hence, the time-evolution operator $\hat{U}$ satisfies the equation $i\partial_t \hat{U}(t) = \hat{h}_{\text{HF}}(t)\hat{U}(t)$. The HF hamiltonian is evaluated with the density matrix obtained from the previous time-step. We will propagate the Green's functions with a small time-step Δ, during which we assume that the Hamiltonian is approximately constant on the interval $[t, t + \Delta]$ and $\hat{h}_{\text{HF}}(t_1) \approx \bar{h}_{\text{HF}}(t)$ as well as the collision integrals $I^{\gtrless,\rceil,\lceil}$ stay constant. We now define the time-evolution operator for the time-propagation to be $\hat{U}(t_1) = e^{i\bar{h}_{\text{HF}}(t)t_1}$. Furthermore, we take the Hartree-Fock Hamiltonian to be a a sum of the one-particle part of the Hamiltonian and the Hartree-Fock self-energy $\bar{h}_{\text{HF}}(t) = \hat{h}_0(t + \Delta/2) + \Sigma_{\text{HF}}(t)$, where the one-body hamiltonian, being a known function of time, is evaluated at half of the time-step. Now, together with equations of motion (5.20) we have

$$
\begin{aligned}
i\partial_{t_1} g^{>}(t_1, t_2) &= \hat{U}^{\dagger}(t_1) I_1(t_1, t_2) \hat{U}(t_2), && (5.24)\\
-i\partial_{t_2} g^{<}(t_2, t_1) &= \hat{U}^{\dagger}(t_1) I_2(t_1, t_2) \hat{U}(t_2), && (5.25)\\
i\partial_{t_1} g^{\rceil}(t_1, -i\tau) &= \hat{U}^{\dagger}(t_1) I^{\rceil}(t_1, -i\tau), && (5.26)\\
-i\partial_{t_2} g^{\rceil}(-i\tau, t_2) &= I^{\lceil}(-i\tau, t_2) \hat{U}(t_2). && (5.27)
\end{aligned}
$$

From these equations we see that in order to be able to propagate the Green's function in time we need to know what is the time-evolution of the collision integrals $I^{\gtrless,\lceil,\rceil}$. From the assumption that the collision integrals $I^{\gtrless,\rceil,\lceil}$ are constant on the interval $[t, t + \Delta]$ we have that $I_1^{>}(t_1, t_2) \approx \bar{I}^{>}(t_2)$ and $I_2^{<}(t_1, t_2) \approx \bar{I}_2^{<}(t_1)$. Evaluating the equations of motion for the transformed Green's functions at $g^{<}(t_1, t + \Delta)$ and $g(t + \Delta, t + \Delta)$ we see that they satisfy the following equations [164]

$$
\begin{aligned}
g^{>}(t + \Delta, t_2) &= \hat{U}(\Delta) g^{>}(t, t_2) - \frac{1}{\bar{h}_{\text{HF}}} \left[1 - e^{-i\Delta\bar{h}_{\text{HF}}}\right] \bar{I}_1^{>}(t_2), && (5.28a)\\
g^{<}(t_1, t + \Delta) &= g^{<}(t_1, t)\hat{U}^{\dagger}(\Delta) - \bar{I}_2^{<}(t_1) \frac{1}{\bar{h}_{\text{HF}}} \left[1 - e^{-i\Delta\bar{h}_{\text{HF}}}\right]. && (5.28b)
\end{aligned}
$$

The mixed terms $g^{\lceil}(-i\tau, t+\Delta)$ and $g^{\rceil}(t+\Delta, -i\tau)$ can be found to satisfy the following

$$g^{\lceil}(-i\tau, t+\Delta) = g^{\lceil}(-i\tau, t)\hat{U}^{\dagger}(\Delta) - \bar{I}^{\lceil}(-i\tau)\frac{1}{\bar{h}_{\rm HF}}\left[1 - e^{-i\Delta\bar{h}_{\rm HF}}\right], \tag{5.29a}$$

$$g^{\rceil}(t+\Delta, -i\tau) = \hat{U}(\Delta)g^{\rceil}(t, -i\tau) - \frac{1}{\bar{h}_{\rm HF}}\left[1 - e^{-i\Delta\bar{h}_{\rm HF}}\right]\bar{I}^{\rceil}(-i\tau). \tag{5.29b}$$

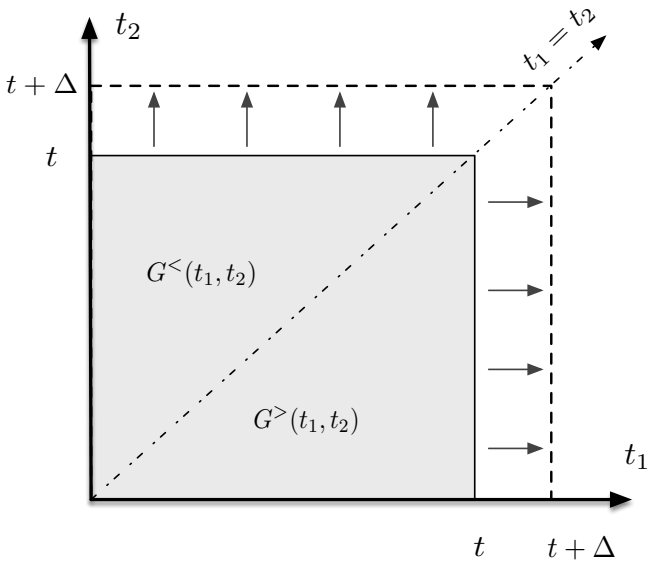

Figure 5.1: The double time-plane for the greater and lesser Green's functions $G^{\gtrless}(t_1, t_2)$.

The time-diagonal propagation is a bit more tedious but $g(t+\Delta, t+\Delta)$ can be found to satisfy the resulting equation

$$\begin{aligned} g^{<}(t+\Delta, t+\Delta) &= \hat{U}(\Delta)g^{<}(t,t,)\hat{U}^{\dagger}(\Delta) - i\hat{U}(\Delta)\left[\int_0^{\Delta} d\bar{t}\,\hat{U}^{\dagger}(\bar{t})\,\bar{I}_{12}^{<}(t)\,\hat{U}(t)\right]\hat{U}^{\dagger}(\Delta) \\ &= \hat{U}(\Delta)\left[g^{<}(t,t) + \sum_{n=0}^{\infty} C^n\right]\hat{U}^{\dagger}(\Delta), \end{aligned} \tag{5.30}$$

where we introduced a short hand notation $\bar{I}_{12} = \bar{I}_1^{<}(t_1, t_2) - \bar{I}_2^{<}(t_1, t_2) = [\bar{I}_1(t_2, t_1)^{>}]^{\dagger} - \bar{I}_2^{<}(t_1, t_2)$ and $C^n = \frac{i\Delta}{n+1}[\bar{h}_{\rm HF}, C^{n-1}]$ with the initial term $C^0 = -i\Delta I_{12}$ [164]. We see that the right hand sides of equations (5.28), (5.30) and (5.29) depend as well on the time $t+\Delta$, therefore in practice we need to take the time-step twice. For the first time we evaluate the right hand sides of Eqs. (5.28), (5.30) and (5.29) after which the values for the collision integrals and for the Hartree-Fock self-energy are taken to be averages evaluated at times t and $t+\Delta$ as $I = [I(t) + I(t+\Delta)]/2$ and $\Sigma_{\rm HF} = [\Sigma_{\rm HF}(t) + \Sigma_{\rm HF}(t+\Delta)]/2$. The actual time-step for the Green's functions is then taken by using these averaged quantities.

5.1.1 GENERALIZED KADANOFF-BAYM ANSATZ

In previous section we saw that the two-time propagation of Kadanoff-Baym equations can be quite tedious. Together with the memory kernel involving integrations over all earlier times is causing the computational effort grows as a function of time as t^3 compared to the propagation of one-time wave function equations in TDDFT where the computational effort goes as t^2 (with memory kernel). One way to reduce the computational cost is to use the Generalized Kadanoff-Baym Ansatz (GKBA) derived by Lipavský [167] for non-equilibrium situation where the two time propagator $G^{\gtrless}(t_1, t_2)$ is approximated with the reduced one-particle density matrix $G^<$ times the retarded Green's function accounting for correlations between different times. By construction the GKBA is exact for equal times which gives reasons to believe that for short time intervals the approximation should work relatively well.

We will start by deriving the GKBA as it is presented by Lipavský [167], Hermans [168] and Balzer [169]. We will again omit the space-spin indices for notational simplicity. First of all, we split the lesser propagator into a lower and upper diagonal as

$$G^<_L(t_1, t_2) = \theta(t_1 - t_2)G^<(t_1, t_2) \tag{5.31}$$

$$G^<_U(t_1, t_2) = -\theta(t_2 - t_1)G^<(t_1, t_2), \tag{5.32}$$

where for example the lower propagator will satisfy the equation of motion

$$i\partial_{t_1} G^<_L(t_1, t_2) = i\delta(t_1, t_2)G^<(t_1, t_2) + i\theta(t_1 - t_2)G^<(t_1, t_2). \tag{5.33}$$

To find a construction for the lesser propagator in terms of the one particle reduced density matrix and retarded / advanced propagators we will need to evaluate convolutions

$$\int dt_3 \, [G^R(t_1, t_3)]^{-1} G^<_L(t_3, t_2) \tag{5.34}$$

$$\int dt_3 \, G^<_U(t_3, t_2)[G^A(t_1, t_3)]^{-1}. \tag{5.35}$$

If we succeed in this, we will have an expression for the $G^<$ propagator when we multiply Eq. (5.34) from the left with G^R and Eq. (5.35) from the right with G^A with integration over the intermediate coordinate. Let us start by considering the convolution $\int dt_3 \, [G^R(t_1, t_3)]^{-1} G^<_L(t_3, t_2)$. Using the definition for the inverse retarded Green's function $[G^R]^{-1} = [G_0]^{-1} - \Sigma^R$ where G_0 is some a non-interacting reference Green's function and Σ^R is some many-body self-energy. The inverse of G_0 can be obtained from the homogeneous solution for the equation of motion as $[G_0(t_1, t_2)]^{-1} = \delta(t_1, t_2)(i\partial_{t_1} - \hat{h}(t_1))$ and $[G_0(t_1, t_2)]^{-1} = \delta(t_1, t_2)(i\overleftarrow{\partial}_{t_2} - \hat{h}(t_2))$.

Inserting all this into equation (5.34) we obtain

$$\begin{aligned}\int dt_3\,[G^R(t_1,t_3)]^{-1}G_L^<(t_3,t_2) &= i\delta(t_1,t_2)G^<(t_1,t_2)+i\theta(t_1,t_2)\partial_{t_1}G^<(t_1,t_2)\\ &\quad-\int dt_3\,\hat{h}(t_3)G_L^<(t_3,t_2)-\int dt_3\,\Sigma^R(t_1,t_3)G_L^<(t_3,t_2)\end{aligned}\tag{5.36}$$

which simplifies with the use of the definition for the lower propagator (5.31) together with the definition for the inverse of the non-interacting Green's function $[G_0]^{-1}$ to form

$$\begin{aligned}\int dt_3\,[G^R(t_1,t_3)]^{-1}G_L^<(t_3,t_2) &= i\delta(t_1,t_2)G^<(t_1,t_2)+\theta(t_1,t_2)\int dt_3\,[G_0(t_1,t_3)]^{-1}G^<(t_3,t_2)\\ &\quad-\int dt_3\,\Sigma^R(t_1,t_3)G_L^<(t_3,t_2).\end{aligned}\tag{5.37}$$

If we now solve for $[G_0]^{-1}$ from the equation for the inverse of the retarded Green's functon $[G^R]^{-1}=[G_0]^{-1}-\Sigma^R$ we get

$$\begin{aligned}\int dt_3\,[G^R(t_1,t_3)]^{-1}G_L^<(t_3,t_2) &= i\delta(t_1,t_2)G^<(t_1,t_2)+\theta(t_1,t_2)\int dt_3\,[G^R(t_1,t_3)]^{-1}G^<(t_3,t_2)\\ &\quad+\theta(t_1,t_2)\int dt_3\,\Sigma^R(t_1,t_3)G^<(t_2,t_2)\\ &\quad-\int dt_3\,\Sigma^R(t_1,t_3)G_L^<(t_3,t_2),\end{aligned}\tag{5.38}$$

where the last two terms cancel due to the definition (5.34). Furthermore, utilizing the equality

$$\int dt_3\,[G^R(t_1,t_3)]^{-1}G^{\gtrless}(t_3,t_2)=\int dt_3\,\Sigma^{\gtrless}(t_1,t_3)G^A(t_3,t_2)\tag{5.39}$$

we obtain

$$\begin{aligned}\int dt_3\,[G^R(t_1,t_3)]^{-1}G_L^<(t_3,t_2) &= i\delta(t_1,t_2)G^<(t_1,t_2)+\theta(t_1,t_2)\int dt_3\Sigma^<(t_1,t_3)G^A(t_3,t_2)\\ &\quad-\theta(t_1,t_2)\int dt_3\theta(t_1,t_3)[G^R(t_1,t_3)]^{-1}G^<(t_3,t_2)\end{aligned}\tag{5.40}$$

where the last term corrects for the step function. Using again the definition for the inverse retarded Green's function together with relation $\int dt_3\,[G_0(t_1,t_3)]^{-1}G^{\gtrless}(t_3,t_1)=\int dt_3\,G^{\gtrless}(t_1,t_3)[G_0(t_3,t_1)]^{-1}=0$ we have

$$\begin{aligned}\int dt_3\,[G^R(t_1,t_3)]^{-1}G_L^<(t_3,t_2) &= i\delta(t_1,t_2)G^<(t_1,t_2)+\theta(t_1,t_2)\int dt_3\Sigma^<(t_1,t_3)G^A(t_3,t_2)\\ &\quad+\theta(t_1,t_2)\int dt_3\,\theta(t_1,t_3)\Sigma^R(t_1,t_2)G^<(t_3,t_2).\end{aligned}\tag{5.41}$$

Similarly, we can study the term $\int dt_3\, G_U^<(t_3,t_2)[G^A(t_1,t_3)]^{-1}$ in Eq. (5.35) yielding

$$\begin{aligned}\int dt_3\, G_U^<(t_3,t_2)[G^A(t_1,t_3)]^{-1} &= i\delta(t_1,t_2)G^<(t_1,t_2)\\ &\quad -\theta(t_1,t_2)\int dt_3\,\theta(t_1,t_3)G^R(t_1,t_3)\Sigma^<(t_3,t_2)\\ &\quad -\theta(t_1,t_2)\int dt_3\,\theta(t_1,t_3)G^<(t_1,t_3)\Sigma^A(t_3,t_2). \qquad (5.42)\end{aligned}$$

Now multiplying Eq. (5.41) from left with G^R and Eq. (5.42) from right with G^A and integrating over the intermediate coordinate we obtain

$$\begin{aligned}G^<(t_1,t_2) &= -G^R(t_1,t_2)\rho(t_2)+\rho(t_1)G^A(t_1,t_2)\\ &\quad +\int_{t_2}^{t_1}dt_3\int_{t_0}^{t_2}dt_4 G^R(t_1,t_3)\Sigma^<(t_3,t_4)G^A(t_4,t_2)\\ &\quad +\int_{t_2}^{t_1}dt_3\int_{t_0}^{t_2}dt_4 G^R(t_1,t_3)\Sigma^<(t_3,t_4)G^<(t_4,t_2)\\ &\quad +\int_{t_2}^{t_1}dt_3\int_{t_0}^{t_2}dt_4 G^R(t_1,t_3)\Sigma^<(t_3,t_4)G^A(t_4,t_2)\\ &\quad +\int_{t_2}^{t_1}dt_3\int_{t_0}^{t_2}dt_4 G^<(t_1,t_3)\Sigma^A(t_3,t_4)G^A(t_4,t_2) \qquad (5.43)\end{aligned}$$

where we used the definition for the one particle reduced density matrix given as a equal time limit of the lesser Green's function $\rho(t) = -iG^<(t,t)$. It is obvious, that we can derive also a similar equation for the $G^>$. Now the GKBA is done by keeping only the non-integral terms giving

$$\begin{aligned}G^<(t_1,t_2) &= -G^R(t_1,t_2)\rho(t_2)+\rho(t_1)G^A(t_1,t_2)\\ &= i\mathcal{A}(t_1,t_2)[\theta(t_1,t_2)\rho(t_2)+\theta(t_2-t_1)\rho(t_1)], \qquad (5.44a)\\ G^>(t_1,t_2) &= G^R(t_1,t_2)\bar\rho(t_2)-\bar\rho(t_1)G^A(t_1,t_2)\\ &= i\mathcal{A}(t_1,t_2)[\theta(t_1,t_2)\bar\rho(t_2)+\theta(t_2,t_1)\bar\rho(t_1)], \qquad (5.44b)\end{aligned}$$

where we introduced the GKB ansatz also for the greater propagator with definition $\bar\rho(t) = 1-\rho(t) = iG^>(t,t)$ and $\mathcal{A}$ denotes the spectral function. For practical proposes we need to find an expression for the retarded and advanced propagators. Since these are two-time variables we cannot treat them at the same approximation level as the rest of the time-propagation. To perform time-propagation we will propagate the time-diagonal part of the greater and lesser Green's functions Eq. (5.30) while the off-diagonal retarded and advanced propagators need to be known. We will determine these propagators at the Hartree-Fock level satisfying following equation of motion

$$\left[i\partial_{t_1}-\hat h_{\rm HF}(t_1)\right]G^{R/A}(t_1,t_2)=\delta(t_1,t_2) \qquad (5.45)$$

where $\hat{h}_{\text{HF}} = \hat{h}_0 + \Sigma_{\text{HF}}$. The solution for this gives us the retarded and advanced Hartree-Fock propagators as

$$G^{R/A}(t_1, t_2) = \mp\theta[\pm(t_1 - t_2)]\mathcal{T}e^{-i\int_{t_2}^{t_1} dt_3 \hat{h}_{\text{HF}}(t_3)}. \tag{5.46}$$

where $\mathcal{T}$ is the time-ordering operator. From the Kadanoff-Baym Eqs. (5.1) for the equal time propagation of $G^<$ Eq. (5.30) we need to determine the collision integral $I_{12}^<$ defined as

$$\begin{aligned} I_{12}^<(t) &= I_1^<(t,t) - I_2^<(t,t) = I_1^<(t,t) + [I_1^<(t,t)]^\dagger \\ &= \int_{t_0}^{t} dt_3 \left[\Sigma^>(t,t_3)G^<(t_3,t) - \Sigma^<(t,t_3)G^>(t_3,t)\right. \\ &\quad \left. + G^<(t,t_3)\Sigma^>(t_3,t) - G^>(t,t_3)\Sigma^<(t_3,t)\right]. \end{aligned} \tag{5.47}$$

Inserting the GKB-ansatz (5.44) for the greater and lesser propagators as well as the solution for the retarded and advanced propagators at HF-level Eq. (5.46), we obtain the GKBA approximation for the collision integral I_{12}

$$\begin{aligned} I_{12}^<(t) &= \int_{t_0}^{t} dt_3 \Big\{ \left[\Sigma^>(t,t_3)G^<(t_3,t_3) - \Sigma^<(t,t_3)G^>(t_3,t_3)\right] e^{-i\int_{t_3}^{t} dt_4\, \hat{h}_{\text{HF}}(t_4)} \\ &\quad + e^{-i\int_{t_3}^{t} dt_4\, \hat{h}_{\text{HF}}(t_4)} \left[G^<(t_3,t_3)\Sigma^>(t_3,t) - G^>(t_3,t_3)\Sigma^<(t_3,t)\right] \Big\} \end{aligned} \tag{5.48}$$

where the self-energy is evaluated at the chosen level. It is to be noted that for isolated systems the GKBA approach becomes exact at the Hartree-Fock level while for the embedded systems, discussed in the next section, we would need to replace Eq. (5.45) with the inhomogeneous one

$$\left[i\partial_{t_1} - \hat{h}_{\text{HF}}(t_1)\right] G^R(t_1, t_2) = \delta(t_1, t_2) + \int dt_3\, \Sigma^R_{\text{EM}}(t_1, t_3)G^R(t_3, t_2) \tag{5.49}$$

where Σ^R_{EM} is the so-called embedding self-energy. If we used this equation the numerical advantage of the GKBA would be lost. By approximating the embedding self-energy in the wide-band limit given as $\Sigma^R_{\text{EM}}(t_1, t_2) = -(i/2)\Gamma_{\text{EM}}\delta(t_1, t_2)$ (see next section for details) all we need to know now is that Γ_{EM} is a positive-semidefinite self-adjoint matrix. This allows us to write the retarded and advanced propagators as

$$G^{R/A}(t_1, t_2) = \mp\theta[\pm(t_1 - t_2)]\mathcal{T}e^{-i\int_{t_2}^{t_1} dt_3 \hat{h}_{\text{HF}}(t_3) - i\Gamma_{\text{EM}}/2}. \tag{5.50}$$

In addition we need to take into account the embedding self-energy in the time-stepping procedure like we would need to do for the solving the standard embedded Kadanoff-Baym equations introduced in the next section. It is to be noted that since the equal-time limit of the lesser Green's function gives us the one-particle reduced density matrix which obeys the equation of motion

$$\frac{d}{dt}\rho(t) + i[h_{\text{HF}}, \rho(t)] = -(I_1^<(t,t) + I_2^>(t,t)) \tag{5.51}$$

where the collision integrals I_1 and I_2 are as in Eq. (5.1) but without the imaginary track. Therefore, we see that the GKBA leads to closed kinetic equations for the one particle reduced density matrix involving scattering integrals, which demonstrates the fact that the quantum dynamics is non-Markovian, *i.e.,* we have introduced memory into our description. It is to be noted that the GKBA is an approximation for the real time lesser and greater propagator only and so far the equilibrium version is unknown. This means that during the time-propagation we need to build the correlations adiabatically in by starting the time-propagation from the non-interacting system and letting the system to relax on the correlated ground-state.

In article VI [6] we compared the full two-time Kadanoff-Baym (KBE) calculations with the GKBA. In the left panel of Fig. 5.2 we illustrate the performance of the GKBA in open systems at Hartree-Fock level. We have two- and four-site chain connected to semi-infinite leads. For the two-site chain we show the density of the first site while for the four-site chain we show the current at the right lead interface with bias voltages 1.6 and 2.4. In both of the cases the agreement between the GKBA and the KBE is satisfactory, although some discrepancy for the steady-state value of the site density in the two-site chain can be observed. For the four-site chain we see that all the features of the transient currents as well as the damping towards steady-state value is well captured with the GKBA. We also benchmarked the GKBE against the KBE in a more complicated system modeling a photovoltaic junction as a donor acceptor complex which is connected to left and right reservoirs [170]. Also for this system we found very good agreement between GKBA and KBE as seen in the right panel of Fig. 5.2 where we show the donor HOMO-LUMO densities denoted by n_l and n_h as well as the acceptor occupations n_i, $i = 1, 2, 3, 4$. The KBE is represented by dotted lines. The GKBA0 scheme denotes the GKBA with HF propagators and is denoted by the dashed lines while the GKBA-SC refers to GKBA approximation with the quasi-particle propagator (see Eq. (36) of paper IV for details [6]).

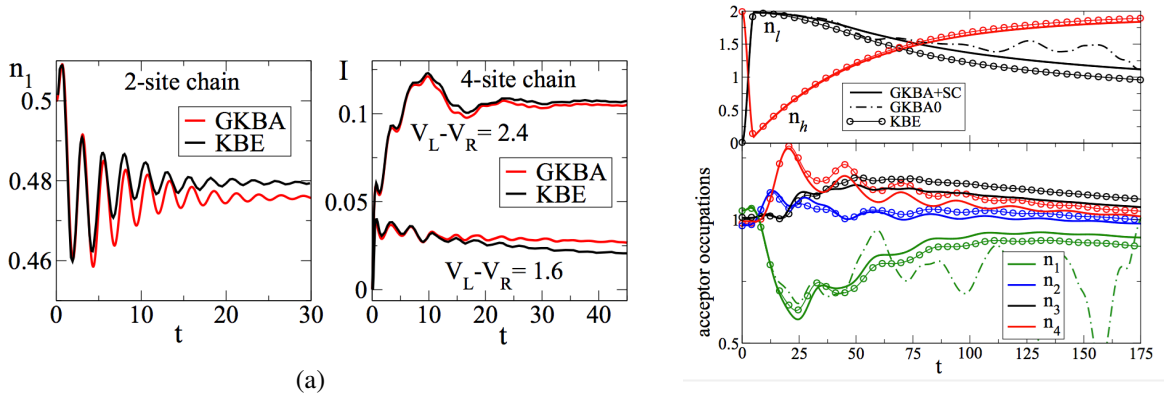

Figure 5.2: a) Comparison of GKBA with KBE of densities for 2-site chain and currents for 4-site chain. b) Comparison of GKBA with KBE for photovoltaic junction perturbed with a light pulse. n_l and n_h denote LUMO and HOMO densities respectively while n_i, $i = 1, 2, 3, 4$ denote the acceptor densities (see article IV [6] for details, Figs. from Latini et al. Phys. Rev. B **89** 0 75306 (2014) [6]).

5.1.2 EMBEDDED KADANOFF-BAYM EQUATIONS

The description of quantum transport through a nano-junction or a molecule involves modeling an open system consisting of semi-infinite electrodes attached to a finite central system, which is eventually driven out of equilibrium. With the non-equilibrium Green's function technique and the Kadanoff-Baym equations together with embedding technique we are able to project the infinite system to a finite one where the semi-infinite leads come into play via an embedding self-energy. The non-equilibrium Green's function technique allows us to take into account electron-electron interactions beyond mean-field allowing us to include non-local memory effects to our description [10, 171, 1, 3]. We are also able to drive the system out of equilibrium by various ways: by applying a bias voltage (ramp-up, smoothly switched-on or AC bias) or by a laser field. These are major improvements towards a more realistic description of transport problem and towards a better understanding of dynamics of open quantum systems. Other theories usually neglect the electron-electron interactions, like in scattering theory, or they are concentrated on the steady-state properties like the Meir-Wingreen approach [162, 13]. Some of the previous approaches to the quantum transport problems partition the system into three different regions; left and right lead having their own chemical potentials and to the central system. At time t_0 these three parts are connected and the current flows through the system [172]. Partitioning the system initially is purely a theoretical trick to simplify the problem, which does not give physically correct results in the transient regime. To describe these transient currents the system has to be treated as a whole and the driving perturbation is the bias voltage applied over the system.

5.1.3 EMBEDDING OF SEMI-INFINITE LEADS

One of the complications in describing transport through a molecular junction is that we have an open infinite system at hand. Therefore, we need to rely on some approximations. First, we could truncate the problem and take only a finite part of the leads into account. This works well if our central system is small enough and we do not need to propagate too far in time. In that case we are able to include a large enough portion of the leads without causing any artificial reflection effects from the boundary of the lead. However, if the central region is large or the characteristic dynamics are slow the extra computational effort from including the lead directly into the calculation will become eventually too large. Therefore, it is advantageous to develop a method which gives us a way to treat the leads without increasing the computational effort. The embedding technique will allow us to include the whole semi-infinite lead without introducing artificial reflections from the boundary while keeping the computational cost at the level of solving the central system only.

In our first example of the embedding technique we will show how to project an infinite open system (see Fig. 5.3) to an interacting finite central region. We will start from the equation of motion for the full

system derived in Sec. 3.3 given in matrix form as

$$[i\partial_{z_1}\boldsymbol{I} - \boldsymbol{H}(z_1)]\boldsymbol{G}(z_1, z_2) = \delta(z_1, z_2)\boldsymbol{I} + \int_{\mathcal{C}} dz_3\, \boldsymbol{\Sigma}_{\text{MB}}(z_1, z_3)\boldsymbol{G}(z_3, z_2), \tag{5.52}$$

where z is a variable on the contour $\mathcal{C}$ and $\boldsymbol{I}$ denotes identity matrix. In the localized (site) basis the Hamiltonian will consist of the Hamiltonian for the leads $\boldsymbol{h}_{\alpha\alpha}$ ($\alpha = \text{L,R}$), the Hamiltonian for the central region $\boldsymbol{h}_{\text{CC}}$, and of the coupling or hybridization between the leads and the central region $\boldsymbol{h}_{\text{C}\alpha}$ and $\boldsymbol{h}_{\alpha\text{C}}$. We will assume that there is no direct connection between the left and right lead. We will need this assumption to be able to project the Eq. (5.52) into a closed form. If for the description of the problem it is necessary to include interactions between the leads, a possible way would be to increase the central region in order to include some of the lead region as well [171]. Now we can write the Hamiltonian in the following block-matrix form

$$\boldsymbol{H}(z) = \begin{pmatrix} \boldsymbol{h}_{\text{LL}} & \boldsymbol{h}_{\text{LC}} & 0 \\ \boldsymbol{h}_{\text{CL}} & \boldsymbol{h}_{\text{CC}} & \boldsymbol{h}_{\text{CR}} \\ 0 & \boldsymbol{h}_{\text{RC}} & \boldsymbol{h}_{\text{RR}} \end{pmatrix}(z). \tag{5.53}$$

We only consider the central region as interacting whereas the leads are effectively noninteracting (it is possible to include a Hartree field in the leads). As a consequence, the many-body self-energy has non-vanishing elements only for the central region because the diagrammatic expansion starts and ends with an interaction line (all being contained in the central region). Thus, the many-body self-energy has the following block-matrix form

$$\boldsymbol{\Sigma}_{\text{MB}}(z, z') = \begin{pmatrix} 0 & 0 & 0 \\ 0 & \boldsymbol{\Sigma}^{\text{MB}}_{\text{CC}}[\boldsymbol{G}_{\text{CC}}] & 0 \\ 0 & 0 & 0 \end{pmatrix}(z, z'). \tag{5.54}$$

Finally, we have the one-particle Green's function which in block-matrix form reads as

$$\boldsymbol{G}(z, z') = \begin{pmatrix} \boldsymbol{G}_{\text{LL}} & \boldsymbol{G}_{\text{LC}} & \boldsymbol{G}_{\text{LR}} \\ \boldsymbol{G}_{\text{CL}} & \boldsymbol{G}_{\text{CC}} & \boldsymbol{G}_{\text{CR}} \\ \boldsymbol{G}_{\text{LR}} & \boldsymbol{G}_{\text{RC}} & \boldsymbol{G}_{\text{RR}} \end{pmatrix}(z, z'). \tag{5.55}$$

By projecting the equation of motion Eq. (5.52) into CC subspace we obtain

$$\begin{aligned} [i\partial_{z_1}\boldsymbol{I} - \boldsymbol{h}_{\text{CC}}(z_1)]\boldsymbol{G}_{\text{CC}}(z_1, z_2) \;=\; & \boldsymbol{I}\delta(z_1, z_2) + \int_{\mathcal{C}} dz_3\, \boldsymbol{\Sigma}^{\text{MB}}_{\text{CC}}(z_1, z_3)\boldsymbol{G}_{\text{CC}}(z_3, z_2) \\ & + \sum_{\alpha=\text{L,R}} \boldsymbol{h}_{\text{C}\alpha}\boldsymbol{G}_{\alpha\text{C}}(z_1, z_2). \end{aligned} \tag{5.56}$$

We can close this equation by finding an expression for $\boldsymbol{G}_{\alpha\text{C}}(z_1, z_2)$. Introducing a non-interacting Green's function $\boldsymbol{g}(z_1, z_2)$ describing the unconnected systems (LL, CC, RR), which satisfies the following

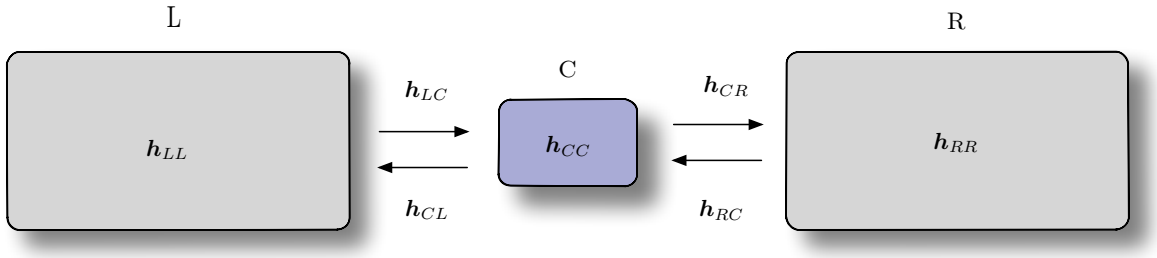

Figure 5.3: Schematics of the transport setup described by semi-infinite leads described by Hamiltonian $\boldsymbol{h}_{\alpha\alpha}$, $\alpha = \mathrm{L,R}$, the interacting central region denoted by $\boldsymbol{h}_{CC}$ as well as the hybridization between the leads and the central system $\boldsymbol{h}_{\mathrm{C}\alpha}$ and $\boldsymbol{h}_{\alpha\mathrm{C}}$.

equation of motion

$$\left(i\partial_{z_1}\boldsymbol{I} + \boldsymbol{H}(z_1) - \boldsymbol{h}^{\,\mathrm{off}}\right)\boldsymbol{g}(z_1, z_2) = \boldsymbol{I}\delta(z_1, z_2) \tag{5.57}$$

where $\boldsymbol{h}^{\,\mathrm{off}}$ describes the off-diagonal part of the total Hamiltonian (5.53). With the help of this we can invert the equation of motion Eq. (5.52) into a form of Dyson equation

$$\begin{aligned}\boldsymbol{G}(z_1, z_2) &= \boldsymbol{g}(z_1, z_2) + \int dz_3\, \boldsymbol{g}(z_1, z_3)\boldsymbol{h}^{off}\boldsymbol{G}(z_3, z_2) \\ &\quad + \int dz_3 dz_4\, \boldsymbol{g}(z_1, z_3)\boldsymbol{\Sigma}_{\mathrm{MB}}(z_3, z_4)\boldsymbol{G}(z_4, z_2).\end{aligned} \tag{5.58}$$

Taking αC-component of this equation gives

$$\boldsymbol{G}_{\alpha\mathrm{C}}(z_1, z_2) = \int dz_3\, \boldsymbol{g}_{\alpha\alpha}(z_1 z_3)\boldsymbol{h}_{\alpha\mathrm{C}}\boldsymbol{G}_{\mathrm{CC}}(z_3, z_2). \tag{5.59}$$

Inserting this to Eq. (5.56) gives us equation of motion for the central region Green's function

$$\begin{aligned}[i\partial_{z_1}\boldsymbol{I} - \boldsymbol{h}_{\mathrm{CC}}(z_1)]\boldsymbol{G}_{\mathrm{CC}}(z_1, z_2) &= \boldsymbol{I}\delta(z_1, z_2) \\ &\quad + \int_{\mathcal{C}} dz_3\, [\boldsymbol{\Sigma}^{\mathrm{MB}}_{\mathrm{CC}}(z_1, z_3) + \boldsymbol{\Sigma}_{\mathrm{EM}}(z_1, z_3)]\boldsymbol{G}_{\mathrm{CC}}(z_3, z_2).\end{aligned} \tag{5.60}$$

This equation has exactly the same form as the equation of motion for the full system, except that now we have an extra term which we call the embedding self-energy defined as

$$\boldsymbol{\Sigma}_{\mathrm{EM}}(z_1, z_2) = \sum_{\alpha=\mathrm{L,R}} \boldsymbol{h}_{\mathrm{C}\alpha}\boldsymbol{g}_{\alpha\alpha}(z_1, z_2)\boldsymbol{h}_{\alpha\mathrm{C}} \tag{5.61}$$

describing the effect of leads. The embedding self-energy includes the time-dependent effects of the leads into our description via the lead Green's function $\boldsymbol{g}_{\alpha\alpha}(z_1, z_2)$, while the strength of the lead–central

system–lead hybridization is described by the coupling hamiltonians $\boldsymbol{h}_{C\alpha}$ and $\boldsymbol{h}_{\alpha C}$. This is a general form of the embedding self-energy which does not assume anything from the structure of the lead.

5.1.4 EMBEDDED TIME-DEPENDENT KOHN-SHAM EQUATIONS

Within TDDFT we are also able to derive embedded Kohn-Sham equations where we need to propagate the central system Kohn-Sham wave functions (see S. Kurth *et al.* [154] for details). As we did in the earlier section within the MBPT, we can partition the infinite open system KS Hamiltonian into a localized basis to left lead, device, and right lead. The KS Hamiltonian in a block-diagonal matrix form reads

$$\begin{pmatrix} \mathbf{H}^{\mathrm{KS}}_{\mathrm{LL}}(t) & \mathbf{H}_{\mathrm{LC}} & 0 \\ \mathbf{H}_{\mathrm{CL}} & \mathbf{H}^{\mathrm{KS}}_{\mathrm{CC}}(t) & \mathbf{H}_{\mathrm{CR}} \\ 0 & \mathbf{H}_{\mathrm{RC}} & \mathbf{H}^{\mathrm{KS}}_{\mathrm{RR}}(t) \end{pmatrix}, \tag{5.62}$$

where $\mathbf{H}^{\mathrm{KS}}_{\mathrm{CC}}(t)$ is the Hamiltonian of the isolated device and $\mathbf{H}^{\mathrm{KS}}_{\alpha\alpha}(t) = \mathbf{H}^{\mathrm{KS}}_{\alpha\alpha}$ is the Hamiltonian of the isolated lead α, $\alpha = L, R$. The terms $\mathbf{H}_{C\alpha}$ and $\mathbf{H}_{\alpha C}$ describe the coupling between lead α and the device. The equation of motion for the single-particle orbitals projected to central region can readily seen to be (see Kurth *et al.* for details [154])

$$[i\partial_t - \boldsymbol{h}^{\mathrm{KS}}_{\mathrm{CC}}(t)]\,\psi_{\mathrm{C}}(t) = \int_0^t \mathrm{d}\bar{t}\; \boldsymbol{\Sigma}^{\mathrm{R}}_{\mathrm{KS,EM}}(t,\bar{t})\psi_{\mathrm{C}}(\bar{t}) + \sum_\alpha \boldsymbol{h}_{C\alpha}\, \boldsymbol{g}^{\mathrm{R}}_{\alpha\alpha}(t,0)\psi_\alpha(0), \tag{5.63}$$

where $\boldsymbol{\Sigma}^{\mathrm{R}}_{\mathrm{KS,EM}}(t,\bar{t})$ is the KS embedding self-energy, $\boldsymbol{g}^{\mathrm{R}}_{\alpha\alpha}$ is the retarded lead Green's function, and $\boldsymbol{h}_{C\alpha}$ describes the coupling between the leads and the central region. Assuming that the exchange-correlation potential is zero in the leads then $\boldsymbol{\Sigma}^{\mathrm{R}}_{\mathrm{KS,EM}}(t,\bar{t})$ can be replaced by $\boldsymbol{\Sigma}^{\mathrm{R}}_{\mathrm{EM}}(t,\bar{t})$ Eq.(5.61).

5.1.5 FORM OF EMBEDDING SELF-ENERGY FOR TIGHT-BINDING SEMI-INFINITE LEAD

As an example of the embedding self-energy in transport situation we consider a linear chain of a one-body tight-binding model described by the Hamiltonian

$$\hat{H}_{lead}(t) = \sum_{\alpha=L,R}\sum_{k,l\in\alpha}^{\infty} \left[t^\alpha_{kl} + W^\alpha(t)\delta_{kl}\right]\hat{d}^\dagger_{k\alpha\sigma}\hat{d}_{l\alpha\sigma} \tag{5.64}$$

where $\alpha = \mathrm{L/R}$ and $t^\alpha_{kl} = (\varepsilon_{k\alpha} - \mu)\delta_{kl} + V^\alpha_{\langle k,l\rangle}$ is the nearest neighbor Hamiltonian of the lead α where $\langle k,l\rangle$ denotes the nearest neighbor indices, $\varepsilon_{k\alpha}$ denotes the onsite energy in the lead α, while $V^\alpha_{\langle k,l\rangle}$ denotes the hopping between nearest neighbor sites. The time-dependent bias in lead α is denoted with $W^\alpha(t)$.

This section will allow us to introduce the basic notation and properties of the lead used later in discussing the numerical results. The main effect of the lead is that when the central system consisting of set of

discrete states is coupled to a continuum of the lead electronic states, this coupling will cause an extra broadening for the central system levels. Therefore, even for the non-interacting system we do not have anymore discrete delta-function like states but levels with certain life-time which are proportional to the imaginary part of the embedding self-energy, commonly called the level broadening and denoted by $\mathbf{\Gamma}_{\text{EM}}$ which is usually a positive-semidefinite self-adjoint matrix. We defined the embedding self-energy to be proportional to the non-interacting lead Green's function in the localized basis and to the coupling hamiltonians as

$$\mathbf{\Sigma}_{\text{EM}}(z_1, z_2) = \sum_{\alpha=\text{L,R}} \boldsymbol{h}_{\text{C}\alpha} \boldsymbol{g}_{\alpha\alpha}(z_1, z_2) \boldsymbol{h}_{\alpha\text{C}}, \tag{5.65}$$

where the coupling matrix elements, being the off-diagonal elements of the full block matrix Hamiltonian Eq. (5.53), are

$$\hat{h}_{\text{off}} = \sum_{ik} \left[V_{ki,\alpha} \hat{d}_k^\dagger \hat{c}_i + V_{ik,\alpha} \hat{c}_i^\dagger \hat{d}_k \right], \tag{5.66}$$

where the indices $i \in$ C and $k \in \alpha$ label the basis functions in the central region C and leads $\alpha =$ L,R respectively. The non-interacting Green's function in delocalized basis can be readily found to be [22, 173]

$$\tilde{g}^<_{\alpha,kl}(t_1, t_2) = i\delta_{kl} f(\varepsilon_{k\alpha}) e^{-i\int_{t_2}^{t_1} dt_3 \, [\varepsilon_{k\alpha} - \mu - W_\alpha(t_3)]}, \tag{5.67}$$

$$\tilde{g}^>_{\alpha,kl}(t_1, t_2) = i\delta_{kl} [f(\varepsilon_{k\alpha}) - 1] e^{-i\int_{t_2}^{t_1} dt_3 \, [\varepsilon_{k\alpha} - \mu - W_\alpha(t_3)]}, \tag{5.68}$$

where again $\varepsilon_{k\alpha}$ is the on-site energy of the lead sites, μ is the chemical potential and $W_\alpha(t)$ is the bias voltage in the lead α while $f(\varepsilon_{k\alpha})$ denotes the Fermi distribution and δ_{kl} is the standard Dirac-delta. We can obtain the lead Green's function in localized site basis via a basis transformation which diagonalizes the lead Hamiltonian $D^\dagger \hat{H}_{lead} D = \text{diag}[\varepsilon_{k\alpha}]$ giving us

$$g_{ij}(t, t') = \left[D \tilde{g}(t, t') D^\dagger \right]_{ij}. \tag{5.69}$$

Therefore, the lesser and greater components in the site basis are

$$g^<_{ij}(t_1, t_2) = i \sum_k D_{ik} f(\varepsilon_{k\alpha}) e^{-i\int_{t_2}^{t_1} dt_3 \, (\varepsilon_{k\alpha} - \mu - W_\alpha(t_3))} D^\dagger_{kj}, \tag{5.70}$$

$$g^>_{ij}(t_1, t_2) = i \sum_k D_{ik} [f(\varepsilon_{k\alpha}) - 1] e^{-i\int_{t_2}^{t_1} dt_3 \, (\varepsilon_{k\alpha} - \mu - W_\alpha(t_3))} D^\dagger_{kj} \tag{5.71}$$

in terms of which we can write the embedding self-energies. For example, the ij-component of the lesser self-energy is

$$\begin{aligned} \Sigma^<_{ij,\alpha,\text{EM}}(t_1, t_2) &= \sum_{kl} V_{i,k\alpha} g^<_{kl}(t_1, t_2) V_{l\alpha,j} \\ &= i \sum_{kl} \sum_m V_{i,k\alpha} D_{km} f(\varepsilon_{m\alpha}) e^{-i\int_{t_2}^{t_1} dt_3 \, (\varepsilon_{m\alpha} - \mu - W_\alpha(t_3))} D^\dagger_{ml} V_{l\alpha,j} \end{aligned}$$

$$= ie^{-i\int_{t_2}^{t_1} dt_3\, W_\alpha(t_3)} \int \frac{d\varepsilon}{2\pi} f(\varepsilon)\Gamma_{ij,\alpha}(\varepsilon)e^{-i(\varepsilon-\mu)(t_1-t_2)}, \tag{5.72}$$

where we defined so-called level-broadening or the linewidth function $\mathbf{\Gamma}_{\text{EM}}$ in local site basis as

$$[\mathbf{\Gamma}]_{ij,\alpha,\text{EM}}(\varepsilon) = 2\pi \sum_{klm} V_{i,k\alpha} V_{l\alpha,j} D_{km} \delta(\varepsilon - \varepsilon_{m\alpha}) D^\dagger_{ml}. \tag{5.73}$$

Similarly we can derive the greater embedding self-energy

$$\Sigma^{>}_{ij,\alpha,\text{EM}}(t_1,t_2) = ie^{-i\int_{t_2}^{t_1} dt_3\, W_\alpha(t_3)} \int \frac{d\varepsilon}{2\pi}[f(\varepsilon)-1]\Gamma_{ij,\alpha}(\varepsilon)e^{-i(\varepsilon-\mu)(t_1-t_2)}. \tag{5.74}$$

The other components of the embedding self-energies needed to propagate the Kadanoff-Baym equations can be obtained from the definitions of the mixed and Matsubara components in terms of the lesser and greater Green's functions.

Our problem has now reduced to the determination of the exact form for the level broadening $\mathbf{\Gamma}_{\text{EM}}(\varepsilon)$, which clearly will need to depend on the energy spectrum of the lead. This can be seen by diagonalizing the tight-binding Hamiltonian for the leads [173] yielding following eigenvalues and eigenvectors

$$\lambda_k = \varepsilon_\alpha \pm 2V_\alpha \cos\left(\frac{\pi k}{N+1}\right), \tag{5.75}$$

$$x_n^{(k)} = (-1)^{n+1}\sqrt{\frac{2}{N+1}} \sin\left(\frac{n\pi k}{N+1}\right), \tag{5.76}$$

where N is number of sites in the tight-binding chain (eventually we will take the limit $N \to \infty$), $k = 1, ..., N$ and $n = 1, ..., N$, and V_α is the hopping between the sites in the lead. The eigenvectors determine now the transformation matrix $\mathbf{D}$ and the level-broadening matrix can now be written with these eigenvectors as

$$\Gamma_{ij,\alpha,\text{EM}}(\varepsilon) = 2\pi V_{i,1} V_{1,j} \sum_{k=1}^{N} x_1^{(k)} \delta(\varepsilon - \varepsilon_{k\alpha}) x_1^{(k)}. \tag{5.77}$$

Assuming infinite leads the spacing between energy levels will be small and the number of levels will be infinite, therefore we will turn the summation over k into a integration and the the limit $N \to \infty$ together with the change of integration variables according to $y = -2V_\alpha \cos\left(\frac{k\pi}{N+1}\right) \Rightarrow \cos\left(\frac{k\pi}{N+1}\right) = -\frac{-y}{2V_\alpha}$ and using an identity $\sin^2\left(\frac{k\pi}{N+1}\right) = 1 - \frac{y^2}{4V_a^2}$ gives an expression for the level broadening [173]

$$\begin{aligned}\Gamma_{ij,\alpha,\text{EM}}(\varepsilon) &= \frac{2V_{i,1}V_{1,j}}{V_\alpha}\int_{-2V_\alpha}^{2V_\alpha} dy \sqrt{1-\frac{y^2}{4V_\alpha^2}}\delta(\varepsilon-\varepsilon_\alpha+\mu-y) \\ &= \frac{2V_{i,1}V_{1,j}}{V_\alpha}\sqrt{1-\frac{\varepsilon^2}{4V_\alpha^2}}\theta(2V_\alpha-|\varepsilon|).\end{aligned} \tag{5.78}$$

Inserting this equation to the expressions of the greater and lesser components of the embedding self-energy we obtained our result. For time-independent bias voltages or if the system has reached a steady-state we

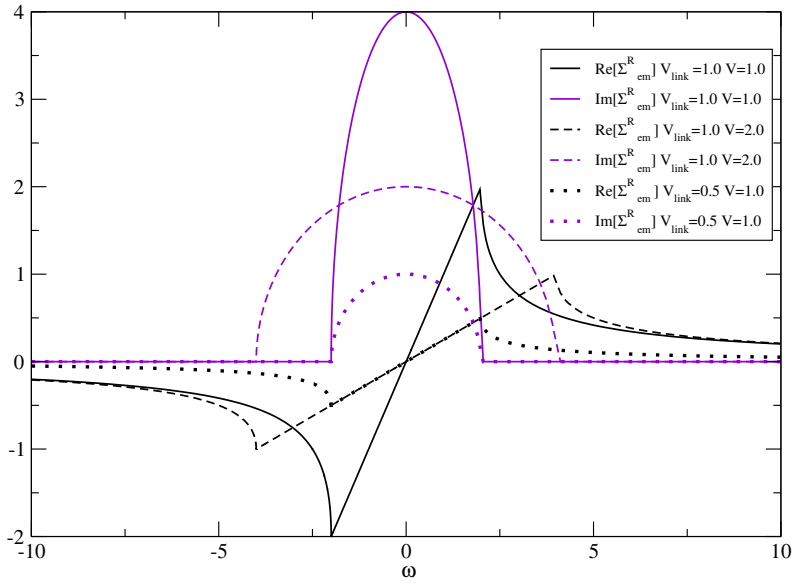

Figure 5.4: Real and imaginary part of the retarded component embedding self-energy. V_{link} denotes the coupling between central region and the leads while V denotes the hopping between the lead sites.

can Fourier transform the embedding as

$$\Sigma^{\gtrless}_{\text{EM},\alpha}(t_1 - t_2) = \int \frac{d\omega}{2\pi} e^{i\omega(t_1-t_2)} \Sigma^{\gtrless}_{\text{EM},\alpha}(\omega) \tag{5.79}$$

where

$$\Sigma^{<}_{\text{EM},\alpha}(\omega) = i f_\alpha(\omega - W_\alpha)\Gamma_{\text{EM}}(\omega - W_\alpha), \tag{5.80}$$

$$\Sigma^{>}_{\text{EM},\alpha}(\omega) = i[f_\alpha(\omega - W_\alpha) - 1]\Gamma_{\text{EM}}(\omega - W_\alpha), \tag{5.81}$$

giving us the retarded and advanced embedding self-energies $\Sigma^{R/A}_{\text{EM},\alpha}(t_1,t_2) = \mp\theta(\pm(t_1-t_2))[\Sigma^{>}_{\text{EM},\alpha}(t_1,t_2) - \Sigma^{<}_{\text{EM},\alpha}(t_1,t_2)]$ in Fourier space as

$$\Sigma^{R/A}_{\text{EM},\alpha}(\omega) = \Lambda_{\alpha,\text{EM}}(\omega) \mp \frac{i}{2}\Gamma_{\alpha,\text{EM}}(\omega), \tag{5.82}$$

where the real part of the retarded embedding self-energy is defined as the Hilbert transform of the broadening $\Gamma_{\text{EM}} = \sum_{\alpha=L,R} \Gamma_{\alpha,\text{EM}}$

$$\Lambda_\alpha(\omega) = \mathcal{P}\int \frac{d\omega'}{\pi} \frac{\Gamma_{\alpha,\text{EM}}(\omega')/2}{\omega - \omega'}. \tag{5.83}$$

The retarded embedding self-energy for the tight-binding leads in Fourier space can compactly be written as

$$\Sigma^R_{\mathrm{EM},\alpha}(\omega) = \Lambda_{\alpha,\mathrm{EM}}(\omega) - \frac{i}{2}\Gamma_{\alpha,\mathrm{EM}}(\omega) = \frac{V_{1\alpha,i}V_{j,1\alpha}}{2V_\alpha^2}\begin{cases} \omega_\alpha - \sqrt{\omega_\alpha^2 - 4V_\alpha^2} & ,\omega_\alpha > 2|V_\alpha| \\ \omega_\alpha + \sqrt{\omega_\alpha^2 - 4V_\alpha^2} & ,\omega_\alpha < -2|V_\alpha| \\ \omega_\alpha - i\sqrt{4V_\alpha^2 - \omega_\alpha^2} & ,|\omega_\alpha| < 2|V_\alpha| \end{cases} \tag{5.84}$$

where $\omega_\alpha = \omega - \varepsilon_\alpha + \mu - W_\alpha$, with the lead-on-site parameter a and the hopping parameter between the lead sites b. The chemical potential is denoted by μ, the applied bias for the lead α by W_α, and $V_{1\alpha,0}, V_{0,1\alpha}$ are the left/right couplings between leads and the central site. In Fig. 5.4 we show the real and imaginary part for the retarded component of the self-energy with different parameters. The spectral function of the non-interacting coupled system reads

$$\mathcal{A}(\omega) = \frac{1}{2\pi}\frac{\Gamma_{\mathrm{EM}}(\omega)}{[\omega - \varepsilon - \Lambda_{\mathrm{EM}}(\omega)]^2 + [\Gamma_{\mathrm{EM}}(\omega)/2]^2}. \tag{5.85}$$

We see that the band width of the lead is given by the nearest neighbour hopping parameter V_α, which determines the width of the non-zero domain for $\mathrm{Im}\,[\Sigma^R_{\mathrm{EM}}]$. The coupling parameter V_{link} on the other hand determines the magnitude of the $\mathrm{Im}\,[\Sigma^R_{\mathrm{EM}}]$ yielding larger broadening for the central region levels. The real part of the retarded self-energy determines the sift of central region levels compared to the unconnected system. The *wide-band* approximation is obtained by approximating Σ^R_{EM} at zero frequency $\Sigma^R_{\mathrm{EM}}(\omega = 0)$ yielding the real part to be zero while the imaginary part is frequency independent constant having value $\Gamma = 2V_{1\alpha,i}V_{j,1\alpha}/V_\alpha^2$.

5.1.6 Embedding of a Finite Region

The charge transport and charge transfer in large molecules has attracted a lot of interest for their potential use as light-based devices. We will now introduce a way to use the embedding technique to study energy transfer through long organic molecules by using many-body perturbation theory together with the Kadanoff-Baym equations. The system is excited at the one end of the molecule and a charge cloud is transported to the other end-group via the connecting wire, usually a large organic molecule, which will transfer the electronic excitation energy.

In order to study the charge and energy transfer through a large organic molecule we need to reduce the system size to be able to handle the system numerically. Therefore, we divide the system in two parts A and B, A denoting the middle carbon backbone based structure whereas B denotes the end-groups (see Fig. 5.5). Consequently, the Hamiltonian matrix, the Green's function, and the self-energy matrices attain the following block matrix from

$$\boldsymbol{H} = \begin{pmatrix} \boldsymbol{H}_{AA} & \boldsymbol{H}_{AB} \\ \boldsymbol{H}_{BA} & \boldsymbol{H}_{BB} \end{pmatrix}, \quad \boldsymbol{G} = \begin{pmatrix} \boldsymbol{G}_{AA} & \boldsymbol{G}_{AB} \\ \boldsymbol{G}_{BA} & \boldsymbol{G}_{BB} \end{pmatrix}, \quad \boldsymbol{\Sigma} = \begin{pmatrix} 0 & 0 \\ 0 & \boldsymbol{\Sigma}_{BB} \end{pmatrix}. \tag{5.86}$$

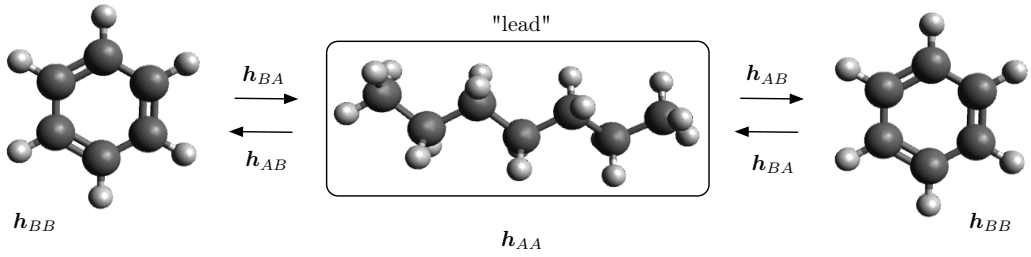

Figure 5.5: Schematics showing the division of the system into end-groups and to embedded central region.

We will treat the electron-electron interactions only on the end-groups which reduces the self-energy matrix to have only the $\mathbf{\Sigma}_{BB}$ element. Extracting from the equation of motion of the Green's function Eq. (3.51) the equation for the $\boldsymbol{G}_{BB}(z,z')$ only, and with the help of the non-contacted non-interacting Green's function of the subsystem A

$$\big[i\frac{d}{dz}\mathbf{1} - \boldsymbol{H}_{AA}(z)\big]\boldsymbol{g}_{AA}(z,z') = \delta(z,z')\mathbf{1} \tag{5.87}$$

we obtain a closed equation for the Green's function $\boldsymbol{G}_{BB}(z,z')$ only,

$$\big[i\frac{d}{dz}\mathbf{1} - \boldsymbol{H}_{BB}(z)\big]\boldsymbol{G}_{BB}(z,z') = \delta(z,z')\mathbf{1} + \int_\gamma d\bar{z}\big[\mathbf{\Sigma}_{\text{EM}}(z,\bar{z}) + \mathbf{\Sigma}_{BB}(z,\bar{z})\big]\boldsymbol{G}_{BB}(\bar{z},z'), \tag{5.88}$$

where $\mathbf{\Sigma}_{em}(z,z')$ is now the embedding self-energy having a general form

$$\mathbf{\Sigma}_{\text{EM}}(z,z') = \boldsymbol{H}_{BA}(z)\boldsymbol{g}_{AA}(z,z')\boldsymbol{H}_{AB}(z'). \tag{5.89}$$

As an example we give the lesser component of the embedding self-energy

$$\begin{aligned}\Sigma^<_{\text{EM},rs}(t,t') &= \sum_{ij}\sum_{k,l\in B} V_{r,i}U_{ik}g^<_{kk}(t,t')U^\dagger_{lj}V_{j,s} \\ &= i\sum_k V_{n_A,1_B}U_{1_B,k}f(\varepsilon_k)\exp[-i\varepsilon_k(t-t')]U^\dagger_{k,n_C}V_{n,B_A},\end{aligned} \tag{5.90}$$

as well as the greater component of the embedding self-energy

$$\begin{aligned}\Sigma^>_{\text{EM},rs}(t,t') &= \sum_{ij}\sum_{k,l\in B} V_{r,i}U_{ik}g^<_{kk}(t,t')U^\dagger_{lj}V_{j,s} \\ &= i\sum_k V_{n_A,1_B}U_{1_B,k}[f(\varepsilon_k)-1]\exp[-i\varepsilon_k(t-t')]U^\dagger_{k,n_B}V_{n_B,n_A},\end{aligned} \tag{5.91}$$

where the $V_{i,j}$ are the coupling matrix elements, $U_{i,j}$ are the elements of the unitary transformation matrix between the site and orbital basis, $g(t,t')$ is the non-interacting Green's function in the embedded region,

$f(\varepsilon)$ is the Fermi-Dirac distribution and ε_k are the eigenenergies of the embedded region. Therefore, in practice the calculation of the embedding self-energy reduces to the finding of these eigenenergies, *e.g.*, to the diagonalization of the Hamiltonian matrix describing the embedded region.

As an example system we study a chain consisting of fourteen sites. The two sites at the end-groups (system B) are treated as interacting while the ten middle sites (system A) we treat via the embedding self-energy. The system is described by a Hamiltonian $\hat{H} = \hat{H}_A + \hat{H}_B + \hat{H}_{AB}$, where

$$\hat{H}_A = \sum_{i=1\in A,\sigma}^{N_A} \varepsilon_{i\sigma}^A \hat{c}_{i\sigma}^\dagger \hat{c}_{i\sigma} + \sum_{i=1,\sigma}^{N_A-1} \left[V_A \hat{c}_{i\sigma}^\dagger \hat{c}_{i+1\sigma} + h.c.\right] \tag{5.92}$$

describes the embedded region. The on-site potential is denoted by $\varepsilon_{i\sigma}^A$, where i is the site index and σ labels the spin index, $\hat{c}^\dagger, \hat{c}$ are the creation and the annihilation operators in the embedded region, and V_A denotes the hopping between sites. The interacting end groups are described by the following Hamiltonian

$$\begin{aligned}\hat{H}_B &= \sum_{i\in B}^{N_B} [\varepsilon_{i\sigma}^B(t) + W_i(t)] \hat{d}_{i\sigma}^\dagger \hat{d}_{i\sigma} + \sum_{i=1,\sigma}^{N_B-1} \left[V_B \hat{d}_{i\sigma}^\dagger \hat{d}_{i+1\sigma} + h.c.\right] \\ &\quad + \frac{1}{2} \sum_{i,j=1,\, i,j\in B\sigma\sigma'}^{N_B} w_{ij} \hat{d}_{i\sigma}^\dagger \hat{d}_{j\sigma'}^\dagger \hat{d}_{j\sigma'} \hat{d}_{i\sigma},\end{aligned} \tag{5.93}$$

where $\varepsilon_{i\sigma}^B$ is the on-site potential for the end-group sites, $W_i(t)$ is a time-dependent external perturbation on the site i, $\hat{d}^\dagger, \hat{d}$ are the creation and the annihilation operators for the end-group sub-system, V_B is the hopping between neighboring sites and w_{ij} is the interaction strength having the form $w_{ij} = U$ if $i = j$ and $w_{ij} = w_{ii}/2|i-j|$ if $i \neq j$. The tunneling Hamiltonian between the sub-system A and B is

$$\hat{H}_{AB,BA} = -\sum_{ij,\sigma} [(V_{i,j} \hat{c}_{i\sigma}^\dagger \hat{d}_{j\sigma} + V_{j,i} \hat{d}_{j\sigma}^\dagger \hat{c}_{i\sigma}) + h.c.], \tag{5.94}$$

where $V_{i,j}$ denotes the coupling element between the site i in sub-system A and site j in sub-system B.

We benchmark the embedded scheme against the full interacting calculation of the Kadanoff-Baym method to test our embedding scheme. We take the nearest neighbor hopping terms to equal to -1.0 everywhere, *i.e.*, $V_A = V_B = V_{i,j} = -1.0$. We apply a perturbation on the first site with step-like perturbation at $t = 0$, *i.e.*, $W_i(t) = 0.5\theta(t)$ for $i = 1$ and $W_i(t) = 0$ otherwise.

It is clear that for the non-interacting system the embedded and the full calculation will yield the same result for the observables. Therefore, we consider an interacting system with interaction strength $U = 0.5$. In Fig. 5.6 we show the time-dependent density for the first and last site without with embedding treatment for HF and 2B approximations. We see a slight difference between the embedded calculation as we would expect, since in the embedded case we have only the two end sites interaction on the both ends of the noninteracting chain compared to the interacting 14-site chain. We notice that the density profile is

slightly out of the phase but the qualitative features are in a good agreement which suggest that the optical spectrum should be fairly reasonable compared to the one obtained from the full calculation.

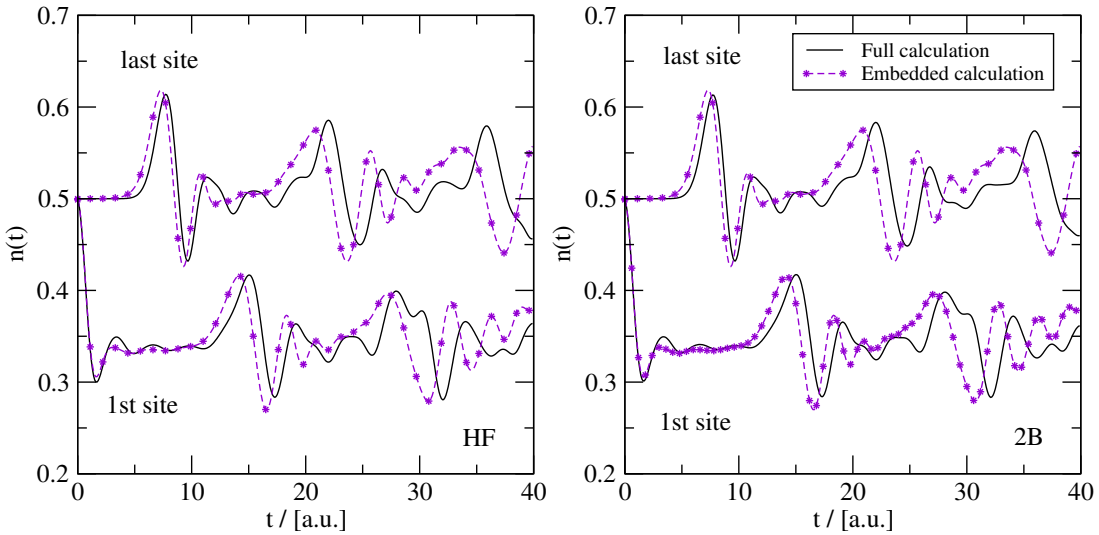

Figure 5.6: Density of the first and last site compared with the embedded and full calculation. The system is driven out of equilibrium by applying a constant potential of $W_1 = 0.5$ to the first site.

5.2 TIME-DEPENDENT MEIR-WINGREEN FORMULA

For the purposes of quantum transport calculations we need to evaluate the time-dependent current through the central-region–lead interface which we will denote by $I_\alpha(t)$, where $\alpha = \mathrm{L,R}$. This current will be proportional to the total change of the particle number in the lead α denoted by $\hat{n}_\alpha$. Thus, by the continuity equation

$$I_\alpha(t) = \frac{d}{dt}\hat{n}_\alpha(t) = -i\frac{d}{dt}\boldsymbol{G}^<_{\alpha\alpha}(t,t) = -i\mathrm{Tr}_\alpha\left[\partial_t \boldsymbol{G}^<_{\alpha\alpha}(t,t') + \partial_{t'}\boldsymbol{G}^<_{\alpha\alpha}(t,t')\right]_{t=t'}. \tag{5.95}$$

From the equation of motion with the Hamiltonian for the transport setup Eq. (5.52) we can extract the $\alpha\alpha$ component of the lesser Green's function

$$i\partial_t \boldsymbol{G}^<_{\alpha\alpha}(t,t') = \delta(t,t')\mathbf{1}_{\alpha\alpha} + \boldsymbol{h}_{\alpha\alpha}(t)\boldsymbol{G}^<_{\alpha\alpha}(t,t') + \boldsymbol{h}_{\mathrm{C}\alpha}(t)\boldsymbol{G}^<_{\alpha\mathrm{C}}(t,t'), \tag{5.96}$$

$$i\partial_{t'} \boldsymbol{G}^<_{\alpha\alpha}(t,t') = -\delta(t,t')\mathbf{1}_{\alpha\alpha} - \boldsymbol{G}^<_{\alpha\alpha}(t,t')\boldsymbol{h}_{\alpha\alpha}(t') - \boldsymbol{G}^<_{\alpha\mathrm{C}}(t,t')\boldsymbol{h}_{\mathrm{C}\alpha}(t'). \tag{5.97}$$

Inserting these equations back into the equation for the time-dependent current trough the interface α Eq. (5.95) we find

$$I_\alpha(t) = \mathrm{Tr}_\alpha\left[\boldsymbol{G}^<_{\alpha\mathrm{C}}(t,t)\boldsymbol{h}_{\mathrm{C}\alpha}(t) + \boldsymbol{G}^<_{\alpha\mathrm{C}}(t,t)\boldsymbol{h}_{\mathrm{C}\alpha}(t)\right]. \tag{5.98}$$

Using the symmetry property $[\boldsymbol{h}_{\alpha \mathrm{C}} \boldsymbol{G}^{<}_{\mathrm{C}\alpha}(t,t')]^{\dagger} = -\boldsymbol{G}^{<}_{\mathrm{C}\alpha}(t',t)\boldsymbol{h}_{\alpha C}$ we can write the equation for the current to be proportional to the real part of the trace over the central system states as a product of the coupling Hamiltonian and Green's function over the contact

$$I_{\alpha}(t) = -2\mathrm{Re}\left\{\mathrm{Tr}_{\alpha}[\boldsymbol{G}^{<}_{\alpha\mathrm{C}}(t,t)\boldsymbol{h}_{\mathrm{C}\alpha}(t)]\right\} = -2\mathrm{Re}\left\{\mathrm{Tr}_{\mathrm{C}}[\mathbf{G}^{<}_{\mathrm{C}\alpha}(t,t)\boldsymbol{h}_{\alpha\mathrm{C}}(t)]\right\}. \tag{5.99}$$

From this equation (Eq. (5.98)) we see that the current through the interface α is proportional to the coupling Hamiltonian $\boldsymbol{h}_{\alpha\mathrm{C}}$ as well as to the Green's function $\boldsymbol{G}_{\alpha\mathrm{C}}$. This is very intuitive since the stronger the coupling, the easier the current flows while the Green's function describes the propagation of the particle from the lead to the central region. To write the current without referring to the lead indices we will solve the equation of motion for the $\boldsymbol{G}^{<}_{\mathrm{C}\alpha}$ component of the Green's function as (see Eq. (5.59))

$$\boldsymbol{G}_{\mathrm{C}\alpha}(t,t') = \int_{\mathcal{C}} d\bar{t}\, \boldsymbol{G}_{\mathrm{CC}}(t,\bar{t})\boldsymbol{h}_{\mathrm{C}\alpha}\boldsymbol{g}_{\alpha\alpha}(\bar{t},t') \tag{5.100}$$

from which we obtain the lesser component as

$$\begin{aligned} \boldsymbol{G}^{<}_{\mathrm{C}\alpha}(t,t') &= \int d\bar{t}\big[\boldsymbol{G}^{<}_{\mathrm{CC}}(t,\bar{t})\boldsymbol{h}_{\mathrm{C}\alpha}\boldsymbol{g}^{A}_{\alpha\alpha}(\bar{t},t') + \boldsymbol{G}^{R}_{\mathrm{CC}}(t,\bar{t})\boldsymbol{h}_{\mathrm{C}\alpha}\boldsymbol{g}^{<}_{\alpha\alpha}(\bar{t},t')\big] &(5.101)\\ &\quad + \int_{0}^{-i\beta} d\bar{\tau}\boldsymbol{G}^{\rceil}_{\mathrm{CC}}(t,\bar{\tau})\boldsymbol{h}_{\mathrm{C}\alpha}\boldsymbol{g}^{\lceil}_{\alpha\alpha}(\bar{\tau},t'). &(5.102)\end{aligned}$$

Thus, we obtain the equation for the time-dependent current to be

$$\begin{aligned} I_{\alpha}(t) = -2\mathrm{Re}\Bigg\{\mathrm{Tr}_{\mathrm{C}}\Bigg[&\int_{0}^{\infty} d\bar{t}[G^{<}_{\mathrm{CC}}(t,\bar{t})\Sigma^{A}_{\alpha,\mathrm{EM}}(\bar{t},t) + G^{R}_{\mathrm{CC}}(t,\bar{t})\Sigma^{<}_{\alpha,\mathrm{EM}}(\bar{t},t)] \\ &+ \int_{0}^{-i\beta} d\bar{\tau} G^{\rceil}_{\mathrm{CC}}(t,\bar{\tau})\Sigma^{\lceil}_{\alpha,\mathrm{EM}}(\bar{\tau},t)\Bigg]\Bigg\}, \end{aligned} \tag{5.103}$$

which we call the time-dependent *Meir-Wingreen formula*. The equation for the current depends only on the central region Green's function while the leads come into play via the embedding self-energy. The many-body part of the self-energy is implicitly coded in the Green's function via the Dyson equation. The first two terms in the current equation (5.103) involving integrations over the earlier times take the history effects into account while the last term, depending on the times on the imaginary track as well as on the real axis, describes the initial correlations.

The time-dependent version of the *Meir-Wingreen formula* (5.103) reduces to the standard steady-state version [162] by taking the limit $t \to \infty$. This assumes that in this limit the Green's functions are time-translationally invariant, *i.e.*, they depend only on the time-difference of the arguments. We will also need to assume that the Green's function and self-energy will vanish if the separation between their time arguments goes to infinity, *i.e.,* the initial correlation terms approaches to zero. By letting $t_0 \to -\infty$, after a Fourier transformation and some algebra we obtain

$$I_\alpha = -i\mathrm{Tr}_\mathrm{C}\left\{\int_{-\infty}^{\infty}\frac{d\omega}{2\pi}\mathbf{\Gamma}_{\alpha,\mathrm{EM}}(\omega)\left[\boldsymbol{G}^<_{\mathrm{CC}}(\omega) - 2\pi i f_\alpha(\omega)\mathcal{A}_{\mathrm{CC}}(\omega)\right]\right\} \tag{5.104}$$

where $\mathbf{\Gamma}_{\alpha,\mathrm{EM}}$ is the imaginary part of the retarded embedding self-energy for lead $\alpha = L, R$ and $f_\alpha(\omega) = f(\omega + W_\alpha)$ is the Fermi distribution for the lead α and $\mathcal{A}_{\mathrm{CC}}$ is the spectral function for the central region.

We can also check that the continuity equation is satisfied for the currents, *i.e.*, $I_L = -I_R = I$ implied by the charge conservation. From the equation (5.103) in the long time limit we obtain the following formula for the current in frequency space

$$I_\alpha = \int\frac{d\omega}{2\pi}\mathrm{Tr}_C\left[\mathbf{\Sigma}^<_{tot,\alpha}(\omega)\boldsymbol{G}^>_{\mathrm{CC}}(\omega) - \mathbf{\Sigma}^>_{tot,\alpha}(\omega)\mathbf{G}^<_{\mathrm{CC}}(\omega)\right] \tag{5.105}$$

where $\mathbf{\Sigma}_{tot,\alpha} = \mathbf{\Sigma}_{\mathrm{MB}} + \mathbf{\Sigma}_{\mathrm{EM},\alpha}$. If we now look at the difference between the currents flowing through the left and right interface $\Delta I = I_L + I_R$ we have

$$\Delta I = \int\frac{d\omega}{2\pi}\mathrm{Tr}_C\left[\mathbf{\Sigma}^<_{tot}(\omega)\boldsymbol{G}^>_{\mathrm{CC}}(\omega) - \mathbf{\Sigma}^>_{tot}(\omega)\boldsymbol{G}^<_{\mathrm{CC}}(\omega)\right] \tag{5.106}$$

which for conserving approximations is zero according to equation (3.124).

5.3 NUMERICAL SIMULATIONS

In this section we will demonstrate some basic properties and phenomena of the quantum transport problem which will help the reader to understand the results presented in the articles I-III. We will start by considering transport through a linear chain consisting of five sites described by tight-binding model connected to semi-infinite non-interacting one dimensional tight-binding leads (see Eq. (2.37)). The tight-binding parameters characterizing the lead $h^\alpha_{kl} = (\varepsilon_{k\alpha} - \mu)\delta_{kl} + V^\alpha_{\langle k,l\rangle}$, where $\varepsilon_{k\alpha}$ is the on-site energy and $V^\alpha_{\langle k,l\rangle} = V^\alpha$ is the hopping between the lead sites, are chosen as follows. We take $\varepsilon_{k\alpha}$ to be equal to the chemical potential, resulting half-filling for the lead energy states, while the value for the nearest neighbor hopping V^α is taken to be -2.0. The on-site parameter for the central region system ε_C is taken to be zero while the nearest neighbor hopping is taken to be $V_\mathrm{C} = -1.0$. The form of the electron-electron interaction is taken to mimic the Coulomb interaction by $w_{ij} = w_{ii}/(2|i-j|)$ if $i \neq j$ and $w_{ij} = w_{ii}$ if $i = j$. Furthermore, we will take the on-site repulsion between electrons to be $w_{ii} = 2.0$. The coupling parameter V_{link} between the central system and the leads is 0.35 and we use atomic units. First we will solve the system at equilibrium characterized by a chemical potential μ and the inverse temperature β. At t_0 we will drive the system out of equilibrium by a bias voltage of the form

$$W_\mathrm{L}(t) = \begin{cases} W\sin^2(\omega t) & t < \frac{\pi}{2\omega} \\ W & t \geq \frac{\pi}{2\omega} \end{cases}, \tag{5.107}$$

i.e. we switch the bias slowly as $\sin^2$ and when the maximum amplitude is reached the bias is kept constant at W. Furthermore, the bias for the right lead is taken to be the negative of the bias on the left lead as $W_R(t) = -W_L(t)$. We chose the amplitude for the bias to be $W = 0.8$ while the frequency for the switching is $\omega = 1.0$. In Fig. 5.7a we will show the current through the right interface with the HF, 2B and GW self-energy approximations. We will observe a big difference in the currents between the uncorrelated HF approximation and the correlated 2B and GW approximations. We can understand this from the Meir-Wingreen formula which basically states that the magnitude of the current is proportional to the spectral weight inside the bias window, which determined by the biased Fermi-levels of the left and right lead as $[\mu - |W_R|, \mu + |W_L|]$. The bias window is demonstrated by the green dashed box in Fig. 5.7b which shows the spectral density for the three different self-energy approximations.

From Fig. 5.7b) we see that the HOMO-LUMO levels in the HF approximation are peaked at the Fermi levels of the left and right lead respectively, *i.e.,* at the edges of the bias window. As a consequence, there is hardly any spectral weight inside the bias window. Thus, the current within the HF approximation is close to zero. Within the correlated many-particle self-energy approximations, where the quasi-particle life-time is much larger, and hence the spectral function is more broadened, there is more spectral weight inside the bias window yielding higher absolute value for the current [10, 173]. The transient structure of the current can be analyzed by Fourier transformation, where the peaks in the Fourier spectra shown in the inset of Fig. 5.7b can be identified as transitions from the left/right lead to the HOMO/LUMO levels respectively.

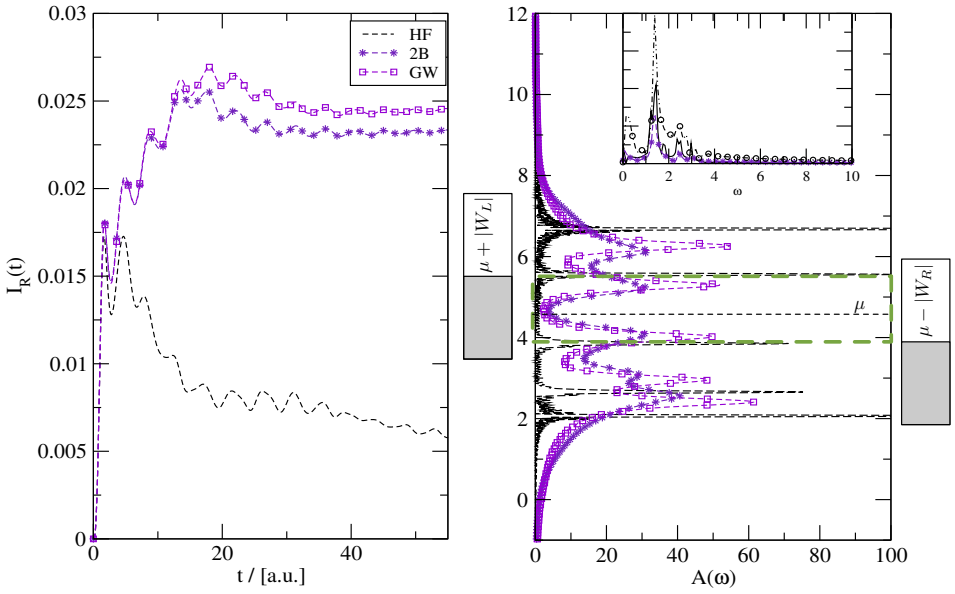

Figure 5.7: Quantum transport through 5-level system connected to semi-infinite leads. a) Time-dependent current $I_R(t)$ through central system – right lead interface. b) Spectral density for HF, 2B and GW approximations. The green box denotes the bias window. Inset shows the Fourier spectra of the current.

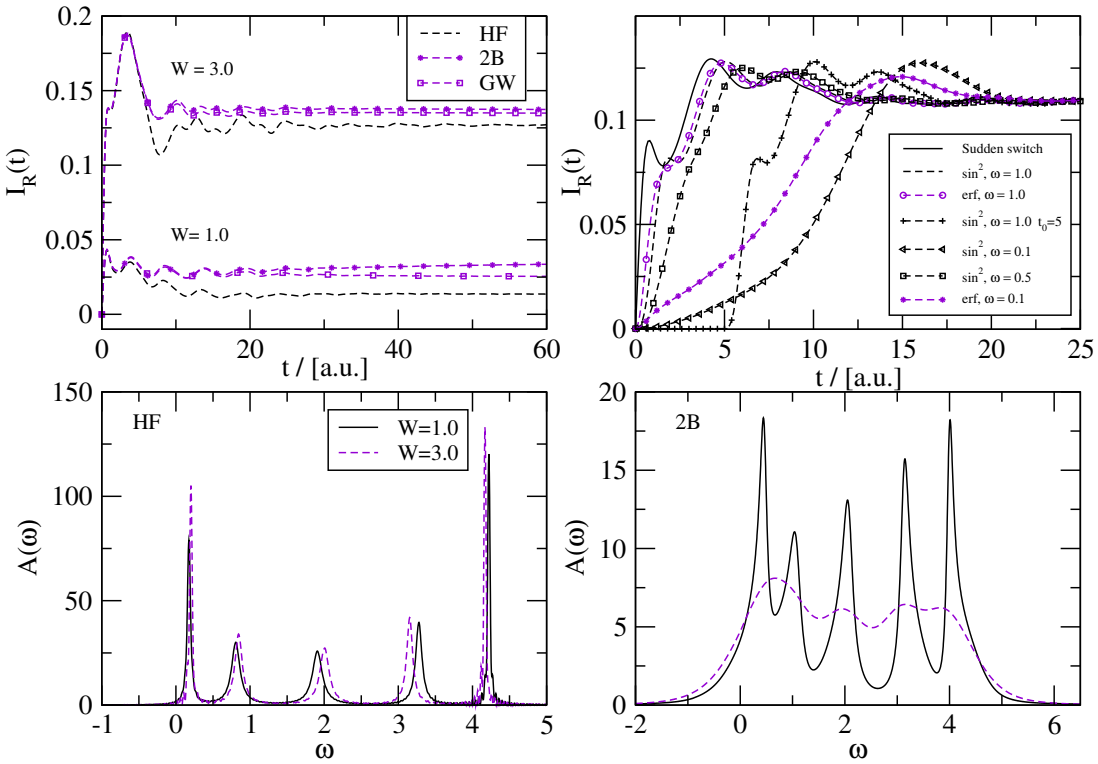

Figure 5.8: *Upper left panel:* Time-dependent current at different levels of approximation. *Upper right panel:* Time dependent currents with different switching of bias voltage. The amplitude of the bias is $W = 1.0$. *Lower panel:* Spectral functions for HF and 2B approximation at different values of bias. All the results are done for the parameters presented in the text.

In the upper left panel Fig. 5.8 we show the time-dependent current with HF, 2B and GW approximations for parameters $V_{link} = 0.5$, $V_\alpha = -2.0$, $V_C = -1.0$, $w_{ii} = 2.0$ and $\mu = 2.61$ with two different values of bias $W = W_L - W_R = 1.0$ and $W = W_L - W_R = 3.0$. We see an enhancement of current due to the increased bias window and consequent increase of spectral mass inside the bias window. A more interesting phenomena due to increase of bias is the enhanced quasi-particle scattering causing a collapsing of the spectral function under higher values of bias [158, 57, 10]. This can be seen clearly in the lower panel of the Fig. 5.8 in which we plot the HF and 2B spectral functions for the bias values $W = 1.0$ and $W = 3.0$, where the 2B spectral function at the bias $W = 3.0$ is more broader compared to the spectral function at bias $W = 1.0$. On the other hand, in the HF spectra we notice only a bias dependent gap closing and no collapsing. The broadening of the spectral function under bias for correlated approximations is due the fact that when adding and removing particles the many-particle interactions lead to a fast decay of many-particle states. Finally, in the upper right panel of Fig. 5.8 we plot the current for 2B approximation with different switchings of the bias voltage. We introduced a third smooth switching in the form of the error function

$$W_{\mathrm{L}}(t) = \begin{cases} W \,\mathrm{erf}(\omega t) & t < \frac{\pi}{2\omega} \\ W & t \geq \frac{\pi}{2\omega} \end{cases} \tag{5.108}$$

where the bias of the right lead is $W_R(t) = -W_L(t)$. This result demonstrates the fact that if the steady-state is reached it does not depend on the applied bias voltage. As we will see later in this chapter there can be multiple steady-states and in order to obtain a different steady-state we need to perturb the system in other ways than just by changing the type of bias. Later we will also notice that if the steady-state is not reached, the change in the bias conditions can very easily lead to another (stable) solution (see [3]).

Now it is clear that if we increase the bias, we will have more levels inside the bias window. Hence, the value for the current will be larger. We can plot the current as a function of time and voltage as seen in Fig. 5.9 and obtain the step-like structure for the IV-characteristics. In Fig. 5.9 we also notice that for large bias values the current starts actually to decrease, this is called the negative differential resistance (NDR) regime where due to the finite band-width of the leads the overlap between the left and right energy band will start to eventually to decrease with increasing of the bias.

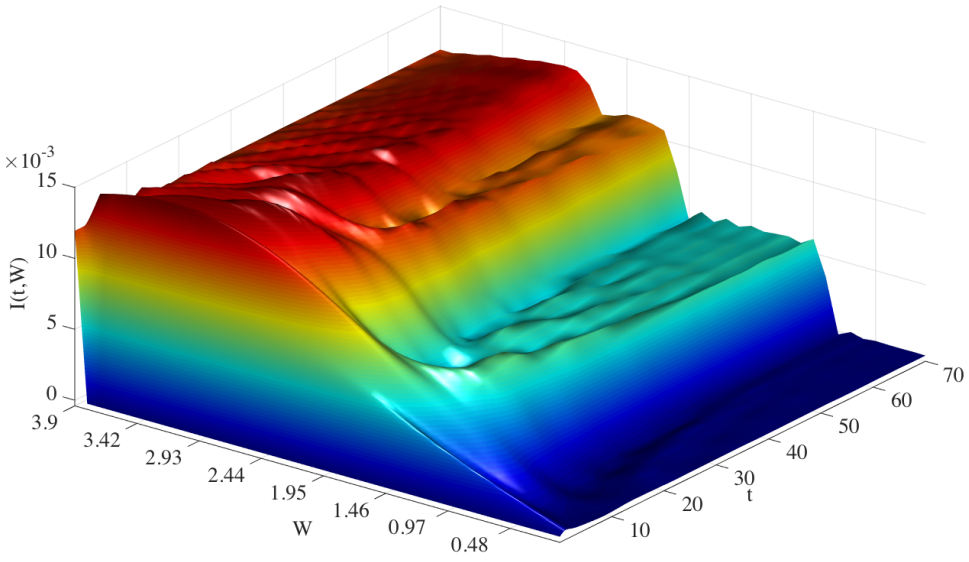

Figure 5.9: Current as a function of time and bias for HF approximation for five level system with parameters $V_{link} = 0.1$, $V_{\mathrm{C}} = -1.0$, $w_{ii} = 2.0$ and $V_\alpha = -2.0$. We see that by increasing the bias the current develops a step-like structure as a higher levels participate in the charge transport.

5.3.1 COMPARISON OF DIFFERENT APPROXIMATIONS FOR NON-EQUILIBRIUM DYNAMICS

To compare TDDFT method with MBPT for quantum transport we studied the interacting resonant level model or the Anderson impurity model [92]. This allowed us to compare these two approaches to numerically exact time-dependent density matrix (tDMRG) results. The Anderson impurity model is described by the Hamiltonian (see also section 2.2 in chapter 2)

$$\begin{aligned}
\hat{h}_{\mathrm{C}} &= \sum_{\sigma} \varepsilon_0 \hat{d}^{\dagger}_{\sigma} \hat{d}_{\sigma} + \frac{1}{2} \sum_{\sigma,\sigma'} U \hat{d}^{\dagger}_{\sigma} \hat{d}^{\dagger}_{\sigma'} \hat{d}_{\sigma'} \hat{d}_{\sigma}, \\
\hat{h}_{\alpha}(t) &= \sum_{\substack{i=-\infty \\ i\neq 0,\sigma}}^{\infty} \Big(\varepsilon_{\alpha} + W_{\alpha}(t) \Big) \hat{c}^{\dagger}_{i\sigma\alpha} \hat{c}_{i\sigma\alpha} - \sum_{\substack{i=-0 \\ i\neq 0,\sigma}}^{\infty} \Big(V_{\alpha} \hat{c}^{\dagger}_{i\sigma\alpha} \hat{c}_{i+1\sigma\alpha} + H.c. \Big), \\
\hat{h}_{\mathrm{T}} &= -\sum_{\sigma} \Big(V_{link}\, \hat{d}^{\dagger}_{\sigma} \hat{c}_{1\sigma L} + V_{link}\, \hat{d}^{\dagger}_{\sigma} \hat{c}_{1\sigma R} + H.c. \Big),
\end{aligned} \tag{5.109}$$

where $\hat{d}$ operators create and annihilate an electron in the impurity site described by on-site energy ε_0 and U is the on-site electron-electron repulsion term. The operators $\hat{c}$ are the fermionic creation and annihilation operators for the leads described by the hamiltonian $\hat{h}_{\alpha}$, the parameter ε_{α} describes the on-site energy and the time-dependent bias is denoted by $W_{\alpha}(t)$. The hopping between the nearest neighbor sites in the lead is described by parameter V_{α} and the hybridization parameter between the leads and the impurity is denoted by V_{link}.

We will use the MBPT approach using the two-time Kadanoff-Baym equations together with the HF, 2B, GW and T-matrix approximations (see section 5.1 in chapter 5 and 3.4 in chapter 3). The TDDFT approach is used with the modified ABALDA approximation for the exchange-correlation potential $v_{\mathrm{xc}}[n]$ (see section 4.1 in chapter 4). These two methods are benchmarked against tDMRG results presented by F. Heidrich-Meisner, A. E. Feiguin, and E. Dagotto, in *Phys. Rev. Lett.* **79**, 235336 (2009) [174]. At t_0 the infinite connected system is in equilibrium at zero temperature with Fermi energy ε_F. The initial state is determined in MBPT approaches by solving the Dyson equation on the imaginary axis (see section 5.1 in chapter 5). Within TDDFT the initial state is obtained via a self-consistent static DFT calculation [175] with a modified BALDA for the exchange-correlation potential. At t_0 we suddenly switch on the bias W_{α} in the lead $\alpha = \mathrm{L,R}$ after which we follow the time-evolution of the system until the steady-state is reached. We choose the lead on-site energies to be zero, $\varepsilon_L = \varepsilon_R = 0$ and the hopping in the left and right lead are the same $V_L = V_R = V$. Values of all the parameters will be given in units of the lead hopping V. Since we are especially interested in the correlation effects in the quantum transport, we will study only the weak coupling regime , *i.e.*, $V_{\mathrm{link}} \ll V$, where the correlation effects are enhanced.

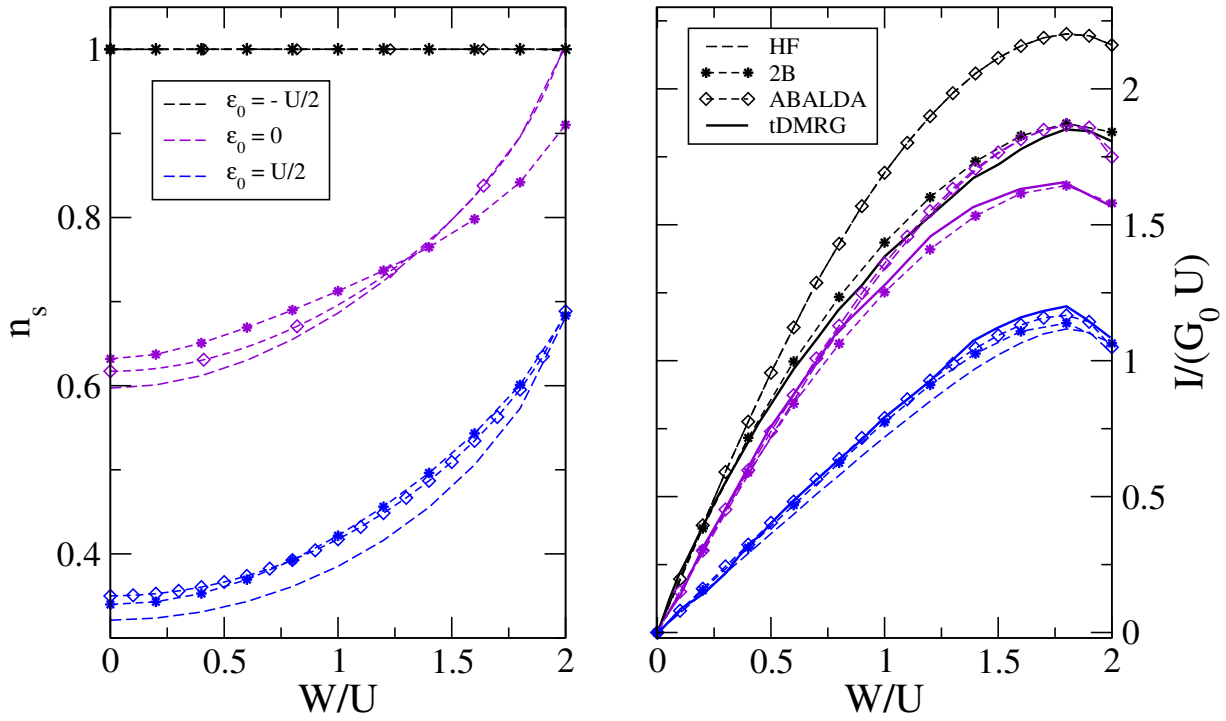

Figure 5.10: The steady-state density voltage (left panel) and current voltage (right panel) for the anderson impurity model with onsite energies $\varepsilon_0 = -U/2, 0, U/2$ with HF, ABALDA of TDDFT and 2B of MBPT compared to tDMRG. $U = 1.0$ and $V_{link} = 0.5$.

In Fig. 5.10 we show the voltage-density and voltage-current characteristics for the Anderson impurity with uncorrelated HF approximation and correlated ABALDA of TDDFT and 2B approximation of MBPT compared to tDMRG with different values for the on-site energy $\varepsilon_0 = U/2, 0, -U/2$ with symmetrically applied bias $W_L = -W_R = W$ and with the coupling parameter $V_{link} = 0.5$ (in article I [1] one can see also the asymmetrically applied bias). For the MBPT approximations we are showing only 2B approximation because the GW and T-Matrix approximations are very close to the 2B. In the left panel of Fig. 5.10 we show the density as a function of the bias. For the particle-hole symmetric point $\varepsilon_0 = -U/2$ all the approximations correctly predict the impurity site to be half-filled. Above the particle-hole symmetric point we see that the uncorrelated HF approximation and the correlated ABALDA and 2B approximations all produce approximately the same estimate for the density in the impurity. The density in the impurity is higher for higher values of bias voltages $W/U > 1$, since the coupling is weak and the driving bias voltage overcomes the Coulomb repulsion which causes the density approach the particle-hole symmetric point.

In the right panel of Fig. 5.10 we display the steady-state current as a function of the bias voltage W with different values for the on-site energy of the impurity ε_0. For small bias all the approximations yield the same value for the steady-state current which is on top of the tDMRG results for all values of the on-site energy. By increasing the bias we start to see some differences between the different approximations. Especially for the particle hole-symmetric point the uncorrelated HF approximation (dashed line) and the

correlated ABALDA for TDDFT (dashed line with diamonds) differ from the tDMRG results (solid line) and yield the same value for the steady-state current. On the other hand, we see that the correlated 2B approximation follows relatively closely to the tDMRG results. Despite the discrepancies in the values for the steady-state current as a function of the bias voltage we see that the differential conductances given by the slopes of the IV curves are in close agreement in all of the approximations, which agrees with the Friedel sum rule that relates the conductance to the density [176].

We also compared the different MBPT approximations and TDDFT to tDMRG in the time-domain to study their performance in the description of the transient phenomena. We take the lead-impurity parameter to be $V_{\text{link}} = 0.3535$ which will slightly enhance the effect of correlations compared to the steady-state results. In Fig. 5.11 we demonstrate the behavior of transient currents as a function of time. We study two different values for the symmetrically applied bias $W_L = W_R = W/2$ with $W = 0.4, 1.0$. The electron-electron repulsion term is taken to be $U = 0.5$. Since the tDMRG is a method for finite systems, we see the reflection effects from the system boundaries at a long propagation time. We see that all the correlated many-particle results are in close agreement with the tDMRG results. The 2B approximation performs most accurately, as it produces the same steady-state value as the tDMRG as well as the characteristic bump in the transient region. On the other hand, we see that the HF and ABALDA approximations overestimate the steady-state value for the current, especially at low bias voltage. The HF and ABALDA are also overestimating the transient bump. One reason for the lack of transient bump in the HF approximation arises from the fact that, at the HF level the initial correlations in the current formula Eq. (5.103) are missing, which causes extra damping [177]. Thus, the time-local approximations have a tendency to overshoot the transient currents [10].

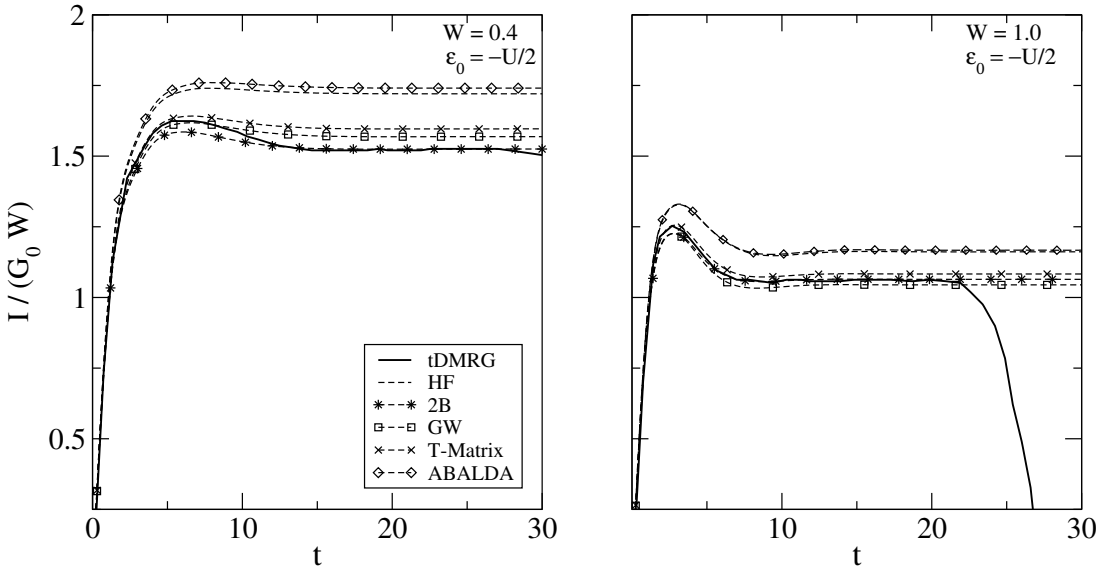

Figure 5.11: Transient currents for symmetrically applied bias $W_L = W_R = W/2$. The electron-electron repulsion term is $U = 0.5$ and the lead-impurity is $V_{\text{link}} = 0.3535$.

The main finding from our comparison results is that the correlated 2B approximation yields the best estimate for the transient and steady-state value for the current when compared to the benchmark tDMRG results. We did not have benchmark data for the density on the impurity level, but as we see from Fig. 5.10 and from the Fig. (3) and Fig. (7) of article I [1], all of the correlated approximations yield very similar estimate for the density at the impurity. When increasing the electron-electron repulsion at the dot (see Fig. (7) of article I [1]), the HF approximation will start to differentiate from the correlated approximations when looking at the density at the impurity. While the ABALDA, assuming that 2B is closest to the exact, performs well. On the other hand for the currents we see again, that ABALDA overestimates the steady-state value, compared to the 2B approximation. We thus conclude that the the ABALDA approximation with TDDFT produces very accurately the density at the interacting dot, while it overestimates the steady-state and transient currents. From the MBPT approximations the 2B approximation performs best for the system and parameters studied when compared to benchmark tDMRG results.

We can explain the discrepancy between the ABALDA currents compared to other correlated approximations by studying the electron density deep inside the leads which is uniquely determined by the Fermi energy ε_F and thus same for all approximations. We will denote by n_g the ground state density at site j_d in the lead far from the impurity site so that $n_j = n_g$ for all $j > j_d$. When we apply a bias voltage, no change in density is observed until after a time $t_d = j_d/v$. The velocity of the density wave-front v moving into the right lead as seen in Fig. 5.12, where we illustrate the density profile for the first 20 sites in the right lead for 2B approximation. In Fig. 5.12 we see a density wave moving into the right lead with velocity v. We also notice the Friedel oscillations in the density profile as a function of the site number.

To see if the deficiencies in the ABALDA are due to the time-space locality of the xc-potential we will study the steady-state value for the density deep inside the lead, for which we can derive an estimate as a function of the ground-state density deep inside the lead n_g, speed of the density wave front v and the value of the steady-state current I. We can do this by studying an interval in the right lead $[j_d, j_d + N_d]$ where $N_d \gg 1$, which in equilibrium contains $n_g N_d$ electrons. At time t_0 we apply the bias voltage $W_L = 0.4$ and $W_R = 0$,it takes the time $t \sim t_d$ for the density wave-front to reach the site j_d, and it takes the time $T_d = N_d/v$ for the wave-front to propagate through the interval $[j_d, j_d + N_d]$ that we are interested in. The local steady-state is reached for times $t > t_d + T_d$ and the number of electrons in the interval $[j_d, j_d + N_d]$ is then given by

$$n_s N_d = n_g N_d + \int_{t_d}^{t_d+T_d} dt\, I_d(t) \sim n_g N_d + I_s T_d, \tag{5.110}$$

where I_s the value of the steady-state current. From this we conclude that the steady-state density in the lead far from the impurity is

$$n_s = n_g + I_s/v. \tag{5.111}$$

This equation shows that if different approximations yield a different value for the steady-state current they will also yield a different value for the steady-state density deep in the leads.

We note that for the half-filled leads the velocity of the density wave front will be close to the Fermi velocity and given by $v = 2V$ for tight-binding lead. We can now calculate the difference in the steady-state and the ground state values, $n_s - n_g$, for the density far from the impurity with different approximations as seen in Fig. 5.13. From the Fig. 5.13 we notice that the ABALDA overestimates the density difference $n_s - n_g$ far from the impurity while it gives a good estimate for the density at the interacting impurity. This means that the xc-potential is good at the impurity but approximating v_{xc} to be zero in the leads is a too simple approximation. From the Sham-Schlüter equation (see Eq. 4.27), relating the v_{xc} and the many-body self-energy Σ, we see that since the Green's function has non-zero components everywhere, must v_{xc} have more than only one non-zero element. In other words, we need to have an exchange-correlation potential which has nonzero values in the leads.

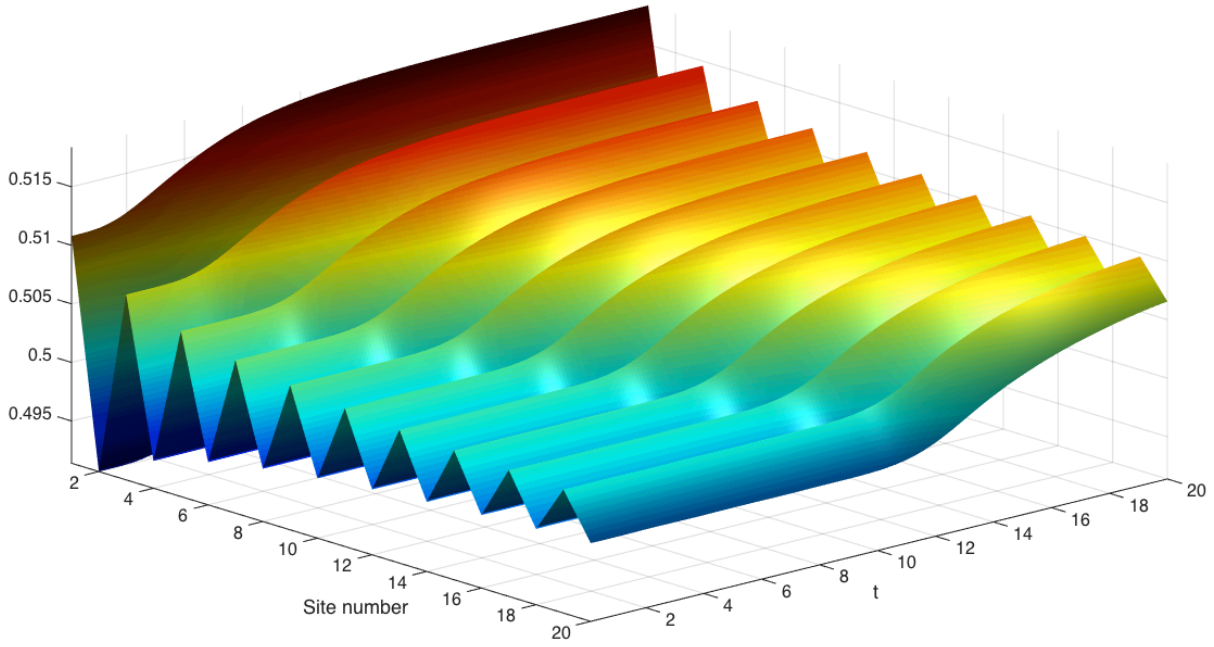

Figure 5.12: Time-dependent density in the right lead within the 2B approximation for a system with Fermi energy $\varepsilon_F = 0$, and $\varepsilon_0 = 0.2$, $V_{\text{link}} = 0.2$ and $U = 0.6$). The system is driven out of equilibrium by an external bias $W_L = 0.4$ and $W_R = 0$. A density wave entering the lead can clearly be observed.

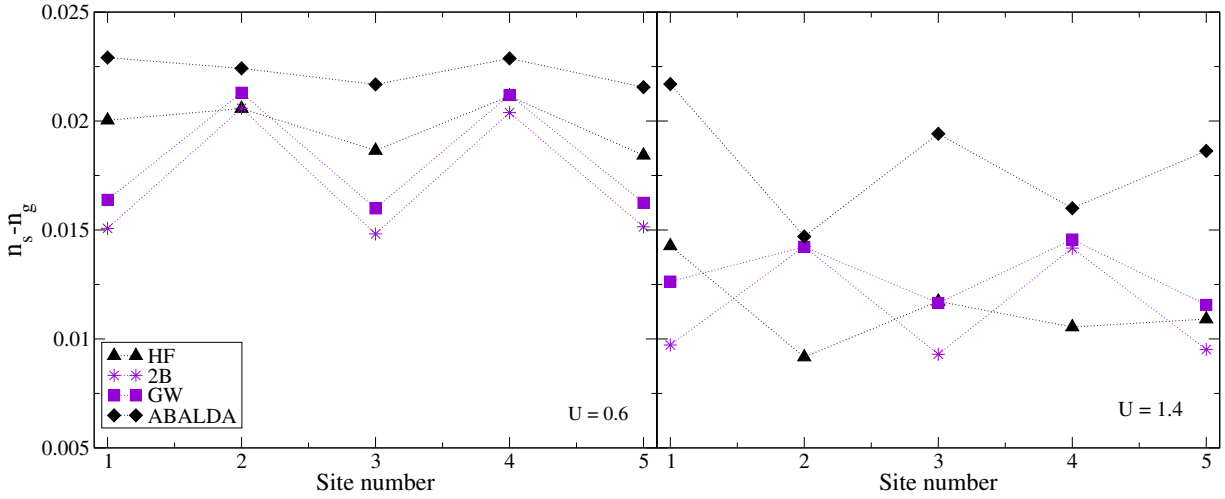

Figure 5.13: Difference between steady-state and ground state density in the right lead for a system with Fermi energy $\varepsilon_F = 0$, and $\varepsilon_0 = 0.2$, $V_{\text{link}} = 0.2$ and for different values of the charging energy $U = 0.6$ (top panel) and $U = 1.4$ (bottom panel). The system is driven out of equilibrium by an external bias $W_L = 0.4$ and $W_R = 0$.

5.3.2 Bistability and non-linear Phenomena

The question of uniqueness of the steady-state in correlated non-equilibrium quantum or classical systems is an interesting fundamental problem [178, 179, 2, 3] which gained attention in the field of quantum transport after experimental observation of hysteresis behavior in IV-characteristics of double barrier resonant tunneling structures [50, 51]. Theoretically this hysteresis or multi-stability phenomenon has been studied at mean-field level by several authors [180, 181, 182] explaining the occurrence of multiple solutions to be caused by electrostatic build-up in the quantum well at the negative differential resistance regime [50]. The increased interest towards molecular electronics and the possibility of molecular devices at large differential resistance regime to behave analogously to double barrier resonant tunneling structures has given a new attention to the multi-stability problem.

The theoretical studies done on the multi-stability problem at the nano-scale have mainly been limited to Hartree-Fock approximation or static density functional theory, where the effects of memory are discarded [183, 179]. In our work we studied whether the multi-stability can be found in correlated approximations beyond the Hartree-Fock and static DFT approximations when the time non-local effects are taken into account. To study the multi-stability phenomenon we first solved the steady-state equations at mean-field level to find the regime for the occurrence of multi-stability in our model systems. After which we performed full time-dependent Kadanoff-Baym calculations with correlated self-energies as well as adiabatic TDDFT calculations [175, 184]. Due to our time-dependent description of the quantum

transport process we were also able to answer the question whether it is possible to switch between multiple steady-states in the time domain.

We started our analysis for the multi-stability phenomenon by deriving a density self-consistency equation for the steady-state density $n_j := \lim_{t\to\infty} n_j(t)$ at the site $j \in \mathrm{C}$ in the central region. At the steady-state all the real-time Green's functions and thus all of the real-time self-energies will depend only on the difference of the time-arguments. Therefore, by taking $t_0 \to -\infty$ we can Fourier transform our objects into the frequency space. Now the density at site j can be calculated from the central region Green's function as

$$\langle \hat{n}_j \rangle = -i[\boldsymbol{G}^{<}_{\mathrm{CC}}(t,t^+)]_{jj} = \int \frac{d\omega}{2\pi i}[\boldsymbol{G}^{<}_{\mathrm{CC}}(\omega)]_{jj}. \tag{5.112}$$

The lesser Green's function for the central system can be obtained from the Dyson equation by utilizing the Langreth rules

$$\mathbf{G}^{<}_{\mathrm{CC}}(\omega) = \boldsymbol{G}^{R}_{\mathrm{CC}}(\omega)\boldsymbol{\Sigma}^{<}_{tot}\boldsymbol{G}^{A}_{\mathrm{CC}}(\omega) + \boldsymbol{\Delta}^{<}(\omega), \tag{5.113}$$

where the retarded and advanced Green's functions are $\boldsymbol{G}^{R}(\omega) = [\omega - \hat{h}_{\mathrm{C}} - \Sigma^{R}_{tot}(\omega)]^{-1}$ and $[\boldsymbol{G}^{R}(\omega)]^{\dagger} = [\boldsymbol{G}^{A}(\omega)]$. The total self-energy is given as a sum of many-body and embedding self-energies as $\boldsymbol{\Sigma}_{tot} = \boldsymbol{\Sigma}_{\mathrm{MB}} + \boldsymbol{\Sigma}_{\mathrm{EM}}$ and the term $\boldsymbol{\Delta}$ is

$$\boldsymbol{\Delta}^{<}(\omega) = \left[1 + \boldsymbol{G}^{R}_{\mathrm{CC}}(\omega)\boldsymbol{\Sigma}^{R}_{tot}(\omega)\right] \boldsymbol{G}^{<}_{0,\mathrm{CC}}(\omega) \left[1 + \boldsymbol{\Sigma}^{A}_{tot}(\omega)\boldsymbol{G}^{A}_{\mathrm{CC}}(\omega)\right], \tag{5.114}$$

where $\boldsymbol{G}^{<}_{0,\mathrm{CC}}(\omega)$ is the equilibrium Green's function of the contacted system [57]. This term is zero (except in some special cases). Which can be seen by solving for the self-energy in Dyson equation giving $\boldsymbol{\Sigma}^{R,A}_{tot}(\omega) = [\boldsymbol{G}^{R,A}_{0,\mathrm{CC}}(\omega)]^{-1} - [\boldsymbol{G}^{R,A}_{\mathrm{CC}}(\omega)]^{-1}$ and using the equilibrium fluctuation-dissipation relations for the non-interacting Green's function $\boldsymbol{G}^{<}_{0,\mathrm{CC}}(\omega) = -f(\omega-\mu_C)[\boldsymbol{G}^{R}_{0,\mathrm{CC}}(\omega) - \boldsymbol{G}^{A}_{0,\mathrm{CC}}(\omega)]$, giving

$$\boldsymbol{\Delta}^{<}(\omega) = 2i\eta f(\omega-\mu_C)\boldsymbol{G}^{R}_{\mathrm{CC}}(\omega)\boldsymbol{G}^{A}_{\mathrm{CC}}(\omega), \tag{5.115}$$

where η is a small positive infinitesimal. The product of retarded and advanced Green's functions will not depend on the small imaginary part η. Thus, when taking $\eta \to 0$ we have $\boldsymbol{\Delta}^{<} \to 0$. Now we can write the density for site j as

$$\begin{aligned} n_j \;=\; & \Bigg[\int \frac{d\omega}{2\pi} \boldsymbol{G}^{R}_{\mathrm{CC}}(\omega) \left[\boldsymbol{\Gamma}_{L,\mathrm{EM}}(\omega) f_L(\omega) + \boldsymbol{\Gamma}_{R,\mathrm{EM}}(\omega) f_R(\omega)\right] \mathbf{G}^{A}_{\mathrm{CC}}(\omega) \\ & -i\boldsymbol{G}^{R}_{CC}(\omega)\boldsymbol{\Sigma}^{<}_{\mathrm{MB}}(\omega)\mathbf{G}^{A}_{\mathrm{CC}}(\omega) \Bigg]_{jj}, \end{aligned} \tag{5.116}$$

where we wrote explicitly the lesser component of the self-energy $\boldsymbol{\Sigma}^{<}_{\alpha,\mathrm{EM}} = i f_\alpha(\omega)\boldsymbol{\Gamma}_{\alpha,\mathrm{EM}}(\omega)$, with $\boldsymbol{\Gamma}_{\alpha,\mathrm{EM}} = -2\mathrm{Im}\left[\boldsymbol{\Sigma}^{R}_{\alpha,\mathrm{EM}}\right]$, $\alpha = \mathrm{L,R}$ (see section 5.1.5 of chapter 5). The Fermi function for the lead α is defined as $f_\alpha(\omega) = f(\omega + W_\alpha)$ For the Anderson impurity model the equation for the density reduces to

simple Meir-Wingreen type integral for the density

$$n = \int_{-\infty}^{\infty} \frac{d\omega}{2\pi} \frac{\Gamma_{L,\mathrm{EM}}(\omega) f_L(\omega) + \Gamma_{R,\mathrm{EM}}(\omega) f_R(\omega) - i\Sigma^{<}_{\mathrm{MB}}(\omega)}{(\omega - \varepsilon_0 - \mathrm{Re}\left[\Sigma^R_{\mathrm{MB}}(\omega)\right] - \Lambda_{\mathrm{EM}}(\omega))^2 + (\mathrm{Im}\left[\Sigma^R_{\mathrm{MB}}(\omega)\right] - \Gamma_{\mathrm{EM}}(\omega)/2)^2}. \tag{5.117}$$

where $\Gamma_{\mathrm{EM}} = \Gamma_{L,\mathrm{EM}} + \Gamma_{R,\mathrm{EM}}$ and $\Lambda_{\mathrm{EM}} = \Lambda_{L,\mathrm{EM}} + \Lambda_{R,\mathrm{EM}}$. For the Hartree-Fock approximation this equation reduces to simple self-consistent equation for the density at the interacting impurity since $\mathrm{Im}\left[\Sigma_{\mathrm{MB}}\right] = \Sigma^{<}_{\mathrm{MB}} = 0$ and $\mathrm{Re}\left[\Sigma^R_{\mathrm{MB}}\right] = nU$ where U is the electron-electron repulsion term.

From the Eq. (5.117) we can now solve for the steady-state density at the impurity as seen in Fig. 5.14. At the upper panel of Fig. 5.14 we consider a single impurity level connected to semi-infinite leads described by following parameters: $V_{link} = 0.7$, $W_L = 3.0$, $W_R = 0.0$, $\varepsilon_C = 0.0$, $\varepsilon_\alpha = \varepsilon_F = 0.6$. The leads are half-filled such that the Fermi-level of lead α is positioned at $\varepsilon_F + W_\alpha$. All energies are measured in units of the lead nearest neighbor hopping parameter V. In the biased system the band-width of the leads is $[\varepsilon_F + W_\alpha - 2V, \varepsilon_F + W_\alpha + 2V]$. With these parameters we are able to find several solutions for the steady-state density at the impurity in function of the electron-electron repulsion U within HF approximation. The maximum number of three different solutions for the steady-state density is obtained for the electron-electron interaction strengths at the interval $[3.95, 4.64]$ as seen from the upper left panel of Fig. 5.14. One special feature of the low density solution n_1 and high density solution n_3 is that $n_{1,3} = 2 - n_{3,1}$, *i.e.*, they resemble the weights of the Green's function at the Coulomb blockade regime

$$G^R_{\sigma\sigma'} \approx \frac{2 - n_\sigma}{\omega - \varepsilon_\sigma - \Sigma^R_{\mathrm{EM}}(\omega)} + \frac{n_\sigma}{\omega - \varepsilon_\sigma - U - \Sigma^R_{\mathrm{EM}}(\omega)} \tag{5.118}$$

although it is not necessary that the density n_σ has the exact same value as one of the solutions. This resemblance of Coulomb blockade solutions and bistability still requires further investigations.

In the lower panel of Fig. 5.14 we show the solutions for the steady-state density at the interacting impurity with the following parameters $V_{\mathrm{link}} = 0.3$, $W_L = 1.8$, $W_R = -1.0$, $\varepsilon_C = 0.0$, $\varepsilon_\alpha = \varepsilon_F = 0.6$. The leads are again half-filled. With these parameters we are able to find several solutions for the steady-state density at the impurity in function of the electron-electron repulsion U within HF approximation. The maximum number of five solutions for the steady-state is obtained for the interaction strengths $[1.88, 2.08]$ and again the high-low density solutions are symmetric to each other. We can analyze the stability of the solutions by utilizing the fixed point theorem. This means in practice that a solution is stable if $\left|\frac{dg(n)}{dn}\right|_{\tilde{n}} < 1$, where $g(n)$ is the right hand side of Eq. (5.117). This implies the stability of solutions $\tilde{n}_1$ and $\tilde{n}_3$ for the situation shown in upper left panel of Fig. 5.14, while the solutions $\tilde{n}_1$, $\tilde{n}_3$ and $\tilde{n}_5$ are stable for the situation demonstrated in upper right panel of Fig. 5.14.

To study the multi-stability in time-domain and to see which one of the solutions is reachable by time propagation we choose $U = 4.0$ for the parameters possessing three fixed point steady-state solutions and $U = 2.0$ for the parameters with five different solutions for the density. We will denote these two different parameter sets as A and B, $A = \{U = 2.0, V_{\mathrm{link}} = 0.3, W_L = 1.8, W_R = -1.0, \varepsilon_C = 0.0\}$ and $B = \{U = 4.0, V_{link} = 0.7, W_L = 3.0, W_R = 0.0, \varepsilon_C = 0.0, \}$. For both of the parameter sets we

have $\varepsilon_\alpha = \varepsilon_F = 0.6$. The values for the steady-state densities corresponding to the parameter set A are $\tilde{n}_1 = 0.66$, $\tilde{n}_2 = 1.16$ and $\tilde{n}_3 = 1.32$ while for the parameter set B the corresponding densities for the HF approximation are $\tilde{n}_1 = 0.17$, $\tilde{n}_2 = 0.54$, $\tilde{n}_3 = 1.0$, $\tilde{n}_4 = 1.46$ and $\tilde{n}_5 = 1.83$. Since the ABALDA is a time-local approximation we can derive a similar self-consistency equation for the density as in the HF case, just by replacing $\hat{h}_{\rm CC}$ with $\hat{h}^{KS}_{\rm CC} = \varepsilon_0 + v_H[n] + v_{\rm xc}[n](j)$. This will result three fixed point densities for the parameter set A: $\tilde{n}_1 = 0.80$, $\tilde{n}_2 = 1.0$ and $\tilde{n}_3 = 1.28$ (see upper right panel in Fig. 5.17a) and also three fixed point solutions for the density for the parameter set B: $\tilde{n}_1 = 0.18$, $\tilde{n}_2 = 1.00$, $\tilde{n}_3 = 1.82$ (see Fig. (2) of article III [3]).

In Fig. 5.16a we show the time-dependent densities for the parameter set A with various self-energy approximations and ABALDA for TDDFT. We solve for the system at the ground state and ramp up the

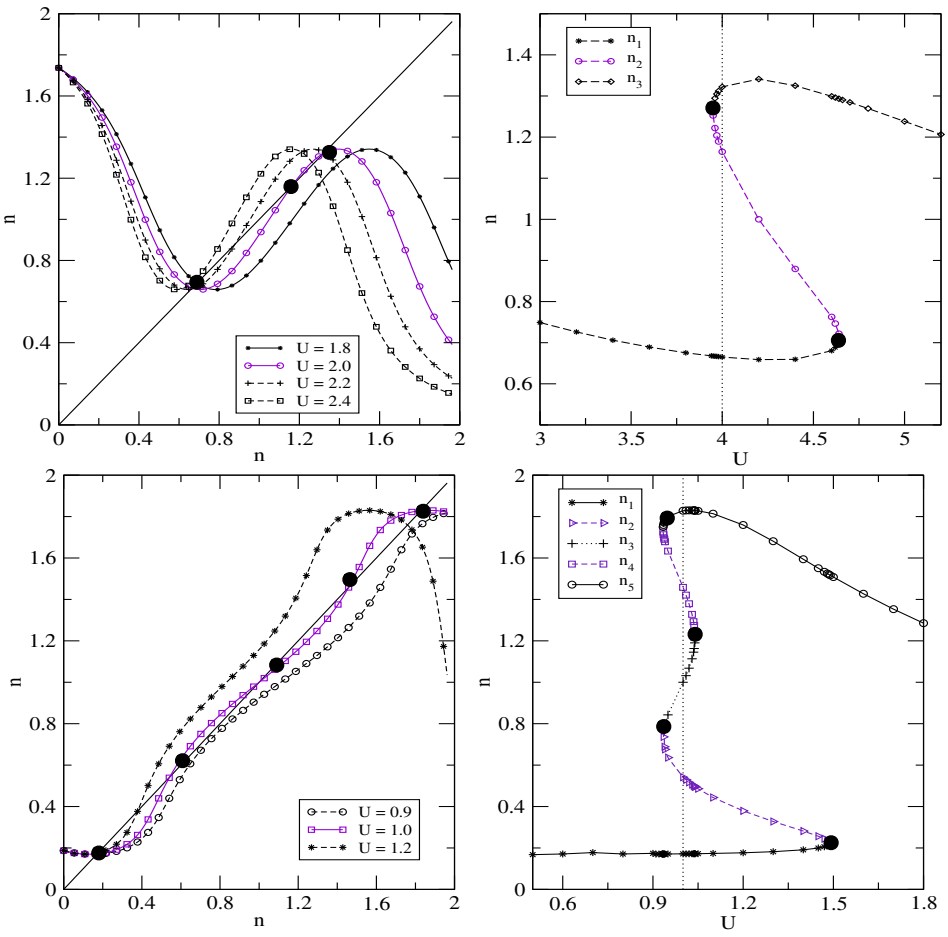

Figure 5.14: Solutions for the steady-state density at HF level obtained from Eq. 5.117. Upper panel: $V_{link} = 0.7$, $W_L = 3.0$, $W_R = 0.0$. Lower panel: $V_{\rm link} = 0.3$, $W_L = 1.8$, $W_R = -1.0$, The dashed line in upper right panel corresponds to $U = 4.0$ and in the lower right panel $U = 1.0$.

bias at t_0 after which we follow the system's time evolution. We notice that in both of the cases: HF and ABALDA, the system goes in to the steady-state value of the density given by fixed point n_1. To switch to an another steady-state we will apply a time-dependent kick on the impurity in form of the exponentially decaying gate voltage of the form

$$V_g(t) = \begin{cases} V_g e^{-\gamma t} & , \text{ if } 0 < t < T_g \\ -V_g e^{-\gamma(t-T_g)} & , \text{ if } T_g < t < 2T_g \\ V_g e^{-\gamma(t-2T_g)} & , \text{ if } t > 2T_g \end{cases}. \tag{5.119}$$

Applying the kick with amplitude of the gate $V_g = 3.0$ and the decay rate $\gamma = 0.2$ together with the bias at t_0 we are able to reach the fixed point solution n_3 for the steady-state density, both in HF approximation and ABALDA. The middle fixed point solution n_2 is not reachable by time-propagation. The closest time-dependent solution for the n_2 fixed point in both HF approximation and ABALDA is obtained with the gate of $V_g = 3.0$ and the decay rate $\gamma = 1.0$, but the steady-state value for the density will be either n_1 or n_3. If we apply the gate at a later time $t > t_0$ or we wait until the gate voltage has decayed and apply it again, we see that we are able to switch between the n_1 and n_3 fixed point solutions for the density both in HF and ABALDA as seen in Fig 5.16a. Naturally the different fixed point solutions for the density lead to multiple solutions for the steady-state current. We are also able to derive a Meir-Wingreen equation for the steady-state current I_{st} in terms of the density n

$$I_{st} = \int \frac{d\omega}{2\pi} \frac{[f_L(\omega) - f_R(\omega)]\Gamma_{L,\text{EM}}(\omega)\Gamma_{R,\text{EM}}(\omega)}{(\omega - \varepsilon_0 - V_g - Un - \Lambda_{\text{EM}}(\omega))^2 + (\Gamma_{\text{EM}}(\omega)/2)^2}. \tag{5.120}$$

For the parameter set A we have the following values for the current corresponding to the three fixed points of the steady-state density $\tilde{I}_1 = 0.055$, $\tilde{I}_2 = 0.12$ and $\tilde{I}_3 = 0.08$, from which $\tilde{I}_1$ and $\tilde{I}_2$ are stable solutions corresponding to the $\tilde{n}_1$ and $\tilde{n}_2$ solutions for the steady-state density. For the parameter set B we have four solutions for the current $\tilde{I}_1 = 0.0052$, $\tilde{I}_2 = 0.035$, $\tilde{I}_3 = 0.056$ and $\tilde{I}_4 = 0.027$ from which two are again stable: $\tilde{I}_1$ corresponding to both $\tilde{n}_1$ and $\tilde{n}_5$ solutions for the density as well as $\tilde{I}_4$ corresponding to $\tilde{n}_3$ fixed point for the density. In Fig. 5.16b we show the time-dependent current and density for the parameter set B. In a similar way as seen for the parameter set B we are again able to switch between the stable fixed points both for density and current in time domain while the unstable fixed points are just solutions with finite life time.

For the correlated many-body approximations we are not able to write a simple self-consistency equation in terms of the density only, since the many-body self-energy depends also on the frequency. However, we can try to see if the correlated approximations possess multiple solutions for the same parameters as HF and ABALDA. In Fig. 5.16a we show the 2B, GW and T-matrix solutions for the time-dependent density which possess only one solution for the steady-state density despite the attempts to find other solutions by applying the gate voltage kick. We can understand the occurrence of only one solution by looking at the steady-state spectral functions presented in Fig. 5.17a. First of all we note that the left lead energy

band is at $[1.6, 5.6]$ with $\mu_L = 3.6$ and the right lead energy band is at $[-1.4, 2.6]$ with $\mu_R = 0.6$. The HF spectral function corresponding to the three fixed point solutions is shown on the left panel of Fig. 5.17a.

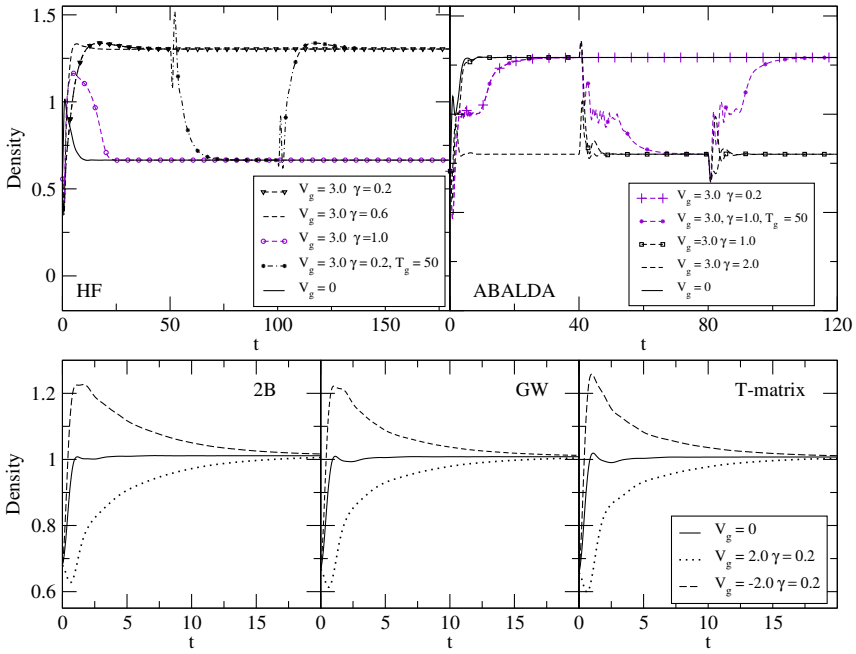

Figure 5.15: a) The time-dependent density and current with parameter set A.

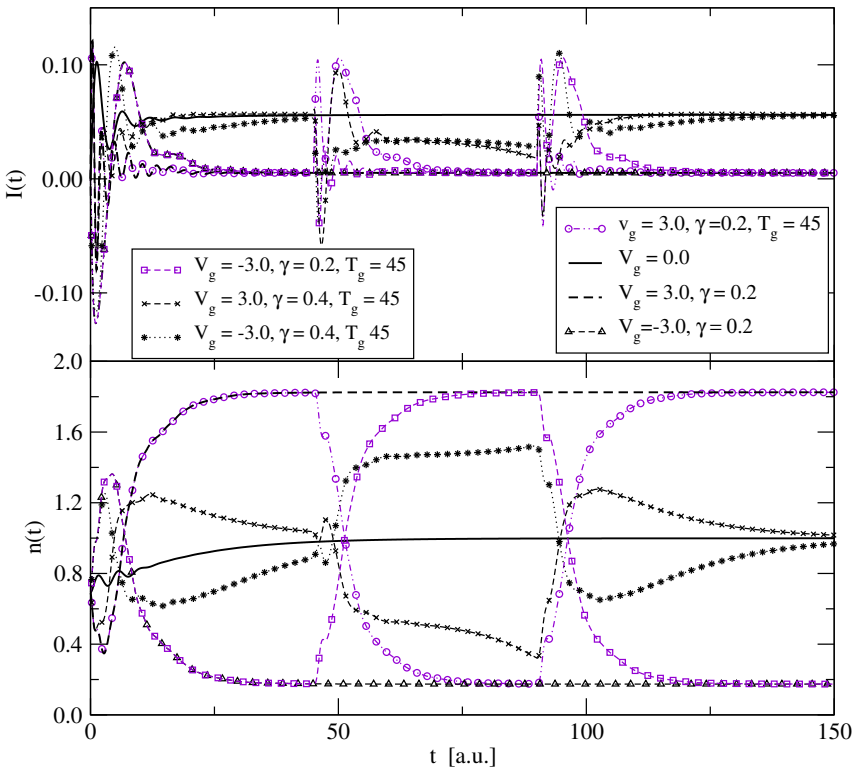

Figure 5.16: The time-dependent density and current with parameter set B.

We see that the spectral functions corresponding to the stable solutions $\tilde{n}_1$ and $\tilde{n}_3$ are clearly separable and are peaked approximately around the Fermi level of the left/right lead respectively. The unstable solution on the other hand is peaked on the top of the right lead energy band, and therefore the middle solution will very likely to slip into the solution $\tilde{n}_3$. We display also the spectral functions for ABALDA although it is a spectral function of a KS system and thus should not be regarded as a true spectral function. For the correlated many-body approximations we now see that the spectral functions are extremely broad due to enhanced quasi-particle scattering at a finite bias [10] and the spectral weight spreads almost uniformly over the entire lead energy spectrum extending even well beyond the band width of the leads. Therefore, it is almost impossible to posses multiple steady-state solutions in these simple systems by only considering electron correlations. The multi-stability could occur again when vibrational degrees of freedom are taken into account [185]. In Fig 5.17b we show the non-equilibrium spectral function $\mathcal{A}(T, w)$ (see Eq. (3.41)) with a snapshot of spectral function during the transition from $\tilde{n}_1$ to $\tilde{n}_3$. This snap shot of the spectra is very close to the unstable state $\tilde{n}_2$ and although this state is not a stable state it can be observed in the non-equilibrium spectral function.

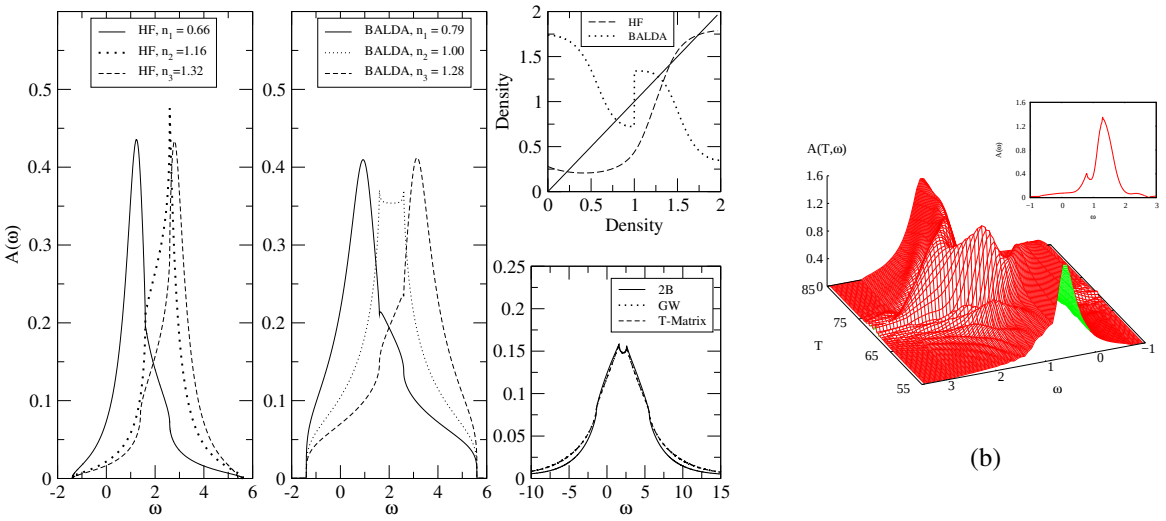

Figure 5.17: a) Spectral functions $\mathcal{A}(\omega)$ for the parameter set A at various levels of approximation. b) Non-equilibrium spectral function $\mathcal{A}(T, \omega)$ within HF approximation for switch from density n_1 to n_2 with parameter set A. Snapshot is showing the spectral function corresponding to density n_2.

Naturally the phenomenon of multi-stability is not restricted to the Anderson impurity model only and it is actually more likely to be found in systems possessing a more complicated level structure. In our work we studied also a two site Hubbard model connected to two semi-infinite, non-interacting tight-binding leads (see article III [3]). We could again find several fixed point solutions for the steady-state density from which some are again stable and reachable via time propagation while the rest are unstable. An interesting result was obtained with parameters V_{link} = 0.4, W_{L} = 2.2, W_{R} = -1.2, U = 2.0, $V_{1,2}$ = 0.4, $\varepsilon_\alpha = \varepsilon_F = 0.6$, $\varepsilon_1^C = \varepsilon_2^C$ = 0 and β = 90, with the half-filled leads. With these parameters together with asymmetrically applied gate voltage $V_{g,1} = 1.0$ and $V_{g,2} = 0$ with decay rate $\gamma = 0.2$ the HF approximation possess a

persistent oscillatory solution as shown in left panel of Fig. 5.18. These oscillations are very sensitive to the initial bias condition which can be seen by applying the bias smoothly as $W_a = W_\alpha \sin^2(\omega_\alpha t)$ and otherwise $W_\alpha(t) = W_\alpha$ with $\omega_\alpha = 0.04$, instead of abruptly ramping up the bias will destroy these oscillations.

We can analyze the nature of these oscillations by studying the equation of motion for the density matrix ρ for the isolated Hubbard dimer. The density matrix satisfies the Heisenberg equation of motion

$$i\partial_t \rho(t) = [\hat{h}_{\text{HF}}, \rho(t)], \tag{5.121}$$

where the HF Hamiltonian reads

$$\hat{h}_{HF}(t) = \begin{pmatrix} \varepsilon_1 + \frac{1}{2}Un_1 & V_{12} \\ V_{21} & \varepsilon_2 + \frac{1}{2}Un_2 \end{pmatrix}. \tag{5.122}$$

By defining following quantities

$$\begin{aligned} \Delta n(t) &= n_1(t) - n_2(t) = \rho_{11}(t) - \rho_{22}(t) && (5.123)\\ J(t) &= iV_{12}[\rho_{21}(t) - \rho_{12}(t)] && (5.124)\\ K(t) &= V_{12}[\rho_{21}(t) + \rho_{12}(t)] && (5.125) \end{aligned}$$

we can derive the following set of coupled equations of motion

$$\begin{aligned} \frac{d}{dt}\Delta n(t) &= 2J(t) && (5.126)\\ \frac{d}{dt}J(t) &= \left(-2V_{12}^2 + \frac{1}{2}K(t)U\right)\Delta n(t) + \Delta\varepsilon K(t) && (5.127)\\ \frac{d}{dt}K(t) &= -\frac{1}{2}UJ(t)\Delta n(t) - \delta\varepsilon J(t) && (5.128) \end{aligned}$$

where $\Delta\varepsilon = \varepsilon_1 - \varepsilon_2$. For our situation the on-site potentials for both sites are equal , *i.e.*, $\varepsilon_1 = \varepsilon_2$ and we can solve for $\Delta n(t)$

$$\Delta\ddot{n}(t) = 2\dot{J}(t) = -(4V_{12}^2 - K(t)U)\Delta n(t) \tag{5.129}$$

where $K(t) = -U/8(\Delta n(t))^2 + D$ and D is a real constant number related to the initial conditions via relation $D = V_{12}[\rho_{12}(0) + \rho_{21}(0)] + \frac{U}{8}[\Delta n(0)]^2$. Thus, the equation of motion for the density difference reads

$$\Delta\ddot{n}(t) + (4V_{12}^2 - UD)\Delta n(t) + \frac{U^2}{8}(\Delta n(t))^3 = 0. \tag{5.130}$$

This equation is of the form of a classical anharmonic oscillator and as a consequence it supports oscillating solutions. Solving Eq. (5.130) for the constant D as

$$D = \frac{\Delta\ddot{n}(t)}{U\Delta n(t)} + \frac{4V_{12}^2}{U} + \frac{U}{8}[\Delta n(t)]^2 \tag{5.131}$$

and use estimates for the densities from the long-time limit, *i.e.,* after the transients have died out and average D over oscillation period in Fig. 5.18, since for the connected Hubbard dimer D is not a constant in time. In the right panel of Fig. 5.18 we show the oscillation frequency and amplitude as a function of the inter-site hopping V_{12} of the Hubbard dimer connected to semi-infinite biased leads for a gate voltage kick of amplitude $V_{g,1} = 1.0$ with different decay rates γ. These oscillation frequencies and amplitudes are compared to those of the isolated Hubbard dimer. Indeed, we find quantitative similarities between the behavior of the oscillations for the connected and isolated dimer. This allows us to conclude that the connected Hubbard dimer in the quantum transport situation can, under certain parameters, behave as anharmonic oscillator and possess artificial oscillatory solutions. It is to be noted that both the oscillations and the multi-stability of the steady-state solutions disappears when including correlation effects beyond the mean-field level.

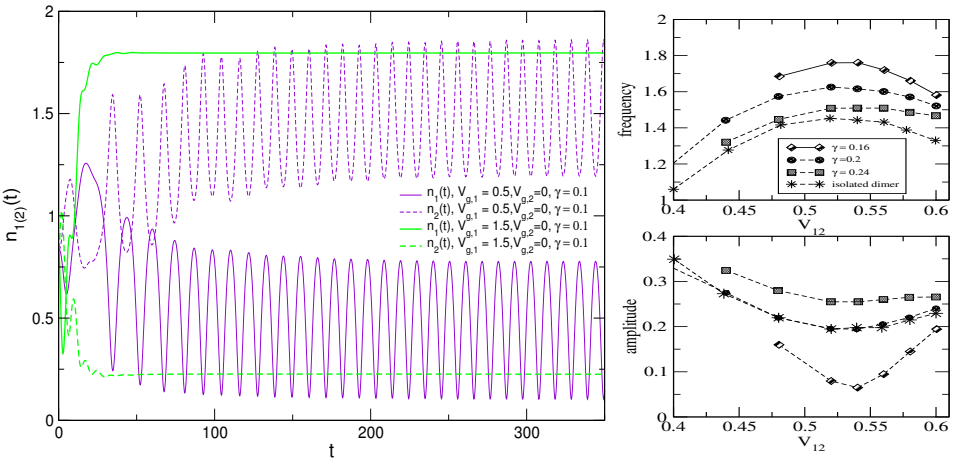

Figure 5.18: *Left panel:* Densities of the first and second site within HF approximation for Hubbard dimer connected to leads. *Right panel:* Oscillation frequency and amplitude of the density oscillations found in Hartree-Fock for certain gate switchings of the Hubbard dimer connected to biased leads as function of the hopping between the Hubbard sites. For comparison, oscillation frequencies and amplitudes are given for the isolated Hubbard dimer in HF approximation described by Eq. (5.130) (Fig. at the left panel from Khosravi *et al.* Phys. Rev. B **85** 075103 (2012)).

To conclude this section, we described the method of Kadanoff-Baym equations to study non-equilibrium dynamics of many-particle systems. We showed how to reduce a computational cost in time-propagation by introducing generalized Kadanoff-Baym anstaz, and in space by treating parts of the system via embedding self-energy. We demonstrated the basic concepts of quantum transport problem by analyzing briefly a five-level system. In addition, we studied the Anderson impurity model in out-of-equilibrium situations with various levels of approximation. We found remarkable agreement between 2B approximation within many-body perturbation theory and numerically exact time-dependent density matrix renormalization group technique. The mean-field approximations can possess artificial behavior in terms of multiple steady-states and undamped oscillations for the density and current. It is to be pointed out that the multiple steady-states could be restored beyond mean-field approximations when vibrational degrees of freedom are taken into account [185].

6

CONCLUSIONS

We have studied many-particle systems in and out of equilibrium by using many-body perturbation theory with non-equilibrium Green's functions and time-dependent density functional theory. The work has consisted of theory development as well as of numerical simulations. We started the discussion by introducing the many-particle problem together with an introduction to many-body perturbation theory and time-dependent density functional theory. A large part of the work done in this thesis consists of describing the time-dependent quantum transport problem, where our purpose was to understand the quality of many-particle self-energy approximations in non-equilibrium systems as well as uniqueness of the steady-state. Some preliminary developments towards description of photoemission processes with the Kadanoff-Baym equations as well as description of time-dependent quantum transport with realistic systems were also introduced but not presented here.

For the interacting Anderson impurity model we studied the electron transport within the TDDFT and MBPT frameworks. Results obtained in the ground state, transient and steady-state regimes are compared with numerically exact time-dependent density matrix renormalization group method. We found that in particular the 2B approximation of MBPT compare nicely. Regarding the TDDFT approach we find that the ABALDA performs very well and yields accurate densities on the interacting site but in many cases overestimates the steady-state current. This problem was linked to an overestimation of the lead-densities within the ABALDA. The result strongly suggest that it is necessary to go beyond the local approximation. For the multi-stability problem we showed that only the stable solutions are accessible via time propagation. By superimposing an exponentially decaying gate voltage we were able to switch between the different steady-states. For the systems considered we found that by inclusion of dynamical XC-effects will destroy the multi-stability phenomenon. We also concluded that in order to find bistable regimes beyond mean-field approximations one should include other degrees of freedom such as vibrations of nuclear coordinates.

The second part of this thesis consisted of studying many-body perturbation theory for the homogeneous electron gas, where the main goal was to answer the long standing question of the role of vertex corrections versus dressing of the Green's functions. This is an enormous project of its own and this question still

remains partially unanswered. Instead, we managed to construct a diagrammatic approach for construction self-energy approximations with positive-semi definite spectral and response properties. We derived a Lehmann-like representation of the exact self-energy and showed that it is given by the sum of squares of irreducible correlators. In the partitioned Feynman diagrams, one half of the partition consists of time-ordered quantities and the other half consists of anti-time-ordered quantities. The partitioning can be seen as cutting the diagram in half along the lesser/greater Green's function lines. After partitioning a self-energy or polarization diagram, we search for the minimal set of half-diagrams in order to write the approximation at hand as a perfect square of half-diagrams. The positivity of the spectral function is guaranteed by the fact that the sum of the products of the half-diagrams is the sum of perfect squares. In its simplicity these cutting rules can be seen as drawing rules for diagrams, and as an extension of the Feynman rules. First we need to draw the diagrams and by assigning a label to the internal vertices we are able to extend to a minimal set of diagrams any MBPT approximation and to generate PSD spectral functions.

In conclusion this thesis work has constituted developments of the time-dependent description of non-equilibrium quantum problem, with specialization to quantum transport situation as well as of developments in the description equilibrium properties of many-particle system. The future developments include a time-dependent description of photoemission and pump-probe processes with Kadanoff-Baym equations as well as a more thorough understanding of the photoemission process at a theoretical level. Also a thorough understanding of the role of vertex corrections for many-particle problem and to examine how the results obtained with it will compare with experiment is an interesting research line.

APPENDIX

A

BiCGSTAB and BiCGSTAB(l) Algorithms for Dyson Equation

Here we present the BiCGSTAB and BiCGSTAB(l) algorithms used for solving the Dyson equation.The Dyson equation in the form of $\mathbf{Ax} = \mathbf{b}$ was

$$\sum_{k=1}^{n}\sum_{q=0}^{m}\Big[\delta_{ik}\delta_{pq} \quad - \quad F_{ik}(\tau_p,\tau_q)\Big]G_{kj}^{M}(\tau_q) = \delta_{ij}g_i(\tau_q) \tag{A.1}$$

by combining the orbital index i and the grid index p into a single index Q_1 we obtain the matrix equations

$$\sum_{Q_2=1}^{nm} A_{Q_1,Q_2}x_{Q_2}^{(j)} = b_{Q_1}^{(j)} \tag{A.2}$$

where we have defined the unknown and the inhomogeneous part as

$$x_{Q_2}^{(j)} \quad = \quad x_{kq}^{(j)} = G_{kj}^{M}(\tau_q) \tag{A.3}$$

$$b_{Q_1}^{(j)} \quad = \quad b_{ip}^{(j)} = \delta_{ij}g_i^{M}(\tau_p). \tag{A.4}$$

A.0.3 BiCGSTAB

One of the algorithms used to solve the Dyson equation in the routine is biconjugate gradient stabilized method BiCGSTAB [165].

The iteration cycle starts with determining initial guess for the Green's function which in our case is taken to be the Hartree-Fock Green's function. Also other DFT-based initial guesses would be possible. So we assume

$$x_{Q_2}^{(0)} = G_{kj}^{\mathrm{HF}}(\tau_q) \tag{A.5}$$

to be given. With this initial guess we compute the first guess for the self-energy $\Sigma_{ij}^{M,c}(\tau_q)$. With this given self-energy the equation (A.2) is solved using the following BiCGSTAB - algorithm. First we compute the initial guess for the residuals

$$r_{Q_1}^{(0)} = b_{Q_1}^{(0)} - \sum_{Q_2}^{nm} A_{Q_1Q_2} x_{Q_2}^{(0)} \tag{A.6}$$

$$\tilde{r}_{Q_1}^{(0)} = r_{Q_1}^{(0)} \tag{A.7}$$

Then the following is repeated until the convergence is reached, here $q = 1, 2, ...$ is the index for the iteration cycle. At the beginning we choose to convergence criterion to be $\Delta = ||r_{Q_1}|| = 1$

if $\langle r_{Q_1}^{(q+1)} \cdot \tilde{r}_{Q_1}^{(0)} \rangle = 0$ **then** method fails.
if $(q == 1)$ **then**
The first guess for the error reduction polynomial is taken to be the first guess for the residual

$$p_{Q_1}^{(0)} = r_{Q_1}^{(0)} \tag{A.8}$$

else

$$\beta_{q+1} = \frac{\langle r_{Q_1}^{(q+1)} \cdot \tilde{r}_{Q_1}^{(0)} \rangle}{\langle \sum_{Q_2}^{nm} A_{Q_1Q_2} p_{Q_2}^{(q)} \cdot \tilde{r}^{(0)} \rangle} \frac{\alpha_q}{\omega_q} \tag{A.9}$$

$$p_{Q_1}^{(q+1)} = r_{Q_1}^{(q+1)} + \beta_{q+1} \big[p_{Q_1}^{(q)} - \omega_q \sum_{Q_2}^{nm} A_{Q_1Q_2} p_{Q_2}^{(q)} \big] \tag{A.10}$$

end if

$$\alpha_q = \frac{\langle r_{Q_!}^{(q)} \cdot \tilde{r}_{Q_1}^{(0)} \rangle}{\langle \sum_{Q_2}^{nm} A_{Q_1Q_2} p_{Q_2}^{(q)} \cdot \tilde{r}_{Q_1}^{(0)} \rangle} \tag{A.11}$$

$$s_{Q_1}^{(q)} = r_{Q_1}^{(q)} - \alpha^q \sum_{Q_2}^{nm} A_{Q_1Q_2} p_{Q_1}^{(q)} \tag{A.12}$$

$$\omega_q = \frac{\langle \sum_{Q_2}^{nm} A_{Q_1Q_2} s_{Q_2}^{(q)} \cdot s_{Q_1}^{(q)} \rangle}{\langle \sum_{Q_2}^{nm} A_{Q_1Q_2} s_{Q_2}^{(q)} \cdot \sum_{Q_2}^{nm} A_{Q_1Q_2} s_{Q_2}^{(q)} \rangle} \tag{A.13}$$

$$x_{Q_1}^{(q+1)} = x_{Q_1}^{(q)} + \alpha_q p_{Q_1}^{(q)} + \omega_q s_{Q_1}^{(q)} \tag{A.14}$$

$$r_{Q_1}^{(q+1)} = s_{Q_1}^{(q)} - \omega_q \sum_{Q_2}^{nm} A_{Q_1 Q_2} s_{Q_2}^{(q)} \tag{A.15}$$

if $(\Delta < tol)$ then x_{Q_1} is our solution for $G_{kj}^{M}(\tau_q)$ with given self-energy $\Sigma_{ij}^{M,c}(\tau_q)$. with this G we can calculate a new approximation for the self-energy and continue the self-consistency cycle until the convergence is reached. For the continuation it is also necessary that $\omega_q \neq 0$.

A.0.4 BiCGSTAB(L)

Another algorithm we us to solve the Dyson equation is called BiCGSTAB(l) [166]. which is an enhanced version of the BiCGSTAB. The problem of BiCGSTAB is that the minimal residual polynomial has only real roots and it can be a poor approximation for the matrices with complex eigenvalues. We again choose the Hartree-Fock Green function to be our initial guess

$$x_{Q_2}^{(0)} = G_{kj}^{\mathrm{HF}}(\tau_q) \tag{A.16}$$

and we compute the first initial guess for the residuals

$$\tilde{r}_{Q_1}^{(0)} = r_{Q_1}^{(0)} = b_{Q_1}^{(0)} - \sum_{Q_2}^{nm} A_{Q_1 Q_2} x_{Q_2}^{(0)} \tag{A.17}$$

At the start we also set $\Delta = ||r_{Q_1}|| = 1$ and $u^{-1} = 0$, $\alpha = 0$ and $\omega = 1$. Then we repeat the following procedure until the convergence is reached $(q = 1, 2, ...)$.

$$\rho_0 = -\omega \rho_0 \tag{A.18}$$

for $i = 0, ..., l-1$ **do**

$$\rho_1 = \langle \hat{r}_{Q_1}^{(j)} \cdot \tilde{r}_{Q_1}^{(0)} \rangle \tag{A.19}$$

$$\beta = \alpha \frac{\rho_1}{\rho_0} \tag{A.20}$$

$$\rho_0 = \rho_1 \tag{A.21}$$

for $i = 0, ..., j$ **do**

$$\hat{u}_{Q_1}^{(i)} = \hat{r}_{Q_1}^{(i)} - \beta \hat{u}_{Q_1}^{(i)} \tag{A.22}$$

end for

$$\hat{u}_{Q_1}^{(j+1)} = \sum_{Q_2}^{nm} A_{Q_1 Q_2} \hat{u}_{Q_2}^{(j)} \tag{A.23}$$

$$\gamma = \langle \hat{u}_{Q_2}^{(j+1)} \cdot \tilde{r}_{Q_1}^{(0)} \rangle \tag{A.24}$$

$$\alpha = \frac{\rho_0}{\gamma} \tag{A.25}$$

for $i = 0, ..., j$ **do**

$$\hat{r}_{Q_1}^{(i)} = \hat{r}_{Q_1}^{(i)} - \alpha \hat{u}_{Q_1}^{(i+1)} \tag{A.26}$$

end for

$$\hat{r}_{Q_1}^{(j+1)} = \sum_{Q_2}^{nm} A_{Q_1 Q_2} \hat{r}_{Q_2}^{(j)} \tag{A.27}$$

$$\hat{x}_{Q_1}^{(0)} = \hat{x}_{Q_1}^{(0)} + \alpha \hat{u}_{Q_1}^{(0)} \tag{A.28}$$

end for

for $j = 0, ..., l$ **do**

for $i = 0, ..., j - 1$ **do**

$$\tau_{ij} = \frac{\langle \hat{r}_{Q_1}^{(j)} \cdot \hat{r}_{Q_1}^{(i)} \rangle}{\sigma_i} \tag{A.29}$$

$$\hat{r}_{Q_1}^{(j)} = \hat{r}_{Q_1}^{(j)} - \tau_{ij} \hat{r}_{Q_1}^{(j)} \tag{A.30}$$

end for

end for

$$\gamma_l = \gamma_l' \tag{A.31}$$

$$\omega = \gamma_l \tag{A.32}$$

for $j = l-1, ..., 1$ **do**

$$\gamma_j = \gamma'_j - \sum_{i=j+1}^{l} \tau_{ji}\gamma_i \tag{A.33}$$

end for

for $j = 1, ..., l-1$ **do**

$$\gamma''_j = \gamma'_{j+1} - \sum_{i=j+1}^{l-1} \tau_{ji}\gamma_{i+1} \tag{A.34}$$

end for

$$\begin{aligned}
\hat{x}^{(0)}_{Q_1} &= \hat{x}^{(0)}_{Q_1} + \gamma_1 \hat{r}^{(0)}_{Q_1} && \text{(A.35)}\\
\hat{r}^{(0)}_{Q_1} &= \hat{r}^{(0)}_{Q_1} - \gamma'_l \hat{r}^{(l)}_{Q_1} && \text{(A.36)}\\
\hat{u}^{(0)}_{Q_1} &= \hat{u}^{(0)}_{Q_1} - \gamma_l \hat{u}^{(l)}_{Q_1} && \text{(A.37)}
\end{aligned}$$

for $j = 1, ..., l-1$ **do**

$$\begin{aligned}
\hat{x}^{(0)}_{Q_1} &= \hat{x}^{(0)}_{Q_1} + \gamma''_j \hat{r}^{(j)}_{Q_1} && \text{(A.38)}\\
\hat{r}^{(0)}_{Q_1} &= \hat{r}^{(0)}_{Q_1} - \gamma'_j \hat{r}^{(j)}_{Q_1} && \text{(A.39)}\\
\hat{u}^{(0)}_{Q_1} &= \hat{u}^{(0)}_{Q_1} - \gamma_j \hat{u}^{(j)}_{Q_1} && \text{(A.40)}
\end{aligned}$$

end for

if ($\Delta < tol$) then x_{Q_1} is our solution for $G^M_{kj}(\tau_q)$ with given self-energy $\Sigma^{M,c}_{ij}(\tau_q)$. with this G we can calculate a new approximation for the self-energy and continue the self-consistency cycle until the convergence is reached.

Bibliography

[1] A.-M. Uimonen, E. Khosravi, A. Stan, G. Stefanucci, S. Kurth, R. van Leeuwen, and E.K.U.Gross. *Phys. Rev. B*, 84:115103, 2011.

[2] A.-M. Uimonen, E. Khosravi, G. Stefanucci, S. Kurth, R. van Leeuwen, and E.K.U. Gross. *Journal of Physics, Conf. Ser.*, 220:012018, 2010.

[3] E. Khosravi, A.-M. Uimonen, A. Stan, G. Stefanucci, S. Kurth, R. van Leeuwen, and E.K.U. Gross. *Phys. Rev. B*, 85:075103, 2012.

[4] G. Stefanucci, Y. Pavlyukh, A.-M. Uimonen, and R. van Leeuwen. *Phys. Rev. B*, 90:115134, 2014.

[5] A.-M. Uimonen, G. Stefanucci, Y. Pavlyukh, and R. van Leeuwen. *Phys. Rev. B*, 91:115104, 2015.

[6] S. Latini, E. Perfetto, A.-M. Uimonen, R. van Leeuwen, and G. Stefanucci. *Phys. Rev. B*, 89:075306, 2014.

[7] A.-M. Uimonen, G. Stefanucci, and van R. Leeuwen. *The Journal of Chemical Physics*, 140:18A526, 2014.

[8] P. Rinke, A. Qteish, J.Neugebauer, C. Freysoldt, and M. Scheffler. *New Journal of Physics*, 7:126, 2004.

[9] P. Rinke, A. Qteish, J. Neugebauer, and M. Scheffler. *Physica Status Solidi (B)*, 245:929–945, 2008.

[10] P. Myöhänen, A. Stan, G. Stefanucci, and R. van Leeuwen. *Phys. Rev. B*, 80:115107, 2009.

[11] J. C. Cuevas and E. Scheer. *Molecular Electronics, An Introduction to Theory and Experiment*. World Scientific, Singapore, 2010.

[12] S. Datta. *Electronic Transport in Mesoscopic Systems*. Cambridge University Press, New York, 1995.

[13] H. Haug and A.-P. Jauho. *Quantum Kinetics in Transport and Optics of Semiconductros*. Springer-Verlag, Berlin, 1996.

[14] D. K. Ferry and S. M. Goodnick. *Transport in Nanostrucuture*. Cambridge University Press, Cambridge, 1997.

[15] Y. V. Nazarov and Y. M. Blanter. *Quantum Transport, Introduction to Nanoscience*. Cambridge University Press, Cambridge, 2009.

[16] D. A. Ryndyk, R. Gutierrez, B. Song, and G. Cuniberti. In I. Burghardt, V. May, D.A. Micha, and E.R. Bittner, editors, *Energy Transfer Dynamics in Biomaterial Systems*, volume 93 of *Springer Series in Chemical Physics*, page 213. Springer-Verlag, 2009.

[17] M. Di Ventra. *Electrical Transport in Nanoscale Systems*. Cambridge University Press, 2008.

[18] R. F. Willis B. Feuerbacher, B.Fitton. *Photoemission and the electronic properties of surfaces*. John Wiley & Sons, New York, 1978.

[19] R. F. Egertons. *Electron Energy-Loss Spectroscopy in the Electron Microscope*. Springer-Verlag, New York, 2011.

[20] G. Strinati. *Rivista Del Nuovo Cimento*, 11(2):1–86, 1988.

[21] P Danielewicz. *Annals of Physics*, 152(2):239–304, 1984.

[22] G. Stefanucci and R. van Leeuwen. *Nonequilibrium Many-Body Theory of Quantum Systems: A Modern Introduction*. Cambridge University Press, Cambridge, 2013.

[23] L. Kadanoff and G. Baym. *Quantum statistical mechanics Green's function methods in equilibrium and nonequilibrium problems*. W.A. Benjamin, New York, 1962.

[24] G. Mahan. *Many-particle physics*. Kluwer Academic/Plenum Publishers, New York, 3rd ed. edition, 2000.

[25] E. K. U. Gross, E. Runge, and O. Heinonen. *Many-Particle Theory*. IOP Publishing, Bath, 1991.

[26] M. Cini. *Topics and Methods in Condensed Matter Theory*. Springer-Verlag, Berlin Heidelberg, 2007.

[27] A. L. Fetter and J. D. Walecka. *Quantum Theory of Many-Particle Systems*. Dover Publications, 1971.

[28] R. D. Mattuck. *A Guide to Feynman Diagrams in the Many-Body Problem*. Dover Publications, New York, 1976.

[29] A. A. Abrikosov, L. P. Gorkov, and I. E. Dzyaloshinski. *Methods of Quantum Field Theory in Statistical Physics*. Dover Publications, New York, 1965.

[30] L. Hedin and S. Lundqvist. In David Turnbull and Henry Ehrenreich Frederick Seitz, editor, *Solid State Physics*, volume 23, pages 1–181. Academic Press, New York, 1970.

[31] C. Berthod. Applications of the many-body formalism in condensed matter physics. University Lecture, 2014.

[32] J. W. Negele. *Quantum many-particle systems*. Perseus Books, Reading, MA, 1998.

[33] L. V. Keldysh. *Sov. Phys. JETP*, 20:1018, 1965.

[34] R. M. Dreizler and E. K. U. Gross. *Density Functional Theory: An Approach to the Quantum Many-Body Problem*. Springer-Verlag, New York, 1990.

[35] U. von Barth. *Physica Scripta*, T109:9–39, 2004.

[36] E. Engel and R. M. Dreizler. *Density Functional Theory: Advanced Course*. Springer-Verlag, Berlin-Heidelberg, 2011.

[37] R. P. Parr and W. Yang. *Density Functional Theory of Atoms and Molecules*. Oxford University Press, Oxford, 1989.

[38] W. Koch and M. C. Holthausen. *A Chemist's Guide to Density Functional Theory*. Wiley-VCH Verlag GmbH, Weinheim, 2001.

[39] C. A. Ullrich. *Time-Dependent Density-Functional Theory,* Concepts and Applications. Dover Science Books, Oxford, 2012.

[40] M. A. L. Marques, C. A. Ullrich, F. Nogueira, A. Rubio, K. Burke, and E. K. U. Gross. *Time-Dependent Density Functional Theory*. Springer Heidelberg, 2006.

[41] M. A. L. Marques, N. T. Maitra, F. M. S. Nogueira, E. K. U. Gross, and A. Rubio. *Fundamentals of Time-Dependent Density Functional Theory*. Springer Heidelberg, 2012.

[42] R. van Leeuwen. *Int. J. Mod. Phys. B*, 15:1969, 2001.

[43] G. Stefanucci C.-O. Almbladh R. van Leeuwen, N. E. Dahlen and U. von Barth. *Int. J. Mod. Phys. B*, 15:1969, 2001.

[44] R. van Leeuwen, N.E. Dahlen, G. Stefanucci, C.-O. Almbladh, and U. von Barth. In Miguel Marques, Carsten Ullrich, Fernando Nogueira, Angel Rubio, Kieron Burke, and Eberhard Gross, editors, *Time-Dependent Density Functional Theory*, volume 706 of *Lecture Notes in Physics*, pages 33–59. Springer Berlin / Heidelberg, 2006.

[45] R. van Leeuwen. *Progress in Theoretical Chemistry and Physics*, 14:43–68, 2003.

[46] J. L. Dormann, D. Fiorani, and E. Tronc. In M. Bonitz and D. Semkat, editors, *Progress in Nonequilibrium Green's Functions II*, page 427. World Scientific, Singapore, 2003.

[47] G. Baym. *Phys. Rev.*, 127:1391–1401, 1962.

[48] G. Baym and L. P. Kadanoff. *Phys. Rev.*, 124:287–299, 1961.

[49] G. Vignale and W. Kohn. *Phys. Rev. Lett.*, 77:2037, 1996.

[50] V. J. Goldman and D. C. Tsui. *Phys. Rev. Lett.*, 58:12, 1987.

[51] F. W. Sheard and G. A. Toombs. *Appl. Phys. Lett.*, 52:15, 1988.

[52] C. Rostgaard, K. W. Jacobsen, and K. S. Thygesen. *Phys. Rev. B*, 81(8):085103, 2010.

[53] A. Stan, N. E. Dahlen, and R. van Leeuwen. *Europhys Lett.*, 76:298, 2006.

[54] A. Stan, N. E. Dahlen, and R. van Leeuwen. *J. Chem. Phys*, 130:114105, 2009.

[55] W. G. Aulbur, L. Jonsson, and J. W. Wilkins. *Solid State Phys.: Adv. Res. Appl.*, 54:1, 2000.

[56] B. Holm and U. von Barth. *Phys. Rev. B*, 57(4):2108, 1998.

[57] K. S. Thygesen and A. Rubio. *Phys. Rev. B*, 77:115333, 2008.

[58] G. D. Mahan. *Comments Cond. Mat. Phys.*, 16(6):333–354, 1994.

[59] S. Hong and G. D. Mahan. *Phys. Rev. B*, 50(12):8182, 1994.

[60] C. Verdozzi, R. W. Godby, and S. Holloway. *Phys. Rev. Lett.*, 74(12):2327–2330, 1995.

[61] H. J. DeGroot, R. T. M. Ummels, and (P. A.

[62] P. Minnhagen. *J. Phys. C*, 7(17):3013, 1974.

[63] R. Del Sole, Lucia Reining, and R. W. Godby. *Phys. Rev. B*, 49(12):8024–8028, 1994.

[64] E. L. Shirley. *Phys. Rev. B*, 54(11):7758–7764, 1996.

[65] H. Ness, L. K. Dash, M. Stankovski, and R. W. Godby. *Phys. Rev. B*, 84(19):195114, 2011.

[66] Y. Takada. *Phys. Rev. Lett.*, 87(22):226402, 2001.

[67] Y. Takada and H. Yasuhara. *Phys. Rev. Lett.*, 89(21):216402, 2002.

[68] P. Romaniello., S. Guyot, and L. Reining. *J. Chem. Phys.*, 131:154111, 2009.

[69] A. Schindlmayr and R. W. Godby. *Phys. Rev. Lett.*, 80(8):1702, 1998.

[70] A. Schindlmayr, T. J. Pollehn, and R. W. Godby. *Phys. Rev. B*, 58:12684, 1998.

[71] G. Källén. *Helvetica Physica Acta*, 25:417, 1952.

[72] H. Lehmann. *Il Nuovo Cimento*, 11(4):342–357, 1954.

[73] H. Ueba and B. Gumhalter. *Progress in Surface Science*, 82:193, 2007.

[74] L.S. Cederbaum and W. Domcke. *Advances in Chemical Physics*, 36:205, 2007.

[75] C. N. Berglund and W. E. Spicer. *Phys. Rev.*, 136:A1030–A1044, 1964.

[76] G. D. Mahan. *Phys. Rev.*, 2:4334, 1970.

[77] C. O. Almbladh and L. Hedin. *Handbook on Synchrotron radiation*, 1:607, 1983.

[78] C. O. Almbladh. *Physica Scripta*, 32:341, 1985.

[79] P. C. Martin, J., and Schwinger. *Phys. Rev.*, 115:1342–1373, 1959.

[80] T. Matsubara. *Prog. Theor. Phys.*, 14:351–378, 1955.

[81] E. Wigner. *Phys. Rev.*, 46:1002–1011, 1934.

[82] P. Gori-Giorgi, M. Seidl, and G. Vignale. *Phys. Rev. Lett.*, 103:166402, 2009.

[83] P. Gori-Giorgi and M. Seidl. *Phys. Chem. Chem. Phys.*, 12:14405–14419, 2010.

[84] R. Pariser and R. G. Parr. *J. Chem. Phys.*, 21:466, 1953.

[85] R. Pariser and R. G. Parr. *J. Chem. Phys.*, 21:767, 1953.

[86] J. A. Pople. *Trans. Faraday Soc.*, 49:1275–1385, 1953.

[87] J. A. Pople. *Proc. Phys. Soc.*, 68:81, 1955.

[88] J. Lindberg and Y. Öhrn. *The Journal of Chemical Physics*, 49:716, 1968.

[89] K. Ohno. *Theoretica chimica acta*, 2:219–227, 1964.

[90] K. Schulten, I. Ohmine, and M. Karplus. *The Journal of Chemical Physics*, 64:4422, 1976.

[91] N. Mataga and K. Nishimoto. *Zeitschrift für Physikalische Chemie*, 13:140, 1957.

[92] P. W. Anderson. *Phys. Rev.*, 124:41–53, 1961.

[93] R. Balian and C. De Dominicis. *Nuclear Physics*, 16:502–517, 1960.

[94] L. Hedin. *Phys. Rev.*, 139:A796–A823, 1965.

[95] F. Aryasetiawan and O. Gunnarsson. *Rep. Prog. Phys.*, 61:237, 1998.

[96] G. D. Mahan. *Comment. Cond. Mat. Phys.*, 16:333, 1994.

[97] L. Hedin. *J. Phys.: Condens. Matter*, 11:R489, 1999.

[98] R. van Leeuwen and G. Stefanucci. *Phys. Rev. B*, 85:115119, 2012.

[99] R. Kubo. *Rep. Prog. Phys.*, 29:255, 1966.

[100] A. Damascelli, Z. Hussain, and Z.-X. Shen. *Rev. Mod. Phys.*, 75:473–541, 2003.

[101] A. Damascelli. *Physica Scripta*, T109:61–74, 2004.

[102] R. Comin and A. Damascelli. *arXiv:1303.1438 [cond-mat.str-el]*, 2013.

[103] F. Giustino. GW & ARPES (talk). http://www.yambo-code.org/theory/giustino.pdf.

[104] M. S. Hybertsen and S. G. Louie. *Comment. Condens. Matter Phys.*, 13:223, 1987.

[105] G. Onida, L. Reining, and A. Rubio. *Rev. Mod. Phys.*, 74:601–659, 2002.

[106] M. Guzzo. *Dynamical correlation in solids: a perspective in photoelectron spectroscopy*. PhD thesis, Ecole polytechnique Palaiseau, 2012.

[107] G. D. Mahan. *Int. J. Mod. Phys. B*, 6:3381, 1992.

[108] E. Engel and S. H. Vosko. *Phys. Rev. B*, 42(8):4940–4953, 1990.

[109] D. J. W. Geldart and R. Taylor. *Can. J. Phys.*, 48:155, 1970.

[110] D. F. DuBois. *Annals of Physics*, 7:174–237, 1959.

[111] D. F. DuBois. *Annals of Physics*, 8:24–77, 1959.

[112] B. Holm. *Self-Consistency and the GW Approximation*. PhD thesis, Department of Theoretical Physics, Lund University, 1997.

[113] G. F. Giuliani and G. Vignale. *Quantum Theory of the Electron Liquid*. Cambridge University Press, Cambridge, 2005.

[114] J. M. Luttinger and J. C. Ward. *Phys. Rev.*, 118:1417–1427, 1960.

[115] P. M. Chaikin and T. C. Lubensky. *Principles of Condensed Matter Physics*. Springer-Verlag, Cambridge, 2003.

[116] N Säkkinen, M Manninen, and R van Leeuwen. *New J. Phys.*, 14(1):013032, 2012.

[117] K. Balzer, S. Hermanns, and M. Bonitz. *EPL (Europhysics Letters)*, 98(6):67002, 2012.

[118] E. E. Salpeter and H. A. Bethe. *Phys. Rev.*, 84:1232–1242, 1951.

[119] D. Sangalli, P. Romaniello, G. Onida, and A. Marini. *J. Chem. Phys.*, 134(3):034115, 2011.

[120] T. Olsen and K. S. Thygesen. *J. Chem. Phys.*, 140(16):164116, 2014.

[121] R. E. Cutkosky. *J. Math. Phys.*, 1(5):429–433, 1960.

[122] M. Veltman. *Physica*, 29(3):186–207, 1963.

[123] R. L. Kobes and G. W. Semenoff. *Nucl. Phys. B*, 260(3-4):714–746, 1985.

[124] R. L. Kobes and G. W. Semenoff. *Nucl. Phys. B*, 272(2):329–364, 1986.

[125] R. Kobes and G. Semenoff. *Phys. Rev. B*, 34(6):4338–4341, 1986.

[126] S. Jeon. *Phys. Rev. D*, 47(10):4586–4607, 1993.

[127] C.-O. Almbladh. *J. Phys. Conf. Ser.*, 35:127–144, 2006.

[128] P. Hohenberg and W. Kohn. *Phys. Rev.*, 136:B864–B871, 1964.

[129] W. Kohn and L. J. Sham. *Phys. Rev.*, 140:A1133–A1138, 1965.

[130] L. J. Sham and M. Schlüter. *Phys. Rev. Lett.*, 51:1888–1891, 1983.

[131] R. van Leeuwen. *Phys. Rev. Lett.*, 76:3610, 1996.

[132] E. Runge and E. K. U. Gross. *Phys. Rev. Lett.*, 52:997–1000, 1984.

[133] R. van Leeuwen. *Phys. Rev. Lett.*, 82:3863–3866, 1999.

[134] M. Ruggenthaler and R. van Leeuwen. *EuroPhys. Lett.*, 95:13001, 2011.

[135] M. Petersilka, U. J. Gossmann, and E. K. U. Gross. *Phys. Rev. Lett.*, 76:1212–1215, 1996.

[136] M. Ruggenthaler, M. Penz, and R. van Leeuwen. *Journal of Physics: Condensed Matter*, 27:203202, 2015.

[137] R. van Leewuen. *International Journal of Modern Physics B*, 15:1969, 2001.

[138] M. E. Casida. In D. E. Chong, editor, *Recent Advances in Density Functional Methods*, volume 1, pages 155–192. World Scientific, Singapore, 1995.

[139] M. E. Casida. In J. M. Seminario, editor, *Recent Developments and Applications in Modern Density Functional Theory*, volume 4, pages 391–439. Elsvier, Amsterdam, 1996.

[140] P. Elliot, F. Furche, and K. Burke. In K. B. Lipkowitz and T. R. Cundari, editors, *Reviews in Computational Chemistry*, volume 26, pages 91–165. Wiley, New Jersey, 2009.

[141] E.K.U. Gross, C.A. Ullrich, and U. J. Gossmann. In E.K.U. Gross and R.M. Dreizler, editors, *Density Functional Theory*, volume 337, page 149. Plenum, New York, 1995.

[142] E. K. U. Gross, J. F. Dobson, and M. Petersilka. In R.F. Nalewajski, editor, *Density Functional Theory II*, volume 181 of *Topics in Current Chemistry*, pages 81–172. Springer Berlin Heidelberg, 1996.

[143] R. van Leeuwen, N. E. Dahlen, G. Stefanucci, C.-O. Almbladh, and U. von Barth. In M. Marques, C. Ullrich, F. Nogueira, A. Rubio, K. Burke, and E. K. U Gross, editors, *Time-Dependent Density Functional Theory*, volume 706 of *Lecture Notes in Physics*, pages 33–59. Springer-Verlag, 2006.

[144] C. Verdozzi. *Phys. Rev. Lett.*, 101:166401, 2008.

[145] Elliott H. Lieb and F.Y. Wu. *Physica A: Statistical Mechanics and its Applications*, 321(1–2):1 – 27, 2003.

[146] N. A. Lima, M. F. Silva, L. N. Oliveira, and K. Capelle. *Phys. Rev. Lett.*, 90:146402, 2003.

[147] S. Kurth, G. Stefanucci, E. Khosravi, C. Verdozzi, and E.K.U. Gross. *Phys. Rev. Lett.*, 104:236801, 2010.

[148] N. A. Lima, L. N. Oliveira, and K. Capelle. *Europhys. Lett.*, 60:601, 2002.

[149] L. Hedin and J. D. Lee. *Journal of Electron Spectroscopy and Related Phenomena*, 124(2-3):289–315, 2002.

[150] N. Agrait, A. L. Yeyati, and J. M. van Ruitenbeek. *Physics Reports*, 377:81 – 279, 2003.

[151] N. A. Zimbovskaya and M. R. Pederson. *Physics Reports*, 509:1–87, 2011.

[152] H. Choi and C. Mody. *Social Studies of Science*, 39(1):11–50, 2009.

[153] M. A. Reed, C. Zhou, C. J. Mulller, T. P. Burgin, and J. M. Tour. *Science*, 278:252–254, 1997.

[154] S. Kurth, G. Stefanucci, C.-O. Almbladh, A. Rubio, and E. K. U. Gross. *Phys. Rev. B*, 72:035308, 2005.

[155] J. Taylor, H. Guo, and J. Wang. *Phys. Rev. B*, 63:245407, 2001.

[156] M. Brandbyge, J.-L. Mozos, P. Ordejón, J. Taylor, and K. Stokbro. *Phys. Rev. B*, 65:165401, 2002.

[157] S.-H. Ke, H. U. Baranger, and W. Yang. *Phys. Rev. B*, 70:085410, 2004.

[158] K. S. Thygesen. *Phys. Rev. Lett.*, 100:166804, 2008.

[159] S. Datta Y. Xue and M. A. Ratner. *Chemical Physics*, 281:151–170, 2002.

[160] J. P. Bergfield and C. A. Stafford. *Phys. Rev. B*, 79:245125, 2009.

[161] M. Strange, C. Rostgaard, H. Häkkinen, and K. S. Thygesen. *Phys. Rev. B*, 83:115108, 2011.

[162] Y. Meir and N.S. Wingreen. *Phys. Rev. Lett.*, 68:2512, 1992.

[163] N. E. Dahlen and R. van Leeuwen. *The Journal of Chem. Phys.*, 122:164102, 2005.

[164] A. Stan, N. E. Dahlen, and R. van Leeuwen. *The Journal of Chem. Phys.*, 130:224101, 2009.

[165] H. A. van der Vorst. *SIAM Journal on Scientific and Statistical Computing*, 13:631, 1992.

[166] G. L. G. Sleijpen, H. A. van der Vorst, and D. R. Fokkema. *Numerical Algorithms*, 7:75–109, 1994.

[167] P. Lipavský, V. Špička, and B. Velický. *Phys. Rev. B*, 34:6933–6942, 1986.

[168] S. Hermans, K. Balzer, and M. Bonitz. *Physica Scripta*, T151:014036, 2012.

[169] K. Balzer and M. Bonitz. *Nonequilibrium Green's Function Approach to Inhomogeneous Systems*. Springer-Verlag, Berlin Heidelberg, 2013.

[170] G. Li, A. Nitzan, and M. A. Ratner. *Phys. Chem. Chem. Phys.*, 14:14270–14276, 2012.

[171] P. Myöhänen, R. Tuovinen, T. Korhonen, G. Stefanucci, and R. van Leeuwen. *Phys. Rev. B*, 85:075105, 2012.

[172] M. Cini. *Phys. Rev. B*, 22:5887, 1980.

[173] A.-M. Uimonen. Many-body approach to time-dependent quantum transport. Master's thesis, University of Jyväskylä, Finland, 2009.

[174] F. Heidrich-Meisner, A. E. Feiguin, and E. Dagotto. *Phys. Rev. B*, 79:235336, 2009.

[175] G. Stefanucci and C.-O. Almbladh. *Europhys. Lett.*, 67:14, 2004.

[176] H. Mera, K. Kaasbjerg, Y. M. Niquet, and G. Stefanucci. *Phys. Rev. B*, 81:035110, 2010.

[177] P. Myöhänen, A. Stan, G. Stefanucci, and R. van Leeuwen. *Europhys. Lett.*, 4:67001, 2008.

[178] A. Dhar. *Advances in Physics*, 47(2008):457–537.

[179] A.A. Dziohev and D.S. Kosov. *The Journal of Chemical Physics*, 135(2011):174111.

[180] J. O. Sofo and A. Balsero. *Phys. Rev. B*, 42(7292), 1990.

[181] T. Fiig and A.-P. Jauho. *Surface Science*, 267(392), 1992.

[182] P. L. Pernas and F. Florens. *Phys. Rev. B*, 47(4779), 1993.

[183] C. F. A. Negre, P. A. Gallay, and C. G. Sánchez. *Chem. Phys. Lett.*, 460:220–224, 2008.

[184] S. Kurth, G. Stefanucci, C.-O. Almbladh, A. Rubio, and E. K. U. Gross. *Phys. Rev. B*, 72(035308), 2005.

[185] E. Y. Wilner, H. Wang, G. Cohen, M. Thoss, and E. Rabani. *Phys. Rev. B*, 88:045137, 2013.

PUBLICATIONS